MOLECULAR TOOLS FOR ELUCIDATING COPPER BIOCHEMISTRY:

Water-soluble fluorescent probes and robust affinity standards

A Dissertation
Presented to
The Academic Faculty

by

M. Thomas Morgan

In Partial Fulfillment
of the Requirements for the Degree
Doctor of Philosophy in Chemistry

Georgia Institute of Technology
May 2013

MOLECULAR TOOLS FOR ELUCIDATING COPPER BIOCHEMISTRY:

Water-soluble fluorescent probes and robust affinity standards

Approved by:

Dr. Christoph J. Fahrni, Advisor
School of Chemistry & Biochemistry
Georgia Institute of Technology

Dr. Laren M. Tolbert
School of Chemistry and Biochemistry
Georgia Institute of Technology

Dr. Seth R. Marder
School of Chemistry and Biochemistry
Georgia Institute of Technology

Dr. Lakeshia J. Taite
School of Chemical and Biomolecular Engineering
Georgia Institute of Technology

Dr. Joseph W. Perry
School of Chemistry and Biochemistry
Georgia Institute of Technology

Date Approved: March 26 2013

ACKNOWLEDGEMENTS

I would like to thank my advisor, Dr. Christoph Fahrni, for initiating inspiring projects, providing helpful advice, and upholding scientific standards which, in my opinion, far exceed the current norm within the fluorescent probe field. I would also like to thank Dr. Manjusha Verma and Aneese Chaudry, who helped get me started in the Fahrni laboratory and whose work laid the foundation for my own. Additionally, I thank former student Jonathan Hofmekler for providing much amusement and for quickly synthesizing previously reported copper(I) probes when we needed them for comparison purposes.

I especially thank fellow graduate student Pritha Bagchi, with whom I have worked extensively in the development of fluorescent probes and affinity standards for copper(I). Her patience and perseverance in obtaining high quality experimental data surpass that of anyone else I know, including myself, and without her contributions my own work would not have progressed nearly so far.

Finally, I thank those outside of the laboratory who helped to support me through these years, including my parents Mike and Karen Morgan, my late grandfather Addison Way Carter, from whom I gained much of my earliest scientific knowledge, and my loving wife Sara, who has patiently supported me throughout my time at Georgia Tech.

TABLE OF CONTENTS

LIST OF TABLES

LIST OF FIGURES

LIST OF SCHEMES

LIST OF SYMBOLS AND ABBREVIATIONS

~	Approximately
[14]aneS_4-*a*	1,4,8,11-Tetrathiacyclotetradecane
[14]aneS_4-*b*	1,4,8,12-Tetrathiacyclotetradecane
[16]aneS_4	1,5,9,13-Tetrathiacyclohexadecane
2,2-DMP	2,2-dimethoxypropane
Å	Angstrom
ad	Apparent doublet
AU	Arbitrary units
br.	Broad
calcd	Calculated
Cu(I)	Copper in the monovalent oxidation state with unspecified coordinating ligands
Cu^+	Free aquocopper(I) ion
d	Doublet
DABCO	1,4-diazabicyclo[2.2.2]octane
DCM	Dichloromethane
DMF	Dimethylformamide
DMSO	Dimethylsulfoxide
$E(A/A^-)$,	Ground-state electrochemical reduction potential of a PET acceptor
E(D+/D)	Donor potential (Reduction potential of the corresponding radical cation)
EI	Electron-impact ionization
equiv.	Molar equivalents
ESF	Ethenesulfonyl fluoride

ESI	Electrospray ionization
ESPT	Excited-state proton transfer or proton shift
EtOAc	Ethyl acetate
EtOH	Ethanol
FWHM	Full width at half maximum
h	Hour
HPLC	High performance (high pressure) liquid chromatography
ICP-MS	Inductively coupled plasma-mass spectrometry
IR	Infrared spectroscopy
IRF	Instrument response function
J	NMR coupling constant
$K_{Cu(I)}$	Cu(I)-ligand complex stability constant
$K'_{Cu(I)}$	Cu(I)-binding affinity (apparent stability constant) at specified pH
k_{nr}	Excited-state nonradiative deactivation rate constant
k_r	Excited-state radiative deactivation rate constant
LG	Leaving group
M	Molar
m	Multiplet
MALDI	Matrix-assisted laser desorption-ionization
Me	Methyl
meV	Millielectron-volt
MHz	Megahertz
min	Minute
mM	Millimolar
MOPS	N-(3-sulfopropyl)morpholine

MS	Mass spectrometry
Ms	Methanesulfonyl
ms	Millisecond
MTBE	*tert*-butyl methyl ether
n.d.	Insufficient signal to noise ratio for determination
n-BuLi	*n*-Butyllithium
NMR	Nuclear magnetic resonance spectroscopy
ORTEP	Oak Ridge thermal ellipsoid plot
p	Pentet (quintet)
PAGE	Polyacrylamide gel electrophoresis
PET	Photoinduced electron transfer
PG	Protective group
ppm	Parts per million
PPTS	Pyridinium *para*-toluenesulfonate
pyr	Pyridine
q	Quartet
R	Alkyl group
RP-HPLC	Reversed-phase HPLC
rt	Room temperature
s	Singlet
sat.	Saturated
SHE	Standard hydrogen electrode reference potential
t	Triplet
t-BuLi	*tert*-Butyllithium
TCEP	Tris(2-carboxyethyl)phosphine, a disulfide reducing agent

TFA	Trifluoroacetic acid
THF	Tetrahydrofuran
TLC	Thin-layer chromatography
TMG	1,1,3,3-Tetramethylguanidine
TsOH	*para*-Toluenesulfonic acid
UV	Ultraviolet
V	Volt
β_2	Ligand-metal 2:1 association constant. $\beta_2 = [ML_2]/([M][L]^2)$
ΔE_{00}	Zero-Zero transition energy for electronic excitation of a fluorophore
ΔG	Gibbs free energy of reaction
µM	Micromolar
σ^c	Computationally derived effective Hammett substituent constant
σ_m	Hammett substituent constant for a group in the *meta* position
σ_p	Hammett substituent constant for a group in the *para* position
$\Sigma\sigma$	Sum of Hammett substituent constants

SUMMARY

Copper is an essential trace element for living organisms and has both known and additional suspected roles in human health and disease. The current understanding of copper metabolism is substantial but incomplete, particularly in regard to its storage and exchange at the subcellular level, although available evidence indicates exchangeable intracellular copper is in the monovalent oxidation state. Selective fluorescent probes with sufficient sensitivity to detect Cu(I) availability at physiologically relevant levels and at subcellular resolution would be valuable tools for studying copper metabolism. As a contribution toward this goal, this work describes the development of Cu(I)-selective fluorescent probes with greatly improved aqueous solubility, contrast ratio, and fluorescence quantum yield. This work also describes the development of water-soluble, 1:1-binding chelators that form colorless, air-stable copper(I)-complexes. By acting as copper(I) buffering agents and affinity standards, these compounds can serve a complementary role to fluorescent probes in the study of copper biochemistry.

Chapter 1 gives a short introduction to the biological importance of copper, the current knowledge regarding intracellular exchangeable copper, the techniques available for detection of copper in biological samples, and the potential benefits of more effective copper(I)-selective fluorescent probes and affinity standards.

Chapter 2 provides an introduction to fluorescence turn-on probes based on photoinduced electron transfer (PET), then describes pilot studies in organic solvents that laid the groundwork for the development of high-contrast Cu(I)-selective fluorescent probes that operate in aqueous solution. The pilot studies

began with demonstrations of the utility of 1,3,5-triarylpyrazolines as electronically tunable fluorophores, then progressed to contrast optimization of triarylpyrazoline-based methanolic Cu(I)-probes. While the author contributed to the synthetic aspects of the latter work, this chapter is intended primarily as a literature review and is referenced frequently in the subsequent chapters.

Chapter 3 describes the development of CTAP-2,[1] a water-soluble Cu(I)-selective fluorescent probe designed to operate on the tunable PET-based fluorescence switching mechanism previously demonstrated with the methanolic Cu(I)-probes described in Chapter 2. To achieve aqueous solubility without producing a strongly amphiphilic, detergent-like structure, CTAP-2 is based on a balanced hydrophilic functionalization approach combining a tetrahydroxylated thiazacrown Cu(I)-ligand with a sulfonated triarylpyrazoline fluorophore. Much of Chapter 3 is devoted to the initially challenging synthesis of this structure. CTAP-2 was found to dissolve directly in water to milimolar concentrations, a characteristic never before reported for Cu(I)-selective fluorescence turn-on probes, and yielded a 65-fold emission enhancement on Cu(I)-saturation, slightly exceeding the maximum contrast ratio of 50 observed for its methanolic forerunners, although providing only a modest fluorescence quantum yield of 8.3%. Linear profiles of absorbance and fluorescence versus concentration of CTAP-2 and its Cu(I)-complex revealed no evidence of aggregation at typical working concentrations in aqueous solution. Experiments by Pritha Bagchi demonstrated that CTAP-2 is able to selectively detect the copper-bound form of the metallochaperone Atox1 within a native electrophoresis gel, thus demonstrating another potentially important application of Cu(I)-selective fluorescence turn-on probes beyond cellular imaging.

During our careful characterization of CTAP-2, another Cu(I)-selective fluorescent probe, Coppersensor-3 (CS3),[2] was reported to yield an even higher

contrast response to Cu(I) in aqueous solution, although it contained no water-solubilizing functional groups and the published emission spectrum was suspiciously cut off at shorter wavelengths while still at over half-maximum intensity. Dynamic light scattering experiments conducted by Pritha Bagchi revealed that not only CS3 but also the earlier aqueous Cu(I)-probes CS1 and CTAP-1 form colloidal aggregates at micromolar concentrations in aqueous solution, while CTAP-2 does not. Based on these results, it appears that CTAP-2 is actually the first truly water-soluble Cu(I)-selective fluorescence turn-on probe.

Chapter 4 describes an initial unsuccessful attempt to improve upon the fluorescence contrast ratio and quantum yield offered by CTAP-2, followed by detailed studies to determine the factors responsible for the low fluorescence quantum yield. Analysis of time-resolved fluorescence decay profiles revealed that the fluorescence quantum yield and contrast ratio of both CTAP-2 and the new probe are limited by formation of multiple Cu(I)-coordination species providing varying degrees of PET inhibition, presumably due to incomplete Cu(I)-N coordination as previously observed for the methanolic Cu(I)-probes described in Chapter 2. Furthermore, the fluorescence quantum yield in aqueous solution of both protonated CTAP-2 and a quaternary ammonium-based fluorophore analog are significantly lower than typically observed for related triarylpyrazolines in organic solvents, indicating the presence of an additional unknown fluorescence quenching pathway. This was initially suspected to be donor-excited PET, but solvent isotope effects revealed that it is actually an excited-state protonation or proton shift, which is hereafter referred to by the general term excited-state proton transfer (ESPT). Two distinct ESPT pathways were identified, an acid-mediated pathway that becomes important only at millimolar hydronium concentrations, and a separate pathway that occurs even in neutral solution and is unaffected by addition of base but inhibited by replacement

of H_2O with D_2O as the solvent. The latter pathway limits the maximum quantum yield available from the CTAP-2 fluorophore to about 30% in aqueous solution.[3]

Chapter 5 describes the development of water-soluble Cu(I)-probes that significantly exceed CTAP-2 in contrast ratio and quantum yield by iterative improvement of both the fluorophore and ligand designs. The knowledge gained through the experiments described in Chapter 4 was essential to this process. Based on evidence that the ESPT-mediated fluorescence quenching of 1,3,5-triarylpyrazolines in protic solvents is suppressed by strong electron-withdrawing groups on the 1-aryl ring, we replaced both the 3-aryl *p*-cyano- and 1-aryl *p*-sulfonate substituents of the CTAP-2 fluorophore with sulfonamide moieties, which are significantly stronger than $-SO_3^-$ and comparable to -CN in terms of electron-withdrawing power. This modification succeeded in inhibiting ESPT but also appeared to provide a higher-than-optimal PET driving force, resulting in an impressive contrast ratio of 160 but a modest fluorescence quantum yield of 14% after optimization of the ligand design. To decrease the PET driving force while maintaining ESPT inhibition, the 3-aryl sulfonamide substituent was isomerized from a strongly electron-withdrawing arenesulfonamide at the para-position to a weakly electron-withdrawing N-arylmethanesulfonamide at the meta-position, while the 1-aryl sulfonamide moiety was left unmodified. The resulting probe gave a remarkable 180-fold fluorescence turn-on response and reached a fluorescence quantum yield of 41% upon Cu(I)-saturation, which should be quite sufficient for imaging applications, although further modifications to improve the binding affinity will likely be necessary to detect Cu(I) at normal physiological concentrations.

Chapter 6 describes the development of sulfonated, thioether-based tetradentate Cu(I)-ligands as robust affinity standards. Two symmetrical tripodal thioether-amine ligands were initially synthesized and characterized. X-ray

crystallographic studies revealed 1:1 Cu(I) complexes as expected, with coordination modes similar to those of related non-sulfonated tripodal ligands. Both of these sulfonated tripods and their respective Cu(I)-complexes are water-soluble, air-stable, and can be isolated by crystallization, making them useful as affinity standards, but the respective Cu(I)-binding affinities are so far separated at neutral pH that these two ligands alone cannot provide a continuous range of buffered Cu^{+} concentrations. This gap was bridged using a tetrasulfonated derivative of the thiocrown ligand [16]aneS_4. Although [16]aneS_4 itself has a similar Cu(I)-complex stability constant to the lower affinity tripodal ligand, placement of the solubilizing functional groups on the middle carbons of opposing trimethylene bridges of the macrocycle yielded a substantial increase in Cu(I)-binding affinity, presumably through preorganization of the free ligand. Like the tripodal amines, the sulfonated thiocrown also yielded a crystalline, water-soluble, air-stable Cu(I)-complex, making it well suited to use as an affinity standard or copper buffer. An extensive series of experiments conducted by Pritha Bagchi using the three sulfonated Cu(I)-chelators as well as several previously reported ligands yielded a web of accurately cross-verified Cu(I) affinities with several anchor points. The new series of Cu(I)-affinity standards can be used directly in ligand competition experiments to determine the Cu(I)-binding affinities of certain copper proteins, as has been demonstrated by Pritha Bagchi using the bacterial copper chaperone CusF, and can presumably be expanded by addition of higher affinity ligands to allow competition experiments with a wider range of biological Cu(I)-ligands.

CHAPTER 1

INTRODUCTION

Copper, like iron and zinc, is an essential trace element for known life forms. Various enzymes essential for human life require copper as a cofactor, including lysyl oxidase, which is required for connective tissue maturation, and cytochrome C oxidase, the terminal component of the respiratory electron transport chain and the primary target of cyanide toxicity.[4] Despite the essentiality of copper, free copper ions, either Cu(I) or Cu(II), exert strong toxic effects, and copper is therefore tightly regulated in biological systems. Defects in copper transport are known to be the underlying cause of Menkes disease and Wilson's disease, and there is evidence suggesting that copper may also be involved in the pathology of much more common human ailments including Alzheimer's disease and Parkinson's disease[4,5].

Given the importance of copper to both fundamental biology and human health, a large and continually evolving body of knowledge has amassed regarding the metabolism and homeostasis of this element, particularly in identification of the genes and proteins involved;[6] however, many important questions about copper biochemistry remain unanswered, particularly with regard to storage, mobilization, and distribution at the subcellular level.[6,7] For example, experiments have demonstrated rapid and substantial cellular uptake or efflux of Cu depending on the copper concentration of the surrounding medium, suggesting the presence of kinetically labile intracellular copper,[8] yet arguments based on the kinetics of Cu incorporation into the enzyme superoxide dismutase indicate that intracellular free copper concentrations must lie well below the level of a single ion per cell.[9] Furthermore, based on available kinetic data regarding the reaction of Cu(I) with dioxygen[10] and of Cu(II) with glutathione,[11] a persuasive argument can be made that free aqueous copper ions, either Cu^{+} or Cu^{2+}, *cannot* exist in significant quantities under

normal intracellular conditions: Free aqueous Cu^{+} is highly reactive toward dioxygen, converting to Cu^{2+} with an estimated half-life of 15 ms in air-saturated water at 25°C.[12] Aqueous Cu^{2+}, however, is highly reactive toward the ubiquitous intracellular free thiol glutathione, and would be reduced in milliseconds by the millimolar glutathione concentrations present in healthy eukaryotic cells.[12] Therefore, free aqueous copper ions of either oxidation state are incompatible with the coexistence of high concentrations of glutathione and molecular oxygen typically present in animal cells, and intracellular copper trafficking must proceed via associative exchange of copper between high affinity ligands rather than by dissociation to free Cu^{+} or Cu^{2+} ions. Several "copper chaperones" (including Atox1 and CCS) are now known to deliver Cu(I) ions to other proteins through an associative exchange mechanism, but little is currently known about the chemical nature and subcellular localization of the high capacity labile copper pools.[4] Also currently unknown is the thermodynamic effective Cu^{+} concentration in various cellular compartments under normal physiological conditions and in disease states. Robust techniques to probe the kinetic accessibility and thermodynamic availability of Cu(I) in biological systems should help to answer these questions.

While total copper concentrations can currently be determined at subcellular spatial resolution by direct detection techniques such as synchrotron-based x-ray fluorescence imaging (SXRF) and secondary ion mass spectrometry (SIMS), selective determination of kinetically available copper requires detection reagents that interact chemically with copper ions to produce a measurable signal.[13] Historically, imaging of kinetically labile copper at the tissue level has been accomplished using chromogenic precipitating agents such as dithiooxamide (rubeanic acid) and *p*-dimethylamino-benzylidene rhodanine,[14] but the sensitivity offered by these methods is sufficient only for detection of the highly elevated copper levels present in certain disease states.[13]

Compared to chromogenic reagents, optical fluorescence turn-on probes offer much greater detection sensitivity and spatial resolution. These properties, combined with

the nondestructive nature of optical fluorescence microscopy, allow imaging of labile metal cation pools in live cells.[13,15] Cation-selective fluorescent probes that respond reversibly to analyte binding offer the additional capability of dynamic imaging of metal ion fluxes within a given cell, which is not possible with direct detection techniques based on x-ray fluorescence or mass spectrometry.[13] In this regard, such fluorescent indicators also provide an advantage over fluorogenic chemodosimeters, which yield an irreversible fluorescence response upon interaction with the analyte.[16]

While selective fluorescent probes for redox-inactive cations such as Ca(II) and Zn(II) have already seen widespread use,[13,15] the design of fluorescence turn-on probes for Cu(I) is more challenging due to the ability of this ion to act as a fluorescence quencher.[17-19] Prior to the beginning of this work, only two biologically applicable Cu(I) selective fluorescence turn-on probes, CTAP-1[8] and Coppersensor-1 (CS1)[20] had been reported. Both probes gave a significant increase in fluorescence emission in response to high-dose copper supplementation in live cells, but the direct physiological significance of the observed response is uncertain. This is in part because the contrast ratio, or fold increase in fluorescence output upon analyte binding, is relatively low for both CTAP-1 and CS1 (4.6 and 10, respectively), thus providing a limited ability to distinguish actual differences in Cu(I) availability from local variations in probe concentration. Furthermore, these lipophilic probes do not dissolve directly in water and were instead introduced into aqueous buffer by dilution of a DMSO stock solution,[8,21] yet no experiments were performed to ascertain whether the resulting solutions actually contain the monomeric probe as opposed to an aggregate. Therefore, it was uncertain whether the species characterized in aqueous buffer are actually the same as observed in cellular imaging experiments, particularly for CS1, which contains no charged or strongly hydrophilic functional groups.[20]

With the ultimate goal of creating better tools for investigating copper(I) biochemistry, Fahrni *et al*. proceeded on a quest to improve the fluorescence contrast

ratio and quantum yield available from water-soluble Cu(I)-selective fluorescent probes. This effort, which commenced with pilot studies in organic solvents,[22-26] eventually lead to the development of CTAP-2,[1] a Cu(I)-selective fluorescent probe which dissolves directly in water and yields a strong 65-fold fluorescence turn-on response, albeit with a somewhat reduced fluorescence quantum yield of 8.3% versus 15% for CTAP-1. Elucidation of the causes of this low fluorescence quantum yield ultimately paved the way for an improved water-soluble Cu(I) probe providing more than double the contrast ratio and a nearly five-fold higher fluorescence quantum yield versus CTAP-2, at last fully meeting the challenge of obtaining a strong yet reversible fluorescence turn-on response to Cu(I) in aqueous solution. The development of bright, high-contrast, water-soluble fluorescence turn-on probes for Cu(I) described in this dissertation constitutes a significant step in the evolution of Cu(I)-responsive fluorescent probes from proof-of-concept to mainstream analytical tools for studying Cu(I)-biochemistry.

In addition to fluorescent probes, this work also describes the development of new water-soluble, 1:1-binding chelators that form colorless, air-stable complexes with Cu(I) for use as robust affinity standards and copper buffering agents. In contrast to Cu(I) selective fluorescence probes, which are intended for use as indicators to report the Cu(I) availability set by more abundant biological ligands, these chelators and their respective Cu(I) complexes can be mixed in various ratios to set the thermodynamically buffered Cu^{+} concentration to a particular desired level while allowing spectrophotometric or fluorimetric monitoring of the copper occupancy of other ligands present in the solution. This capability could serve a variety of purposes in the study of copper biochemistry, including calibration of Cu(I)-selective fluorescent probes, detection of new Cu(I)-binding proteins by selective metalation, and accurate determination of the Cu(I)-binding affinity of known copper proteins.

References

(1) Morgan, M. T.; Bagchi, P.; Fahrni, C. J. *J. Am. Chem. Soc.* **2011**, *133*, 15906.

(2) Dodani, S. C.; Domaille, D. W.; Nam, C. I.; Miller, E. W.; Finney, L. A.; Vogt, S.; Chang, C. J. *Proc. Natl. Acad. Sci. U. S. A.* **2011**, *108*, 5980.

(3) Morgan, M. T.; Bagchi, P.; Fahrni, C. J. *Dalton Trans.* **2013**, *42*, 3240.

(4) Kim, B.-E.; Nevitt, T.; Thiele, D. J. *Nat. Chem. Biol.* **2008**, *4*, 176.

(5) Gaggelli, E.; Kozlowski, H.; Valensin, D.; Valensin, G. *Chem. Rev.* **2006**, *106*, 1995.

(6) Nevitt, T.; Ohrvik, H.; Thiele, D. J. *Biochim. Biophys. Acta.* **2012**, *1823*, 1580.

(7) Lutsenko, S. *Curr. Opin. Chem. Biol.* **2010**, *14*, 211.

(8) Yang, L.; McRae, R.; Henary, M. M.; Patel, R.; Lai, B.; Vogt, S.; Fahrni, C. J. *Proc. Natl. Acad. Sci. U. S. A.* **2005**, *102*, 11179.

(9) Rae, T. D.; Schmidt, P. J.; Pufahl, R. A.; Culotta, V. C.; O'Halloran, T. V. *Science* **1999**, *284*, 805.

(10) Mi, L.; Zuberbühler, A. D. *Helv. Chim. Acta* **1991**, *74*, 1679.

(11) Gorren, A. C.; Schrammel, A.; Schmidt, K.; Mayer, B. *Arch. Biochem. Biophys.* **1996**, *330*, 219.

(12) Morgan, M. T.; Bagchi, P.; Fahrni, C. J. In *Encyclopedia of Inorganic and Bioinorganic Chemistry*; John Wiley & Sons: 2013; Vol. in press.

(13) McRae, R.; Bagchi, P.; Sumalekshmy, S.; Fahrni, C. J. *Chem. Rev.* **2009**, *109*, 4780.

(14) Okamoto, K.; Utamura, M. *Acta Sch. Med. Univ. Imp. Kioto* **1938**, *20*, 573.

(15) Domaille, D. W.; Que, E. L.; Chang, C. J. *Nat. Chem. Biol.* **2008**, *4*, 168.

(16) Hyman, L. M.; Franz, K. J. *Coord. Chem. Rev.* **2012**, *256*, 2333.

(17) Kim, H.-S.; Ahner, B. A. *Anal. Chim. Acta* **2006**, *575*, 223.

(18) Rapisarda, V. A.; Volentini, S. I.; Farías, R. N.; Massa, E. M. *Anal. Biochem.* **2002**, *307*, 105.

(19) Strambini, G. B.; Gabellieri, E. *Journal of Physical Chemistry* **1991**, *95*, 4347.

(20) Zeng, L.; Miller, E. W.; Pralle, A.; Isacoff, E. Y.; Chang, C. J. *J. Am. Chem. Soc.* **2006**, *128*, 10.

(21) Miller, E. W.; Zeng, L.; Domaille, D. W.; Chang, C. J. *Nat. Protoc.* **2006**, *1*, 824.

(22) Cody, J.; Mandal, S.; Yang, L.; Fahrni, C. J. *J. Am. Chem. Soc.* **2008**, *130*, 13023.

(23) Verma, M.; Chaudhry, A. F.; Fahrni, C. J. *Org. Biomol. Chem.* **2009**, *7*, 1536.

(24) Verma, M.; Chaudhry, A. F.; Morgan, M. T.; Fahrni, C. J. *Org. Biomol. Chem.* **2010**, *8*, 363.

(25) Chaudhry, A. F.; Verma, M.; Morgan, M. T.; Henary, M. M.; Siegel, N.; Hales, J. M.; Perry, J. W.; Fahrni, C. J. *J. Am. Chem. Soc.* **2010**, *132*, 737.

(26) Chaudhry, A. F.; Mandal, S.; Hardcastle, K. I.; Fahrni, C. J. *Chem. Sci.* **2011**, *2*, 1016.

CHAPTER 2

SETTING THE STAGE: PHOTOINDUCED ELECTRON TRANSFER, ELECTRONIC TUNING, AND CONTRAST-OPTIMIZED FLUORESCENT PROBES FOR COPPER(I) IN NONAQUEOUS SOLUTION

2.1. Introduction

CTAP-1, the first fluorescence turn-on probe for aqueous Cu(I), was introduced by Fahrni and coworkers in 2005. This probe operates on a photoinduced electron transfer (PET)-based fluorescence switching mechanism and gives a 4.6-fold enhancement in fluorescence emission upon analyte binding.[1] While preliminary cellular imaging with CTAP-1 yielded results qualitatively consistent the subcellular distribution of Cu(I) by x-ray fluorescence microscopy,[1] a significantly larger fluorescence enhancement factor, preferably at least 50, would be desirable for biological imaging applications. In addition to improving the overall signal-to-noise ratio, a higher fluorescence enhancement factor, or contrast ratio, also reduces the likelihood that any local accumulation of the free probe will be misinterpreted as the presence of the analyte. With the ultimate goal of achieving a high contrast fluorescence turn-on response to aqueous Cu(I), Fahrni *et al.* conducted a series of pilot investigations on contrast optimization of PET-based fluorescence turn-on probes utilizing a tunable 1,3,5-triarylpyrazoline fluorophore platform.[2,3,4,5] These studies, which were conducted in nonaqueous solution to avoid interference from aggregation effects, culminated in the development of methanolic Cu(I)-probes with contrast ratios up to 50 and revealed the primary factor hindering further improvement, which turned out to involve the

coordination mode to Cu(I) rather than the inherent properties of the fluorophore.[4,5] While the author was involved in the latter two works, this was primarily in optimizing the synthesis of intermediates to allow preparation of probe libraries. Nevertheless, these publications constitute an essential backdrop for the development of the aqueous Cu(I) probes presented in subsequent chapters, and are therefore described in a fair degree of detail. Although this chapter is to serve primarily as a literature review, the author's synthetic work is described in the experimental section.

2.2. Fluorescence turn-on probes based on photoinduced electron transfer (PET)

As mentioned in Chapter 1, the design of fluorescence turn-on probes for copper(I) is complicated by the propensity of this cation to act as a fluorescence quencher. Since direct binding of Cu(I) to a fluorophore typically results in a fluorescence turn-off response, the design of a fluorescence turn-on probe for this cation depends on coupling the output of the fluorophore to the interaction of Cu(I) with a remote binding site. This can be achieved using photoinduced electron transfer (PET) as a fluorescence quenching mechanism, which is the design strategy of CTAP-1.[1] The process of fluorescence, fluorescence quenching by PET, and the utilization of PET to design fluorescence turn-on probes are described below.

2.2.1. The Process of fluorescence and quenching by PET

The process of fluorescence begins with absorption of a photon by the fluorophore in its ground state (S_0) to produce an excited electronic state (normally the first singlet excited state S_1). In simplified terms, the excitation can be viewed as promotion of an electron from the highest occupied molecular orbital (HOMO) to the lowest unoccupied molecular orbital (LUMO) of the fluorophore. The actual electronic transition is extremely rapid, initially producing S_1 in the geometry preferred by S_0 (Franck-Condon state, FC). After geometrical relaxation and energy loss by vibrational

cooling, the fluorophore returns to the ground electronic state S_0 by emission of a photon of lower energy (Figure 2.1).[6] As S_0 is initially produced in the preferred geometry of S_1, a second vibrational cooling also occurs, yielding a Stokes shift, or energy difference between excitation and emission maxima, equal to the combined vibrational energy losses.

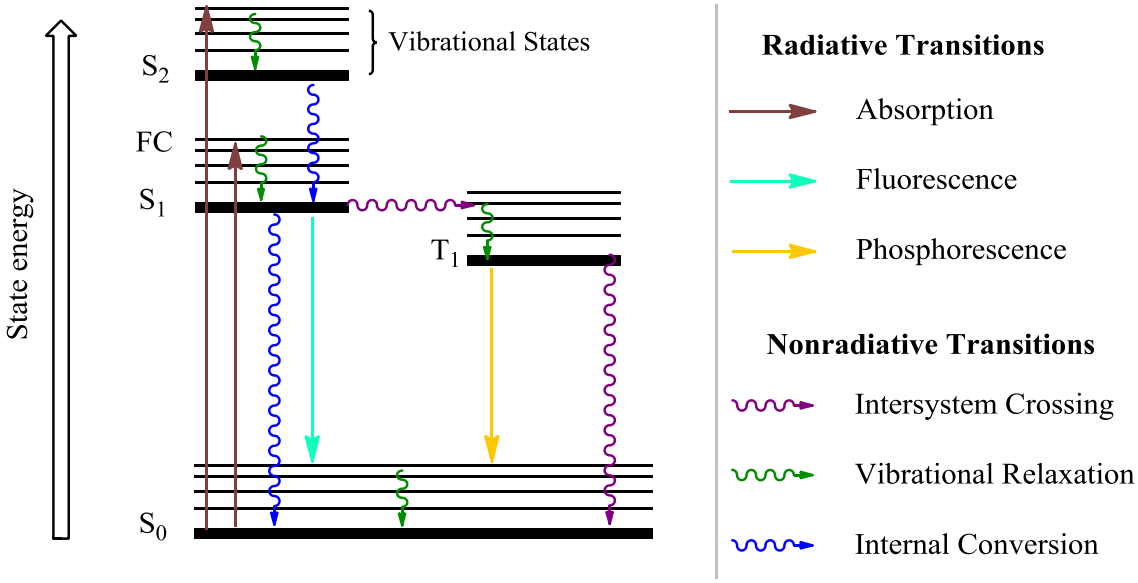

Figure 2.1: Generalized Jablonski diagram for organic fluorophores

If an electron donor, a separate moiety capable of facile one-electron oxidation, is coupled to the fluorophore, then electron transfer can occur from the donor to the excited fluorophore, filling the vacancy in the fluorophore HOMO and blocking the normal radiative transition to S_0. The ion pair resulting from electron transfer usually undergoes rapid nonradiative charge recombination to return the original ground state of the system. This process is known as acceptor-excited photoinduced electron transfer, and the net

result is efficient nonradiative conversion of S_1 back to S_0, resulting in quenching of fluorescence (Figure 2.2).[6]

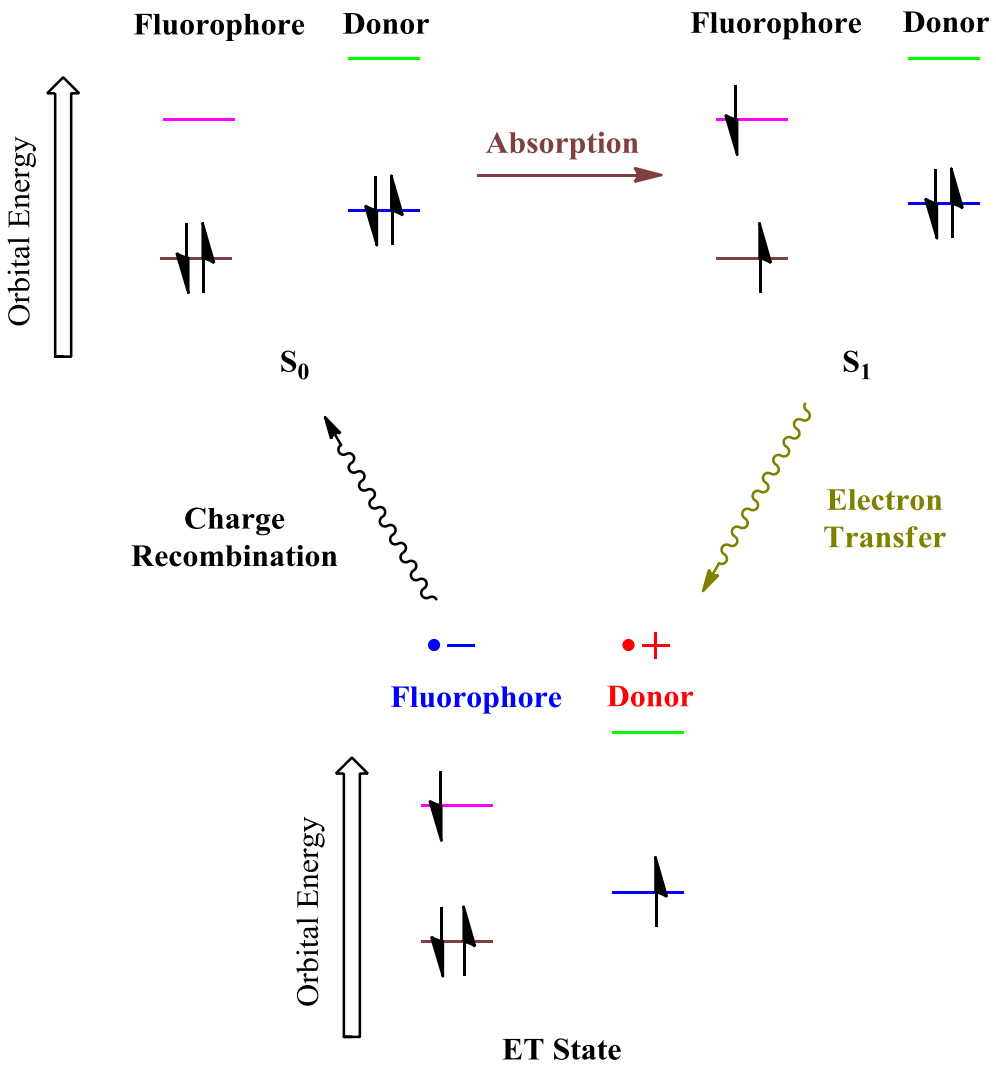

Figure 2.2: Simplified diagram of the PET process

2.2.2. A Fluorescence turn-on response by inhibition of a fluorescence quenching pathway

If the electron donor in the system described above includes an appropriately designed cation binding site, then binding of the cation can impede oxidation of the electron donor. The result is a reduced rate of PET and a corresponding increase in fluorescence emission: a fluorescence turn-on response. Due to the indirect coupling between the cation and the fluorophore, this approach can be effective even for cations that normally behave as fluorescence quenchers provided that the cation-mediated quenching mechanism depends on short-range interactions.

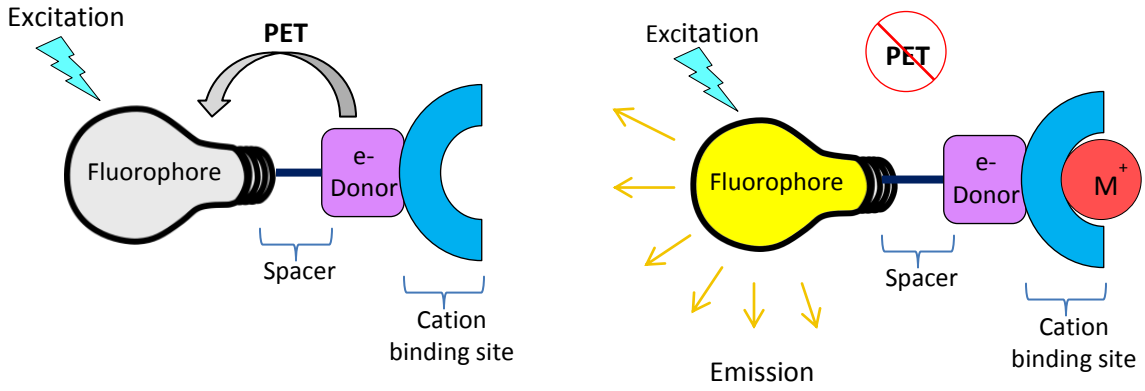

Figure 2.3: Conceptual diagram of a PET-based fluorescence turn-on probe

2.2.3. Relationships between PET driving force, PET rate, and fluorescence contrast ratio

2.2.3.1. The Relationship between PET rate constants and fluorescence contrast ratio

For a PET-based fluorescence turn-on probe to achieve a high contrast ratio, the fluorescence of the free probe must be quenched as efficiently as possible. At the same time, binding of the analyte must suppress PET quenching to the extent that the analyte-

bound probe recovers a significant fraction of the intrinsic fluorescence quantum yield of the free fluorophore. Assuming that binding of the analyte to the donor has no significant effect on the absorption spectrum of the fluorophore, the contrast ratio (fluorescence enhancement factor) upon analyte binding is the ratio of the fluorescence quantum yield of the analyte-bound probe to that of the free probe. The relevant quantum yields can be calculated as described below.[2] The quantum yield of the fluorophore in the absence of PET (Φ_f^0) is given by Equation 2.1, where k_r is the rate constant of radiative deactivation of the excited state (fluorescence emission) and k_{nr} is the sum of the rate constants of all nonradiative deactivation pathways.

$$\Phi_f^0 = \frac{k_r}{k_r + k_{nr}} \qquad (2.1)$$

If PET serves as an additional nonradiative deactivation pathway, then the fluorescence quantum yield (Φ_f) is given by Equation 2.2, where $k_0 = k_r + k_{nr} = 1/\tau_f$, τ_f is the fluorescence lifetime in the absence of PET, and k_{et} is the rate constant of PET.

$$\Phi_f = \frac{\Phi_f^0 k_0}{k_0 + k_{et}} \qquad (2.2)$$

Accordingly, the fluorescence enhancement factor (f_e) upon analyte binding is given by Equation 2.3, where Φ_f' is the fluorescence quantum yield in the presence of analyte and k_{et}' is the rate constant of PET in the presence of the analyte.

$$f_e = \frac{\Phi_f'}{\Phi_f} = \frac{k_0 + k_{et}}{k_0 + k_{et}'} \qquad (2.3)$$

2.2.3.2. Dependence of the PET rate constant on the PET driving force

For systems such as 1,3,5-triarylpyrazolines where the donor is separated from the fluorophore by a saturated carbon spacer, the electronic coupling between the two units is relatively small and the electron transfer can be modeled as a nonadiabatic reaction according to semiclassical Marcus theory.[7,8] The relationship between electron transfer rate constant and electron transfer driving force (ΔG_{et}) is then given by Equation 2.4, where h is Planck's constant, k_B is Boltzmann's constant, T is the absolute temperature, λ is the reorganization energy, and H_{DA} is the electronic coupling between the state preceding electron transfer and the electron transfer state.

$$k_{\mathrm{et}} = \left(\frac{4\pi^3}{\mathrm{h}^2 \lambda k_B T}\right)^{1/2} {H_{DA}}^2 \exp\left[-\frac{(\Delta G_{et} + \lambda)^2}{4\lambda k_B T}\right] \qquad (2.4)$$

According to Equation 2.4, the rate of electron transfer increases with increasing driving force (more negative ΔG_{et}), provided that $-\Delta G_{et}$ is less than the reorganization energy λ. At larger values of $-\Delta G_{et}$, the electron transfer rate actually decreases with increasing driving force. This regime, known as the Marcus inverted region, is not normally reached by systems such as 1,3,5-triarylpyrazolines utilized in fluorescent probe design,[2] so an increase in $-\Delta G_{et}$ results in a reduced fluorescence quantum yield via an increased k_{et}.

2.2.3.3. Dependence of the PET driving force on donor and fluorophore parameters

The value of ΔG_{et} can be estimated from physical parameters of the fluorophore and donor according to the Rehm-Weller equation[9] (Eq. 2.5), where $E(D^+/D)$ is the reduction potential of the oxidized donor, $E(A/A^-)$ is the ground state reduction potential of the fluorophore, ΔE_{00} is the excited state energy (zero-zero transition energy) for the S_0 to S_1 transition of the fluorophore, and w_p is a Coulombic stabilization term

corresponding to the energy released (negative value) when the ions generated by electron transfer are brought from infinite separation to their actual spatial separation in the product ion pair or zwitterion. The magnitude of w_p is small compared to the other terms in polar solvents due to dielectric screening.

$$\Delta G_{et} = E(\mathrm{D}^+/\mathrm{D}) - E(\mathrm{A}/\mathrm{A}^-) - \Delta E_{00} + w_p \qquad (2.5)$$

It is important to note that the $E(D^+/D)$ term, also known as the donor potential, is written as a reduction potential although the electron transfer involves oxidation of the donor. Therefore, a more positive value of $E(D^+/D)$ corresponds to weaker driving force for electron transfer (more positive ΔG_{et}), while a more positive value of $E(A/A^-)$ or ΔE_{00} corresponds to a stronger PET driving force.

2.2.4. Triarylpyrazolines as tunable fluorophore platforms for PET based fluorescence turn-on probes

Based on Equation 2.5, it is possible to adjust the driving force for electron transfer, and hence the quantum yield of the fluorophore in the absence and presence of analyte, by manipulating the fluorophore parameters $E(A/A^-)$ and ΔE_{00}. By careful tuning of these parameters, it is possible to maximize the ratio of the two quantum yields and thus the contrast ratio. Compared to other common fluorophore platforms, 1,3,5-triaryl-Δ^2-pyrazolines are advantageous for such tuning because $E(A/A^-)$ and ΔE_{00} can be varied selectively and in a highly predictable manner: Electron-withdrawing substituents on the 3-aryl ring strongly increase $E(A/A^-)$, while electron-withdrawing substituents on the 1-aryl ring primarily increase ΔE_{00}.[3] The reason for this behavior is apparent from the frontier molecular orbital structure of the parent 1,3,5-triphenylpyrazoline (Figure 2.4): The HOMO is shifted toward the 1-aryl ring, while the LUMO has much greater density on the 3-aryl ring. An electronegative substituent on the 1-aryl ring will lower the energy

of the HOMO with little effect on the LUMO, thus increasing the HOMO-LUMO gap and therefore the excited state energy. Analogous substitution of the 3-aryl ring will strongly lower the LUMO energy while also lowering the HOMO energy to a lesser extent, thus greatly facilitating ground state reduction while slightly reducing the excited state energy.

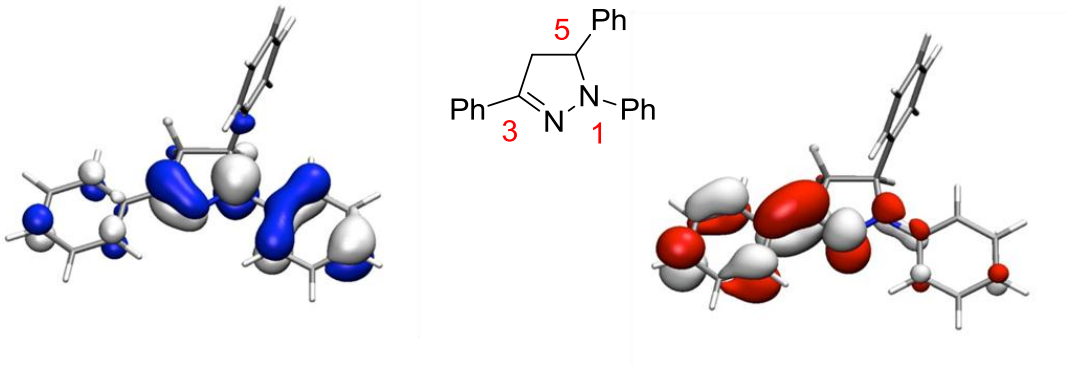

HOMO LUMO

Figure 2.4: Frontier molecular orbitals of 1,3,5-triphenyl-Δ^2-pyrazoline
Calculations carried out by Dr. Christoph Fahrni

In addition to the tunability achievable through functionalization of the 1- and 3-aryl rings, the 5-aryl ring, which is not part of the fluorophore π-system, can be functionalized with an electron-donating group to provide a built-in PET donor for a fluorescence turn-on probe. This design strategy is exemplified by CTAP-1,[1] the first fluorescence turn-on probe for aqueous Cu^+ (Figure 2.4).

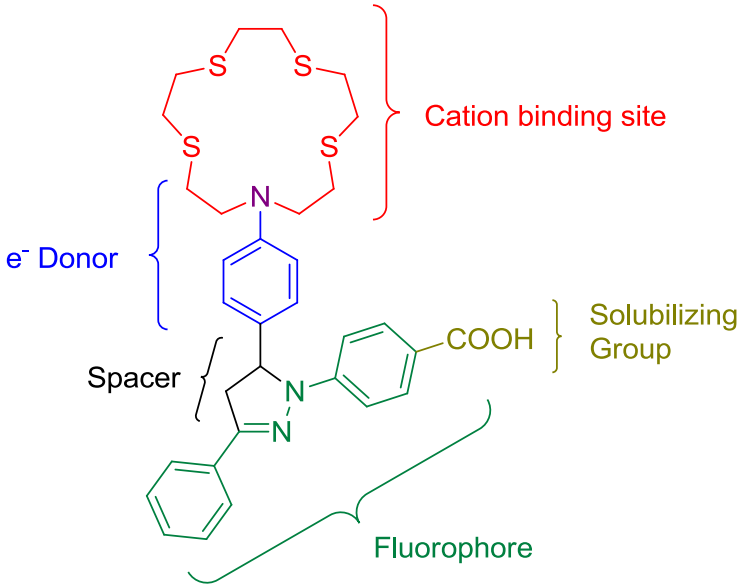

Figure 2.5: The Anatomy of CTAP-1

As noted in the introduction, CTAP-1, which was not systematically optimized by electronic tuning, gave a contrast ratio of only 4.6 upon saturation with Cu(I). To pave the way for higher contrast PET-based Cu(I) probes, Cody et al. conducted a detailed experimental and computational investigation into maximizing the fluorescence contrast ratio by tuning the fluorophore parameters $E(A/A^-)$ and ΔE_{00}.[2] Using a series of 1,3,5-triarylpyrazolines bearing an N,N-dimethylaniline moiety as a pH sensitive PET donor, the values of H_{DA} and λ were estimated by fitting experimentally derived electron transfer driving forces and rate constants to Equation 2.4 (See Section 2.2.3.2). Based on the fitted values (18 cm^{-1} and 0.54 eV, respectively) and a representative k_0 value of 2.8 x 10^8 s^{-1}, an expression was derived for the fluorescence enhancement factor (f_e) as a function of the switching potential $\Delta E(D^+/D)$, which is the change in donor potential upon analyte binding, and the initial electron transfer driving force before binding of the analyte ($-\Delta G^0_{et}$). A contour plot of the theoretical contrast ratio versus $\Delta E(D^+/D)$ and $-\Delta G^0_{et}$ is shown below (Figure 2.5).

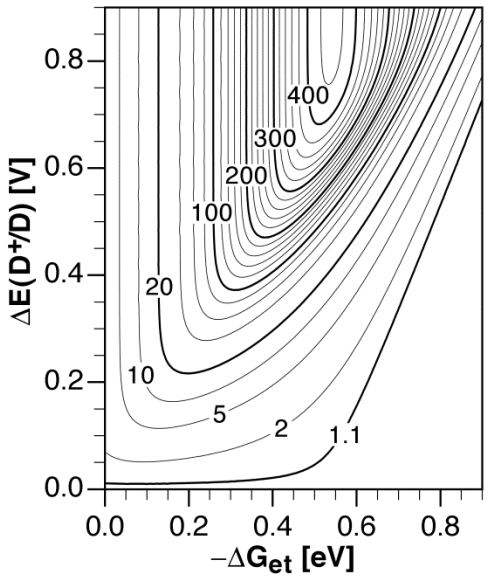

Figure 2.6: Predicted contrast ratio as a function of PET driving force and switching potential for 1,3,5-triarylpyrazolines. Reprinted with permission from Cody, J.; Mandal, S.; Yang, L.; Fahrni, C. J., *J. Am. Chem. Soc.* **2008,** *130* (39), 13023-13032. © 2008 American Chemical Society.

As shown in Figure 2.5, that the maximum possible contrast ratio depends on the switching potential $\Delta E(D^+/D)$, a property governed by the design of the donor and its cation binding site. Furthermore, the initial electron transfer driving force $-\Delta G^0_{et}$ must be tuned within a narrow range to achieve the maximum contrast ratio available for a given switching potential. Protonation of the dimethylamino moiety of the pyrazolines should result in a very large increase in donor potential, and the maximum fluorescence enhancement factor observed in this study (400) corresponded to the derivative with the largest estimated $-\Delta G^0_{et}$ value (0.56 eV, approximately equal to the estimated reorganization energy). The observed maximum fluorescence enhancement is consistent with the relationship plotted in Figure 2.5, which predicts a maximum fluorescence enhancement factor of just over 400.

2.3. Electronically tuned Cu(I) selective fluorescent probes

Tuning the PET driving force is expected to be more critical for achieving a high-contrast response to a soft cation such as Cu(I) than for a strong, hard Lewis acid such as the proton. In contrast to protonation, which renders the arylamine PET donor essentially inert towards oxidation, Cu(I)-coordination may give only a small increase in $E(D^+/D)$. In this scenario, an insufficient initial PET driving force will give a low contrast ratio due to incomplete fluorescence quenching of the free probe, and excessive PET driving force will also give a low contrast ratio due to residual fluorescence quenching of the Cu(I)-bound form. Therefore, a high contrast ratio can only be achieved if the initial PET driving force is tuned within a narrow range. For example, according to Figure 2.5, an increase in $E(D^+/D)$ of 0.4 eV upon analyte binding can give a fluorescence enhancement of over 100-fold, but only if $-\Delta G^0_{et}$ lies between 0.24 and 0.40 eV. The low contrast ratio observed for CTAP-1 is presumably due in part to an insufficient PET driving force, because the fluorescence quantum yield of the free probe is relatively high (3%).

2.3.1. Probe design

2.3.1.1. Ligand design

In addition to the low PET driving force as described above, another limiting factor for the contrast ratio of CTAP-1 may be the design of the Cu(I) binding site. The CTAP-1 ligand (Figure 2.6, structure **2.1**) contains five donor atoms, but Cu(I) usually exhibits a maximum coordination number of four, even in macrocyclic ligands containing more than four donor atoms.[10] It is therefore likely that the CTAP-1-Cu(I) is actually a fluxional 4-coordinate complex, and the predominant species in solution may not have a direct Cu-N bond. To enforce coordination of the arylamine nitrogen to Cu(I), a macrocyclic arylamine-thioether ligand with only four donor atoms was devised (structure **2.2**). In addition to the reduction in donor atom number, the linkers between

adjacent donor atoms were lengthened from two CH_2 units to three. This modification should provide a sufficient macrocyclic cavity size for Cu(I), which is too large to fit within a similar 12 or 13 membered macrocycle.[11] Furthermore, the switch from 5-membered to 6-membered chelate rings is expected to increase the Cu(II)/Cu(I) reduction potential of the ligand-copper complex[12] and thus the selectivity for Cu(I).

2.1
(CTAP-1 ligand)

2.2

Figure 2.7: Structural comparison of the CTAP-1 ligand and revised ligand **2.2**

2.3.1.2. Fluorophore design

Based on the previous electronic tuning study on triarylpyrazoline-based pH probes,[2] the optimum value of the initial PET driving force ($-\Delta G^0_{et}$) for 1,3,5-triarylpyrazoline-based Cu(I) probes should be greater than zero and presumably less than 0.56 eV (the optimum value for the proton probes). Based on a previous study of polyfluorinated 1,3,5-triarylpyrazolines[3] and the measured donor potential of free ligand **2.2** (0.45 eV), it was determined that 3,5-difluoro-substitution of the 3-aryl ring would provide $-\Delta G^0_{et}$ values ranging from 0.03 to 0.56 eV as the 1-aryl ring is varied stepwise from phenyl to pentafluorophenyl.[4] The probe structures chosen for synthesis (**2.3a-f**) are shown in Figure 2.7. For more direct comparison to the previously described proton

probes,[2] stuctures **2.4b-f** were also included.[5] Structure **2.4a** was omitted due to the anomalously low quantum yield previously observed for the parent triarylpyrazoline bearing an unsubstituted 5-aryl ring.[2]

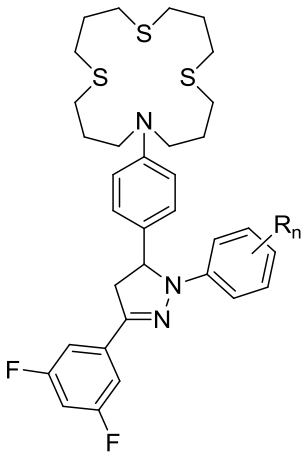

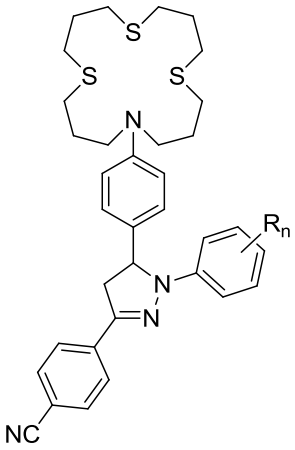

Cmpd.	R_n
2.3a	H
2.3b	3-F
2.3c	2,5-F_2
2.3d	2,3,5-F_3
2.3e	2,3,5,6-F_4
2.3f	2,3,4,5,6-F_5

Cmpd.	R_n
2.4a	H (not prepared)
2.4b	3-F
2.4c	2,5-F_2
2.4d	2,3,5-F_3
2.4e	2,3,5,6-F_4
2.4f	2,3,4,5,6-F_5

Figure 2.8: Structures of Cu(I) probes **2.3a-f** and **2.4b-f**

2.3.2. Synthesis

Ligand **2.2** was prepared by macrocyclization of bis(3-mercaptopropyl) sulfide[13] (**2.5**) with N,N-bis(3-iodopropyl)aniline[14] (**2.6**) by syringe pump addition of both components to a large volume of solvent in the presence of base (Scheme 2.1). Although the use of cesium carbonate in DMF[15] has become the standard procedure for the preparation of macrocyclic polythioethers, we found that use of the liquid strong base

1,1,3,3-tetramethylguanidine (TMG) in acetonitrile greatly facilitated workup at the expense of only a small reduction in yield when the reaction was conducted on a multigram scale.

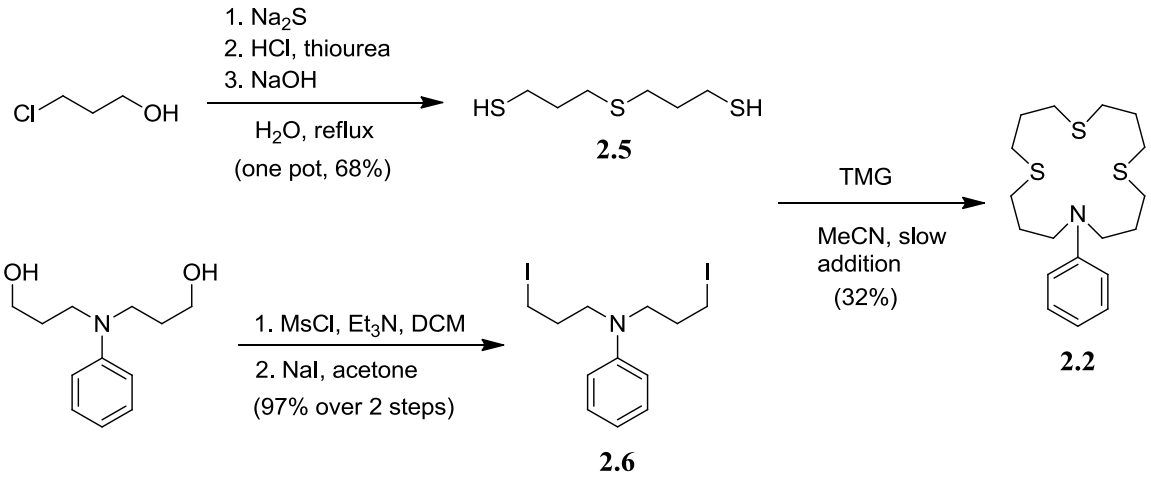

Scheme 2.1: Synthesis of N-arylthiazacrown ligand **2.2**

Triarylpyrazolines analogous to **2.3** and **2.4** had been previously prepared via condensation of arylhydrazines with the appropriately substituted chalcone derivatives, which in turn were prepared by condensation of aryl aldehydes with substituted acetophenones.[1,2,3] By this methodology, the triarylpyrazoline 1-, 3-, and 5-aryl rings are derived from the arylhydrazine, the substituted acetophenone, and the aryl aldehyde, respectively. Accordingly, ligand **2.2** was subjected to Vilsmeier formylation to give aldehyde **2.7**, which could then be condensed with 3,5-difluoroacetophenone or 4-cyanophenone to give the respective chalcone derivatives **2.8** (Scheme 2.2) and **2.9** (Not shown).

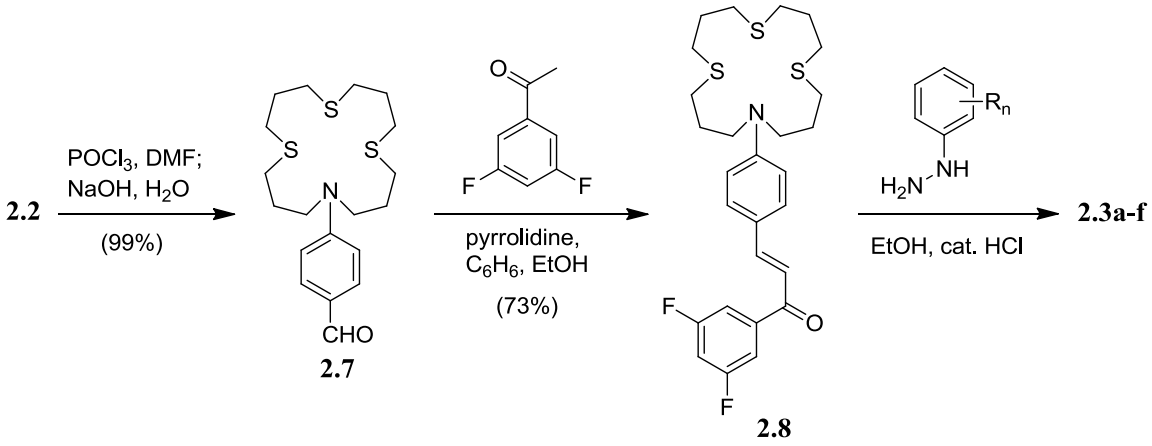

Scheme 2.2: Synthesis of probes **2.3a-f**

Preparation of chalcone **2.8** was initially problematic. The standard conditions previously employed to prepare related chalcones[1,2] (piperidine, ethanol, reflux) were unsuccessful with 3,5-difluoroacetophenone due to nucleophilic substitution of the aryl fluoride by piperidine.[3] The conditions previously utilized to prepare chalcones from fluorinated acetophenones[3] (NaOH, ethanol, rt) were also unsatisfactory, giving an impure product in only 21% yield (experiments conducted by Dr. Manjusha Verma). The author then found that the yield and purity of the product can be greatly improved by using pyrrolidine as the condensation catalyst, conducting the reaction at only 40°C to avoid nucleophilic aromatic substitution, and adjusting the solvent composition to promote complete dissolution of the starting materials while allowing the product to crystallize during the course of the reaction. This *in situ* crystallization should improve the yield by protecting the desired product from further reactions. Under these conditions, pure **2.8** was obtained in 73% yield by simple filtration from the reaction mixture.

The final products **2.3a-f**[4] and **2.4b-f**[5] were prepared by Dr. Manjusha Verma and Aneese Chaudhry by condensation of chalcones **2.8** and **2.9**, respectively, with the appropriate arylhydrazines under acid catalysis.

2.3.3. Contrast optimization

The steady state photophysical characteristics of probes **2.3a-f** and **2.4b-f** are given in Table 2.1. Since the probes were not intended for direct biological application, they were characterized in methanol rather than in aqueous solution to avoid interference from aggregation effects. The values reported of ΔG^0_{et} were estimated using excited-state energies determined in methanol and potentials $E(D^+/D)$ and $E(A/A^-)$ measured in acetonitrile, which has a similar dielectric constant but a larger accessible potential range compared to methanol.[4]

Table 2.1: Photophysical properties of probes **2.3a-f** and **2.4b-f**

Cmpd.	Abs. λ_{max}/nm	Em. λ_{max}/nm	ΔE_{00}/eV[a]	ΔG^0_{et}/eV	Φ_f Free	Φ_f Cu(I)[b]	f_e[c]
2.3a	371	476	2.97	-0.03	0.058	0.20	3
2.3b	366	461	3.04	-0.13	0.029	0.19	7
2.3c	355	451	3.12	-0.23	0.0084	0.12	14
2.3d	350	436	3.19	-0.34	0.0014	0.07	50
2.3e	330	420	3.35	-0.52	<0.001	0.024	n.d.
2.3f	323	423	3.38	-0.59	<0.001	0.0063	n.d.
2.4b	394	487	2.85	-0.22	0.0072	0.15	21
2.4c	381	480	2.92	-0.31	0.0033	0.095	29
2.4d	373	464	3.00	-0.39	0.0024	0.048	20
2.4e	356	445	3.13	-0.47	0.0010	0.020	20
2.4f	350	448	3.15	-0.54	<0.001	0.020	n.d.

[a] Estimated as the mean of the absorption and emission maxima on an energy scale. [b] Probes were saturated with Cu(I) provided as $Cu(MeCN)_4PF_6$. [c] Fluorescence enhancement factor (contrast ratio) given as the ratio of the fluorescence quantum yield of the Cu(I) saturated probe to that of the free probe. Data acquired by Aneese Chaudhry.

For both probe series, the absorption and emission maxima shift to shorter wavelengths with increasing fluorination of the 1-aryl ring, corresponding to a stepwise increase in ΔE_{00} from 2.97 to 3.38 eV for **2.3a-f** and 2.85 to 3.15 eV for **2.4b-f**. The overall PET driving force increases accordingly (ΔG^0_{et} becomes more negative), and the fluorescence quantum yields decrease for both the free and Cu(I)-saturated probes. The decline is more rapid for the free probes than for their Cu(I) complexes, resulting in maximum contrast at intermediate values of $-\Delta G^0_{et}$. The optimum contrast ratios achieved with the two probe series are 50 and 29 for derivatives **2.3d** and **2.4c**, respectively. These dramatic improvements over the contrast ratio of 4.6 observed for CTAP-1 come at the expense of relatively minor reductions in fluorescence quantum yield (0.070 for **2.3d** and 0.095 **2.4c** vs. 0.15 for CTAP-1). Notably, the less quenched derivative **2.4b** achieves a contrast ratio of 21 with the same final quantum yield as CTAP-1, demonstrating a substantial improvement in performance beyond that due to electronic tuning alone. The ligand design modification described in Section 2.3.1.1 was intended to produce such an effect, although it is possible that the observed improvement is actually due to the change of solvent or an increase in the intrinsic fluorophore quantum yield.

2.3.4. Incomplete fluorescence recovery due to ternary complex formation

2.3.4.1. Degree of fluorescence recovery versus the unquenched fluorophore

Although the contrast ratios of probes **2.3d**, **2.4b**, and **2.4c** represent a marked improvement over CTAP-1, the fluorescence quantum yields of the Cu(I) saturated probes remain relatively low. By contrast, acidification of the probe solutions in the absence of Cu(I) increased the quantum yields to around 0.5 (Table 2.2), a typical value for 1,3,5-triarylpyrazolines in methanolic solution.[16] Protonation presumably occurs on the nitrogen of the N,N-dialkylaniline PET donor, resulting in complete inhibition of PET

as previously observed.[2] Furthermore, the emission maxima were identical for the free, Cu(I)-bound, and protonated probes, indicating that the site of protonation is indeed the arylamine moiety and not the pyrazoline ring itself. Assuming the fluorescence quantum yield under acidic conditions represents the intrinsic quantum yield of the isolated triarylpyrazoline fluorophore in methanolic solution, the degree of fluorescence recovery upon Cu(I)-coordination can be determined as the ratio of the quantum yield of the Cu(I) saturated probe to that of the protonated probe. These values are given in Table 2.2.

Table 2.2: Fluorescence recoveries upon Cu(I)-saturation

Compound	Φ_f Cu(I)-sat.	Φ_f Acidic[a]	Fluorescence Recovery[b]	f_e Cu(I) sat.	f_e Acidic[c]
2.3d	0.070	0.47	15%	50	335
2.4b	0.15	0.53	28%	21	74
2.4c	0.095	0.54	18%	29	164

[a] Fluorescence quantum yield in the presence of 180 mM CF_3COOH. [b] Φ_f (Cu(I)-sat.)/Φ_f(Acidic). [c] Φ_f(Acidic)/ Φ_f(free). Primary data acquired by Aneese Chaudhry.

From the data in Table 2.2, it is clear that the contrast-optimized probes recover only a small fraction of the intrinsic fluorophore quantum yield upon coordination to Cu(I). This low fluorescence recovery limits not only the brightness but also the contrast of the Cu(I) probes. This is shown by the much higher contrast ratios obtained by protonation than for Cu(I)-coordination, especially for **2.3d**. As mentioned previously, a lower contrast ratio might be expected for coordination to the soft Cu(I) cation than for protonation due to weaker inhibition of PET. This would also manifest as a lower fluorescence quantum yield at the value of ΔG^0_{et} that gives the highest contrast ratio. However, even if the initial PET driving force ($-\Delta G^0_{et}$) is set significantly below the value required for maximum contrast (probe **2.4b**), the fluorescence quantum yield of the Cu(I)-saturated probe is still less than a third of that available from the triarylpyrazoline

fluorophore. Therefore, it appears that an additional factor is also hindering fluorescence recovery.

2.3.4.2. Potential causes of incomplete fluorescence recovery

Although Cu(I) may quench fluorescence by direct interaction with a fluorophore,[17,18] the low fluorescence recoveries observed for probe series **2.3** and **2.4** cannot be explained by this effect: Upon titration of a 6.5 μM solution of probe **2.3d** with Cu(I), the fluorescence intensity increased linearly up to 1 molar equivalent (consistent with high affinity binding) but then leveled off to an essentially constant value up to 2 molar equivalents, indicating that excess Cu(I) has no significant quenching effect at low micromolar concentrations.

Another seemingly likely explanation for the low fluorescence recovery would be photoinduced electron transfer from the probe-bound Cu(I) center to give a Cu(II) complex, but previously observed electron self-exchange rate constants for Cu(I)/Cu(II) centers are usually less than 10^4 and never more than 10^6 M^{-1} s^{-1}.[19] Therefore, electron transfer from Cu(I) should be far too slow to compete with fluorescence emission, which occurs on a nanosecond timescale for 1,3,5-triarylpyrazolines. Indeed, time resolved fluorescence spectroscopy revealed a lifetime of 3.76 ns for **2.4b** in acidic solution (180 μM TFA), which corresponds to an excited state deactivation rate constant (k_0) of 2.7 x 10^8 s^{-1} in the absence of PET.

When applied to Cu(I)-saturated **2.4b**, the above technique yielded unexpected results. As shown in Figure 2.9, the decay profile of **2.4b**-H^+ is monoexponential, which is indicated by its linearity when plotted on a logarithmic y-axis (blue trace). This is the expected behavior for a homogeneous population of fluorophores with a single radiative deactivation pathway. By contrast, **2.4b-Cu(I)** gave a multiexponential fluorescence decay profile, which is visible in Figure 2.9 as an obvious curvature in its fluorescence decay profile (red trace). The decay profile of **2.4b**-Cu(I) fits best to a triexponential

model with components of 84 ps (35%), 0.77 ns (36%) and 3.23 ns (29%) implying the presence of three distinct species in comparable abundance that do not equilibrate on the timescale of fluorescence emission (Figure 2.9).

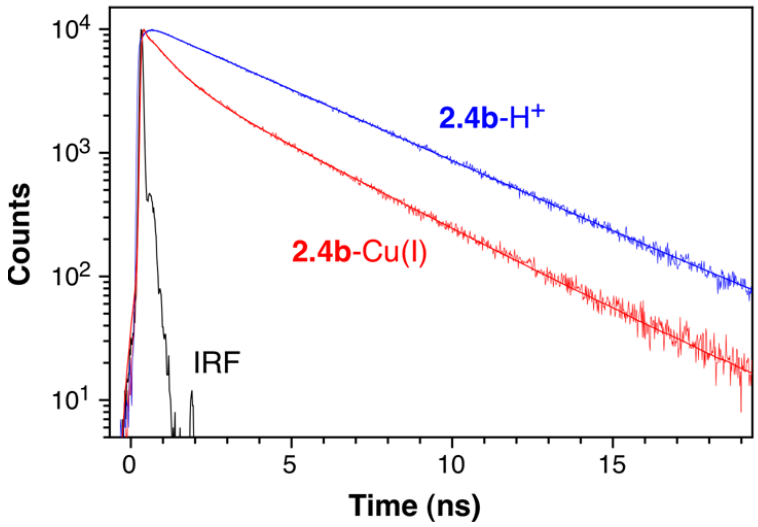

Figure 2.9: Fluorescence decay profiles of **2.4b** in the presence of 10μM Cu(I) or 180 mM TFA. Data acquired by Aneese Chaudhry. Adapted with permission from reference[5] © 2010 American Chemical Society.

In contrast to the fluorescence decay profile, the 2D fluorescence excitation-emission profile[5] of **2.4b**-Cu(I) was consistent with a homogeneous fluorophore population and very similar to that of **2.4b**-H^+, implying that the nature of the fluorophore and the radiative deactivation pathway are essentially identical for all emissive species present under both conditions. Furthermore, pump-probe transient absorption spectroscopy experiments[5] identified a very similar ^{1}ET state for **2.4b** and **2.4b**-Cu(I) and a similar radiative ^{1}CT (charge transfer) state for **2.4b**-Cu(I) and **2.4b**-H^+, but no photoproducts could be detected for **2.4b**-Cu(I) that did not have a counterpart in either free **2.4b** or **2.4b**-H^+, thus providing no evidence for electron transfer from the Cu(I) center. Taken together, these data indicate that **2.4b**-H^+ and all species of **2.4b**-

Cu(I) have effectively the same fluorophore, so the structural differences responsible for the distinct fluorescence lifetimes of the three apparent **2.4b**-Cu(I) species probably lie in the coordination mode of the thiazacrown ligand to Cu(I).

2.3.4.3. Evidence for ternary complex formation

Distinct coordination species would be expected to give different NMR chemical shifts for the protons of the ligand, so the behavior of the ligand **2.2**-Cu(I) was investigated by ^{1}H NMR in deuterated methanol.[5] Titration of ligand **2.2** with the Cu(I) salt $Cu(CH_3CN)_4PF_6$ gave a single set of sharp resonances which steadily increased in chemical shift, reaching saturation at 1 molar equivalent of Cu(I). This indicates that the coordination equilibria of ligand **2.2** at room temperature are much faster than the NMR timescale. Cooling the solution to -40°C failed to prevent rapid equilibration, but the aromatic ring protons *ortho* and *para* to the amine nitrogen showed a surprisingly large decrease in chemical shift with decreasing temperature. By contrast, the chemical shifts of the protons alpha to sulfur in the ligand backbone remained essentially constant (Figure 2.10).

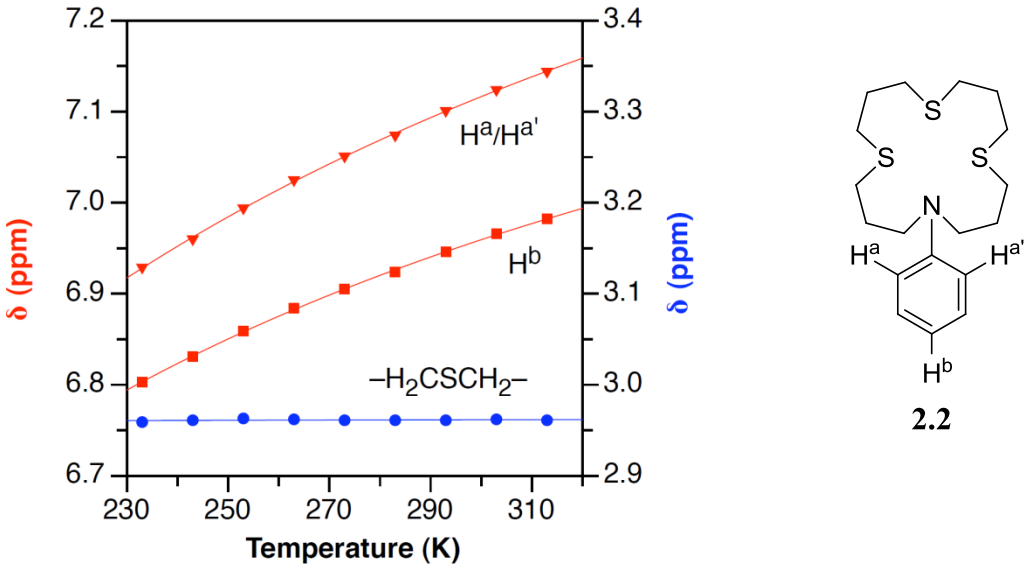

Figure 2.10: Temperature dependence of NMR chemical shifts for **2.2**-Cu(I). Data acquired by C. J. Fahrni. Adapted with permission from reference[5] © 2010 American Chemical Society

All three protons $H^a/H^{a'}$ and H^b show increases in chemical shift for the Cu(I)-complex versus the free ligand, which is presumably due to a reduction in π-donation from the amine nitrogen into the aromatic ring upon coordination to Cu(I). Therefore, a decrease in chemical shift with decreasing temperature is consistent with an equilibrium involving an exothermic, entropically unfavorable conversion of a species with the expected tetradentate coordination mode of the thiazacrown to one or more species lacking a Cu-N bond. The most logical explanation for a loss of entropy upon Cu-N bond dissociation is that the released coordination site on Cu(I) is occupied by a solvent molecule (the counterion, PF_6^-, is usually non-coordinating).

In further support of a mechanism involving Cu-N bond dissociation and ternary complex formation, computational modeling identified steric clashes between the aromatic ring and ligand backbone in the energy minimized structure of [**2.2**-Cu(I)]$^+$ (Figure 2.11A) which could be relieved by coordination of a methanol molecule to the

Cu(I) center with cleavage of the Cu-N bond. Two energy-minimized ternary complex structures were found, one possessing a hydrogen bond from the methanol OH to the slightly pyramidalized thiazacrown nitrogen (Figure 2.11B) and the other with no hydrogen bond and a nearly trigonal planar geometry about the thiazacrown N. (Figure 2.11C). The predicted gas phase association enthalpies were -12.4 and -10.2 kcal/mol for B and C, respectively.

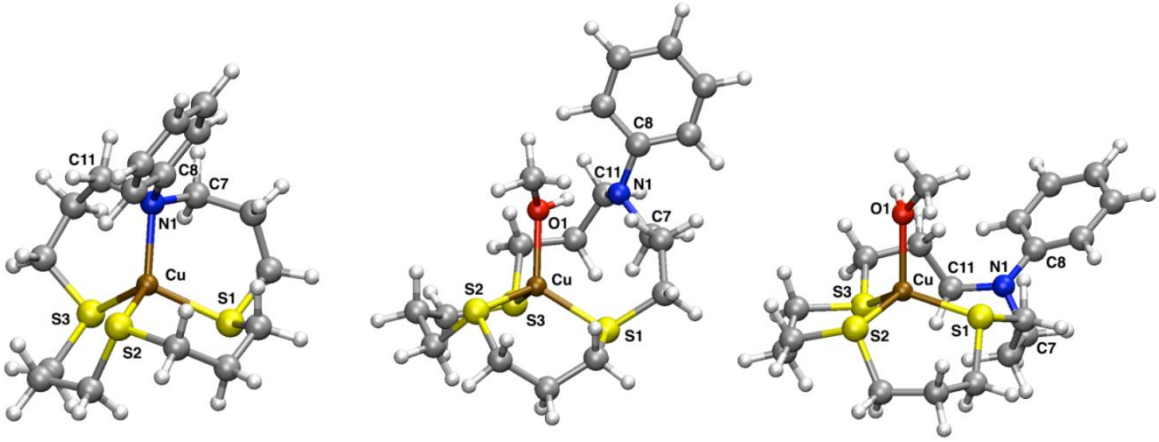

t,t,t-[**2.2**-Cu]$^+$ (A)

t,t-[**2.2**-Cu-MeOH]$^+$ (B)

c,t-[**2.2**-Cu-MeOH]$^+$ (C)

Figure 2.11: Computationally predicted structures of **2.2**-Cu(I) coordination species Geometries optimized at the B3LYP/6-31G(d) level of theory. Calculations carried out by C. J. Fahrni. See reference[5] supporting information for full details.

Although the above structures were computed in the gas phase, they are consistent with the three observed fluorescence lifetimes, presumably corresponding to the 3.23, 0.77, and 0.084 ns components for the binary complex, H-bonded ternary complex, and non-H-bonded ternary complex, respectively. The decreasing pyramidalization about N for the ternary complexes should correspond to an increase in π-donor strength and therefore a reduction in $E(D^+/D)$ compared to the binary complex. Thus, it appears that the major factor underlying the incomplete fluorescence recovery and resultant low

quantum yields of probe series **2.3** and **2.4** is sterically driven Cu-N bond dissociation and concomitant ternary complex formation with solvent molecules. In fact, if the speciation of **2.4b**-Cu(I) could be restricted exclusively to the binary complex presumably responsible for the 3.23 ns fluorescence decay component, the fluorescence quantum yield should increase more than three-fold from 0.15 to 0.46 based on the fluorescence quantum yield of 0.53 and lifetime of 3.76 ns observed for the protonated probe (assuming no difference in k_r).

2.4. Conclusions

The works summarized in this chapter proved that it is possible to obtain a high contrast (50-fold) fluorescence turn-on response to the redox-active Cu(I) cation using PET-based probes. By modifying the design of the copper binding site and also optimizing the fluorescence contrast ratio via electronic tuning, the fluorescence contrast can be increased by an order of magnitude relative to CTAP-1 at the expense of only a two-fold reduction in quantum yield (probe **2.3d**). Alternatively, the contrast can be improved nearly five-fold relative to CTAP-1 with no loss of fluorescence quantum yield (probe **2.4b**). Importantly, it was discovered that primary limiting factor for both the contrast ratio and quantum yield of the new generation of Cu(I) probes is not electron transfer from the Cu(I) center but rather Cu-N bond dissociation in the thiazacrown-Cu(I) complex and concomitant ternary complex formation with solvent molecules. This suggests that further substantial improvements in contrast ratio and quantum yield can be achieved by modifying the design of the arylamine-thioether Cu(I)-binding site to enforce direct coordination of Cu(I) to the arylamine nitrogen. The obvious caveat of these studies is that they were conducted in methanol, whereas Cu(I) probes must operate in aqueous solution for biological applications. Although the PET switching mechanism is certainly sensitive to solvent polarity, methanol is already a rather polar solvent, so the

operation of PET-based probes should not be fundamentally different in aqueous versus methanolic solution. Since both water and methanol are small, hydroxylic solvents with no other coordinating functional groups, a large difference in Cu(I)-coordination chemistry is also unlikely. For the improved probe design strategies described in this chapter to be implemented in aqueous solution, the most significant challenges that must be met are actually the inherent aggregation propensity and low solubility associated with structures presenting a large hydrophobic surface area, which includes both the triarylpyrazoline fluorophores and thioether-rich Cu(I) ligand of probe series **2.3** and **2.4**. These challenges are addressed in the following chapter.

2.5. Experimental section

The syntheses carried out by the author are described below. For other experimental details, see references.[4,5]

General

NMR: δ in ppm vs. $SiMe_4$ (^1H, ^{13}C) or CCl_3F (^{19}F). MS: EI (70eV), selected peaks, *m/z* with relative intensity in parentheses. IR: NaCl windows (neat or film from $CDCl_3$), KBr pellet (solids). TLC: 0.25 mm, Merck silica gel 60 F254. Spots were visualized under 254 nm illumination or with PMA stain (5% phosphomolybdic acid in ethanol).

Bis(3-mercaptopropyl)sulfide (**2.5**)

A mixture of 3-chloro-1-propanol (25 mL, 300 mmol) and $Na_2S{\cdot}9H_2O$ (35 g, 146 mmol) in 120 mL of 0.5% NaOH (*aq*) was refluxed for 12 h under nitrogen. The reaction mixture was cooled to 0 °C, and 37% HCl (*aq*) (100 mL, 1.2 mol) was added, followed by thiourea (34 g, 447 mmol). The mixture was refluxed under nitrogen for 2 days then cooled to 0 °C, and NaOH pellets (93 g, 2.3 mol) were added with rapid stirring. The mixture was refluxed under nitrogen for 4 h, poured over crushed ice, and acidified with

37% aq. HCl (100 mL). The product was extracted with *tert*-butyl methyl ether (3 x 120 mL), and the extract was dried with Na2SO4 and concentrated under reduced pressure to give the product as a colorless oil (21.3 g, 80%). ^{1}H NMR indicated the presence of a trace of 1,3-propanedithiol, and this was completely removed by heating the product to 150 °C for 45 min under a stream of nitrogen (purified yield 18.0 g, 68%). TLC R_f 0.41 (15:1 hexanes: EtOAc). IR (neat) 2929, 2845, 2549, 1435, 1344, 1295, 1251 cm^{-1}. ^{1}H NMR (CDCl3, 400 MHz) δ1.37 (t, J = 8.1 Hz, 2H), 1.88 (p, *J* = 7.0 Hz, 4H), 2.59–2.68 (m, 8H). ^{13}C NMR (CDCl3, 100 MHz) δ23.2, 30.0, 33.0. MS *m/z* 182 ([M^{+}], 100), 107 (65), 74 (67), 41 (65). EI HRMS *m*/*z* calcd for [M^{+}] $C_6H_{14}S_3$ 182.0258, found 182.0265.

N,*N*-Bis(3-iodopropyl)aniline (**2.6**)

A mixture of *N*,*N*-bis(3-hydroxypropyl)aniline[20] (8.10 g, 38.7 mmol) and Et_3N (22 mL,4 equiv.) in CH_2Cl_2 (140 mL) was cooled in an ice bath under a stream of nitrogen, and methanesulfonyl chloride (9.0 mL, 3 equiv.) was added dropwise with rapid stirring over a period of 5 min. The reaction mixture was stirred for 1 h then quenched by adding crushed ice. A solution of NaH_2PO_4 (6.7 g in 40 mL H_2O) was added. The organic layer was separated, dried with Na_2SO_4, and concentrated under reduced pressure. The residue was taken up in acetone (50 mL) and a solution of NaI (17.5 g, 3 equiv.) in acetone (50 mL) was added. The mixture was stirred overnight, diluted with water (200 mL) and extracted with *tert*-butyl methyl ether. The extract was washed twice with water and brine, dried with Na_2SO_4, and concentrated under reduced pressure to give the product as a yellow-brown oil which was used without further purification. Yield 15.4 g (93%). TLC R_f 0.44 (15:1 hexanes: EtOAc). IR (film) 2926, 1598, 1504, 1228, 1199 cm^{-1}. ^{1}H NMR (CDCl3, 400 MHz) δ2.08 (p, *J* = 6.8 Hz, 4H), 3.20 (t, *J* = 6.6 Hz, 4H), 3.42 (t, *J* = 7.0 Hz, 4H), 6.69–6.74 (m, 3H), 7.19 7.25 (m, 2H). ^{13}C NMR($CDCl_3$, 100 MHz) δ3.7, 30.7,

51.6, 112.7, 116.7, 129.3, 147.4. MS *m/z* 429 ([M^+], 26), 274 (100), 146 (28). EI HRMS *m/z* calcd for [M^+] $C_{12}H_{17}I_2N$ 428.9450, found 428.9470.

13-Phenyl-1,5,9-trithia-13-azacyclohexadecane (**2.2**)

Diiodide **2.6** (8.99 g, 21.0 mmol), dithiol **2.5** (3.82 g, 21.0 mmol), and 1,1,3,3-tetramethylguanidine (5.3 mL, 2.0 equiv.) were each dissolved in acetonitrile, placed in 10 mL all-plastic syringes, and diluted to 10 mL. The resulting solutions were simultaneously and continuously added via syringe pump over a period of 60 h to a refluxing solution of 1,1,3,3-tetramethylguanidine (0.66 mL,0.25 equiv.) in acetonitrile (750 mL) under nitrogen. After cooling to rt, the reaction mixture was concentrated under reduced pressure. The residue was stirred with toluene (150 mL) for 1 h. The precipitated salts were filtered out, and the filtrate was chromatographed on silica gel (hexanes-*tert*-butyl methyl ether) to give the product as a colorless, viscous oil. Yield 2.40 g (32%). R_f 0.35 (8:1 hexanes- MTBE), 0.34 (10:1 Hexanes: EtOAc). IR (film) 2916, 2851, 1598, 1504, 1365, 1261 cm^{-1}. ^1H NMR ($CDCl_3$, 400 MHz) δ 1.92 (p, J = 7.0 Hz, 4H), 1.95 (p, J = 7.1 Hz, 4H), 2.62 (t, J = 6.9 Hz, 4H), 2.68 (t, J = 6.9 Hz, 4H), 2.69 (t, J = 7.0 Hz, 4H), 3.46 (t, J = 7.2 Hz, 4H), 6.66 6.71 (m, 3H), 7.19–7.25 (m, 2H). ^{13}C NMR ($CDCl_3$, 100 MHz) δ 27.5, 29.6, 29.8, 30.8, 31.0, 50.4, 112.5, 116.2, 129.2, 148.1. MS *m/z* 355 ([M^+], 100), 221 (18), 193 (17), 180 (27), 146 (46), 120 (29), 106 (26), 77 (11). EI HRMS *m/z* calcd for [M^+] $C_{18}H_{29}NS_3$ 355.1462, found 355.1458.

4-(1,5,9-Trithia-13-azacyclohexadecan-13-yl)benzaldehyde (**2.7**)

N,N-Dimethylformamide (8.5 mL, 110 mmol) was cooled in an ice bath, and $POCl_3$ (5.0 mL, 55 mmol) was added over a period of 30 min. The resulting mixture was added to a solution of ligand **2.2** (2.40 g, 6.75 mmol) in DMF (8 mL). After stirring for 45 min at 75 °C, the mixture was cooled to room temperature, poured into water (200 mL), and made

basic with NaOH. Dichloromethane (50mL) was added, and the mixture was stirred for 1 h. The organic layer was separated, and the aqueous layer was extracted with DCM (2 x 50 mL). The combined organic extracts were concentrated under reduced pressure, and the residue was taken up in benzene (25 mL). The solution was washed with water to remove DMF, dried with Na_2SO_4 and concentrated under reduced pressure to give the product as a yellow-brown oil which solidified after several hours. Yield: 2.56 g (99%). TLC *R*f 0.44 (2 : 1 hexanes: EtOAc). IR (film) 2935, 2848, 1667, 1597, 1524, 1406, 1364, 1198, 1168, 818 cm^{-1}. ^1H NMR(CDCl3, 400 MHz) δ 1.93 (p, *J* = 6.9Hz, 4H), 1.99 (p, *J* =7.0Hz, 4H), 2.64 (t, *J* =6.6Hz, 4H), 2.70 (t, *J* = 6.9 Hz, 4H), 2.72 (t, *J* = 7.0 Hz, 4H), 3.61 (t, *J* = 7.5 Hz, 4H), 6.68 (d, *J* = 9.0 Hz, 2H), 7.72 (d, *J* = 9.0 Hz, 2H), 9.73 (s, 1H). ^{13}C NMR (CDCl3 , 100 MHz) δ 26.9, 29.1, 29.4, 30.5, 30.9, 49.9, 110.8, 124.9, 132.0, 152.3, 189.8. MS *m/z* 383 ([M^+], 100), 249 (15), 208 (26), 174 (44), 134 (25), 87 (13), 41 (14). EI HRMS *m/z* calcd for [M^+] $C_{10}H_{29}NOS_3$ 383.1411, found 383.1392.

Chalcone **2.8**

Aldehyde **2.7** (385 mg, 1.0 mmol) and 3,5-difluoroacetophenone (172 mg, 1.1 mmol) were completely dissolved in 4 mL of ethanol–benzene (1:1) at 40 °C. Pyrrolidine (0.2 mL, 2 equiv.) was added, the reaction flask was sealed, and the mixture was stirred at 40 °C for 24 h. The resulting orange slurry was diluted with 25 mL of ethanol and concentrated to a volume of 10 mL to remove benzene. An additional 15 mL portion of ethanol was added, and the mixture was stirred at 0 °C for 4 h. The orange crystalline product was filtered off and dried under vacuum. Yield: 384 mg (73%). IR (KBr pellet) 2920, 1569, 1521, 1359, 1297, 1158, 984, 809 cm^{-1}. ^1H NMR (CDCl3, 400 MHz) δ 1.93 (p, *J* = 6.9 Hz, 4H), 1.98 (p, *J* = 7.0 Hz, 4H), 2.64 (t, *J* = 6.6 Hz, 4H), 2.70 (t, *J* = 7.0 Hz, 4H), 2.72 (t, *J* = 7.1 Hz, 4H), 3.58 (t, *J* = 7.4 Hz, 4H), 6.66 (d, *J* = 8.9 Hz, 2H), 6.99 (tt, *J* = 8.5, 2.4 Hz, 1H), 7.50 (ddd, *J* = 7.9, 2.4, 1.2 Hz, 2H), 7.53 (d, *J* = 8.9 Hz, 2H), 7.80 (d,

J = 15.4 Hz, 1H). ^{13}C NMR (CDCl3, 100 MHz) δ 27.2, 29.4, 29.6, 30.8, 31.1, 50.1, 107.3 (t, J_{CF} = 25.5 Hz), 111.1 (dd, J_{CF} = 18.7, 7.1 Hz), 111.7, 115.3, 122.0, 131.0, 142.2 (t, J_{CF} = 7.4 Hz), 147.1, 150.3, 162.9 (dd, J_{CF} = 250.2, 12.0 Hz), 187.5 (t, J_{CF} = 1.9 Hz, broad). ^{19}F NMR (CDCl3, 376 MHz) δ -109.2 (t, J = 7.4 Hz, 2F). MS *m/z* 521 ([M+], 100), 387 (23), 312 (30), 286 (35), 141 (21). EI HRMS *m/z* calcd for [M^+] $C_{27}H_{33}NOS_3$ 521.1692, found 521.1726.

2.6. References

(1) Yang, L.; McRae, R.; Henary, M. M.; Patel, R.; Lai, B.; Vogt, S.; Fahrni, C. J. *Proc. Natl. Acad. Sci. U. S. A.* **2005**, *102*, 11179.

(2) Cody, J.; Mandal, S.; Yang, L.; Fahrni, C. J. *J. Am. Chem. Soc.* **2008**, *130*, 13023.

(3) Verma, M.; Chaudhry, A. F.; Fahrni, C. J. *Org. Biomol. Chem.* **2009**, *7*, 1536.

(4) Verma, M.; Chaudhry, A. F.; Morgan, M. T.; Fahrni, C. J. *Org. Biomol. Chem.* **2010**, *8*, 363.

(5) Chaudhry, A. F.; Verma, M.; Morgan, M. T.; Henary, M. M.; Siegel, N.; Hales, J. M.; Perry, J. W.; Fahrni, C. J. *J. Am. Chem. Soc.* **2010**, *132*, 737.

(6) Valeur, B. *Molecular Fluorescence: Principles and Applications*; Wiley-VCH: Weinheim, 2001.

(7) Closs, G. L.; Miller, J. R. *Science* **1988**, *240*, 440.

(8) Marcus, R. A.; Sutin, N. *Biochim. Biophys. Acta* **1985**, *811*, 265.

(9) Rehm, D.; Weller, A. *Israel Journal of Chemistry* **1970**, *8*, 259.

(10) Chaka, G.; Kandegedara, A.; Heeg, M. J.; Rorabacher, D. B. *Dalton Trans.* **2007**, 449.

(11) Krylova, K.; Jackson, K. D.; Vroman, J. A.; Grall, A. J.; Snow, M. R.; Ochrymowycz, L. A.; Rorabacher, D. B. *Inorg. Chem.* **1997**, *36*, 6216.

(12) Addison, A. W. *Inorg. Chim. Acta* **1989**, *162*, 217.

(13) Goodrow, M. H.; Musker, W. K. *Synthesis* **1981**, 457.

(14) Everett, J. L.; Ross, W. C. J. *J. Chem. Soc.* **1949**, 1972.

(15) Buter, J.; Kellogg, R. M. *J. Org. Chem.* **1981**, *46*, 4481.

(16) Rivett, D. E.; Rosevear, J.; Wilshire, J. F. K. *Aust. J. Chem.* **1979**, *32*, 1601.

(17) Rapisarda, V. A.; Volentini, S. I.; Farias, R. N.; Massa, E. M. *Anal Biochem* **2002**, *307*, 105.

(18) Strambini, G. B.; Gabellieri, E. *J. Phys. Chem.* **1991**, *95*, 4347.

(19) Chaka, G.; Sonnenberg, J. L.; Schlegel, H. B.; Heeg, M. J.; Jaeger, G.; Nelson, T. J.; Ochrymowycz, L. A.; Rorabacher, D. B. *Journal of the American Chemical Society* **2007**, *129*, 5217.

(20) Jones, G. B.; Chapman, B. J.; Mathews, J. E. *J. Org. Chem.* **1998**, *63*, 2928.

CHAPTER 3

DEVELOPMENT OF A WATER SOLUBLE, AGGREGATION RESISTANT, HIGH CONTRAST FLUORESCENT PROBE FOR COPPER(I)

The majority of original research presented in this chapter has been published.[1]

3.1. Background: Lipophilicity and aggregation of fluorescent probes

Synthetic fluorescent probes for detection of biological metal ions are generally lipophilic compounds, due in part to the carbon-rich conjugated π-systems common to most organic fluorophores. Additionally, the number of charged or highly polar functional groups in the probe structure is often minimized to allow passive diffusion across lipid bilayer membranes.[2] Although some degree of lipophilicity is beneficial from the standpoint of cell permeability, highly lipophilic substances are subject to strong hydrophobic interactions and therefore exhibit poor aqueous solubility and a propensity to aggregate in aqueous solution. Aggregation of fluorophores can profoundly alter their photophysical properties: spectral shifts, complete fluorescence quenching, or even dramatic fluorescence enhancements have all been observed upon aggregation of fluorescent dyes.[3,4,5] Such effects are likely to confound the photophysical characterization of lipophilic fluorescent probes in aqueous solution. Furthermore, the aggregation state of these probes are likely to be altered by partitioning into lipid bilayers or other hydrophobic domains in a biological environment, thus calling into question the often presumed correspondence between the properties of a fluorescent probe observed upon characterization in aqueous buffer and its behavior in a biological setting.

In the case of Cu(I)-responsive probes, high lipophilicity is especially likely due to the thioether-rich ligand designs typically used to achieve selectivity for the soft Cu(I) cation. The structures of three representative Cu(I)-selective fluorescence turn-on probes are shown in Figure 3.1.

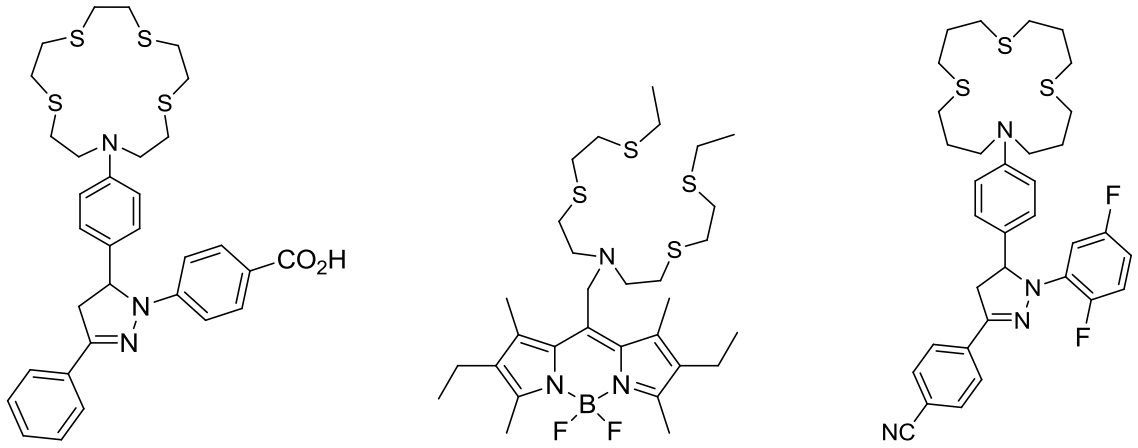

Figure 3.1: Structures of previously reported Cu(I)-selective fluorescent probes

The structures of CS1[6] and **2.4c** (Chapter 2) are dominated by hydrophobic functional groups, and it is unlikely that such structures can exist in stable monomeric aqueous solution at the micromolar concentrations typically used for fluorescence experiments. It is for this reason that **2.4c** and its analogs were characterized in methanolic rather than aqueous solution.[7,8] CTAP-1 contains a carboxylic acid moiety, which should be ionized at neutral pH, to promote aqueous solubility,[9] but placing a strongly hydrophilic functional group at only one end of a relatively large lipophilic molecule creates an amphiphilic structure which may still be very prone to aggregation. For example, Niu *et al* functionalized a distyryl-BODIPY fluorophore comparable in size to CTAP-1 with a tetraanionic sulfonated peptide to achieve water-solubility, but the resulting dye was found to be completely aggregated down to a concentration of 1 μM in

aqueous buffer![4] Since both the fluorophore and the thiazacrown ligand contribute substantially to the lipophilicity of probes such as CTAP-1 and **2.4c**, hydrophilic functionalization of both moieties may be necessary to produce probes of similar architecture that remain monomeric at useful concentrations in aqueous solution.

3.2. Probe design

The research described in Chapter 2 demonstrated that significant improvements in contrast ratio relative to the previously available Cu(I)-selective fluorescent probes CTAP-1 and CS1 can be achieved using a probe design comprising a tetradentate thiazacrown ligand coupled to an electronically tuned triarylpyrazoline fluorophore. These contrast optimized probes, however, were not designed to operate in an aqueous environment and instead were characterized in methanolic solution to avoid interference from aggregation. Therefore, in the work described in this chapter, we sought to develop a probe architecture that would allow application of the newly developed contrast optimization strategy in aqueous solution, with the ultimate goal of creating a higher contrast Cu(I)-selective fluorescence turn-on probe that would be suitable for biological applications.

3.2.1. Hydroxymethylated thiazacrown ligand

To avoid creating a highly amphiphilic structure, we sought to functionalize not only the fluorophore but also the thioether-based Cu(I) binding site with hydrophilic groups. Taking ligand **2.2** as a starting point, we chose to symmetrically functionalize the macrocycle with four equivalent hydroxymethyl groups (design **3.1)**. This modification should substantially decrease lipophilicity without introducing additional stereogenic centers into the final probe structure. To further reduce lipophilicity and perhaps also strengthen the Cu(I)-N interaction, the N-S linkers were shortened from three CH_2 units

to two, giving ligand **3.2**. Although the resulting reduction in macrocycle cavity size might be expected to impair metal binding, studies on macrocyclic tetrathioethers have shown that16- and 14-membered rings provide almost identical Cu(I) binding affinities.[10,11] The progression to the final ligand design is shown in Figure 3.2.

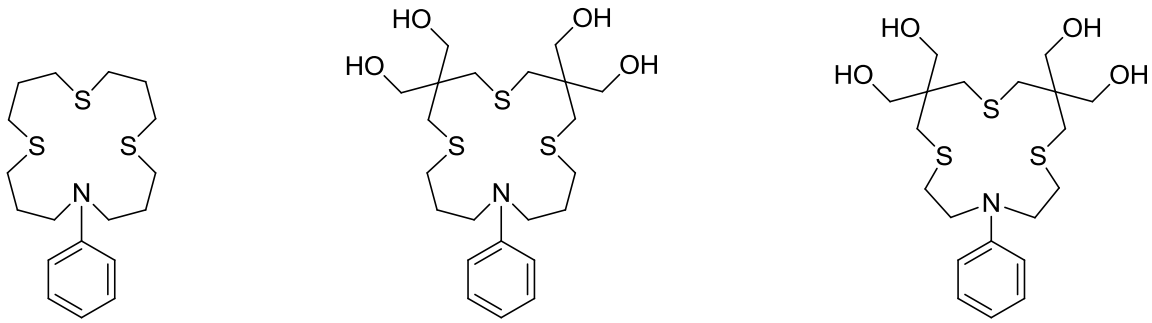

2.2 **3.1** **3.2**

Figure 3.2: Modification of the thiazacrown ligand to reduce lipophilicity

3.2.2. Sulfonated triarylpyrazoline fluorophore

In CTAP-1, the fluorophore was functionalized with a directly attached carboxylic acid as an ionizable group to promote aqueous solubility. This design strategy, however, is not well suited for contrast optimization by the electronic tuning strategy described in Chapter 2: The carboxylate existing in neutral solution would be reprotonated to the neutral form upon acidification, thus preventing the estimation of the intrinsic fluorophore quantum yield by protonation of the PET donor. Furthermore fluorophores bearing carbonyl substituents often exhibit low fluorescence quantum yields due to the existence of low-lying n,π* states, which do not have allowed radiative transitions back to the ground state.[12] Evidence of this effect was previously encountered by Cody *et al.* during preliminary studies of electronically tuned triarylpyrazoline

fluorophores, where derivatives bearing a carboxyl ester moiety on the 1-aryl ring showed dramatic decreases in fluorescence quantum yield with increasing fluorination even in the absence of a PET donor.[13] Both of the above complications can be avoided by replacing the carboxylic acid with a sulfonic acid. As a strong acid, a sulfonic acid moiety will exist solely as an anionic sulfonate group at any pH accessible in dilute aqueous solution, and the use of sulfonates as solubilizing groups for organic fluorophores is well established.[12] Furthermore, judging by the reported Hammett substituent constants of $\sigma_p = 0.36$ for SO_3^- and $\sigma_m = 0.35$ for F,[14] a *para*-sulfonate group has comparable electron-withdrawing power to the *meta*-fluoro- substituent previously employed for electronic tuning (Chapter 2).

3.2.3. Selection of the fluorophore substituents

Based on the results described in Chapter 2, the PET driving force for triarylpyrazoline Cu(I) probes with an N-arylthiazacrown ligand as the 5-aryl ring can be set within an appropriate tunable range using either a 3,5-difluorophenyl or 4-cyanophenyl moiety for the 3-aryl ring (probe series **2.3** and **2.4**, respectively). The PET driving force can then be tuned to maximize the contrast ratio by successive fluorination of the 1-aryl ring. For the new probe series, we selected a 4-cyanophenyl group for the 3-aryl ring because it should be less lipophilic than 3,5-difluorophenyl and also provides longer excitation and emission wavelengths for a given PET driving force (Table 2.1), which would be beneficial if the probe is used for cellular imaging applications. For the 1-aryl ring, the *p*-sulfonate group should already provide similar electron withdrawing power to a single *m*-fluoro-substituent (see above). The unfluorinated compound **3.3a** was therefore expected to be analogous to the slightly under-quenched probe **2.4b** (Chapter 2), thus providing a natural starting point for the tuning series. As in Chapter 2, successive fluorination of the 1-aryl ring should increase the PET driving force over a substantial range, but only designs **3.3b** and **3.3c** were selected for the initial

investigation since fluoro-substituents *ortho* to the sulfonate group may be susceptible to undesired nucleophilic aromatic substitution. The final structures selected for synthesis are shown in Figure 3.3.

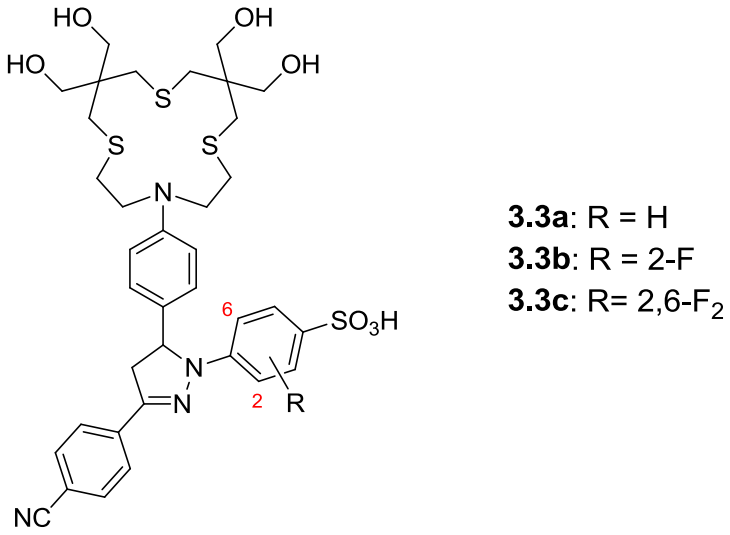

Figure 3.3: Initial probe designs

3.3. Synthesis of the ligand framework

3.3.1. Attempted synthesis via a neopentyl alcohol intermediate

A brief retrosynthetic analysis (Scheme 3.1) identified the commercially available, inexpensive compound pentaerythritol as an obvious starting point for the synthesis of ligand **3.2**.

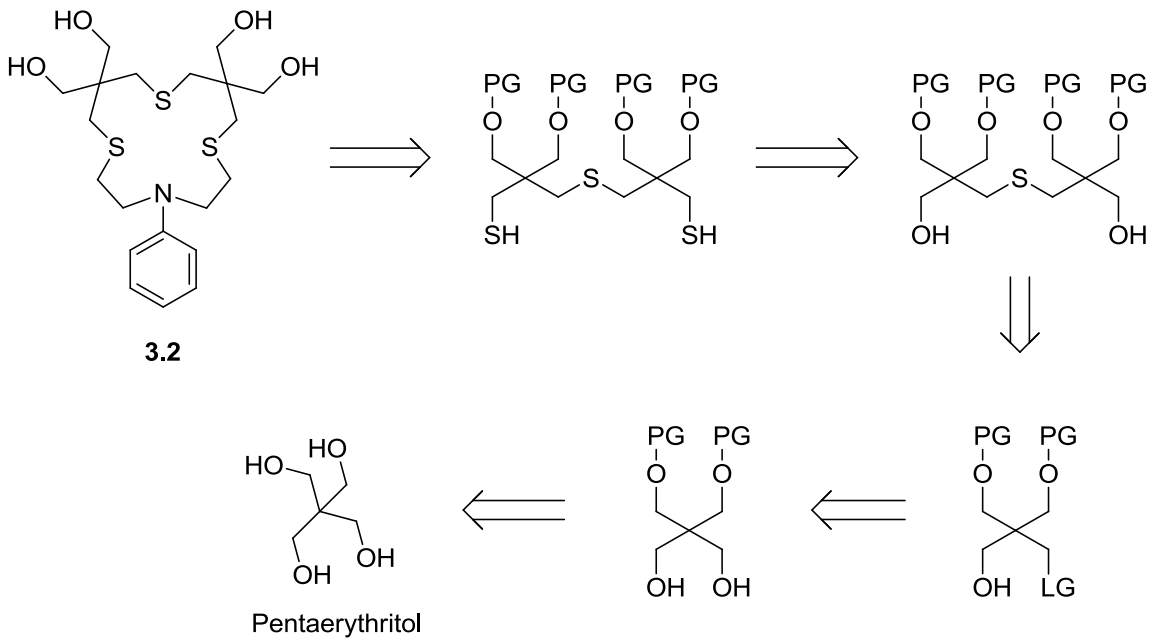

Scheme 3.1: Retrosynthetic analysis for ligand **3.2**

A synthesis based on this approach would require selective protection of two of the four hydroxyl groups of pentaerythritol, followed by selective conversion of one of the two remaining hydroxyls to a suitable leaving group. Pentaerythritol can be converted to the cyclohexanone monoacetal **3.4** in 90% yield,[15] so this reaction was chosen for the first protection step. The resulting diol would be converted to the monomesylate **3.5**. The role of this neopentyl alcohol derivative in the synthesis of **3.2** would then be analogous to that of 3-chloro-1-propanol in the synthesis of ligand **2.2**: The central thioether would be introduced by coupling two equivalents of the alcohol with sodium sulfide, and the resulting thioether-diol **3.6** would subsequently be converted to dithiol **3.7**, which is the immediate precursor for macrocyclization to give the ligand framework. This proposed synthesis is shown in Scheme 3.2.

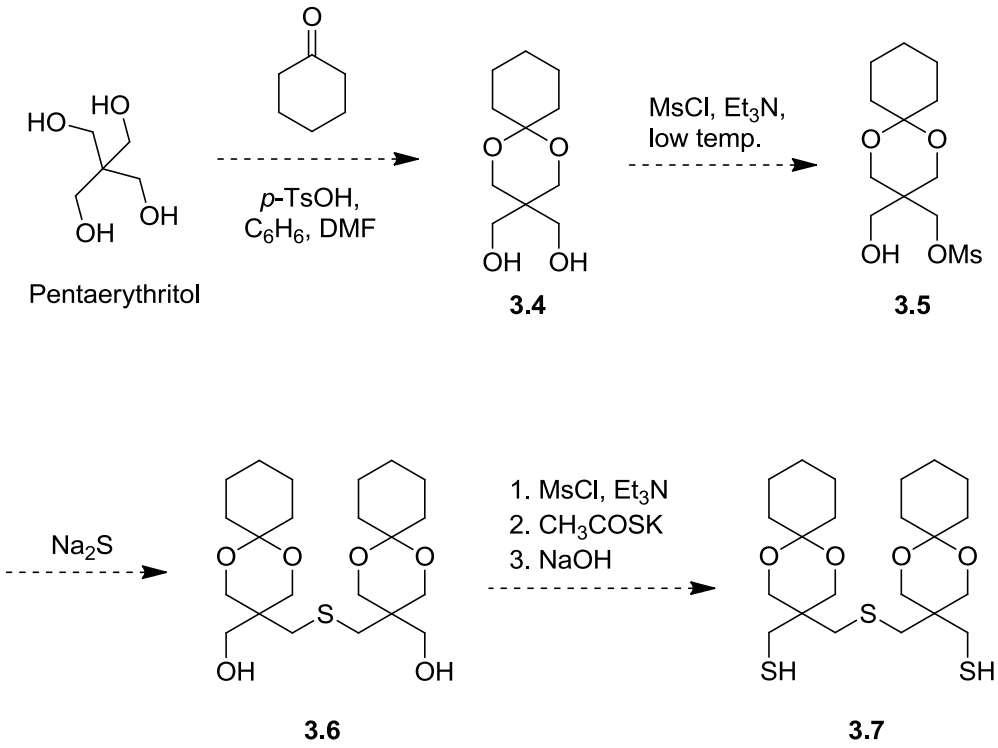

Scheme 3.2: Proposed synthesis of the dithiol intermediate

Intermediate **3.4** was synthesized according to the literature reaction conditions, but the product was isolated by recrystallization from toluene instead of the previously described procedure, which involved kugelrohr distillation followed by column chromatography.[15] This modification substantially improved preparation time and scalability at the expense of a moderate reduction in percent yield. Mesylation of **3.4** was conducted at -78°C using just over one molar equivalent of methanesulfonyl chloride in an attempt to achieve selectivity for the mono-mesylate **3.5**, but a substantial amount of the bis-mesylate **3.8** was also formed (Scheme 3.3). Nevertheless, the desired intermediate **3.5** was isolated in 35% yield by column chromatography and subsequently reacted with sodium sulfide in an attempt to prepare diol **3.6**.

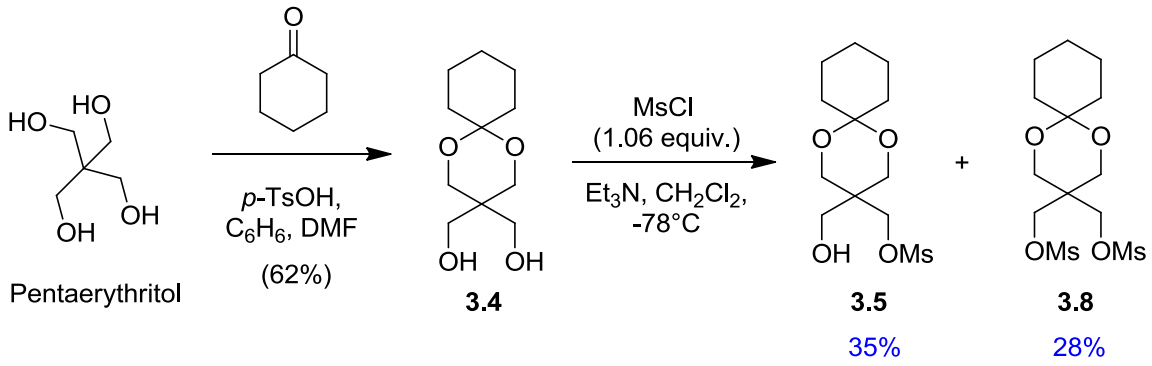

Scheme 3.3: Synthesis of neopentyl alcohol-mesylate intermediate **3.5** (Isolated yields)

3.3.2. Unexpected oxetane formation

The reaction of **3.5** with sodium sulfide was conducted under phase transfer catalysis in an attempt to overcome the low S_N2 reactivity typical of neopentyl electrophiles, but the desired product was not identified. The major product was found to be oxetane **3.9**, which was isolated in 42% yield relative to **3.5** or 76% relative to Na_2S (Scheme 3.4). Substantial unconsumed starting material was also apparent by TLC.

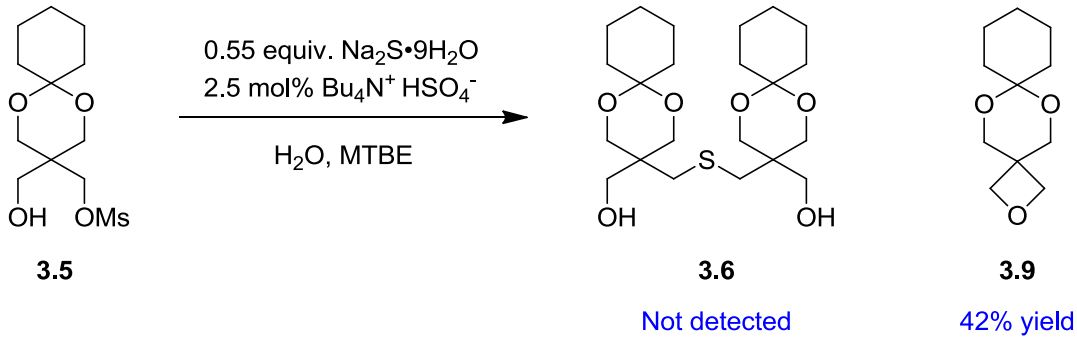

Scheme 3.4: Unexpected oxetane formation under phase-transfer catalysis

Although the low reactivity of neopentyl centers towards intermolecular nucleophilic substitution is well known, it was nevertheless surprising that an alkoxide could not only outcompete the strongly nucleophilic hydrosulfide ion but also form a

strained 4-membered ring in the process. It was thought that this unusual behavior may be due to the high reactivity of alkoxides under phase transfer conditions combined with the high basicity of the sulfide dianion, which actually exists as a mixture of hydrosulfide and hydroxide in aqueous solution.[16] To test this hypothesis, mesylate **3.5** was reacted with ethanethiolate under protic conditions in the presence of excess ethanethiol (pKa 10.6 in H_2O[16]) to minimize both the reactivity and concentration of alkoxide species (Scheme 3.5). In addition to the expected thioether 3.10, a surprisingly large amount of oxetane **3.9** was formed even under these conditions.

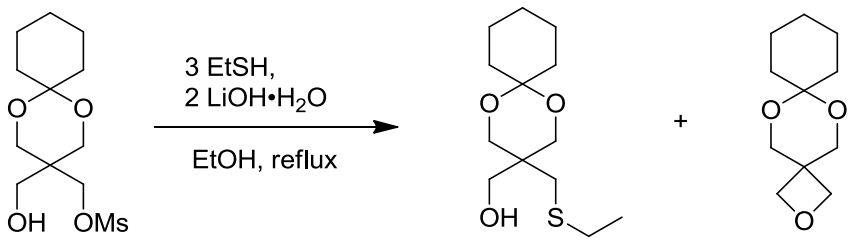

3.5 **3.10** **3.9**

59% 41%

Scheme 3.5: Oxetane formation under protic conditions in the presence of a thiol-thiolate mixture
(Product distribution by ^{1}H NMR)

Clearly, intermediate **3.5** is highly susceptible to oxetane formation, so an entirely different precursor was examined. The commercially available, water soluble bromide **3.11** was reacted with aqueous sodium sulfide at room temperature in an attempt to produce thioether **3.12** (Scheme 3.6). Remarkably, the oxetane **3.13** was the major product and none of the desired thioether could be detected. A small amount of the alkene **3.14** was also formed, presumably by simultaneous elimination of bromide and formaldehyde. An analogous elimination reaction has been previously observed for 3-bromo-2,2-dimethyl-1-propanol and related compounds.[17]

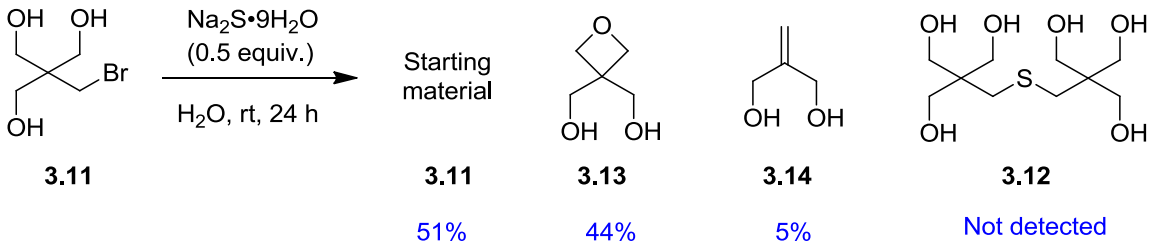

Scheme 3.6: Reaction of bromide **3.11** with aqueous sodium sulfide
(Product distribution by ^{1}H NMR)

3.3.3. Synthesis of the ligand framework by a thietane ring-opening strategy

Based on the results shown in Schemes 3.4, 3.5, and 3.6, it appears that reaction of basic sulfur nucleophiles with hydroxylated neopentyl electrophiles such as **3.5** and **3.11** inevitably results in substantial conversion of the starting material to the corresponding oxetane, which is presumably greatly accelerated by the Thorpe-Ingold effect.[18] This remarkable facility of oxetane formation, however, suggests that the corresponding thietanes should also be easily accessible. A thietane ring can be opened by benzyl bromide to give a 3-bromopropyl thioether,[19] which could presumably be converted to a bis(3-mercaptopropyl) thioether such as **3.7** by coupling with sodium sulfide followed by removal of the benzyl groups. This strategy was realized as shown in Scheme 3.7 via the previously reported thietane **3.15**,[20] which is easily prepared inexpensive starting materials via dibromide **3.16**. Ring opening of the thietane to bromide **3.17** proved to be remarkably efficient, and coupling of this neopentyl bromide with sodium sulfide gave clean conversion to thioether **3.18** after optimization of the reaction conditions. The benzyl groups were removed by dissolving metal reduction to give dithiol **3.19**. Cyclization with diiodide **3.20**, which was prepared in two steps from commercially available N-phenyldiethanolamine, proceeded in good yield to give intermediate **3.21**, an acetonide-protected aldehyde derivative of ligand **3.2**.

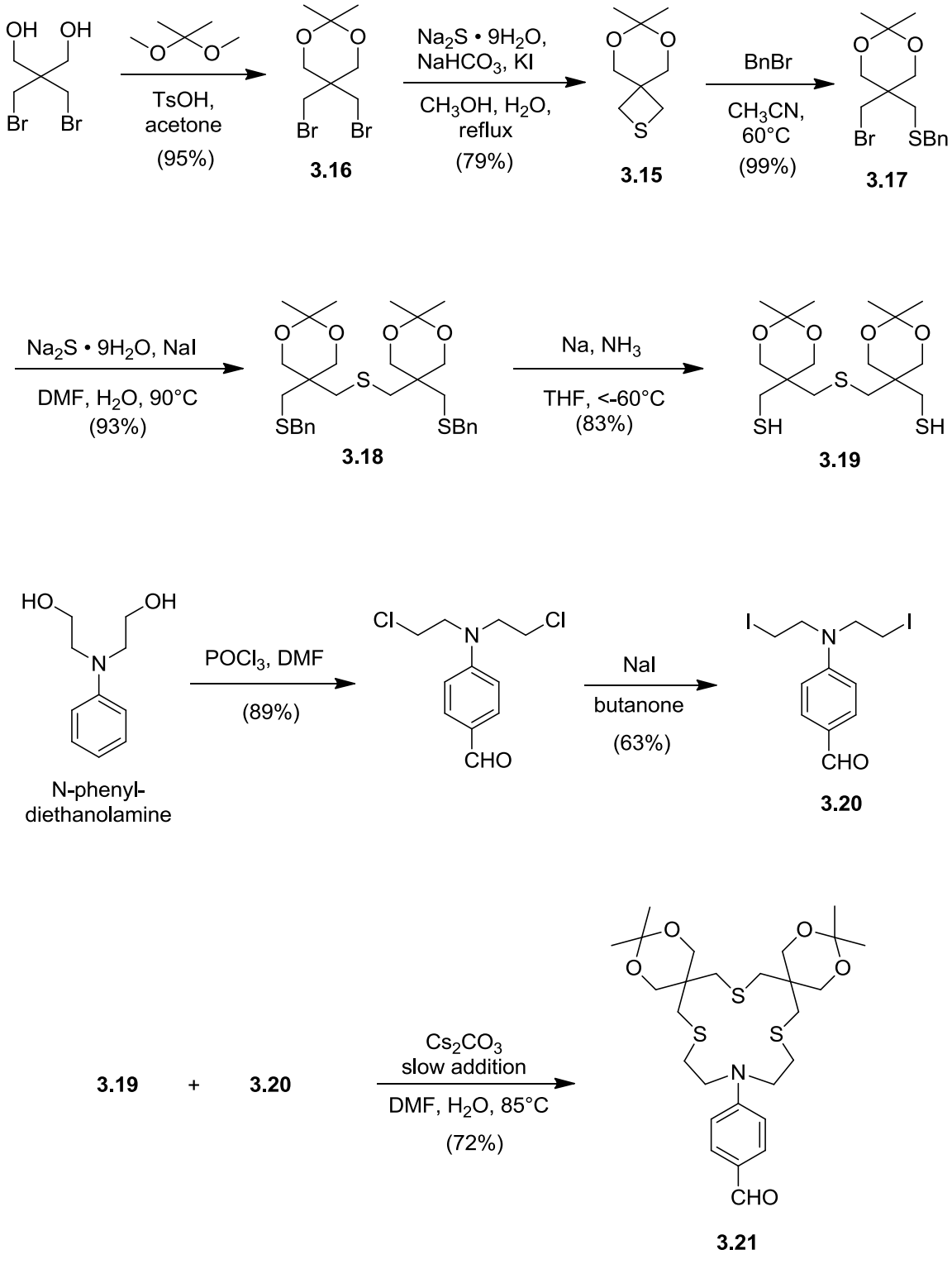

Scheme 3.7: Synthesis of the ligand framework

3.4. Synthesis of the sulfonated triarylpyrazoline fluorophore

3.4.1. Potential synthetic routes

As described in Chapter 2, 1,3,5-triarylpyrazoline-based probes are generally prepared by condensation of a chalcone derivative containing the desired 3- and 5-aryl substituents with an arylhydrazine corresponding to the 1-aryl ring of the desired product. In the case of target compounds **3.3a-c**, a sulfonic acid moiety must somehow be introduced at the para position of the 1-aryl ring. This could in principle be accomplished by direct sulfonation after assembly of the triarylpyrazoline core, but the acetonide-protected N-arylthiazacrown ligand would likely be damaged by electrophilic sulfonating agents. Alternatively, the sulfonic acid group could be introduced at the arylhydrazine stage, but the resulting triarylpyrazolines could not be purified by normal phase chromatography after the cyclization reaction, which sometimes gives fluorescent side products that complicate probe characterization and are difficult to remove by reversed-phase HPLC.[8] Therefore, a desirable route would be to introduce the sulfonic acid moiety in a protected form that could later be unmasked along with the hydroxyl groups of the ligand at the end of the synthesis.

3.4.2. An acetonide-based neopentyl protective group for sulfonic acids

The surprisingly facile oxetane formation observed for the hydroxylated neopentyl mesylate **3.5** presumably involves displacement of the intact methanesulfonate anion as a leaving group, thus suggesting that a similar hydroxylated neopentyl derivative might serve as a protective group for sulfonic acids. The hydroxyl group required for sulfonate displacement could itself be protected with an acid-labile group, thus providing a neopentyl sulfonate that is stable under basic and moderately nucleophilic conditions, but readily cleaved by strong base after a prior acidic deprotection step. Since the ligand

hydroxyl groups were already protected as acid-labile acetonides (intermediate **3.21**), a similar acetonide moiety was incorporated into a neopentyl sulfonate ester to give protective group **3.22**, which could be deprotected as shown in Scheme 3.8:

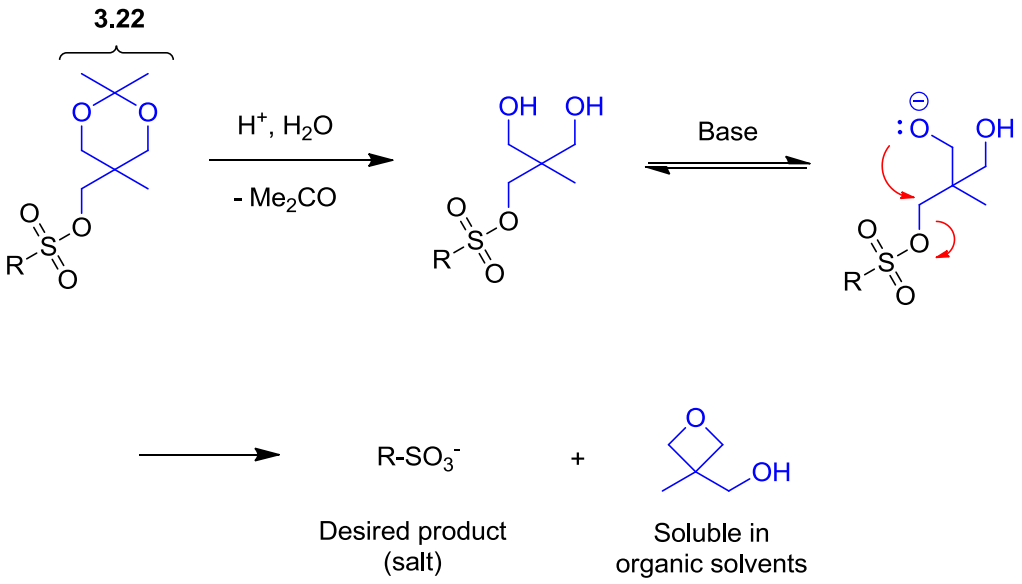

Scheme 3.8: Sulfonate protective group **3.22** and proposed deprotection mechanism

3.4.3. Synthesis of the target probe series 3.3a-c

Synthesis of the arylhydrazine intermediates

As shown in Scheme 3.9, protective group **3.22** was easily introduced by reacting the corresponding alcohol **3.23** with commercially available fluorinated arenesulfonyl chlorides. The resulting fluorinated arenesulfonates **3.24a-c** were converted in high yield to the corresponding arylhydrazines **3.25a-c** by nucleophilic aromatic substitution with hydrazine hydrate. As might be expected, the reactivity of aryl fluorides **3.24a-c** toward hydrazine increased dramatically upon additional fluorination; while the reaction of **3.24a** required heating to proceed in DMSO solution, **3.24c** was so reactive that the reaction

had to be conducted in the less polar solvent acetonitrile to prevent thermal runaway and side product formation.

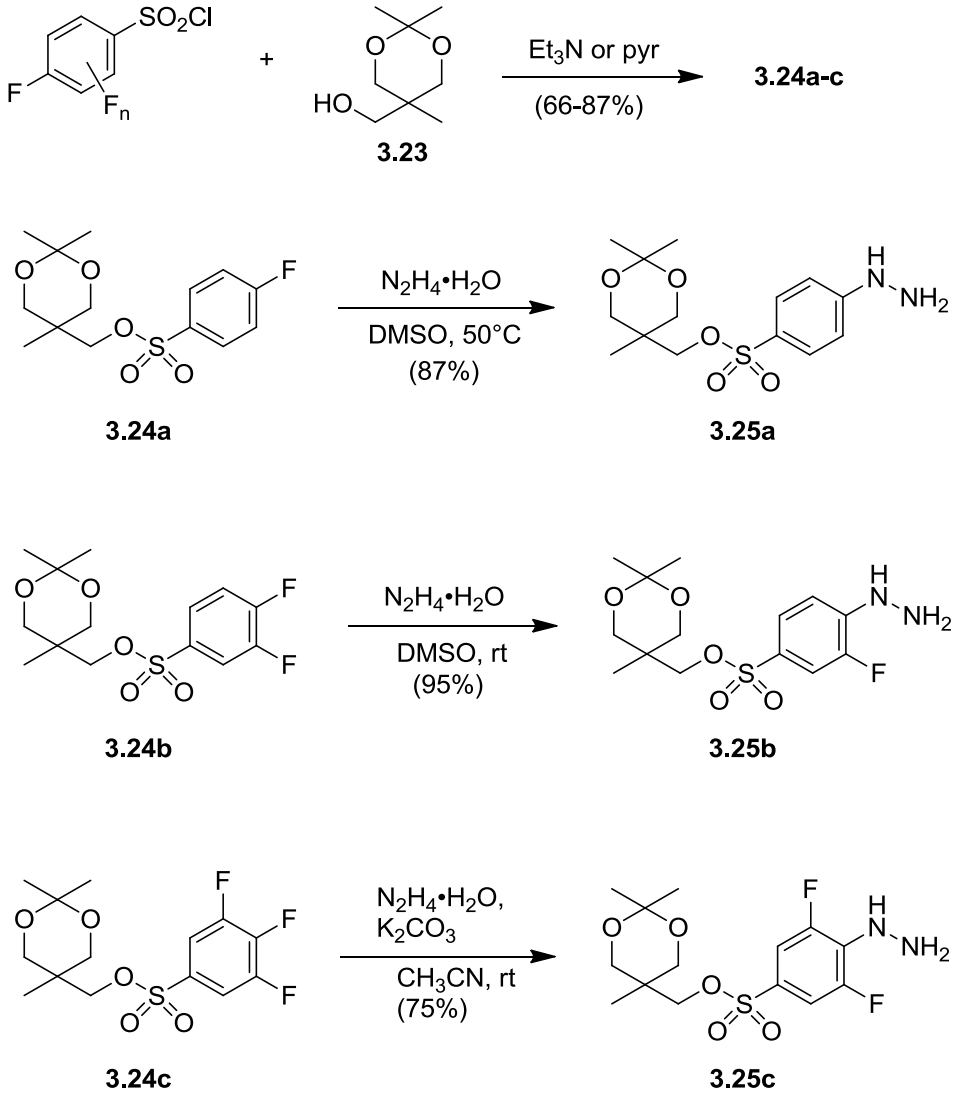

Scheme 3.9: Synthesis of arylhydrazine-sulfonate esters **3.25a-c**

As indicated in Scheme 3.9, protective group **3.22** remained intact even upon heating with hydrazine, demonstrating a remarkable robustness against nucleophilic

displacement, and all of the above reactions were sufficiently clean that the products could be isolated simply by crystallization. Although a few other intramolecularly cleavable neopentyl sulfonate protective groups have been reported,[21-23] **3.22** has significant advantages for the present application: It can be introduced in one step from commercially available alcohol **3.23**, whereas the t-butyl carbamate-based neopentyl protective group NeoN-B[21] requires four synthetic steps to produce the alcohol precursor. Furthermore, it is resistant to both hydrazine and fluoride ion, which is presumably not the case for the more recently introduced silyl ether[22] or carboxylic ester[23] based neopentyl sulfonate protective groups.

Construction of the triarylpyrazoline fluorophore

As shown in Scheme 3.10, the triarylpyrazoline core was assembled by aldol condensation of aldehyde **3.21** with 4-cyanoacetophenone followed by condensation of the resulting chalcone **3.26** with arylhydrazine **3.25a** under mildly acidic conditions. Although the latter resulted in partial cleavage of the acetonide groups, the fully protected intermediate **3.27a** was recovered by including a brief re-acetalization step in the workup procedure to allow for efficient chromatographic purification. Probe **3.3a** was then obtained by complete hydrolysis of the acetonide moieties with trifluoroacetic acid-water mixture followed by treatment with potassium t-butoxide at room temperature to induce sulfonate elimination. This deprotection procedure, although requiring two steps, proved to be reasonably efficient, and the desired product was obtained in 63% yield by crystallization of the zwitterionic acid form. Although the resulting material appeared pure by NMR, it was further purified for photophysical characterization by conversion to the highly soluble ammonium salt followed by RP-HPLC using acetonitrile/aqueous NH_4HCO_3 as the mobile phase. Probes **3.3b** and **3.3c** were then prepared analogously to **3.3a** except that the final products were isolated directly as the ammonium salts by RP-HPLC after deprotection (see Experimental Section for details).

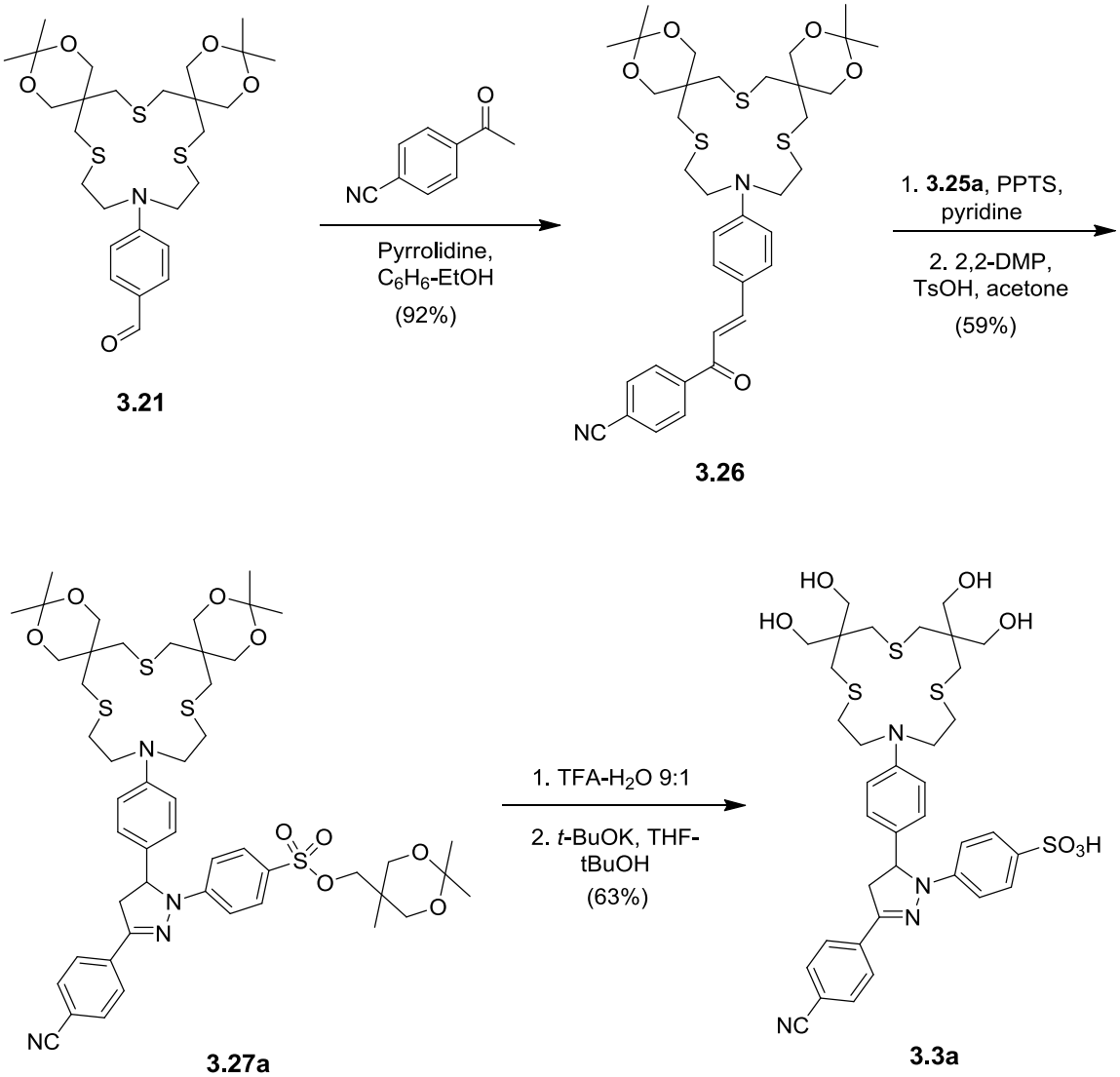

Scheme 3.10: Synthesis of probe **3.3a**

3.5. Initial characterization of the probe series

The ammonium salts of **3.3a-c** dissolve rapidly in pure water, and millimolar stock solutions were easily prepared by direct dissolution without organic cosolvents. This stands in stark contrast to previously reported Cu(I) probes including **2.4c**, CS1 and

even CTAP-1, all of which can be introduced into aqueous solution only by pre-dissolution in an organic solvent such as DMSO. In neutral aqueous buffer (10 mM MOPS, pH 7.2), probes **3.3a-c** gave only very weak fluorescence in the absence of analyte and exhibited large emission enhancements upon saturation with Cu(I). As expected for a PET-based fluorescence switching mechanism, saturation with Cu(I) had no effect on the emission wavelength and only a very small effect on the absorption spectrum for each probe. The absorption and emission maxima shifted toward shorter wavelength from **3.3a** to **3.3c**, giving a stepwise increase in the estimated excited-state energies (ΔE_{00}) from 2.79 to 3.06 eV. The corresponding ΔG^0_{et} values in aqueous solution cannot be directly calculated from the Rehm-Weller equation (see Chapter 2) because the reduction potentials $E(A/A^-)$ are outside of the accessible potential window, but data on related triarylpyrazolines bearing a *p*-cyano substituent on the 3-aryl ring show that $E(A/A^-)$ is little affected by fluorination of the 1-aryl ring.[24] Therefore, the PET driving force ($-\Delta G^0_{et}$) should track the changes in ΔE_{00}. Accordingly, the fluorescence quantum yields of the free and Cu(I) saturated probes **3.3a-c** decrease with increasing excited state energy, corresponding to an increasing rate of PET for both the free and Cu(I)-bound forms (Table 3.1).

Table 3.1: Photophysical properties of probes **3.3a-c**

Probe	Abs. λ_{max}/nm	Em. λ_{max}/nm	ΔE_{00}/eV[a]	Φ_f Free	Φ_f Cu(I)[b]	f_e[c]
3.3a	396	508	2.79	0.0015	0.083	65
3.3b	376	498	2.89	0.0006	0.033	41
3.3c	358	467	3.06	0.0005	0.010	9

[a] Estimated as the mean of the absorption and emission energies for the analyte-free probes. [b] Probes were saturated with Cu(I) by titration with aq. $CuSO_4$ in the presence of 20 μM sodium ascorbate. [c] Fluorescence enhancement factor (contrast ratio) given as the ratio of the emission intensity of the Cu(I)-saturated probe to that of the free probe at 380 nm excitation; emission spectra were integrated over the range $\lambda_{max} \pm 10$ nm to improve signal to noise ratio.

3.6. Reduction of the PET driving force

3.6.1. Probe design

As indicated in Table 3.1, the largest fluorescence enhancement, 65-fold, was observed with **3.3a**, which also possesses the lowest excited state energy and therefore the lowest PET driving force. As demonstrated in Chapter 2, however, the contrast ratio should pass through a maximum at an intermediate value of $-\Delta G^0_{et}$. Therefore, it was unclear whether the optimum contrast ratio is already achieved with **3.3a** or if a derivative with lower excited state energy would offer an even larger fluorescence enhancement. To address this question, we devised probe **3.3d**, in which the electron-withdrawing sulfonate moiety is decoupled from the fluorophore π-system through a saturated carbon spacer.

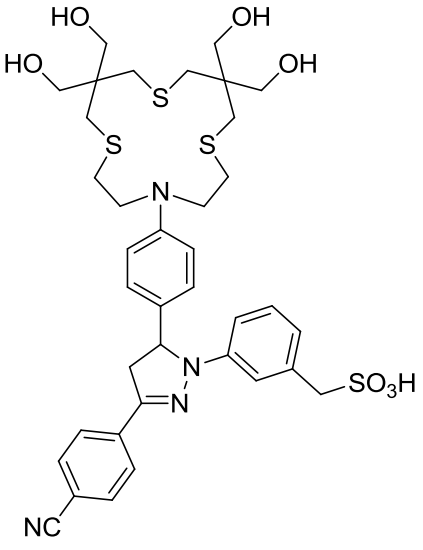

3.3d

Figure 3.4: Structure of probe **3.3d**

3.6.2. Synthesis of probe 3.3d

The synthesis of **3.3d** required a slightly different route than used for **3.3a-c**, because the corresponding arylhydrazine cannot be prepared by nucleophilic aromatic substitution of an aryl fluoride without the activating effect of the strongly electron-withdrawing sulfonate ester on the aromatic ring. Therefore, amine **3.28** was chosen as the arylhydrazine precursor (Scheme 3.11). Synthesis of **3.28** required the sulfonyl chloride **3.29**, which has been previously prepared from the corresponding S-alkyl isothiourea derivative using aqueous chlorine[25] or from the corresponding sodium sulfonate by reaction with thionyl chloride.[26] The former procedure requires handling of chlorine gas and has the potential to produce explosive nitrogen trichloride. The latter procedure was also unsatisfactory; the authors reported no analytical data, and their conditions were found to give a tarry mixture containing more unreacted starting material than desired product. Therefore, a method was devised to generate the sulfonyl chloride by direct oxidative chlorination of the thiol **3.30** with chlorine generated *in situ*: Addition of hydrogen peroxide to a biphasic mixture containing a dichloromethane solution of **3.30** and concentrated hydrochloric acid gave clean conversion to **3.29**, which was obtained in higher yield and purity than previously reported.[25] Coupling with alcohol **3.23** gave the sulfonate ester **3.31**, which was subsequently reduced to amine **3.28** without disturbing the benzylic sulfonate ester or the acetonide moiety using zinc dust in a methanolic acetic acid-ammonium acetate buffer. The planned synthetic route entailed conversion of **3.28** to a crystalline diazonium tosylate[27,28] in the presence of acetone to preserve the acetonide moiety, followed by reduction to the corresponding arylhydrazine after removal of acetone. Attempts to crystallize the diazonium salt were unsuccessful, so the amine was instead reacted with isoamyl nitrite under neutral conditions, a procedure known to convert arylamines to the corresponding 1,3-diaryltriazenes,[29] and then reduced

in one pot to give an amine-arylhydrazine mixture. The arylhydrazine appears to be somewhat unstable and could not be isolated in pure form, but an excess of the crude material was reacted with chalcone **3.26** to give the protected triarylpyrazoline **3.32** in 52% yield. The deprotection procedure developed for the arenesulfonates **3.3a-c** also proved effective for the benzylic methanesulfonate **3.3d**, and the desired product was isolated as the ammonium salt by RP-HPLC (Scheme 3.11).

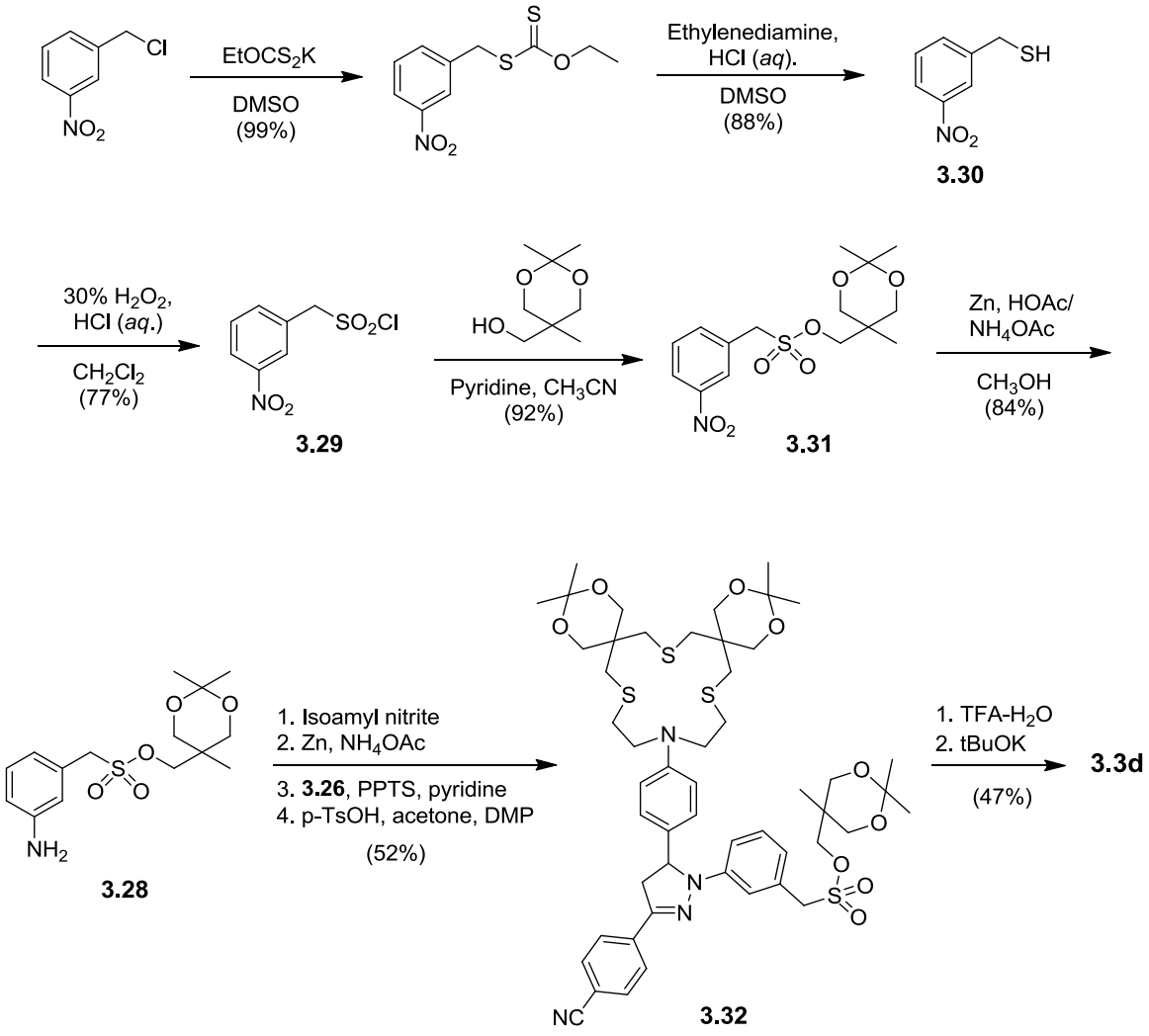

Scheme 3.11: Synthesis of probe **3.3d**

3.6.3. Evaluation of the expanded probe series

Probe **3.3d** gave absorption and emission maxima of 404 and 532 nm, respectively, corresponding to a significantly lower excited state energy of 2.70 eV versus 2.79 eV for **3.3a** (table 3.2). Consistent with a reduced PET driving force, the fluorescence quantum yield of the free probe nearly doubled from 0.15% to 0.26%. The quantum yield of the Cu(I)-saturated form, however, decreased slightly from 8.3% for **3.3a** to 7.7% for **3.3d**, suggesting the presence of an efficient nonradiative deactivation pathway other than acceptor-excited PET. To gauge the intrinsic fluorophore quantum yield of **3.3d** as well as **3.3a-c**, the quantum yields were measured in 5 mM HCl, where the arylamine moiety is expected to be protonated and therefore inactive toward oxidative electron transfer. As in Chapter 2, the fluorescence recoveries upon Cu(I) binding were determined as the ratio of the fluorescence quantum yield of the Cu(I)-saturated probe to that of the protonated probe. As shown in Table 3.2, the lower excited state energy of **3.3d** compared to the other probes does indeed result in a greater fluorescence recovery relative to the unquenched fluorophore upon Cu(I) coordination, but this does not result in a larger fluorescence enhancement factor or improved fluorescence quantum yield relative to **3.3a**-Cu(I) because the fluorophore of **3.3d** apparently possesses an intrinsically lower quantum efficiency in aqueous solution. Interestingly, anomalously low fluorescence quantum yields in methanolic solution have been previously reported for other triarylpyrazolines bearing relatively electron-rich 1-aryl rings.[30,31]

Table 3.2: Fluorescence recoveries and related properties for probes **3.3a-d**

Compound	ΔE_{00}/eV[a]	Φ_f Cu(I)-sat.[a]	Φ_f Acidic[b]	Fluorescence recovery[c]	f_e Cu(I) sat.[a]
3.3d	2.70	0.077	0.10	77%	32
3.3a	2.79	0.083	0.25	33%	65
3.3b	2.89	0.033	0.31	11%	41
3.3c	3.06	0.010	0.62	2%	9

[a] All values determined as in Table 3.1. [b]Fluorescence quantum yield in 5 mM HCl (*aq*). [c] Φ_f (Cu(I)-sat.)/Φ_f(Acidic).

3.7. Further characterization of the optimized probe CTAP-2

As indicated in Table 3.2, probe **3.3a** gives the highest contrast ratio and also the highest fluorescence quantum yield upon Cu(I) saturation. This compound was therefore selected as the optimized probe for further study and given the designation CTAP-2.

3.7.1. Copper(I) binding stoichiometry and reversibility

To confirm that CTAP-2 has the intended 1:1 copper coordination stoichiometry and high binding affinity, a 4.5 μM solution of the probe in deoxygenated buffer (5 mM MOPS-K^+, pH 7.2) was titrated with Cu(I) in 0.5 μM increments up to 8 μM total. Whether Cu(I) was supplied directly from an acetonitrile stock solution of the hexafluorophosphate (Figure 3.5) or produced in situ by reduction of Cu(II) with ascorbate, the fluorescence intensity of CTAP-2 first increased linearly and then saturated sharply at 4.5 μM (1 molar equivalent) of Cu(I). These results indicate clean 1:1 binding with an association constant on the order of 10^9 or higher.

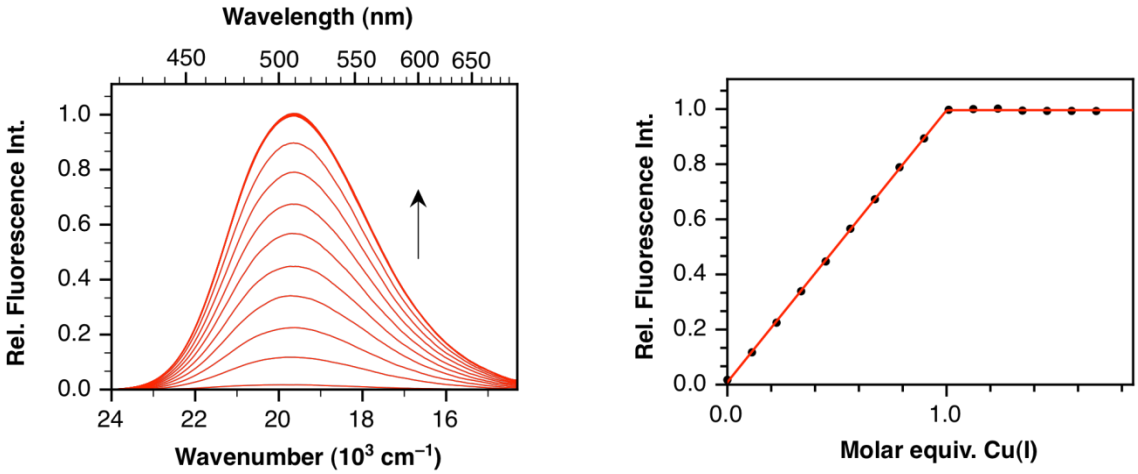

Figure 3.5: Mole-ratio titration of CTAP-2 with Cu(I). Left: Smoothed fluorescence emission spectra. Right: Fluorescence emission intensity at 510 nm versus amount of added Cu(I). Adapted with permission from Ref. 1. © 2011 American Chemical Society.

The response of CTAP-2 to Cu(I) was completely reversed by addition of an excess of the nonselective, high affinity transition metal chelating agent TPEN (N,N,N',N'-tetrakis(2-pyridylmethyl)ethylenediamine), indicating that the response is indeed due to a reversible complexation reaction.

3.7.2. Analyte selectivity

To determine the selectivity of CTAP-2 for Cu(I) over other biologically relevant metal ions, the fluorescence response of the probe to each cation was recorded in the absence and presence of Cu(I). As shown in Figure 3.6, no cation other than Cu(I) gave a significant fluorescence turn-on response, and none of the cations inhibited the response to Cu(I). A moderate concentration (10 mM) of chloride also did not interfere, despite the significant affinity of this anion toward Cu(I).

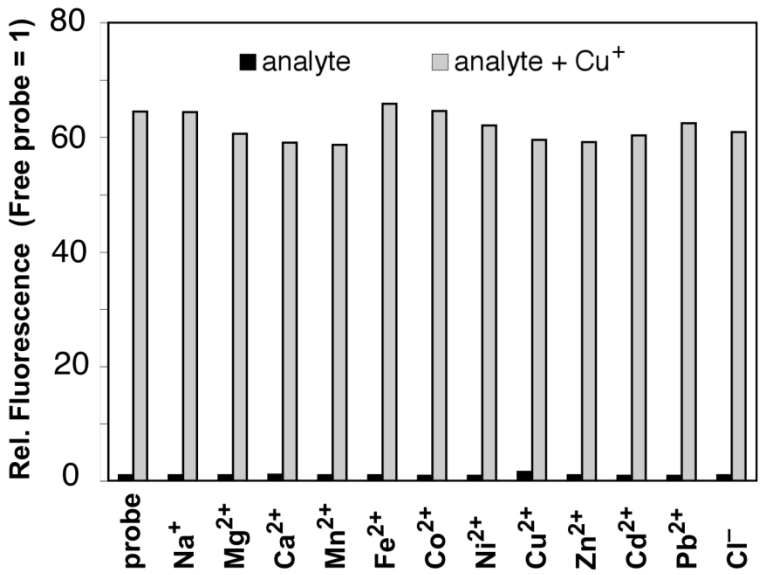

Figure 3.6: Analyte selectivity of CTAP-2. Adapted with permission from Ref. 1.

Although slight fluctuations in the response to Cu(I) are discernible, these were poorly reproducible and are probably due to partial oxidation of Cu(I) during mixing of the solutions in air. Consistent with this notion, the strongest Cu(I) response was observed in the presence of the reducing cation Fe(II).

3.7.3. Copper(I) binding affinity and pKa

The experiments and data fitting described in subsection 3.7.3 were carried out by Pritha Bagchi except where specified otherwise.

Cu(I) binding affinity of CTAP-2

As shown in Figure 3.5, direct titration of micromolar concentrations of CTAP-2 with Cu(I) results in sharp saturation at one molar equivalent of the metal, indicating that the dissociation constant of CTAP-2-Cu(I) is much smaller than the probe concentration used in the experiment. The binding affinity cannot be accurately determined from these data, because essentially all of the metal remains bound to the probe up to the saturation point. The Cu(I)-association constant of CTAP-2 was instead calculated from the much

smaller Cu(II)-association constant and the redox potential of the CTAP-2-bound Cu(II/I) couple. According to the Nernst relationship, these values are related by Equation 3.1, where $E_{Cu(II/I)L}$ is the reduction potential of the ligand-bound Cu(II/I) couple, $E_{Cu(II/I)solv}$ is the "concentration potential", the standard potential of the aqueous Cu(II/I) couple corrected for the activity coefficient of each ion under the conditions of measurement, F is the Faraday constant, $K_{Cu(II)}$ is the ligand-Cu(II) complex stability constant, and $K_{Cu(I)}$ is the ligand-Cu(I) complex stability constant.[32]

$$E_{Cu(II/I)L} = E_{Cu(II/I)solv} - \frac{\ln(10)RT}{F}\log\frac{K_{Cu(II)}}{K_{Cu(I)}} \qquad (3.1)$$

The CTAP-2-Cu(II) complex stability constant was determined by spectrophotometrically monitored titration of CTAP-2 with excess $CuSO_4$ at pH 5 (10 mM PIPES/K^+, 0.1 M $KClO_4$), and the resulting data were fitted over the entire spectral range (250-500 nM) using the Specfit software package[33] to yield a value of log $K_{Cu(II)}$ = 2.97 ± 0.07. The half-wave potential of the CTAP-2-bound Cu(II/I) couple was determined by cyclic voltammetry in the presence of 1 mM $CuSO_4$ in the same PIPES-$KClO_4$ buffer described above, yielding a value of $E_{Cu(II/I)L}$ = +0.626 V (vs. SHE). On the basis of these data and a value of 0.13 V vs. SHE for $E_{Cu(II/I)solv}$,[32] the Cu(I) binding affinity of CTAP-2 was estimated as log $K_{Cu(I)}$ = 11.4 ± 0.1, which corresponds to a dissociation constant of only 4 pM, at pH 5. Given the low pKa of CTAP-2 (see below), these values are not significantly influenced by protonation under the conditions of measurement and thus are unchanged at pH 7.

Acid dissociation constant (pKa) of CTAP-2

As implied by its relatively high fluorescence quantum yield under acidic conditions (Table 3.2), CTAP-2 gives a very strong fluorescence turn-on response upon

protonation of the arylamine PET donor. Therefore the pKa of CTAP-2 is important not only for binding affinity determination but also for the susceptibility of the Cu(I) response to interference from environmental pH. To determine the pKa, which is normally reported on the basis of hydronium concentration rather than activity, the fluorescence emission of CTAP-2 was recorded over a p[H] range from 2.4 to 5.0 at intervals of 0.1 log unit, and the data were analyzed using Specfit to yield a value of 3.97 ± 0.01 at 0.1 M ionic strength. Given this relatively low pKa value and the threefold higher fluorescence quantum yield of CTAP-2-H^+ versus CTAP-2-Cu(I), the contrast ratio of CTAP-2 upon Cu(I) saturation should remain above 30 down to pH 6, which was experimentally verified by the author, and is expected to fall to unity near pH 4.5.

3.7.4. Aggregation effects in aqueous solution

To determine whether CTAP-2 is affected by aggregate formation within the intended working concentration range, the absorbance of both free and Cu(I)-saturated CTAP-2, as well as the fluorescence emission intensity of the latter, were recorded over a range of concentrations from 0.5 to 5 μM in aqueous buffer (10 mM MOPS, pH 7.2). The presence of an aggregate with significantly different photophysical properties than the monomer would be indicated by deviation from linearity in a plot of absorbance or fluorescence intensity versus concentration, because the fraction of the probe in aggregated form should be concentration dependent. As shown in Figure 3.7, the absorption and fluorescence intensity of CTAP-2-Cu(I) scaled linearly with concentration, thus providing no evidence of aggregation up to the maximum working concentration of 5 μM. Higher concentrations are not appropriate for fluorescence measurements due to substantial inner filter effects that would result from the large absorbance of the solution, which is already above 0.13 at 380 nm for the 5 μM point. The slope of the absorbance versus concentration plot revealed a molar absorptivity of

2.66 x 10^4 M^{-1} cm^{-1} at 380 nm, which corresponds to 2.9 x 10^4 M^{-1} cm^{-1} at the absorption maximum of 391 nm for CTAP-2-Cu(I).

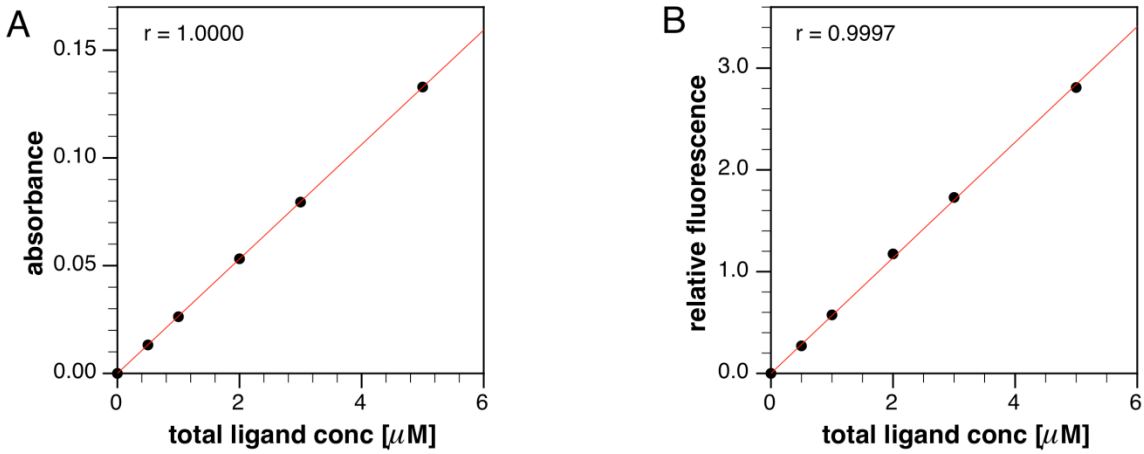

Figure 3.7: Absorbance and fluorescence versus concentration of CTAP-2-Cu(I). A. absorbance at 380 nm. B. fluorescence emission intensity over λ_{max} ± 10 nm at 380 nm excitation.

The absorbance of free CTAP-2 also scaled linearly with concentration up to the intended working maximum of 5 µM (Figure 3.8, inset). To determine whether observable aggregation of CTAP-2 occurs at all in aqueous solution, the absorbance was also measured at higher concentrations using a 0.5 cm path-length cuvette. Deviation from linearity became apparent above 10 µM, indicating that CTAP-2 does aggregate significantly at high concentration. To estimate the fraction of the probe that is likely aggregated at the maximum working concentration, the data were fitted to a simple dimerization model, which is shown as the red trace in Figure 3.8 (see Experimental Section for details).

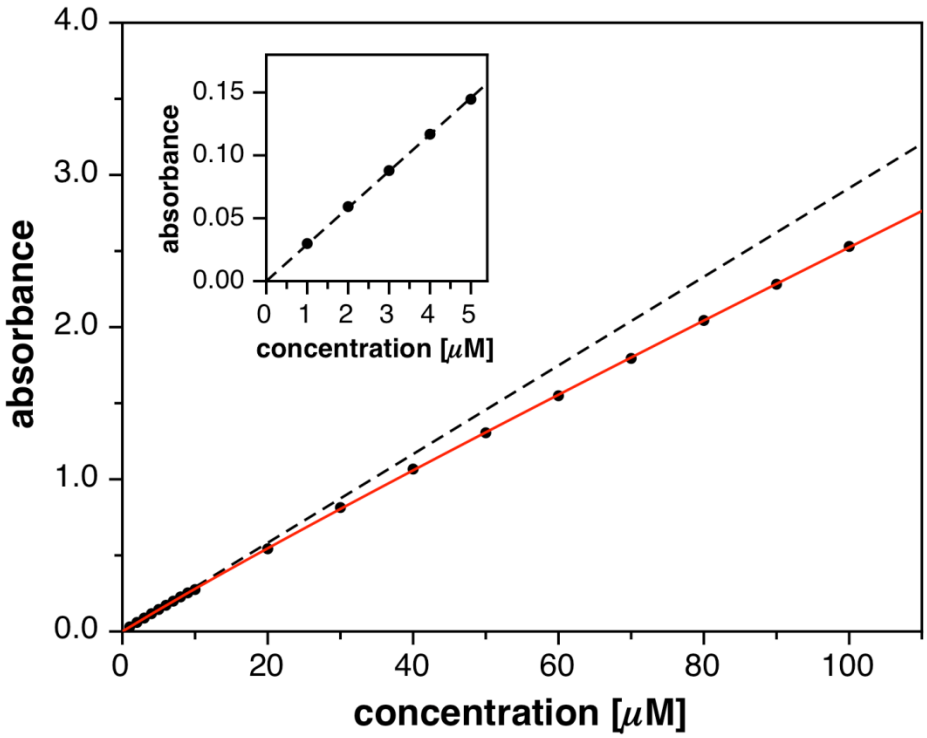

Figure 3.8: Absorbance at 396 nm versus concentration of CTAP-2. All absorbances are scaled to 1 cm path length. Inset: 0-5 μM range. Dashed line: linear fit based on 0-5 μM range. Red curve: dimerization model fit over all data points.

The fit shown in Figure 3.8 yielded a reasonable molar absorptivity of 4.25×10^4 M^{-1} cm^{-1} at 396 nm for the CTAP-2 dimer and a dimerization equilibrium constant of log $K = 3.98 \pm 0.06$, which implies that a 5 μM solution of CTAP-2 would contain about 4 mol% of the dimer. While the exact nature of the CTAP-2 aggregate, and therefore the amount present at a given concentration, is uncertain, the fluorescence contrast ratio of CTAP-2 upon saturation with Cu(I) remained constant within experimental error over a range of concentrations spanning more than an order of magnitude (Table 3.3), indicating that any aggregate that may be present does not have an observable impact on the performance of CTAP-2 within its working concentration range.

Table 3.3: Fluorescence contrast ratio of CTAP-2 at different concentrations

Concentration (μM)[a]	0.35	0.73	1.1	1.5	4.5
Contrast ratio[b]	69	66	64	65	66

[a] The 4.5 μM sample was prepared from a precise stock solution. Other concentrations were calculated from the absorbance at 380 nm (10 cm path length). [b] Ratio of the emission intensity of the Cu(I)-saturated probe to that of the free probe at 380 nm excitation; emission spectra were integrated over the range $\lambda_{max} \pm 10$ nm.

3.8. Applications of CTAP-2

All experiments presented in Section 3.8 were conducted by Pritha Bagchi.

3.8.1. In-gel detection of a copper metallochaperone

During the development of CTAP-2, it was recognized by graduate student Pritha Bagchi that a water-soluble, high contrast Cu(I)-selective fluorescent probe may be useful for the selective detection of proteins bearing an accessible Cu(I)-binding site after separation by native gel electrophoresis. To test this concept, CTAP-2 was applied to a native PAGE gel containing the copper chaperone protein Atox1. Remarkably, CTAP-2 gave visible fluorescent staining only for the copper-loaded form of the protein and not for the metal-free apo form obtained by treatment with cyanide. CTAP-2 also did not respond to carbonic anhydrase, a zinc protein, or to Cu/Zn superoxide dismutase, which contains a copper site buried within the interior of the protein. These results are shown in Figure 3.9. Note that the diffuse appearance of the protein bands is characteristic of the native PAGE method, which is sensitive to the presence of different isoforms of the same protein and typically exhibits lower resolution than standard SDS-PAGE.

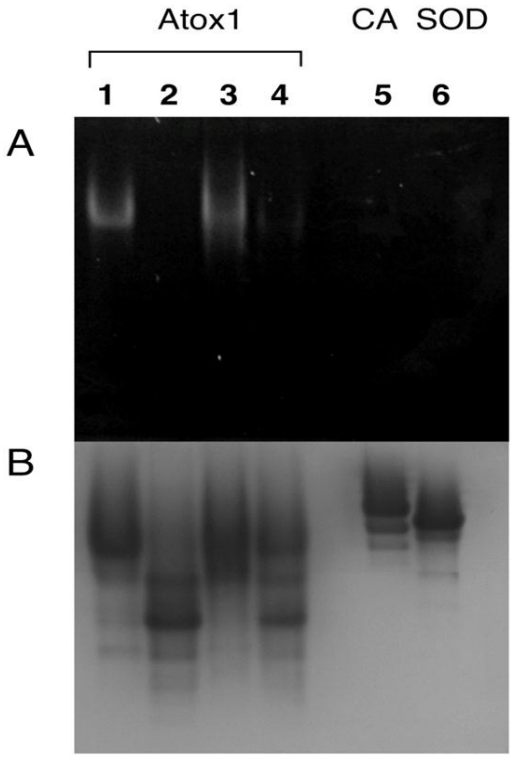

Figure 3.9: Selective in-gel detection of copper-loaded Atox1 with CTAP-2. (A) native PAGE gel incubated with 5 μM CTAP-2, then visualized at 365 nm excitation (emission 537/35 nm BP, UV transillumination mode). (B) same gel stained with Coomassie blue to visualize all proteins. Lane 1: hAtox1 as isolated. Lane 2: hAtox1, KCN. Lane 3: hAtox1, TCEP, $Cu(MeCN)_4PF_6$. Lane 4: hAtox1, TCEP, $Cu(MeCN)_4PF_6$, then KCN. Lane 5: carbonic anhydrase. Lane 6: superoxide dismutase (SOD1). Experiment performed by Pritha Bagchi. Reproduced with permission from Ref. 1. © 2011 American Chemical Society.

Although the results shown in Figure 3.9 indicate that CTAP-2 is able to detect copper bound to the metallochaperone Atox1, the actual detection mechanism is uncertain; the most reliable estimate for the Cu(I)-binding affinity of Atox1 is log $K_{Cu(I)}$ = 17.4,[34] which is one million fold larger than our estimate of log $K_{Cu(I)}$ = 11.4 for CTAP-2. Therefore, CTAP-2 should not be able to extract Cu(I) from its binding site on the protein, and the observed fluorescent species may be a CTAP-2-Cu(I)-Atox1 ternary complex. Such a complex is reasonable given the bidentate coordination mode of Atox1

as well as the macrocycle-Cu(I)-solvent ternary complex formation previously observed with thiazacrown-based probes (Chapter 2).

3.8.2. Preliminary cellular imaging

Despite its hydrophilic nature and the presence of an anionic sulfonate group, CTAP-2 proved to be cell permeant. In live NIH 3T3 mouse fibroblasts grown under copper-supplemented conditions, CTAP-2 gave a perinuclear staining pattern (Figure 3.10) resembling the total copper distribution previously recorded in this cell type by synchrotron X-ray fluorescence microscopy.[9,35]

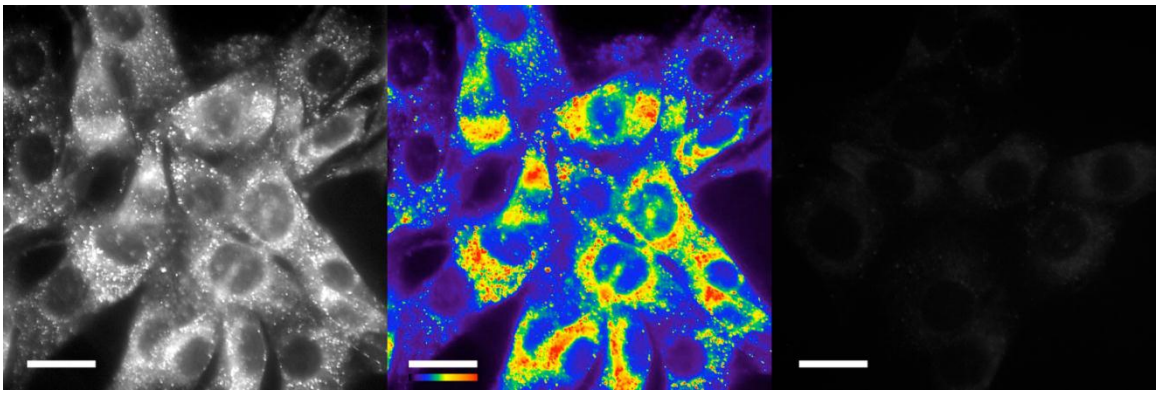

Figure 3.10: Fluorescence micrographs of live copper-supplemented NIH 3T3 cells with and without CTAP-2. Left: Grayscale image of cells incubated with 5 μM CTAP-2 for 1 hour. Center: False color image of the same cells. Right: Control cells not incubated with CTAP-2 showing the cellular autofluorescence background under identical imaging conditions. Scale bar 20 μM. Experiment performed by Pritha Bagchi

Although these preliminary results appear promising, the significance of the observed staining pattern is not yet certain given the considerations of binding affinity and ternary complex formation noted above. Also, the ability of the fluorophore to interact with lipids, which might occur via the uncharged 3-aryl ring, has not yet been investigated. Nevertheless, this experiment with CTAP-2 demonstrates that it is possible

to avoid aggregation in aqueous solution while maintaining cellular permeability using a sulfonated triarylpyrazoline fluorophore platform, a valuable piece of information for the design of future Cu(I) probes.

3.9. Colloidal aggregation of previously reported Cu(I)-selective fluorescent probes

Dynamic light scattering and gel imaging experiments described in this section were conducted by Pritha Bagchi. CS1 and CS3 were synthesized by Jonathan Hofmekler.

As discussed in section 3.1, previously reported Cu(I)-selective fluorescent probes such as CS1[6] and **2.4c**[8] are expected to be too lipophilic to form stable monomeric aqueous solutions at the micromolar concentrations typically employed for fluorescence experiments. Even the carboxylic acid moiety of CTAP-1[9] may be insufficient to prevent aggregation. The aggregation behavior of these probes in aqueous solution, however, had not been experimentally determined. Furthermore, during our studies with CTAP-2, the group that developed CS1 reported the probe Coppersensor-3 (CS3), in which the fluorine atoms of CS1 were replaced by methoxy groups, supposedly resulting in an even higher fluorescence contrast ratio and quantum yield than CTAP-2 upon saturation with Cu(I) in aqueous solution.[36] CS3 also possesses a highly lipophilic structure with no charged functional groups, thus calling into question whether the extensive hydrophilic functionalization of CTAP-2 is actually necessary for reliable Cu(I) sensing in an aqueous environment. Therefore, following the suggestion of a skeptical reviewer during attempted publication of our studies with CTAP-2, we examined the aggregation behavior of the previously reported Cu(I) probes described above and also tested them for the in-gel detection of Atox1 as described for CTAP-2.

Following a widely used procedure for producing aqueous solutions of lipophilic dyes,[9,37] each of the above probes was dissolved in DMSO to a concentration of 1 mM,

then diluted to a concentration of 5 μM in aqueous buffer (10 mM MOPS/K^+ pH 7.2). All of the resulting solutions appeared transparent and homogeneous, but dynamic light scattering experiments revealed the presence of colloidal particles with hydrodynamic radii of 50-100 nm for the previously reported Cu(I) probes (Figure 3.11).

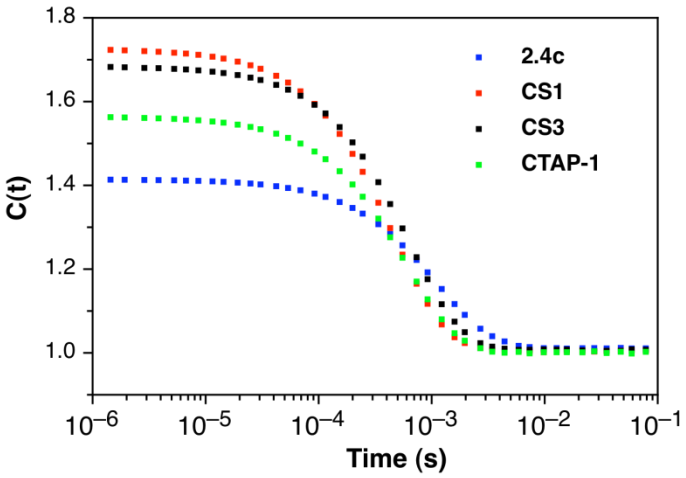

Probe	R_h (nm)[a]	SD (nm)[b]
2.4c	100	12
CS1	49	6
CS3	67	9
CTAP-1	63	6

Figure 3.11: DLS autocorrelation curves and calculated hydrodynamic radii of colloidal particles. [a] Hydrodynamic radius calculated from the Stokes-Einstein relation (averaged over 20 measurements). [b] Standard deviation in calculated R_h. Data acquired by Pritha Bagchi. Adapted with permission from Ref. 1. © 2011 American Chemical Society.

Surprisingly, even the carboxylic acid-functionalized CTAP-1 produced a colloid, and this occurred regardless of whether the stock solution was prepared from the free acid or the potassium salt. Apparently, a single carboxylate group is insufficient to solubilize this relatively large structure to micromolar concentrations. CTAP-2, by contrast, gave no more signal than the background count rate of the buffer, thus confirming the absence of colloidal aggregates. Based on these results, it appears that only CTAP-2 was actually characterized in monomeric form in aqueous solution, and that the photophysical properties previously ascribed to CS1, CS3, and even CTAP-1 are actually due to aggregates, at least in the absence of Cu(I). Therefore, the properties of these lipophilic

probes may be altered by changes in aggregation state in applications involving a mixed-polarity environment, including cellular imaging.

As might be expected based on their colloidal nature in aqueous solution, none of the above previously reported Cu(I)-probes gave detectable selective staining of Cu(I)-loaded hAtox1 in native PAGE gels under the same conditions that were successful with CTAP-2. Therefore, it appears that the substantial effort expended in development of the hydrophilically functionalized CTAP-2 did indeed result in enhanced capabilities for this Cu(I)-selective fluorescent probe.

3.10. Conclusions

Previously reported copper(I)-selective fluorescence turn-on probes based on a lipophilic, thioether-rich ligand coupled to an uncharged fluorophore have a strong propensity to aggregate in aqueous solution, an effect which we long suspected and ultimately proved via dynamic light scattering experiments. Even an ionizable carboxylic acid moiety attached to the fluorophore is not in itself sufficient to prevent aggregation. By combining a polyhydroxylated thiazacrown ligand with a sulfonated triarylpyrazoline fluorophore, we created the highly water-soluble Cu(I)-probe CTAP-2, which is devoid of observable aggregation effects at typical working concentrations of 1-5 μM in aqueous solution, although aggregation can be detected at higher concentrations even for this probe. The balanced solubilization strategy developed for CTAP-2 allows the previously developed strategy of contrast optimization by electronic tuning (Chapter 2) to be deployed in aqueous solution, although in this case CTAP-2 itself turned out to be the optimally tuned member of the probe series. Notably, the change from methanol to water does not adversely affect the tunable PET switching mechamism of triarylpyrazoline-based Cu(I)-probes. In fact, the combination of fluorescence contrast ratio and quantum yield offered by CTAP-2 in aqueous solution (65-fold and 8.3%, respectively) is actually

better than the maximum obtained for its predecessors in methanolic solution (50-fold and 7%, respectively for **2.3d**, see Chapter 2).

The high contrast ratio and aqueous solubility of CTAP-2 allow this probe to be used for the selective in-gel detection of a metallochaperone containing an exchangeable copper(I) site. Although the sensitivity of CTAP-2 itself toward the tested metallochaperone Atox1 is not particularly high, this detection method constitutes an apparently novel and potentially valuable application for Cu(I)-selective fluorescent probes. The existing methods for in-gel detection of copper-containing proteins, laser ablation-ICP-MS[38] and synchrotron-based X-ray fluorescence mapping,[39] are sensitive only to total copper content, whereas Cu(I)-selective fluorescent probes can be used to differentiate the exchangeable Cu(I)-site of a copper trafficking protein from the buried copper site of an enzyme.

CTAP-2 also proved to be cell permeant despite its extensive hydrophilic functionalization, and can be applied for cellular imaging similarly to previous Cu(I) probes such as CTAP-1 and CS1. Recent measurements of the Cu(I) binding affinities of Atox1 and several other copper trafficking proteins, however, give association constants in the range of 10^{17}-10^{19},[40] several orders of magnitude higher than any of the available small molecule Cu(I)-selective fluorescence turn-on probes including CTAP-2. This suggests that intracellular free Cu^{+} concentrations should actually be buffered below the detection limit of any of these probes under normal physiological conditions. Therefore, the interpretation of the observed intracellular staining patterns is uncertain at present and requires further study, ideally with future Cu(I)-probes featuring higher binding affinities.

While CTAP-2 clearly represents an important step in the evolution of Cu(I)-responsive fluorescent probes, it also leaves substantial room for improvement. In addition to the binding affinity considerations mentioned above, the fluorescence quantum yield of Cu(I)-saturated CTAP-2 remains relatively low at 8.3%. By contrast, triarylpyrazoline-based proton probes operating by a similar PET mechanism reach

quantum yields up to 71% in acetonitrile solution,[24] and the 62% quantum yield observed for the difluorinated CTAP-2 derivative **3.3c** under acidic conditions proves that comparable performance is possible even in aqueous solution. The three-fold higher quantum yield of protonated CTAP-2 over the copper-saturated form suggests that a weak Cu(I)-N interaction and associated ternary complex formation as observed for the probes described in Chapter 2 may also limit the fluorescence quantum yield of CTAP-2-Cu(I); however, the quantum yield of protonated CTAP-2 in aqueous solution is approximately half of that shown by its predecessors **2.4b-f** in acidified methanol, suggesting that an additional quenching mechanism is also involved. These limiting factors are investigated in more detail in Chapter 4.

3.11. Experimental Section

3.11.1. Synthesis

General

Materials and reagents: Probe **2.4c**,[7] CTAP-1,[9] CS1,[6] CS3,[36] 5,5-bis(bromo-methyl)-2,2-dimethyl-1,3-dioxane[41] (**3.16)**, and 5-hydroxymethyl-2,2,5-trimethyl-1,3-dio-xane[42] (**3.23)**, were prepared according to published procedures, although the latter is now commercially available. Dry THF (EMD), dry DMSO (EMD), and dry tert-butanol (Alfa Aesar) were used as received. All other reagents and solvents were acquired from standard commercial sources and used as received.

NMR: Spectra were recorded at 400 MHz (^{1}H), 100 MHz (^{13}C), and 376 MHz (^{19}F). Chemical shifts are reported in ppm versus $SiMe_4$ (^{1}H and ^{13}C) or CCl_3F (^{19}F) and are specified at ambient temperature unless noted otherwise. Carbon chemical shifts are referenced indirectly via the solvent chemical shift of 77 ppm ($CDCl_3$) or 49 ppm

(CD_3OD). MS: selected peaks, *m/z*. EI spectra were acquired at 70 eV. IR: NaCl windows (neat or film) or KBr pellet (solids). TLC: 0.25 mm Merck Silica Gel 60 F_{254} visualized under 254 nm illumination or by staining with 5% phosphomolybdic acid in ethanol. Column chromatography: Flash chromatography on Sorbent Technologies standard grade silica gel (70-230 mesh). Reversed-phase HPLC was conducted with a 30 x 1 cm R-18 column at ambient temperature using an elution gradient of 30%-37% MeCN/0.1% aqueous NH_4HCO_3 over 20 minutes. The eluted products were freed of NH_4HCO_3 by repeated dissolution in methanol followed by evaporation under vacuum.

3,3-bis(hydroxymethyl)-1,5-dioxaspiro[5.5]undecane (**3.4**)[15]

Pentaerythritol (24 g, 180 mmol), DMF (240 mL) and benzene (160 mL) were added to a 1 L three-necked flask equipped with a large stir bar, a thermometer, and a rubber septum. The middle neck was then connected to a Dean-Stark trap topped with a reflux condenser and calcium chloride drying tube. The mixture was heated to reflux under stirring (liquid phase 115 °C), and cyclohexanone (12.4 mL, 120 mmol) was added in small portions over 3 hours. The mixture was left at reflux overnight, then allowed to cool and concentrated under reduced pressure. The gummy residue was stirred with water, then extracted with MTBE (4 x 100 mL). The combined extracts were dried and concentrated, and the residue was recrystallized from boiling toluene (220 mL). The product was collected by filtration, washed with hexanes, and dried by suction under warm air to give the product as a colorless, fluffy crystalline powder (14.9 g). After concentration of the mother liquor, a further 1.2 g of crystalline NMR-pure product was collected. Total yield 16.1 g (74 mmol, 61%). mp 125-126°C (first crop). Lit.[15] mp 123-124°C. ^{1}H NMR ($CDCl_3$) δ 1.37-1.43 (m, 2H), 1.49-1.55 (m, 4H), 1.73-1.76 (m, 4H), 2.32 (br. t, J = 4.9 Hz, 2H), 3.73 (s, 4H), 3.76 (br. d, J = 4.8 Hz, 4H).

3-hydroxymethyl-3-methanesulfonyloxymethyl-1,5-dioxaspiro[5.5]undecane (**3.5**)

Diol **3.4** (1.00 g, 4.62 mmol) was dissolved in a mixture of triethylamine (2.0 mL, 3.0 equiv.) and dichloromethane (50 mL) and the solution was cooled under nitrogen in a dry ice-acetone bath (-78°C). Methanesulfonyl chloride (379 µL, 1.06 equiv.) was added dropwise, and the mixture was stirred for 3 hours at -78°C, then allowed to warm slowly to room temperature and washed with a solution of KH_2PO_4 (1.9 g, 3 equiv.) in water (50 mL) to remove excess triethylamine. The organic layer was collected and the aqueous layer was extracted with DCM (25 mL). The combined organic phases were dried with Na_2SO_4 and concentrated under reduced pressure. The residue was separated by column chromatography to give mesylate **3.5** (470 mg, 35%) and bis-mesylate **3.8** (488 mg, 28%). Mesylate **3.5**: ^{1}H NMR ($CDCl_3$) δ 1.38-1.44 (m, 2H), 1.47-1.57 (m, 4H), 1.68-1.71 (m, 2H), 1.79-1.82 (m, 2H), 1.96 (br. t, J = 5.8 Hz, 2H), 3.07 (s, 3H), 3.59 (d, J = 5.8 Hz, 2H), 3.71 (d, J = 12.3 Hz, 2H), 3.79 (d, J = 12.3 Hz, 2H), 4.41 (s, 2H). ^{13}C NMR δ 22.2, 22.3, 25.3, 30.3, 34.2, 36.7, 39.1, 60.98, 61.03, 68.9, 98.6. EI-MS m/z 294 (M^+, 35), 265 (22), 251 (100), 83 (35), 55 (50). EI-HRMS m/z calcd for $C_{12}H_{22}O_6S$ 294.1137, found 294.1135. Bis-mesylate **3.8**: ^{1}H NMR δ 1.38-1.45 (m, 2H), 1.49-1.55 (m, 4 H) 1.73-1.76 (m, 4H), 3.07 (s, 6H), 3.78 (s, 4H), 4.27 (s, 4H).

Attempted synthesis of thioether-diol **3.6** (Scheme 3.4)

A mixture of mesylate **3.5** (328 mg, 1.11 mmol), sodium sulfide nonahydrate (290 mg, 0.55 equiv.), tetrabutylammonium bisulfate (9.3 mg, 2.5 mole %), water (3 mL), and MTBE (10 mL) was stirred under nitrogen overnight. No reaction was apparent by TLC, so the mixture was heated at reflux for four hours. TLC (10:1 DCM-MTBE) then indicated a single major product at R_f 0.46 and traces of UV-active products at R_f >0.9, as well as substantial unreacted starting material (R_f 0.17). The organic layer was collected, and the aqueous layer was extracted with MTBE. The combined organic phases were dried with sodium sulfate and concentrated under reduced pressure, and the residue was separated by column chromatography (DCM-MTBE). The combined minor products

amounted to less than 10 mg of material and were not characterized. The major product was obtained as a colorless solid and identified as the oxetane 7,11,14-trioxadispiro[5.2.3.2]tetradecane (**3.9**). Yield 92.7 mg (468 µmol, 42% relative to **3.5**, 76% relative to $Na_2S \bullet 9\ H_2O$). ^{1}H NMR ($CDCl_3$) δ 1.38-1.43 (m, 2H), 1.50-1.54 (m, 4H), 1.69-1.72 (m, 4 H), 4.03 (s, 4H), 4.46 (s, 4H). ^{13}C NMR ($CDCl_3$) δ 22.4, 25.5, 32.2, 37.9, 65.4, 78.1, 97.9. EI-MS *m/z* 198 (M^+, 55), 169 (25), 155 (100), 83 (58), 55 (70). EI-HRMS *m/z* calcd for $C_{11}H_{18}O_3$ 198.1256, found 198.1262.

Oxetane formation in the presence of a thiol-thiolate mixture (Scheme 3.5)

Mesylate **3.5** (225 mg, 0.679 mmol) and ethanethiol 170 µL, 3 equiv. were dissolved in ethanol (5 mL), and solid lithium hydroxide monohydrate (64 mg, 2 equiv.) was added to the stirred solution. The mixture was refluxed under argon for 3.5 hours then allowed to cool. An aliquot of the mixture was diluted into neutral phosphate buffer (0.5 M KH_2PO_4, 0.5 M Na_2HPO_4, 1 mL), and the resulting suspension was extracted with $CDCl_3$ (2 x 0.7 mL). TLC (10:1 DCM-MTBE) indicated complete consumption of the starting material and formation of two products in comparable abundance, one of which was identical to oxetane **3.9**. The extract was dried with sodium sulfate, filtered through a cotton plug, and concentrated under a stream of argon in a warm water bath to give a colorless oil (16 mg), which was identified as a mixture containing 59 mol% 3-ethylthiomethyl-3-hydroxymethyl-1,5-dioxaspiro[5.5]undecane (**3.10**) and 41 mol% oxetane **3.9** (calculated from the integrated ^{1}H NMR spectrum). Thioether **3.10**: ^{1}H NMR ($CDCl_3$) δ 1.27 (t, J = 7.4 Hz, 3H), 1.38-1.43 (m, 2H), 1.48-1.55 (m, 4H), 1.68-1.72 (m, 2H), 1.78-1.81 (m, 2H), 1.92 (br. t, J = 5.6 Hz, 1H). 2.57 (q, J = 7.4 Hz, 2H), 2.65 (s, 1H), 3.73 (d, J = 11.5 Hz, 2H), 3.73 (overlapping d, $J \approx 6$ Hz, 2H), 3.77 (d, J = 11.5 Hz, 2H). ^{13}C NMR ($CDCl_3$) δ 14.8, 22.5, 25.6, 28.0, 31.2, 33.8, 34.4, 38.7, 63.7, 63.8, 78.2, 98.3. EI-MS *m/z* 260 (M^+, 48), 217 (100), 75 (37), 55 (42). EI-HRMS *m/z* calcd for $C_{13}H_{24}O_3S$ 260.1446, found 260.1453.

Reaction of bromide **3.11** with aqueous sodium sulfide (Scheme 3.6)

Pentaerythritol monobromide (**3.11**) (500.3 mg, 2.51 mmol) and sodium sulfide nonahydrate (302 mg, 0.50 equiv.) were stirred in H_2O (12 mL) under nitrogen for 24 hours. A 0.5 mL aliquot of the mixture was treated with 1 drop of 1% alcoholic phenolphthalein and titrated under a stream of nitrogen to a colorless endpoint with 1 M HCl. The resulting solution, which was neutral to pH paper, was concentrated under reduced pressure. The residue was dissolved in D_2O, filtered , and analyzed by ^{1}H NMR. The product distribution was calculated from the integrated 1H NMR spectrum on the basis of the following signals: Starting material **3.11**: δ 3.49 (s, 2H), 3.60 (s, 6H). Oxetane **3.13**: δ 3.82 (s, 4H), 4.55 (s, 4H). Alkene **3.14**: δ 4.13 (br. s, 4H), 5.17 (br. s, 2H). No other signals were observed except for water and a trace of phenolphthalein. The peak assignments of the starting material were confirmed by comparison to a spectrum of an authentic sample in D_2O. To confirm the identities of the products , the NMR spectrum was also acquired in dry DMSO-d6 as follows: A second aliquot of the reaction mixture was neutralized by bubbling with CO_2 and concentrated to dryness. The residue was stirred with acetone then filtered to remove salts, and the filtrate was concentrated nearly to dryness. The resulting colorless oil was stirred with 1 mL $CDCl_3$, and DMSO-d_6 was added dropwise until the mixture became homogeneous. The solution was concentrated nearly to dryness under a stream of argon in a warm water bath, then diluted with DMSO-d_6 and analyzed by ^{1}H NMR. The identity of the commercially available alkene **3.14** was confirmed by comparison to the ^{1}H NMR spectrum posted by Sigma-Aldrich, and the peaks assigned to oxetane **3.13** are consistent with those previously reported.[43] Starting material **3.11**: δ 3.35 (d, J = 5.3 Hz, 6H), 3.47 (s, 2H), 4.47 (d, J = 5.3 Hz, 3H). Oxetane **3.13**: δ 3.54 (d, J = 5.4 Hz, 4H), 4.27 (s, 4H), 4.76 (t, J = 5.4 Hz, 2H). Alkene **3.14**: δ 3.90 (dt, J = 5.6, 1.4 Hz, 4H), 4.72 (t, J = 5.6 Hz, 2H), 4.97 (p, J = 1.4 Hz, 1H).

7,7-Dimethyl-6,8-dioxa-2-thiaspiro[3.5]nonane (**3.15**)

A mixture of 5,5-bis(bromomethyl)-2,2-dimethyl-1,3-dioxane[41] (**3.16**) (38.67 g, 128 mmol), sodium sulfide nonahydrate (46 g, 1.5 equiv.), sodium bicarbonate (16 g, 1.5 equiv.), potassium iodide (21 g, 1 equiv.), methanol (400 mL) and water (100 mL) was stirred at reflux for 36 hours. The reaction mixture was then concentrated under reduced pressure, diluted with water (250 mL) and extracted with MTBE (3 x 150 mL). The extract was dried with $MgSO_4$, concentrated under reduced pressure, and the residue was crystallized from MTBE-hexane to give the product as colorless crystals. Yield 17.65 g (101 mmol, 79%). Mp 54-55°C (Lit.[41] 51-52°C). ^{1}H NMR ($CDCl_3$, 400 MHz) δ 1.39 (s, 6H), 2.97 (s, 4H), 3.88 (s, 4H). ^{13}C NMR ($CDCl_3$, 100 MHz) δ 23.5, 30.8, 41.0, 68.3, 97.7. IR (KBr pellet) 2998, 2933, 2864, 1370, 1269, 1197, 1116, 1064, 1029, 931, 825, 731 661 cm^{-1}. EI-MS *m/z* 174 (38, $[M]^+$), 159 (100), 99 (68), 85 (63), 59 (48). EI-HRMS *m/z* calcd for $[M]^+$ $C_8H_{14}O_2S$ 174.0715, found 174.0727.

5-((Benzylthio)methyl)-5-(bromomethyl)-2,2-dimethyl-1,3-dioxane (**3.17**).

A mixture of thietane **3.15** (6.63 g, 38.0 mmol), benzyl bromide (6.64 g, 38.8 mmol), and potassium carbonate (100 mg, 0.02 equiv) in acetonitrile (13 mL) was stirred at 60°C in a sealed flask under argon for 2 days and then concentrated under reduced pressure. The residue was taken up in dichloromethane (100 mL), stirred with 2 g silica gel, and filtered through a 2 x 2 cm pad of silica gel. The silica gel was washed with 100 mL of dichloromethane, and the combined filtrate and washing were concentrated under reduced pressure go give the product as a colorless oil. Yield 13.01 g (37.6 mmol, 99%). ^{1}H NMR ($CDCl_3$) δ 1.38 (s, 3H), 1.39 (s, 3H), 2.60 (s, 2H), 3.63 (s, 2H), 3.72 (s, 4H), 3.75 (s, 2H), 7.22-7.36 (m, 5H). ^{13}C NMR ($CDCl_3$) δ 22.4, 24.7, 34.1, 37.1, 37.8, 37.9, 65.5, 98.5, 127.2, 128.5, 128.9, 138.0. IR (neat) 2979, 2939, 2852, 1668, 1590, 1555,

1520, 1402, 1367, 1350, 1190, 1165, 1114, 1086, 1033, 843, 813, 739, 603, 521 cm^{-1}. EI-MS *m/z* 344 (10, $[M]^+$), 329 (13), 286 (21), 189 (21), 91 (100). EI-HRMS *m/z* calcd for $[M]^+$ $C_{15}H_{21}BrO_2S$ 344.0446, found 344.0435.

Bis((5-((benzylthio)methyl)-2,2-dimethyl-1,3-dioxan-5-yl)methyl)sulfane (**3.18**).

To a stirred solution of bromide **3.17** (11.95 g, 34.6 mmol) and potassium iodide (5.74 g, 34.6 mmol) in DMF (50 mL) was added sodium sulfide nonahydrate (5.0 g, 0.6 equiv.) in water (10 mL) followed by additional DMF (20 mL) and the mixture was stirred under nitrogen at 90°C for 20 hours. After cooling, the mixture was poured into water (300 mL) and extracted with MTBE (150 mL). The extract was washed sequentially with water (300 mL + 5 mL brine), 2.5% NaOH solution (2 x 200 mL), and brine (25 mL), dried with sodium sulfate, stirred with 3 g silica gel, filtered, and concentrated under reduced pressure to give the product as a pale yellow oil. Yield 9.02 g (16.0 mmol, 93%). ^{1}H NMR ($CDCl_3$) δ 1.38 (s, 6H), 1.40 (s, 6H), 2.62 (s, 4H), 2.72 (s, 4H), 3.68 (d, *J* = 9.1 Hz, 4H), 3.70 (d, *J* = 9.1 Hz, 4H), 3.72 (s, 4H), 7.21-7.34 (m, 10H). ^{13}C NMR ($CDCl_3$) δ 23.7, 23.8, 34.5, 37.7, 37.9, 38.2, 66.1, 98.3, 127.0, 128.4, 128.9, 138.2. IR (neat) 2990, 2938, 2863, 1494, 1452, 1383, 1371, 1251, 1194, 1153, 1115, 1090, 1056, 1036, 836, 731, 701, 521 cm^{-1}. EI-MS *m/z* 562 (2, $[M]^+$), 561 (6), 471 (55) 297 (22), 265 (36), 181 (34), 91 (100). EI-HRMS *m/z* calcd for $[M-1]^+$ $C_{30}H_{41}O_4S_3$ 561.2167, found 561.2177.

Bis((5-mercaptomethyl-2,2-dimethyl-1,3-dioxan-5-yl)methyl)sulfane (**3.19**)

A 1L 3-neck flask equipped with a stir bar, dry ice condenser, thermometer, and two gas inlets was charged with thioether **3.18** (8.92 g, 15.8 mmol) and THF (150 mL) under nitrogen and cooled in a dry ice/acetone bath. Anhydrous ammonia was then condensed into the stirred mixture until the total volume reached 300 mL. The inlet used

for ammonia was then removed and sodium metal (1.46 g, 4 equiv.) was added in small pieces against a gentle flow of nitrogen at a rate sufficient to maintain the temperature of the reaction mixture between -70 and -60°C. After addition was complete, the dark blue mixture was allowed to stir for 15 minutes and then quenched with ammonium chloride (8.5 g, 10 equiv). The open neck of the reaction flask was then sealed, the dry ice bath was removed, and the ammonia was carefully boiled off using a warm water bath. *Note: the ammonia gas exiting the top of the condenser was collected with an ice-cooled mixture of 500 mL concentrated HCl and 2.5 L water to prevent release to the atmosphere*. Sodium hydroxide solution (5% w/v, 130 mL, 10 equiv.) was then added, and the resulting mixture was diluted with water (200 mL), washed with MTBE (150 mL), and neutralized with citric acid (12.2 g, 4 equiv.), causing the crude product to separate as a yellow oil. The mixture was extracted with MTBE (3 x 100 mL) and the combined extracts were dried with $MgSO_4$, concentrated, and purified by column chromatography (hexane-MTBE) to give the product as a colorless oil. Yield 5.02 g (13.1 mmol, 83%). ^{1}H NMR ($CDCl_3$) δ 1.31 (t, J = 9.1 Hz, 2H), 1.40 (s, 6H), 1.42 (s, 6H), 2.73 (d, J = 9.1 Hz, 4H), 2.74 (s, 4H), 3.70 (d, J = 11.7 Hz, 4H), 3.76 (d, J = 11.7 Hz, 4H). ^{13}C NMR ($CDCl_3$) δ 23.2, 24.1, 27.2, 36.6, 37.7, 65.8, 65.9, 98.3. IR (neat) 2990, 2938, 2863, 2556, 1451, 1419, 1371, 1254, 1195, 1153, 1119, 1065, 934, 832, 729, 521 cm^{-1}. EI-MS *m/z* 382 (60, $[M]^+$), 309 (36), 207 (75), 149 (80), 117 (56), 99 (72), 87 (93), 59 (100). EI-HRMS *m/z* calcd for $[M]^+$ $C_{16}H_{30}O_4S_3$ 382.1306, found 382.1299.

4-(Bis(2-iodoethyl)amino)benzaldehyde (**3.20**)

To a solution of N-phenyldiethanolamine (17.36 g, 95.8 mmol) in DMF (33 mL) was added a cooled solution of phosphorus oxychloride (40 mL, 4.5 equiv.) in DMF (67 mL, 9 equiv.) and the resulting mixture was stirred at 90°C for 4 hours. After cooling to room temperature, the mixture was poured over crushed ice, neutralized with an ice cold

solution of NaOH (70 g, 18 equiv.) in water (200 mL), and stirred for 1 hour at 0°C. The precipitated product was then collected by filtration and recrystallized from ethanol to give the intermediate 4-(bis(2-chloroethyl)amino)benzaldehyde as tan needles. Yield 21.02 g (85.4 mmol, 89%). Mp 88-89°C (Lit.[44] 85-88°C). ^{1}H NMR ($CDCl_3$) δ 3.68 (t, *J* = 6.9 Hz, 4H), 3.84 (t, *J* = 6.9 Hz, 4H), 6.75 (d, *J* = 9.0 Hz, 2H), 7.77 (d, *J* = 9.0 Hz, 2H), 9.78 (s, 1H). ^{13}C NMR ($CDCl_3$) δ 40.0, 53.3, 111.3, 126.7, 132.3, 150.9, 190.1. IR (KBr pellet) 2964, 2746, 1668, 1592, 1560, 1521, 1405, 1361, 1285, 1167, 1140, 962, 819, 750, 715, 605 cm^{-1}. EI-MS *m/z* 245 (28, $[M]^+$), 196 (100), 132 (34), 77 (27), 63 (35). EI-HRMS *m/z* calcd for $[M]^+$ $C_{11}H_{13}Cl_2NO$ 245.0374, found 245.0384.

A solution of 4-(bis(2-chloroethyl)amino)benzaldehyde (9.60 g, 39.0 mmol) and sodium iodide (17.5 g, 3 equiv.) in butanone (60 mL) was stirred at 65°C for 24 hours. The mixture was then allowed to cool, diluted with acetone (100 mL), stirred with 6 g activated carbon, filtered through Celite, and concentrated. The residue was taken up in dichloromethane (200 mL), filtered to remove salts, concentrated, and crystallized from methanol (300 mL) under stirring to give the product as a light green crystalline powder. Yield 10.46 g (24.4 mmol, 63%). Mp 109-109.5°C (Lit.[44] 105-107°C). ^{1}H NMR ($CDCl_3$) δ 3.25 (t, *J* = 8.0 Hz, 4H), 3.85 (t, *J* = 8.0 Hz, 4H), 6.70 (d, *J* = 8.9 Hz, 2H), 7.78 (d, *J* = 8.9 Hz, 2H), 9.79 S, 1H). ^{13}C NMR (CDCl3) δ -0.1, 53.8, 111.1, 126.9, 132.4, 150.2, 190.1. IR (KBr pellet) 2969, 2930, 1665, 1592, 1557, 1517, 1393, 1164, 816 622 cm^{-1}. EI-MS *m/z* 429 (48, $[M]^+$), 302 (42), 288 (100), 155 (52), 147 (42), 133 (44), 91 (32), 77 (33). EI-HRMS *m/z* calcd for $[M]^+$ $C_{11}H_{13}I_2NO$ 428.9087, found 428.9095.

Macrocycle **3.21**

Solutions of dithiol **3.19** (4.87 g, 12.7 mmol) and diiodide **3.20** (5.46 g, 12.7 mmol) in DMF were added simultaneously by syringe pump to a stirred mixture of cesium carbonate (12.4 g, 3 equiv.) in DMF (880 mL) and water (20 mL) under argon at

85°C over a period of 24 hours. The mixture was concentrated to dryness, and the residue was taken up in toluene (200 mL), filtered, and concentrated. The product was isolated by column chromatography (4:1 to 1:1; hexane/ethyl acetate) and recrystallized from methanol to give colorless crystals. Yield 5.12 g (9.21 mmol, 72%). Mp 197-199°C. ^{1}H NMR ($CDCl_3$) δ 1.41 (s, 6H), 1.43 (s, 6H), 2.78 (s, 4H), 2.84 (t, *J* = 6.9 Hz, 4H), 2.86 (s, 4H), 3.69 (d, *J* = 11.8 Hz, 4H), 3.74 (d, *J* = 11.8 Hz, 4H), 3.79 (t, *J* = 6.9 Hz, 4H), 6.66 (d, *J* = 8.9 Hz, 2H), 7.74 (d, *J* = 8.9 Hz, 2H), 9.75 (s, 1H). ^{13}C NMR ($CDCl_3$) δ 22.7, 24.3, 29.9, 33.8, 35.9, 37.6, 52.4, 66.9, 98.5, 111.1, 125.6, 132.1, 151.2, 190.0. IR (KBr pellet) 2983, 2943, 1669, 1593, 1521, 1369, 1192, 1167, 1116, 846, 816 cm^{-1}. EI-MS *m/z* 555 (61, $[M]^+$), 540 (46), 349 (33), 206 (60), 202 (92), 193 (53), 175 (58), 160 (100), 147 (97), 133 (80), 117 (73), 99 (50), 85 (73). EI-HRMS *m/z* calcd for $[M]^+$ $C_{27}H_{41}NO_5S_3$ 555.2147, found 555.2158.

(2,2,5-Trimethyl-1,3-dioxan-5-yl)methyl 4-fluorobenzenesulfonate (**3.24a**)

A solution of 4-fluorobenzenesulfonyl chloride (4.84 g, 24.9 mmol) in acetonitrile (12 mL) was added to a stirred solution of 5-hydroxymethyl-2,2,5-trimethyl-1,3-dioxane[42] (**3.23)** (5.98 g, 37.3 mmol) in pyridine (20 mL, 10 equiv.). After stirring overnight, the mixture was quenched with water (10 mL), diluted with methanol (100 mL), and slowly diluted with crushed ice under rapid stirring until the product began to crystallize. The mixture was then stirred for 3 hours at room temperature followed by 1 hour at 0°C. The product was collected by filtration and washed with water to give a colorless crystalline powder. Yield 6.90 g (21.7 mmol, 87%). Mp 64-65°C. ^{1}H NMR ($CDCl_3$) δ 0.82 (s, 3H), 1.22 (s, 3H), 1.38 (s, 3H), 3.52 (dt, *J* = 12.1, 1.0 Hz, 2H), 3.59 (dt, *J* = 12.1, 1.0 Hz, 2H), 4.13 (s, 2H), 7.21-7.27 (m, 2H), 7.93-7.98 (m, 2H). ^{13}C NMR ($CDCl_3$) δ 17.1, 18.9, 28.0, 33.9, 65.5, 72.9, 98.1, 116.5 (d, J_{CF} = 22.8 Hz), 130.8 (d, J_{CF} = 9.6 Hz), 131.7 (d, J_{CF} = 3.3 Hz), 165.7 (d, J_{CF} = 256.5 Hz). ^{19}F NMR ($CDCl_3$) δ –

103.26 (tt, *J* = 8.2, 5.0 Hz, 1F). IR (KBr pellet) 3434 (br), 2971, 2996, 2878, 1601, 1591, 1494, 1371, 1360, 1187, 1157, 967, 863, 845, 675, 552 cm^{-1}. EI-MS *m/z* 318 (100, $[M–CH_3]^+$), 230(12), 159 (50), 95 (47), 83 (35), 71 (38), 59 (49). EI-HRMS *m/z* calcd for $[M–CH_3]^+$ $C_{13}H_{16}FO_5S$ 303.0702, found 303.0712.

(2,2,5-Trimethyl-1,3-dioxan-5-yl)methyl 3,4-difluorobenzenesulfonate (**3.24b**)

Synthesized as described for **3.24a** using 3.70 g (17.4 mmol) of 3,4-difluoro-benzenesulfonyl chloride to give the product as a colorless crystalline powder. Yield 5.04 g (15.0 mmol, 86%). Mp 54-55°C. ^1H NMR ($CDCl_3$) δ 0.82 (s, 3H), 1.24 (s, 3H), 1.38 (s, 3H), 3.51 (dt, *J* = 12.1, 1.1 Hz, 2H), 3.60 (dt, *J* = 12.2, 1.1 Hz, 2H), 4.17 (s, 2H), 7.37 (ddd, *J* = 9.5, 8.7, 7.4 Hz, 1H), 7.73 (dddd, *J* = 8.6, 3.9, 2.2, 1.5 Hz, 1H), 7.78 (ddd, *J* = 9.3, 7.1, 2.2 Hz, 1H). ^{19}F NMR ($CDCl_3$) δ –128.02 (dddd, *J* = 20.8, 9.7, 7.1, 4.6 Hz, 1F), –133.52 (dt, *J* = 20.4, 7.6 Hz, 1F). IR (KBr pellet) 3092, 2996, 2961, 2876, 1613, 1512, 1374, 1363, 1279, 1210, 1183, 1088, 1078, 969, 962, 917, 852, 840, 680, 618, 582 cm^{-1}. EI-MS *m/z* 336 (100, $[M–CH_3]^+$), 248 12), 177 (37), 113 (36), 85 (26), 71 (30), 59 (52). EI-HRMS *m/z* calcd for $[M–CH_3]^+$ $C_{13}H_{15}F_2O_5S$ 321.0608, found 321.0605.

(2,2,5-Trimethyl-1,3-dioxan-5-yl)methyl 3,4,5-trifluorobenzenesulfonate (**3.24c**)

3,4,5-trifluorobenzenesulfonyl chloride (2.34 g, 10.1 mmol) was added to a solution of 5-hydroxymethyl-2,2,5-trimethyl-1,3-dioxane[42] (**3.23)** (1.8 g, 1.1 equiv.) and triethylamine (2.1 mL, 1.5 equiv.) in dichloromethane (10 mL) and the mixture was stirred for 4 hours at room temperature. The mixture was then quenched with water and extracted with MTBE (50 mL). The extract was washed with 1 M monosodium phosphate (2 x 25 mL), dried with $MgSO_4$, and concentrated under reduced pressure. The residue was recrystallized from MTBE-hexane to give the product as a colorless crystalline powder. Yield 2.11 g (59%, 5.95 mmol). Mp 87-90°C. ^1H NMR ($CDCl_3$) δ

0.83 (s, 3H), 1.25 (s, 3H), 1.38 (s, 3H), 3.48 (dt, *J* = 12.3, 1.2 Hz, 2H), 3.60 (dt, *J* = 12.3, 12. Hz, 2H), 4.21 (s, 2H), 7.61 (t, *J* = 6.3 Hz, 2H). ^{19}F NMR ($CDCl_3$) δ –129.57 (dd, *J* = 19.9, 6.4 Hz, 2F), –150.49 (tt, *J* = 19.9, 6.2 Hz, 1F). IR (KBr pellet) 3082, 2940, 2993, 2882, 1609, 1526, 1441, 1368, 1328, 1180, 1087, 1049, 959, 922, 852, 827, 619, 517 cm^{-1}. EI-MS *m/z* 339 (100, $[M–CH_3]^+$), 266(12), 195 (30), 131 (31), 85 (24), 71 28), 59 (65). EI-HRMS *m/z* calcd for $[M]^+$ $C_{13}H_{14}F_3O_5S$ 339.0514, found 339.0520.

Arylhydrazine **3.25a**

A solution of **3.24a** (1.96 g, 6.16 mmol) and hydrazine hydrate (1.2 mL, 4 equiv.) in DMSO (5 mL) was stirred under argon for 3 hours at 50°C. An additional 1.2 mL hydrazine hydrate and 5 mL DMSO were then added, and the mixture was stirred for an additional 3 hours at 50°C. The reaction mixture was then diluted with water until slightly turbid, stirred at 0°C until crystals appeared, diluted slowly with 170 mL water plus 20 mL methanol, and stirred at 0°C for 1 hour. The product was collected by filtration and washed with cold water to give an off-white crystalline powder. Yield 1.78 g (5.39 mmol, 87%). Mp 115-116°C. ^{1}H NMR ($CDCl_3$) δ 0.82 (s, 3H), 1.26 (s, 3H), 1.38 (s, 3H), 3.56 (s, 4H), 3.69 (s, (br), 2H), 4.04 (s, 2H), 5.73 (s, (br), 1H), 6.87 (d, *J* = 8.9 Hz, 2H), 7.72 (d, *J* = 8.9 Hz, 2H). ^{13}C NMR ($CDCl_3$) δ 17.3, 19.6, 27.4, 33.9, 65.7, 72.1, 98.0, 110.9, 123.4, 130.0, 155.0. IR (KBr pellet) 3330, 2993, 2960, 1632, 1594, 1382, 1375, 1349, 1207, 1186, 1164, 1095, 1082, 975, 824, 810, 692, 568 cm^{-1}. EI-MS *m/z* 330 (29, $[M]^+$), 315 (37), 188 (100), 171 (48), 107 (39), 106 (41). EI-HRMS *m/z* calcd for $[M]^+$ $C_{14}H_{22}N_2O_5S$ 330.1249, 330.1266.

Arylhydrazine **3.25b**

To a stirred solution of **3.24b** (2.22 g, 6.60 mmol) in DMSO (10 mL) was added hydrazine hydrate (2.6 mL, 8 equiv.). The rapidly warming mixture was quickly placed in

a cool water bath, then stirred overnight. The mixture was diluted 1:1 with an equal volume of water, stirred at 0°C, poured into 100 mL of ice water to induce crystallization, diluted with 60 mL methanol to redissolve amorphous material, and then slowly diluted with ice water to 220 mL under continuous stirring. The product was collected by filtration and washed with water to give an off-white crystalline powder. Yield 2.18 g (6.26 mmol, 95%). Mp 132-133°C. ^{1}H NMR ($CDCl_3$) δ 0.82 (s, 3H), 1.26 (s, 3H), 1.38 (s, 3H), 3.55 (dt, *J* = 12.1, 1.1 Hz, 2H), 3.57 (dt, *J* = 12.1, 1.1 Hz, 2H), 3.69 (d (br), *J* = 2.1 Hz, 2H), 4.07 (s, 2H), 5.88 (s (br), 1H), 7.27 (t, *J* = 8.3 Hz, 1H), 7.48 (dd, *J* = 11.1, 2.0 Hz, 1H), 7.63 (ddt, *J* = 8.6, 2.0, 0.8 Hz, 1H). ^{13}C NMR ($CDCl_3$) δ 17.2, 19.3, 27.6, 33.8, 65.6, 72.4, 98.0, 111.6 (d, J_{CF} = 3.8 Hz), 114.4 (d, J_{CF} = 21.1 Hz), 122.3 (d, J_{CF} = 6.7 Hz), 125.9 (d, J_{CF} = 3.0 Hz), 143.8 (d, J_{CF} = 9.6 Hz), 148.6 (d, J_{CF} = 243.5 Hz). ^{19}F NMR ($CDCl_3$) δ –135.37 (dddd, *J* = 11.1, 8.1, 3.1, 0.6 Hz, 1F). IR (KBr pellet) 3343, 2988, 2883, 1635, 1605, 1522, 1375, 1363, 1349, 1202, 1163, 1087, 1000, 974, 912, 839, 806, 677, 574 cm^{-1}. EI-MS *m/z* 348 (32, $[M]^+$), 333 (42), 290 (25), 260 (30), 206 (100), 189 (40), 125 (40), 108 (33), 85 (34). EI-HRMS *m/z* calcd for $[M]^+$ $C_{14}H_{21}FN_2O_5S$ 348.1155, found 348.1158.

Arylhydrazine **3.25c**

To a stirred solution of **3.24c** (1.31 g, 3.70 mmol) in acetonitrile (5 mL) was added potassium carbonate (770 mg, 1.5 equiv.), followed by hydrazine hydrate (270 µL, 1.5 equiv.) and the resulting biphasic mixture was stirred at room temperature overnight. The mixture was then poured into water (100 mL) and extracted with dichloromethane (3 x 25 mL). The combined extracts were dried with Na_2SO_4 and concentrated under reduced pressure. The residue was crystallized from dichloromethane-EtOAc-hexane to give the product as a colorless crystalline powder. Yield 1.02 g (2.78 mmol, 75%). Mp 112-115°C. ^{1}H NMR ($CDCl_3$) δ 0.82 (s, 3H), 1.27 (s, 3H), 1.39 (s, 3H), 3.52 (dt, *J* =

12.1, 1.0 Hz, 2H), 3.59 (dt, *J* = 12.1, 1.0 Hz, 2H), 4.05 (d (br), *J* = 3.8 Hz, 2H), 4.14 (s, 2H), 5.53 (s (br), 1H), 7.37-7.47 (m, 2H). ^{19}F NMR ($CDCl_3$) δ –127.49 - –127.38 (m, 2F). IR (KBr pellet) 3369, 3303, 2992, 2874, 1613, 1512, 1437, 1365, 1302, 1207, 1178, 1089, 1084, 1032, 970, 920, 837, 801, 606, 520 cm^{-1}. EI-MS *m/z* 366 (27, $[M]^+$), 308 (28), 278 (30), 224 (100), 207 (23), 159 (26), 143 (50), 85 (38), 59 (38). EI-HRMS *m/z* calcd for $[M]^+$ $C_{14}H_{20}F_2N_2O_5S$ 366.1061, found 366.1075.

Chalcone **3.26**

A solution of aldehyde **3.21** (2.04 g, 3.67 mmol), 4-cyanoacetophenone (543 mg, 3.74 mmol) and pyrrolidine (0.6 mL, 2 equiv.) in 1:1 benzene-ethanol (15 mL) was stirred at 50°C for 2 days. The reaction mixture was then diluted with ethanol (15 mL), concentrated to 15 mL total volume, diluted with an additional ethanol (15 mL), and stirred at 0°C for 4 hours. The product was collected by filtration as a bright orange crystalline powder. Yield 2.30 g (92%). Mp 197-201°C. ^{1}H NMR ($CDCl_3$) δ 1.41 (s, 6H), 1.43 (s, 6H), 2.78 (s, 4H), 2.84 (t, *J* = 6.9 Hz, 4H), 2.83 (s, 4H), 3.70 (d, *J* = 11.8 Hz, 4H), 3.74 (d, *J* = 11.8 Hz, 4H), 3.76 (t, *J* = 7.9 Hz, 4H), 6.64 (d, *J* = 8.9 Hz, 2H), 7.25 (d, *J* = 15.4 Hz, 1H), 7.54 (d, *J* = 8.9 Hz, 2H), 7.782 (d, *J* = 8.6 Hz, 2H), 7.784 (d, *J* = 15.4 Hz, 1H), 8.05 (d, *J* = 8.5 Hz, 2H). ^{13}C NMR ($CDCl_3$) δ 22.7, 24.3, 30.0, 33.7, 35.9, 37.6, 52.3, 66.8, 98.4, 111.7, 115.1, 116.0, 118.1, 122.5, 128.5, 131.0, 132.2, 142.2, 146.9, 149.0, 188.7. IR (KBr pellet) 2988, 2939, 2229, 1650, 1571, 1517, 1343, 1213, 1173, 1033, 810 cm^{-1}. EI-MS *m/z* 682 (75, $[M]^+$),320 (38), 287 (70), 274 (100), 261 (49), 117 (47), 83 (47). EI-HRMS *m/z* calcd for $[M]^+$ $C_{36}H_{46}N_2O_5S_3$ 682.2569, found 682.2592.

Triarylpyrazoline **3.27a**

A mixture of chalcone **3.26** (540 mg, 0.791 mmol), arylhydrazine **3.25a** (392 mg, 1.18 mmol), pyridinium *p*-toluenesulfonate (200 mg, 1 equiv.) and pyridine (1.9 mL) was

stirred in a sealed flask under argon at 90°C for 6 hours. After cooling to room temperature, the reaction mixture was diluted with 10 mL dichloromethane followed by 10 mL xylenes and concentrated under reduced pressure. The residue was taken up in acetone (20 mL). 2,2-dimethoxypropane (2 mL) was added followed by *p*-toluenesulfonic acid monohydrate (600 mg, 4 equiv.), and the mixture was stirred for 30 minutes at room temperature. It was then made basic with 20% aqueous ammonia (1 mL), poured into water (140 mL) + brine (5 mL), and extracted with MTBE (3 x 25 mL). The combined extracts were dried with $MgSO_4$, concentrated under reduced pressure, and subjected to sequential column chromatography with hexane-ethyl acetate (2:1) followed by benzene-MTBE (7:1) to give the product as a yellow glassy solid. Yield 462 mg (0.464 mmol, 59%). ^{1}H NMR ($CDCl_3$) δ 0.81 (s, 3H), 1.22 (s, 3H), 1.37 (s, 3H), 1.39 (s, 6H), 1.42 (s, 6H), 2.76 (s, 4H), 2.77 (t, *J* = 7.5 Hz, 4H), 2.82 (s, 4H), 3.18 (dd, *J* = 17.4, 5.7 Hz, 1H), 3.55 (s, 4H), 3.64 (t, *J* = 7.2 Hz, 4H), 3.68 (d, *J* = 11.8 Hz, 4H), 3.73 (d, *J* = 11.8 Hz, 4H), 3.84 (dd, *J* = 17.2, 12.2 Hz, 1H), 4.03 (s, 2H), 5.35 (dd, *J* = 12.2, 5.7 Hz, 1H), 6.55 (d, *J* = 8.9 Hz, 2H), 7.06 (d, *J* = 8.9 Hz, 2H), 7.16 (d, *J* = 9.0 Hz, 2H), 7.67 (d, *J* = 8.7 Hz, 2H), 7.69 (d, *J* = 9.0 Hz, 2H), 7.81 (d, *J* = 8.7 Hz, 2H). ^{13}C NMR ($CDCl_3$) δ 17.3, 19.6, 22.9, 24.3, 27.5, 30.1, 33.7, 33.9, 36.1, 37.8, 43.1, 52.4, 63.5, 65.6, 65.7, 67.0, 72.1, 98.0, 98.5, 112.0, 112.3, 113.0, 118.6, 124.4, 126.3, 126.8, 127.8, 129.5, 132.3, 136.3, 146.5, 147.4, 147.6. IR (KBr pellet) 2990, 2937, 2866, 2225, 1611, 1594, 1519, 1500, 1372, 1354, 1192, 1169, 1091, 971, 828, 620 cm^{-1}.

Triarylpyrazoline **3.27b**

A mixture of chalcone **3.26** (610 mg, 0.893 mmol), arylhydrazine **3.25b** (342 mg, 0.982 mmol, 1.1 equiv.), pyridinium *p*-toluenesulfonate (220 mg, 1 equiv.) and pyridine (1.8 mL) was stirred under argon at 80°C for 16 hours. A further 156 mg (0.448 mmol, 0.5 eq) of **3.25b** were added, and the mixture was stirred at 80°C for a further 18 hours

and then at 100°C for 4 hours. The mixture was worked up analogously to **3.27a** to give the product as a yellow glassy solid. Yield 327 mg (0.323 mmol, 36%). ^{1}H NMR ($CDCl_3$) δ 0.78 (s, 3H), 1.24 (s, 3H), 1.38 (s, 3H), 1.39 (s, 6H), 1.42 (s, 6H), 2.74 (t, *J* = 7.3 Hz, 4H), 2.75 (s, 4H), 2.79 (s, 4H), 3.26 (dd, *J* = 17.2, 3.7 Hz, 1H), 3.53-3.61 (m, 8H), 3.67 (d, *J* = 11.8 Hz, 4H), 3.72 (d, *J* = 11.8 Hz, 4H), 3.78 (dd, *J* = 17.2, 11.8 Hz, 1H), 4.08 (s, 2H), 5.74 (dt, *J* = 11.7, 3.7 Hz, 1H), 6.44 (d, *J* = 8.9 Hz, 2H), 6.97 (d, *J* = 8.7 Hz, 2H), 7.42 (dd, *J* = 12.2, 2.0 Hz, 1H), 7.57 (dd, *J* = 8.7, 2.0 Hz, 1H), 7.69 (d, *J* = 8.6 Hz, 2H), 7.79 (t, *J* = 8.1 Hz, 1H), 7.84 (d, *J* = 8.6 Hz, 2H). ^{13}C NMR ($CDCl_3$) δ 17.1, 19.3, 22.9, 24.3, 27.7, 30.1, 33.5, 33.9, 36.0, 37.7, 42.7, 52.3, 65.50, 65.55, 65.59, 66.9, 72.6, 98.0, 98.5, 111.8, 112.2, 116.7 (d, J_{CF} = 16.7 Hz), 118.6, 118.8 (d, J_{CF} = 3.8 Hz), 125.0 (d, J_{CF} = 2.5 Hz), 126.0 (d, J_{CF} = 6.6 Hz), 126.4, 126.8, 128.3, 132.4, 136.2, 137.0 (d, J_{CF} = 8.6 Hz), 146.4, 148.8 (d, J_{CF} = 248.8 Hz), 148.5. ^{19}F NMR ($CDCl_3$) δ –122.99 (ddd, *J* = 11.9, 7.9, 3.8 Hz, 1F). IR (KBr pellet) 2990, 2938, 2866, 2226, 1602, 1519, 1372, 1254, 1174, 1089, 969, 839, 695, 600, 558, 521 cm^{-1}.

Triarylpyrazoline **3.27c**

A mixture of chalcone **3.26** (359 mg, 0.526 mmol), arylhydrazine **3.25c** (269 mg, 0.734 mmol, 1.4 equiv.), pyridinium *p*-toluenesulfonate (203 mg, 1.5 equiv.) and pyridine (1.3 mL) was stirred under argon at 90°C for 16 hours. A further 95 mg (0.26 mmol, 0.5 equiv.) of **3.25c** were added, and the mixture was stirred for 100°C for 8 hours. The reaction mixture was worked up analogously to **3.27a** to give the product as a pale yellow glassy solid. Yield 51 mg (0.049 mmol, 9%). ^{1}H NMR ($CDCl_3$) δ 0.78 (s, 3H), 1.27 (s, 3H), 1.387 (s, 3H), 1.391 (s, 6H), 1.42 (s, 6H), 2.73-2.75 (m, 8H), 2.80 (s, 4H), 3.25 (dd, *J* = 17.1, 6.3 Hz, 1H), 3.50-3.62 (m, 8H), 3.66-3.76 (m, 9H), 4.13 (2H), 5.63 (dd, *J* = 12.0, 6.3 Hz, 1H), 6.46 (d, *J* = 8.9 Hz, 2H), 7.06 (d, *J* = 8.8 Hz, 2H), 7.36 (d, *J* = 6.9 Hz,

2H), 7.67 (d, *J* = 8.2 Hz, 2H), 7.78 (d, *J* = 8.7 Hz, 2H). ^{19}F NMR ($CDCl_3$) δ –115.24 (d, *J* = 7.4 Hz, 2F).

Probe **3.3a** (CTAP-2)

Intermediate **3.27a** (332 mg, 0.333 mmol) was dissolved in a mixture of 90% TFA and 10% H_2O (w/w, 10 mL) and stirred for 12 minutes at room temperature after complete dissolution. The reaction mixture was then diluted with H_2O (5 mL), stirred for an additional 12 minutes, poured into H_2O (75 mL), rinsed in completely with methanol (10 mL), cooled by adding crushed ice, and made basic with 20% aqueous ammonia (14 mL). The resulting suspension was stirred for 30 minutes at 0°C and the intermediate was then collected by filtration, washed with water, and dried under vacuum to give a yellow powder (281 mg). This product was then dissolved in dry DMSO (0.5 mL) under argon, and the resulting viscous solution was diluted with dry THF (3 mL) followed by dry *tert*-butanol (3 mL) under rapid stirring. Potassium *tert*-butoxide (3.8 mL of a freshly prepared 1M solution in THF, 12 equiv.) was added dropwise. The mixture was stirred for 20 minutes at room temperature, then quenched with acetic acid (275 µL) and diluted with dichloromethane (10 mL). The resulting yellow fluorescent precipitate was filtered off, dried under argon flow, and dissolved in water (10 mL). The solution was acidified with 1 M HCl (5 mL), and the resulting yellow precipitate was collected and crystallized from methanol to give the zwitterionic acid form of the product as a yellow crystalline powder. Yield 156 mg (0.202 mmol, 61%) mp > 200°C (decomposes). An analytical sample of the ammonium salt was obtained by dissolving the acid form in dilute aqueous ammonia and subjecting the resulting solution to reversed phase HPLC to give the product as a yellow glassy solid after evaporation. HPLC t_r = 15.2 min (gradient 0-20 min 30%-37% MeCN/0.1% aqueous NH_4HCO_3). ^{1}H NMR (CD_3OD) δ 2.58 (s, 4H), 2.59 (s, 4H), 2.68 (t, *J* = 7.2 Hz, 4H), 3.01 (dd, *J* = 17.5, 6.0 Hz, 1H), 3.49 (s, 8H), 3.61 (t, *J* = 6.6

Hz, 4H), 3.76 (dd, *J* = 17.5, 12.3 Hz, 1H), 5.36 (dd, *J* = 12.3, 6.0 Hz, 1H), 6.48 (d, *J* = 8.9 Hz, 2H), 6.98 (d, *J* = 8.8 Hz, 2H), 7.10 (d, *J* = 8.9 Hz, 2H), 7.60 (d, *J* = 8.9 Hz, 2H), 7.71 (d, *J* = 8.7 Hz, 2H), 7.84 (d, *J* = 8.7 Hz, 2H). ^{13}C NMR (CD_3OD, c = 56 mM) δ 31.2, 33.5, 35.5, 43.7, 45.9, 53.3, 64.5, 65.1, 112.2, 113.3, 114.0, 119.9, 127.4, 128.0, 128.2, 130.0, 133.5, 136.6, 138.5, 146.6, 147.7 (Note: the last resonance corresponds to isochronous shift of two carbon atoms, at a concentration of 22 mM an additional resonance appears at 147.8 ppm). IR (KBr pellet) 2912, 2224, 1595, 1518, 1498, 1394, 1180, 1121, 1027, 823, 742, 635, 558 cm^{-1}. ESI-HRMS *m/z* calcd for $[M]^-$ $C_{36}H_{43}N_4O_7S_4$ 771.2015, found 771.2019.

Probes **3.3b** and **3.3c**

The ammonium salts were prepared analogously to **3.3a** except that the mixed precipitate obtained after quenching with acetic acid was dissolved water and directly purified by rp-HPLC without isolation of the acid forms. No attempt was made to quantitatively isolate the products from the reaction mixtures, so the isolated yields shown do not represent the true chemical yields.

Probe **3.3b**: Yellow glassy solid. Isolated yield 10 mg (0.0126 mmol, 50%). HPLC t_r = 17.3 min (gradient 0-20 min 30%-37% MeCN/0.1% aqueous NH_4HCO_3). ^{1}H NMR (CD_3OD) δ 2.57 (s, 4H), 2.58 (s, 4H), 2.67 (t, *J* = 6.9 Hz, 4H), 3.23 (dd, *J* = 17.3, 4.1 Hz, 1H), 3.48 (s, 8H), 3.58 (t, *J* = 7.0 Hz, 4H), 3.77 (dd, *J* = 17.3, 11.8 Hz, 1H), 5.66 (dt, 11.8, 3.8 Hz, 1H), 6.40 (d, *J* = 8.9 Hz, 2H), 6.94 (d, *J* = 8.7 Hz, 2H), 7.33 (dd, *J* = 12.6, 1.9 Hz, 1H), 7.49 (dd, *J* = 8.5, 1.9 Hz, 1H), 7.65 (t, *J* = 16.6 Hz, 1H), 7.74 (d, *J* = 8.7 Hz, 2H), 7.91 (d, *J* = 8.7 Hz, 2H). ^{19}F NMR (CD_3OD) δ –122.8 (m, 1F). IR (KBr pellet) 2912, 2225, 1605, 1518, 1417, 1185, 1096, 1034, 816, 701, 610, 558 cm^{-1}. ESI-HRMS *m/z* calcd for $[M]^-$ $C_{36}H_{42}FN_4O_7S_4$ 789.1920, found 789.1921.

Probe **3.3c**: Pale yellow glassy solid. Isolated yield 17 mg (0.021 mmol, 42%). HPLC t_r = 18.4 min (gradient 0-20 min 30%-37% MeCN/0.1% aqueous NH_4HCO_3). ^{1}H NMR (CD_3OD) δ 2.59 (s, 4H), 2.60 (s, 4H), 2.71 (t, *J* = 6.9 Hz, 4H), 3.27 (dd, *J* = 17.2, 7.7 Hz, 1H), 3.50 (s, 8H), 3.62 (t, *J* = 7.2 Hz, 4H), 3.74 (dd, *J* = 17.2, 11.9 Hz, 1H), 5.47 (dd, *J* = 11.9, 7.7 Hz, 1H), 6.48 (d, *J* = 8.9 Hz, 2H), 7.08 (d, *J* = 8.7 Hz, 2H), 7.27 (d, *J* = 8.6 Hz, 2H), 7.73 (d, *J* = 8.7 Hz, 2H), 7.86 (d, *J* = 8.7 Hz, 2H). ^{19}F NMR (CD_3OD) δ –116.7 (d, *J* = 8.4 Hz, 2F). IR (KBr pellet) 2915, 2226, 1608, 1520, 1422, 1425, 1185, 1093, 1044, 840, 815, 643, 557 cm^{-1}. ESI-HRMS *m/z* calcd for $[M]^-$ $C_{36}H_{41}F_2N_4O_7S_4$ 807.1826, found 807.1828.

(3-Nitrophenyl)methanethiol (**3.30**)

3-Nitrobenzyl chloride (18.0 g, 10.5 mmol) and potassium ethyl xanthate (20.2 g, 1.2 equiv.) were stirred together in DMSO (200 mL) for 30 minutes. The mixture was diluted with water (500 mL) and extracted with MTBE (300 mL). The extract was washed with water (2 x 300 mL) followed by brine (30 mL), dried with $MgSO_4$, and concentrated under reduced pressure to give the intermediate S-3-nitrobenzyl-O-ethylxanthate as a yellow oil. Yield 26.7 g (10.4 mmol, 99%). ^{1}H NMR ($CDCl_3$) δ 1.43 (t, *J* = 7.1 Hz, 3H), 4.44 (s, 2H), 4.66 (q, *J* = 7.1 Hz, 2H), 7.50 (t, *J* = 8.0 Hz, 1H), 7.70 (d, *J* = 7.7 Hz, 1H), 8.12 (ddd, *J* = 8.2, 2.3, 1.0 Hz, 1H), 8.23 (t, *J* = 1.8 Hz, 1H). ^{13}C NMR ($CDCl_3$) δ 13.7, 39.2, 70.5, 122.5, 123.9, 129.4, 135.1, 138.6, 148.2, 212.6. IR (neat) 2982, 1529, 1224, 1111, 1047, 811, 722, 680 cm^{-1}. EI-MS *m/z* 257 (76, $[M]^+$), 169 (51), 152 (85), 136 (100), 121 (65), 90 (78), 77 (47), 63 (40). EI-HRMS *m/z* calcd for $[M]^+$ $C_{10}H_{11}NO_3S_2$ 257.0180, found 257.0177.

A solution of the above xanthate ester (11.55 g, 44.9 mmol) in DMSO (20 mL) was added to a cooled solution of ethylenediamine (4.8 mL, 1.6 equiv.) and concentrated HCl (1.8 mL, 0.5 equiv.) in DMSO (20 mL). The resulting mixture was stirred for 5

minutes, then diluted with 1 M HCl (100 mL) followed by water (300 mL), and extracted with MTBE (200 mL). The organic layer was extracted with 5% aqueous NaOH (3 x 50 mL) and the combined aqueous extracts were immediately acidified with 30 mL of 37% HCl. The resulting emulsion was extracted with dichloromethane (2 x 30 mL) and the combined organic phases were dried with $MgSO_4$, stirred with 2 g silica gel, filtered, and concentrated under reduced pressure to give the product as a pale yellow oil. Yield 6.71 g (39.7 mmol, 88%). ^{1}H NMR ($CDCl_3$) δ 1.87 (t, *J* = 7.9 Hz, 1H), 3.84 (d, *J* = 7.9 Hz, 2H), 7.51 (t, *J* = 7.9 Hz, 1H), 7.66-7.69 (m, 1H), 8.11 (ddd, *J* = 8.2, 2.2, 1.0 Hz, 1H), 8.21 (tt, *J* = 1.8, 0.4 Hz, 1H). ^{13}C NMR ($CDCl_3$) δ 28.3, 122.1, 123.0, 129.6, 134.2, 143.1, 148.4. IR (neat) 3069, 2031, 1525, 1351, 810, 739, 701, 680, 667 cm^{-1}. EI-MS *m/z* 169 (56, $[M]^+$), 136 (100, 121 (22), 90 (52), 78 (20), 63 (23). EI-HRMS *m/z* calcd for $[M]^+$ $C_7H_7NO_2S$ 169.0197, found 169.0203.

(3-Nitrophenyl)methanesulfonyl chloride (**3.29**)

A round bottom flask containing a magnetic stir bar was charged with thiol **3.30** (6.18 g, 36.5 mmol), dichloromethane (75 mL), and concentrated HCl (60 mL, 20 equiv.), then fitted with a reflux condenser topped with a pressure-equalizing addition funnel containing 30% aqueous hydrogen peroxide (22 mL, 6 equiv.). The first 5 mL of H_2O_2 solution were added, and the mixture was stirred rapidly without external heat until reflux commenced. The remaining H_2O_2 was then added in 2 mL portions at a rate sufficient to maintain gentle reflux. After the mixture had cooled, the green organic layer was separated, carefully decolorized with aqueous Na_2SO_3 (exothermic), dried with $MgSO_4$, and concentrated under reduced pressure. The residue was recrystallized from benzene-cyclohexane to give the product as colorless crystals. Yield 6.60 g (28.0 mmol, 77%). Mp 101-102°C (Lit.[25] 95-100°C). ^{1}H NMR ($CDCl_3$) δ 4.96 (s, 2H), 7.69 (td, *J* = 7.9, 0.7 Hz, 1H), 7.85 (dt, *J* = 7.3, 1.6 Hz, 1H), 8.36 (dd, *J* = 2.2, 1.0 Hz, 1H), 8.37-8.39

(m, 1H). ^{13}C NMR ($CDCl_3$) δ 69.3, 125.1, 126.2, 128.2, 130.4, 137.2, 148.5. IR (film from $CDCl_3$) 3082, 2992, 2930, 1523, 1359, 1265, 1180, 1167, 1141, 907, 877, 816, 810, 754, 684, 672, 535, 509 cm^{-1}. EI-MS *m/z* 237 (1), 235 (2, $[M]^+$), 136 (100), 90 (48), 64 (23). EI-HRMS *m/z* calcd for $[M]^+$ $C_7H_6ClNO_4S$ 234.9706, found 234.9707.

(2,2,5-trimethyl-1,3-dioxan-5-yl)methyl (3-nitrophenyl)methanesulfonate (**3.31**)

A solution of sulfonyl chloride **3.29** (5.00 g, 21.2 mmol) in acetonitrile (20 mL) was added to a solution of 5-hydroxymethyl-2,2,5-trimethyl-1,3-dioxane[42] (**3.23)** (4.07 g, 25.4 mmol) in pyridine (10.4 mL, 10 equiv.) The resulting mixture was stirred overnight, then diluted with water (300 mL) and extracted with toluene (3 x 100 mL). The combined extracts were washed with water (100 mL), dried with $MgSO_4$, and concentrated under reduced pressure. The residue was recrystallized from benzene-cyclohexane to give the product as small colorless needles. Yield 7.00 g (19.5 mmol, 92%). Mp 102-103°C. ^{1}H NMR (CDCl3, 400 MHz) δ 1.32 (s, 3H), 1.39 (s, 3H), 1.43 (s, 3H), 3.54 (d, *J* = 10.0 Hz, 2H), 3.64 (d, *J* = 10.0 Hz, 2H), 4.32 (s, 2H), 4.49 (s, 2H), 7.62 (t, *J* = 7.9 Hz, 1H), 7.81 (dtd, *J* = 7.7, 1.0, 0.4 Hz, 1H), 8.27 (ddd, *J* = 8.2, 2.2, 1.0 Hz, 1H), 8.32 (t, *J* = 1.8 Hz, 1H). ^{13}C NMR (CDCl3, 100 MHz) δ 17.0, 18.8, 28.3, 34.1, 55.2, 65.5, 73.4, 98.3, 124.0, 125.6, 129.9, 130.0, 136.6, 148.4. IR (KBr) 3447 (br), 2995, 2960, 2879, 1532, 1352, 1207, 1175, 1180, 1088, 962, 909, 813, 731, 691, 559 cm^{-1}. EI-MS *m/z* 359 (1, $[M]^+$), 344 (100), 329 (12), 187 (20), 136 (97), 120 (15), 106 (68), 90 (51), 59 (62). EI-HRMS *m/z* calcd for $[M]^+$ $C_{15}H_{21}NO_7S$ 359.1039, found 359.1021.

(2,2,5-trimethyl-1,3-dioxan-5-yl)methyl (3-aminophenyl)methanesulfonate (**3.28**)

To a solution of **3.31** (6.67 g, 18.6 mmol), ammonium acetate (25.4 g, 18 equiv.), and acetic acid (2.2 mL, 2 equiv.) in methanol (220 mL) was added zinc dust (7.3 g, 6 equiv.) in small portions until the reaction was complete by TLC (2:1 hexane-EtOAc).

The mixture was then filtered, concentrated under reduced pressure, diluted with water (80 mL) and extracted with dichloromethane (2 x 80 mL). The combined extracts were washed with 0.2 M tetrasodium EDTA solution (100 mL), dried with $MgSO_4$, and concentrated under reduced pressure. The residue was crystallized from MTBE-hexane to give the product as a colorless crystalline powder. Yield 5.16 g (15.7 mmol, 84%). Mp 72-73°C.^{1}H NMR (CDCl3, 400 MHz) δ 0.82 (s, 3H), 1.41 (s, 3H), 1.43 (s, 3H), 3.57 (d, *J* = 11.5 Hz, 2H), 3.61 (d, *J* = 11.5 Hz, 2H), 3.76 (s (br), 2H), 4.22 (s, 2H), 4.28 (s, 2H), 6.66-6.68 (m, 1H), 6.76-6.78 (m, 2H), 7.15 (t, *J* = 8.0 Hz, 1H). ^{13}C NMR (CDCl3, 100 MHz) δ 17.2, 19.3, 27.9, 34.0, 56.1, 65.6, 73.1, 98.2, 115.6, 116.9, 120.6, 128.6, 129.8, 147.0. IR (KBr) 3462, 3435, 3360, 2988, 2872, 1624, 1465, 1351, 1266, 1184, 1145, 1084, 1032, 1001, 968, 823, 795, 701, 636 517 cm^{-1}. EI-MS *m/z* 329 (31, $[M]^+$), 314 (17), 187 (37), 106 (100), 77 (17), 59 (19). EI-HRMS *m/z* calcd for $[M]^+$ $C_{15}H_{23}NO_5S$ 329.1297, found 329.1299.

Triarylpyrazoline **3.32**

Amine **3.28** (808 mg, 2.43 mmol) was stirred in dichloromethane (6 mL), and isoamyl nitrite (330 µL, 1 equiv.) was added dropwise. After 1 hour, the reaction mixture was concentrated under reduced pressure, redissolved in toluene, and concentrated again. The resulting material was taken up in methanol (12 mL) and ammonium acetate (3.7 g, 20 equiv.), acetic acid (280 µL, 2 equiv.) and zinc dust (1.6 g, 10 equiv.) were added sequentially with rapid stirring. After 15 minutes, the reaction mixture was diluted with methanol, filtered, concentrated under reduced pressure, diluted with water, and extracted with dichloromethane (3 x 20 mL). The combined extracts were washed with tetrasodium EDTA solution, dried with Na_2SO_4, and concentrated under reduced pressure. The residue was fractioned by column chromatography (dichloromethane-MTBE) to give the intermediate arylhydrazine as a brown paste which was used without further purification.

A mixture of the above crude arylhydrazine (145 mg, approx. 0.4 mmol), chalcone **3.26** (143 mg, 0.209 mmol), and pyridinium *p*-toluenesulfonate (104 mg, 2 equiv.) in pyridine (0.7 mL) was stirred for 16 hours at 60°C and then worked up analogously to **3.27a** to give the product as a yellow, highly fluorescent glassy solid. Yield 110 mg (0.109 mmol, 52%). ^{1}H NMR (CDCl3, 400 MHz) δ 0.81 (s, 3H), 1.45 (s, 3H), 1.39 (s, 6H), 1.41 (s, 3H), 1.42 (s, 6H), 2.76 (s, 4H), 2.77 (t, *J* = 6.9 Hz, 4H), 2.82 (s, 4H), 3.10 (dd, *J* = 17.1, 6.4 Hz, 1H), 3.56 (d, *J* = 10.0 Hz, 2H), 3.59 (d, *J* = 10.0 Hz, 2H), 3.63 (t, *J* = 7.3 Hz, 4H), 3.68 (d, *J* = 11.9 Hz, 4H), 3.73 (d, *J* = 11.9 Hz, 4H), 3.76 (dd, *J* = 12.4, 17.1 Hz, 1H), 4.17 (d, *J* = 9.6 Hz, 1H), 4.20 (d, *J* = 9.6 Hz, 1H), 4.29 (d, *J* = 14.0 Hz, 1H), 4.33 (d, *J* = 14.0 Hz, 1H), 5.30 (dd, *J* = 12.4, 6.3 Hz, 1H), 6.54 (d, *J* = 8.9 Hz, 2H), 6.86 (d, *J* = 8.0 Hz, 1H), 6.96 (dd, *J* = 8.3, 1.6 Hz, 1H), 7.09 (d, *J* = 8.9 Hz, 2H), 7.17 (t, *J* = 8.0 Hz, 1H), 7.31 (t, *J* = 1.8 Hz, 1H), 7.63 (d, *J* = 8.7 Hz, 2H), 7.76 (d, *J* = 8.7 Hz, 2H). ^{13}C NMR (CDCl3, 100 MHz) δ 17.2, 19.6, 22.9, 24.3, 27.6, 30.2, 33.7, 34.0, 36.1, 37.8, 42.9, 52.4, 56.7, 63.9, 65.59, 65.63, 67.0, 73.1, 98.1, 98.5, 111.1, 112.3, 113.9, 115.9, 118.9, 121.7, 125.9, 127.0, 128.4, 128.9, 129.4, 132.2, 137.0, 144.1, 144.9, 146.2. IR (KBr pellet) 2990, 2938, 2866, 2224, 1602, 1571, 1519, 1451, 1372, 1256, 1190, 1115, 1090, 967, 838, 730, 522 cm^{-1}.

Probe **3.3d**

This compound was prepared from intermediate **3.32** (25.2 mg, 28 μmol) using same method as for **3.3b-c.** Yellow-orange glassy solid. Isolated yield 13.5 mg (0.017 mmol, 47%). HPLC t_r = 16.0 min (gradient 0-20 min 30%-37% MeCN/0.1% aqueous NH_4HCO_3). ^{1}H NMR (CD_3OD, 400 MHz) δ 2.59 (s, 4H), 2.60 (s, 4H), 2.72 (t, *J* = 7.0 Hz, 4H), 3.03 (dd, *J* = 17.3, 6.6 Hz, 1H), 3.50 (s, 8H), 3.64 (t, *J* = 7.0 Hz), 3.77 (dd, *J* = 17.3, 12.5 Hz, 1H), 3.93 (d, *J* = 13.5 Hz, 1H), 3.98 (d, *J* = 13.5 Hz, 1H), 5.35 (dd, *J* = 12.5, 6.6 Hz, 1H), 6.54 (d, *J* = 8.9 Hz, 2H), 6.84 (dt, *J* = 7.6, 0.8 Hz, 1H), 6.89 (ddd, *J* =

8.3, 2.3, 0.8 Hz, 1H), 7.05 (t, *J* = 7.9 Hz, 1H), 7.07 (d, *J* = 8.8 Hz, 2H), 7.36 (d, *J* = 1.8 Hz, 1H), 7.69 (d, *J* = 8.7 Hz, 2H), 7.85 (d, *J* = 8.7 Hz, 2H). ^{13}C NMR (CD_3OD, 100 MHz) δ 32.1, 34.4, 36.3, 44.5, 46.8, 54.2, 59.7, 65.3, 66.4, 112.5, 114.2, 114.6, 118.3, 120.8, 123.9, 127.9, 129.1, 130.3, 131.8, 134.3, 135.9, 139.9, 146.2, 146.8, 148.6. IR (KBr pellet) 2918, 2224, 1600, 1518, 1488, 1393, 1184, 1134, 1039, 701, 569 cm^{-1}. ESI-HRMS *m/z* calcd for $[M]^-$ $C_{37}H_{45}N_4O_7S_4$ 785.2171, found 785.2187.

3.11.2. Absorption and fluorescence spectroscopy

General

UV-vis absorption spectra were acquired at 22°C with a Varian Cary Bio50 spectrophotometer with constant temperature accessory. Fluorescence spectra were recorded with a PTI fluorimeter. The fluorescence spectra were corrected for the spectral response of the detection system and for the spectral irradiance of the excitation source (via a calibrated photodiode). The path length was 1 cm for absorbance and fluorescence spectra and 10 cm for absorbance measurements used in quantum yield determination.

Absorption and emission spectra

The normalized absorption (blue traces) and emission spectra (red traces) of compounds **3.3a-d** in aqueous solution (10 mM MOPS/K^+, pH 7.2) are shown in Figure 3.12. Emission spectra were monitored in the presence of excess Cu(I) for maximizing the signal/noise ratio. No discernable shifts in emission wavelength were observed upon Cu(I) addition for any of the probes. The beige area indicates the tunable range of the excited state energy ΔE_{00}.

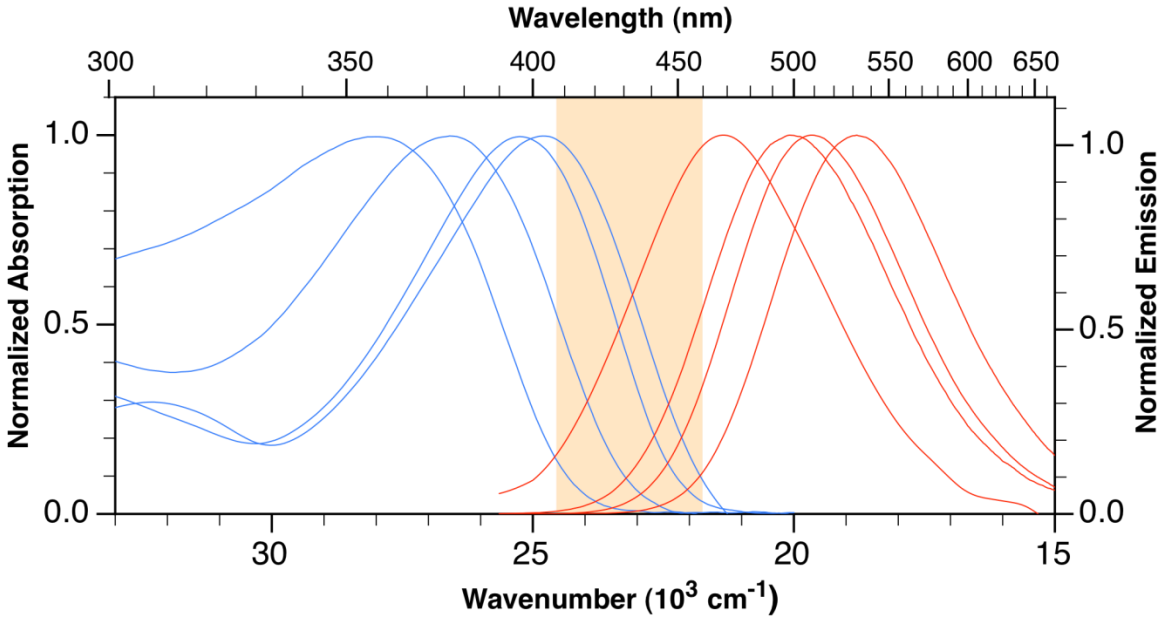

Figure 3.12: Normalized absorption and emission spectra of **3.3a-d**

Fluorescence quantum yields, contrast ratios, and reversibility of response

Quantum yields and fluorescence enhancement factors (contrast ratios) were determined in 10 mM pH 7.2 MOPS buffer, which was filtered through a 0.45 µM membrane filter to prevent interference from dust particles or fibers. For quantum yield determination, excitation was at 380 nm and four data points with absorbances between 0.05 and 0.5 (l = 10 cm) were used for each compound. The probes were saturated with Cu(I) by titration with 250 µM aqueous copper(II) sulfate in the presence of 20 µM sodium ascorbate as a reducing agent. The quantum yields of the copper saturated forms were determined from the slope of the integrated fluorescence emission from 390-700 nm versus absorbance at 380 nm using norharmane in 0.1 N H_2SO_4 (Φ_f = 0.58)[45] as a standard. To reduce errors due to the much lower signal-to-noise ratios of the emission spectra of the free probes, the raw spectra were converted to a wavenumber scale, fitted to a Gaussian function, transformed back to a wavelength scale, and integrated over the acquired spectral range. Fluorescence enhancement factors were determined as the ratio of the slopes of the integrated fluorescence emission (λ_{max} ± 10 nm, raw spectrum) versus

concentration of the Cu(I)-saturated and free probes. For probes **3.3a** (CTAP-2) and **3.3d**, the reversibility of the fluorescence response was confirmed at each absorbance point by adding an excess (10 μM) of the non-selective transition metal chelating agent tetrakis(2-pyridylmethyl)ethylenediamine (TPEN) to the copper saturated probe solutions to remove Cu(I). For both compounds, the fluorescence intensity after addition of TPEN was equal to that of the free probe within experimental error.

Mole ratio titration of CTAP-2 with Cu(I) (Figure 3.5)

A magnetically stirred solution of CTAP-2 (4.5 μM, 3 mL) in deoxygenated MOPS/K^+ buffer (10 mM, pH 7.2) was titrated with 0.6 μL aliquots of 2.5 mM $Cu(MeCN)_4PF_6$ in acetonitrile to provide a final Cu(I) concentration of 0.5 μM per aliquot. Each aliquot was introduced below the surface of the solution, and the fluorescence response (λ_{exc} = 380 nm, λ_{em} = 498-518 nm) was recorded after a 1 minute delay to allow for thorough mixing.

Analyte selectivity of CTAP-2 (Figure 3.6)

A single 4.5 μM solution (100 mL) of CTAP-2 in MOPS buffer (10 mM, pH 7.2) was prepared and the fluorescence spectrum of a 3 mL aliquot of the solution was recorded over the range of 410-700 nm with excitation at 380 nm. Each cation tested was then added as an aqueous stock solution (5 μL) to provide the indicated final concentration (10 mM for Na^+, Mg^{2+}, Ca^{2+}, and Cl^-; 10 μM for others) and the solution was thoroughly mixed by inversion. The fluorescence response was measured after a 1 minute equilibration period. Cu(I) was then added as a 2.5 mM stock solution of [Cu(MeCN)4]PF6 in acetonitrile (6 μL) to provide a final Cu(I) concentration of 5 μM, the solution was quickly mixed, and the fluorescence response was measured after a further 1 minute equilibration period. The fluorescence spectra of all solutions were

integrated over the range of 498-518 nm (λ_{max} ± 10 nm) to maximize signal to noise ratio, and none of the analytes other than Cu(I) produced a significant fluorescence enhancement outside of this range. The cations tested were supplied in the following forms: Mg(II), Ca(II), Co(II), and Ni(II) were provided as nitrates, Na^+ was provided as $NaClO_4$, and Mn(II), Fe(II), Cu(II) and Zn(II) were provided as sulfates. Chloride was supplied as KCl.

Absorbance and fluorescence versus concentration of CTAP-2-Cu(I) (Figure 3.7)

An aliquot of CTAP-2 ammonium salt stock solution (150 μM in H_2O) was added to a 1 cm cuvette containing 3 mL MOPS buffer (10 mM, pH 7.20) under rapid stirring, followed quickly by an aliquot of Cu(I) stock solution (1 mM [Cu(MeCN)4]PF6 in acetonitrile) sufficient to provide 1.3 molar equivalents of Cu(I). After 1 minute of stirring, the fluorescence spectrum was acquired with excitation at 380 nm and integrated over the emission range of 498-518 nm, and the UV absorbance was measured at 380 nm. This process was repeated using the same solution to provide increasing concentrations of CTAP-2-Cu(I) up to 5 μM.

Absorbance versus concentration of free CTAP-2 (Figure 3.8)

Experimental procedure

Aliquots of a 2.0 mM stock solution of CTAP-2 ammonium salt in water were sequentially added to 28.2 mL of MOPS/K^+ buffer (10 mM, pH 7.20) in a 10 cm path length cuvette to provide CTAP-2 concentrations from 1 to 10 μM in 1 μM steps. Aliquots of the same stock solution were added to 1.5 mL of MOPS/K^+ buffer in a 0.5 cm path length cuvette to provide concentrations from 10 to 100 μM in 10 μM steps. The absorbance at 396 nm was recorded at each concentration and the results were divided by the relevant path length.

Dimerization model

The nonlinear data obtained in the above experiment were analyzed assuming a simple dimerization equilibrium, where L represents monomeric CTAP-2 and L_2 represents the dimer (Equation 3.2):

$$2\,L \leftrightarrows L_2 \tag{3.2}$$

The dimerization equilibrium constant, *K*, is given by Equation 3.3, where species given in brackets represent concentrations:

$$K = \frac{[L_2]}{2[L]} \tag{3.3}$$

By mass balance, the dimer concentration, monomer concentration, and total CTAP-2 concentration $[L_{tot}]$ are related by Equation 3.4:

$$[L_{tot}] = [L] + 2[L_2] \tag{3.4}$$

The total absorbance of a solution containing L and L_2 but no other colored species is given by Equation 3.5, where *A* is the absorbance, ε_L and ε_{L_2} are the respective molar absorptivities of the monomer and dimer at the wavelength of measurement, and *b* is the optical path length.

$$A = b\varepsilon_L[L] + b\varepsilon_{L_2}[L_2] \tag{3.5}$$

Solving Equations 3.3 and 3.4 for [L] and $[L_2]$ and substituting the results into Equation 3.5 gives Equation 3.6, which relates the absorbance to the dimerization equilibrium constant and the molar absorptivities of the monomer and dimer:

$$A = \frac{b}{8K}\left(2\varepsilon_{\mathrm{L}}\left(\sqrt{1+8K[\mathrm{L}_{tot}]}-1\right)+\ \varepsilon_{\mathrm{L}_2}\left(4K[\mathrm{L}_{tot}]-\sqrt{1+8K[\mathrm{L}_{tot}]}+1\right)\right) \qquad (3.6)$$

The absorbance versus concentration data were fitted over the entire concentration range using Equation 3.6 with a monomer molar absorptivity (ε_{L}) of 2.91 x 10^4, which was obtained from a linear fit over the 0-5 μM range, to give log K = 3.98 ± 0.06 and $\varepsilon_{\mathrm{L}_2}$ = 4.25 ± 0.08 x 10^4 M^{-1} cm^{-1} at 396 nm.

3.12. References

(1) Morgan, M. T.; Bagchi, P.; Fahrni, C. J. *J. Am. Chem. Soc.* **2011**, *133*, 15906.

(2) Domaille, D. W.; Que, E. L.; Chang, C. J. *Nat. Chem. Biol.* **2008**, *4*, 168.

(3) Hong, Y.; Lam, J. W.; Tang, B. Z. *Chem. Soc. Rev*. **2011**, *40*, 5361.

(4) Niu, S. L.; Ulrich, G.; Ziessel, R.; Kiss, A.; Renard, P. Y.; Romieu, A. *Org. Lett.* **2009**, *11*, 2049.

(5) Tokoro, Y.; Nagai, A.; Chujo, Y. *Tetrahedron Lett.* **2010**, *51*, 3451.

(6) Zeng, L.; Miller, E. W.; Pralle, A.; Isacoff, E. Y.; Chang, C. J. *J. Am. Chem. Soc.* **2006**, *128*, 10.

(7) Verma, M.; Chaudhry, A. F.; Morgan, M. T.; Fahrni, C. J. *Org. Biomol. Chem.* **2010**, *8*, 363.

(8) Chaudhry, A. F.; Verma, M.; Morgan, M. T.; Henary, M. M.; Siegel, N.; Hales, J. M.; Perry, J. W.; Fahrni, C. J. *J. Am. Chem. Soc.* **2010**, *132*, 737.

(9) Yang, L.; McRae, R.; Henary, M. M.; Patel, R.; Lai, B.; Vogt, S.; Fahrni, C. J. *Proc. Natl. Acad. Sci. U. S. A.* **2005**, *102*, 11179.

(10) Bernardo, M. M.; Schroeder, R. R.; Rorabacher, D. B. *Inorg. Chem.* **1991**, *30*, 1241.

(11) Galijasevic, S.; Krylova, K.; Koenigbauer, M. J.; Jaeger, G. S.; Bushendorf, J. D.; Heeg, M. J.; Ochrymowycz, L. A.; Taschner, M. J.; Rorabacher, D. B. *Dalton Trans.* **2003**, 1577.

(12) Valeur, B. *Molecular Fluorescence: Principles and Applications*; Wiley-VCH: Weinheim, 2001.

(13) Cody, J. W. Ph. D. Dissertation, Georgia Institute of Technology, 2006.

(14) Hansch, C.; Leo, A.; Taft, R. W. *Chem. Rev.* **1991**, *91*, 165.

(15) Murguía, M. C.; Vaillard, S. E.; Grau, R. J. *Synthesis* **2001**, 1093.

(16) Tsonopoulos, C.; Coulson, D. M.; Inman, L. B. *J Chem Eng Data* **1976**, *21*, 190.

(17) Searles, S.; Nickerson, R. G.; Witsiepe, W. K. *J. Org. Chem.* **1960**, *24*, 1839.

(18) Beesley, R. M.; Ingold, C. K.; Thorpe, J. F. *J. Chem. Soc.* **1915**, *107*, 1080.

(19) Palmer, D. C.; Taylor, E. C. *J. Org. Chem.* **1986**, *51*, 846.

(20) Chung, S. K.; Ban, S. H.; Kim, S. H.; Kim, B. E.; Woo, S. H. *Bioorg. Med. Chem. Lett.* **1995**, *5*, 1091.

(21) Roberts, J. C.; Gao, H.; Gopalsamy, A.; Kongsjahju, A.; Patch, R. J. *Tetrahedron Lett.* **1997**, *38*, 355.

(22) Seeberger, S.; Griffin, R. J.; Hardcastle, I. R.; Golding, B. T. *Org. Biomol. Chem.* **2007**, *5*, 132.

(23) Rusha, L.; Miller, S. C. *Chem. Commun.* **2011**, *47*, 2038.

(24) Cody, J.; Mandal, S.; Yang, L.; Fahrni, C. J. *J. Am. Chem. Soc.* **2008**, *130*, 13023.

(25) Ziegler, C.; Sprague, J. M. *J. Org. Chem.* **1951**, *16*, 621.

(26) McKew, J. C. *e. a.* U. S., 2006.

(27) Filimonov, V. D.; Trusova, M.; Postnikov, P.; Krasnokutskaya, E. A.; Lee, Y. M.; Hwang, H. Y.; Kim, H.; Chi, K. W. *Org. Lett.* **2008**, *10*, 3961.

(28) Tang, Z. Y.; Zhang, Y.; Wang, T.; Wang, W. *Synlett* **2010**, 804.

(29) Smith, W. B.; Ho, O. C. *J. Org. Chem.* **1990**, *55*, 2543.

(30) Rivett, D. E.; Rosevear, J.; Wilshire, J. F. K. *Aust. J. Chem.* **1979**, *32*, 1601.

(31) Fahrni, C. J.; Yang, L. C.; VanDerveer, D. G. *J. Am. Chem. Soc.* **2003**, *125*, 3799.

(32) Bernardo, M. M.; Heeg, M. J.; Schroeder, R. R.; Ochrymowycz, L. A.; Rorabacher, D. B. *Inorg. Chem.* **1992**, *31*, 191.

(33) Binstead, R. A.; Zuberbühler, A. D.; 3.0.27 ed.; Spectrum Software Associates, Marlborough MA 01752: 2001.

(34) Xiao, Z. G.; Wedd, A. G. *Nat. Prod. Rep.* **2010**, *27*, 768.

(35) McRae, R.; Lai, B.; Fahrni, C. J. *J. Biol. Inorg. Chem.* **2010**, *15*, 99.

(36) Dodani, S. C.; Domaille, D. W.; Nam, C. I.; Miller, E. W.; Finney, L. A.; Vogt, S.; Chang, C. J. *Proc. Natl. Acad. Sci. U. S. A.* **2011**, *108*, 5980.

(37) Miller, E. W.; Zeng, L.; Domaille, D. W.; Chang, C. J. *Nat. Protoc.* **2006**, *1*, 824.

(38) Becker, J. S.; Lobinski, R. *Metallomics* **2009**, *1*, 312.

(39) Ortega, R. *Metallomics* **2009**, *1*, 137.

(40) Xiao, Z. G.; Brose, J.; Schimo, S.; Ackland, S. M.; La Fontaine, S.; Wedd, A. G. *J. Biol. Chem.* **2011**, *286*, 11047.

(41) Nishizono, N.; Sugo, M.; Machida, M.; Oda, K. *Tetrahedron* **2007**, *63*, 11622.

(42) Ouchi, M.; Inoue, Y.; Wada, K.; Iketani, S.; Hakushi, T.; Weber, E. *J. Org. Chem.* **1987**, *52*, 2420.

(43) Vandenberg, E. J.; Mullis, J. C.; Juvet, R. S. *J. Polym. Sci., Part A: Polym. Chem.* **1989**, *27*, 3083.

(44) Wiley, R. H.; Irick, G. *J. Org. Chem.* **1961**, *26*, 593.

(45) Pardo, A.; Reyman, D.; Poyato, J. M. L.; Medina, F. *J. Lumin.* **1992**, *51*, 269.

CHAPTER 4

DECONSTRUCTING THE PERFORMANCE CEILING FOR CTAP-2 AND RELATED PROBES: THE IMPORTANCE OF COPPER-NITROGEN COORDINATION AND EXCITED-STATE PROTON TRANSFER

4.1. Introduction: Incomplete fluorescence recovery in PET-based Cu(I)-probes limits contrast ratio and quantum yield

The previous chapter describes the development of CTAP-2,[1] a water-soluble, high contrast fluorescence turn-on probe for Cu(I) based on a photoinduced electron transfer (PET) switching mechanism. With a contrast ratio of 65, CTAP-2 represents a significant improvement over the first generation aqueous Cu(I)-probe CTAP-1,[2] which gave only a 4.6 fold fluorescence enhancement upon Cu(I)-saturation. The fluorescence quantum yield of Cu(I)-saturated CTAP-2, however, remains relatively low at 8.3%, which is only a third of the 25% quantum yield observed upon protonation of the N-arylthiazacrown PET donor. Similar behavior was previously noted for the forerunners of CTAP-2, the N-arylthiazacrown-based methanolic Cu(I)-probes described in Chapter 2. For example, probe **2.3d**, which provided the highest contrast ratio of 50, gave a fluorescence quantum yield of only 7% upon saturation with Cu(I), corresponding to a recovery of only 18% of the fluorescence output available upon complete PET inhibition by protonation of the thiazacrown nitrogen.[3] Fluorescence recovery can be improved by lowering the PET driving force, but a moderate increase in the fluorescence quantum yield comes at the expense of a substantial reduction in contrast ratio. Accordingly, the

more electron-rich triarylpyrazoline **2.4b** gave a quantum yield of 15% upon saturation with Cu(I), corresponding to 28% fluorescence recovery, but the contrast ratio was reduced to only 21. The low fluorescence recovery was shown to be due to incomplete Cu(I)-N coordination and concomitant coordination of a solvent molecule to the resulting vacancy at the Cu(I) center, resulting in rapidly equilibrating ternary complexes with lower donor potentials and therefore faster rates of quenching by PET compared to the binary probe-Cu(I) complex.[4]

Although CTAP-2 offers a slightly better combination of contrast ratio and quantum yield than the methanolic Cu(I)-probes described above, its fluorescence recovery remains low at 33%, implying that its performance is likely limited by a similar mechanism. Additionally, the 25% fluorescence quantum yield of protonated CTAP-2 is only about half that typically shown by cyano-substituted triarylpyrazolines lacking a PET quencher,[4-6] suggesting that an additional fluorescence quenching mechanism limits the intrinsic quantum yield of the CTAP-2 fluorophore in aqueous solution. The work presented in this chapter,[7] which began as an attempt to improve upon the performance of CTAP-2 by incorporating a new ligand design strategy recently demonstrated in methanolic solution,[6] ultimately shed light on the causes of both the incomplete fluorescence recovery and the low intrinsic fluorophore quantum yield observed for CTAP-2 and related triarylpyrazoline-based aqueous Cu(I)-probes.

4.2. Background: Integrating the aryl ring of the PET donor into the ligand backbone improves fluorescence contrast and quantum yield in methanolic Cu(I)-probes

During the development of CTAP-2, a parallel effort was underway in the Fahrni laboratory to improve the performance of methanolic Cu(I)-probes by addressing the problem of ternary complex formation[4] previously observed for the N-arylthiazacrown

derivatives described in Chapter 2. This project,[6] which served as a basis for the probe design described in this chapter, is summarized below (Section 4.2).

4.2.1. A Revised ligand design to alleviate steric crowding in the Cu(I)-complex and provide an improved switching potential

Computational modeling of the Cu(I)-complexes of ligand 2.2, the N-aryl thiazacrown Cu(I)-receptor/PET donor of the probes described in Chapter 2, revealed that at least part of the driving force for Cu-N bond dissociation and ternary complex formation is due to steric clashes between the ortho-hydrogen atoms of the aromatic ring and the ligand backbone.[4,6] Integration of the aromatic ring of the PET donor into the ligand backbone (ligand 4.1) was expected to alleviate these unfavorable steric interactions and thus suppress ternary complex formation (Scheme 4.1).

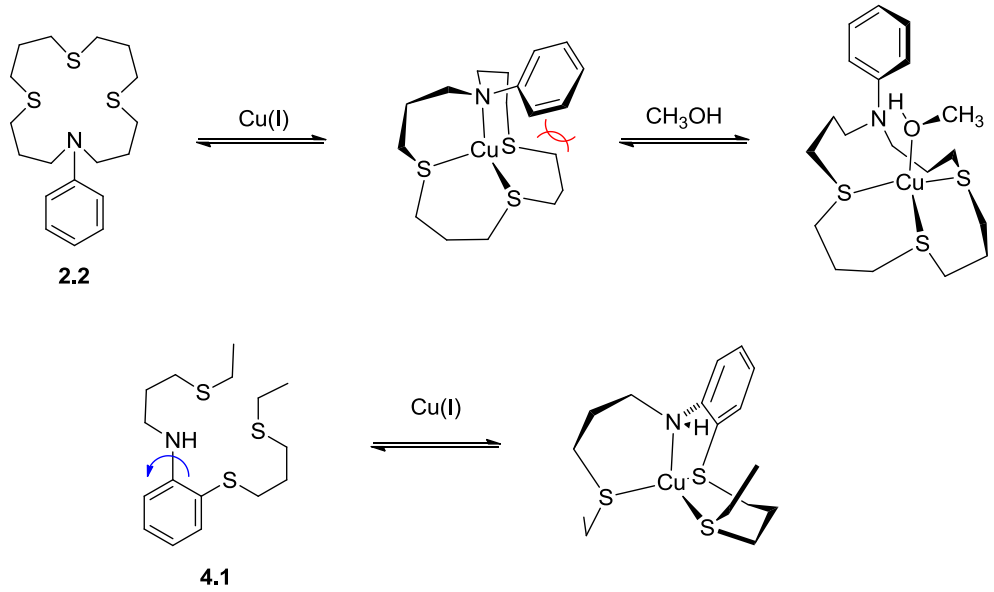

Scheme 4.1: Fusing the PET-donor aryl ring with the ligand backbone to remove the steric driving force for ternary complex formation. Adapted from a similar scheme prepared by Dr. Christoph Fahri.[6]

In addition to inhibiting ternary complex formation, the new design was expected to provide a synergistic conformational and electronic switching effect: binding of Cu(I) to the ligand should induce a conformational change that rotates the NH unit out of the plane of the aromatic ring, thus resulting in reduced π-donation and therefore greater inhibition of PET than would be provided by the Cu-N interaction alone.[6] The switch from macrocyclic to linear topology was purely for synthetic accessibility; this change typically has only a small effect on Cu(I) binding affinity for polythioether ligands.[8]

4.2.2. Integration of the PET donor aryl ring with the ligand backbone markedly improves probe performance

The new ligand design **4.1** was combined with the tunable triarylpyrazoline fluorophore platform previously utilized in methanolic Cu(I)-probe series **2.4b-f** (Chapter 2) to give Cu(I)-probes **4.2b-f** (Figure 4.1).

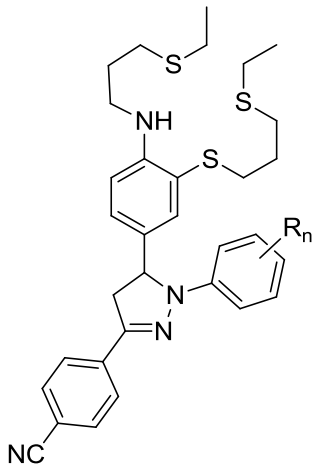

Cmpd.	R_n
4.2b	3-F
4.2c	2,5-F_2
4.2d	2,3,5-F_3
4.2e	2,3,5,6-F_4
4.2f	2,3,4,5,6-F_5

Figure 4.1: Methanolic Cu(I)-probes based on an integrated arylamine ligand design.[6] For consistency with Chapter 2, the designation **4.2a**, which would denote R_n = H, has been omitted.

As shown in Table 4.1, a side-by-side comparison of probes differing in ligand design but with equivalent triarylpyrazoline fluorophores, substitution of the integrated arylamine ligand design **4.1** (probes **4.2b-f**) for the original N-arylthiazacrown design **2.2** (probes **2.4b-f**) results in markedly higher fluorescence quantum yields upon Cu(I) saturation for all derivatives. The fluorescence quantum yields in the absence of Cu(I) are similar for the two probe series, resulting in substantially higher fluorescence contrast ratios for the integrated arylamine ligand design (series **4.2**).

Table 4.1: Comparison of probe series **4.2** to the analogous series **2.4**

Probe	Φ_f Free	Φ_f Cu(I)[a]	f_e[b]	Probe	Φ_f Free	Φ_f Cu(I)[a]	f_e[b]
2.4b	0.007	0.15	21	**4.2b**	0.017	0.57	34
2.4c	0.003	0.095	29	**4.2c**	0.007	0.54	74
2.4d	0.002	0.048	20	**4.2d**	0.002	0.49	210
2.4e	0.001	0.020	20	**4.2e**	0.001	0.24	160
2.4f	<0.001	0.020	n.d.	**4.2f**	<0.001	0.21	n.d.

[a] Probes were saturated with Cu(I) provided as $Cu(MeCN)_4PF_6$. [b]Fluorescence enhancement factor (contrast ratio) given as the ratio of the fluorescence quantum yield of the Cu(I) saturated probe to that of the free probe. Data from references 4 and 6.

Since probe series **2.4** and **4.2** share a common set of fluorophore moieties, the substantially greater fluorescence quantum yields upon Cu(I)-saturation for series **4.2** versus series **2.4** correspond to greater recovery of the intrinsic fluorophore quantum yield upon binding of Cu(I). As the low fluorescence recovery of the series **2.4** probes was found to be due to incomplete Cu(I)-N coordination with ternary complex formation,[4] the greatly improved fluorescence recovery for series **4.2** suggests that the integrated arylamine ligand design **4.1** successfully avoids the ternary complex formation

observed with ligand **2.2** (see Scheme 4.1). Accordingly, the fluorescence decay profile of the contrast-optimized probe **4.2d** upon saturation with Cu(I) that fit well to a monoexponential model, which is consistent with a uniform emitter as opposed to the multiple coordination species apparent in the multiexponential fluorescence decay profiles of probe **2.4b**. Furthermore, the X-ray crystal structure of the complex [**4.1**-Cu(I)]PF_6, which was crystallized from methanol, revealed only a binary comlex with a direct Cu-N bond.[6] Therefore, it appears that the integrated arylamine ligand design strategy improves the fluorescence quantum yield and contrast ratio of PET-based methanolic Cu(I)-probes by suppressing the Cu-N bond dissociation and ternary complex formation that occur with the earlier N-arylthiazacrown ligand design.

4.3. Combining an integrated arylamine ligand architecture with the balanced soulbilization strategy of CTAP-2

As noted in the introduction, the performance of CTAP-2 is presumably limited by incomplete Cu(I)-N coordination and ternary complex formation analogous to that observed for N-arylthiazacrown-based methanolic Cu(I) probe series **2.4**. Since this effect can be abrogated in methanolic solution by integrating the arylamine PET donor into the ligand backbone, an analog of CTAP-2 incorporating this ligand design strategy may provide substantially higher contrast ratio and quantum yield in aqueous solution than CTAP-2 itself, despite the apparently low intrinsic quantum yield of the CTAP-2 fluorophore. For example, the contrast-optimized methanolic Cu(I)-probe **4.2d** gave a fluorescence quantum yield of 0.49 upon saturation with Cu(I) versus 0.64 for the corresponding triarylpyrazoline bearing an unsubstituted 5-aryl ring, corresponding to a fluorescence recovery of 77%. An equivalent fluorescence recovery for CTAP -2, assuming a value of 0.25 for the intrinsic fluorophore quantum yield, would more than double the quantum yield of the Cu(I)-saturated form from 0.083 to 0.19. Assuming no

change in quantum yield for the free probe, this would give a corresponding increase in contrast ratio from 65 to 149.

Combining the integrated arylamine ligand architecture of the ultra-high contrast methanolic Cu(I) probe **4.2d** with the hydroxylated ligand/sulfonated fluorophore solubilization strategy of CTAP-2, we envisaged the aqueous Cu(I) probe **4.3** (Figure 4.2).

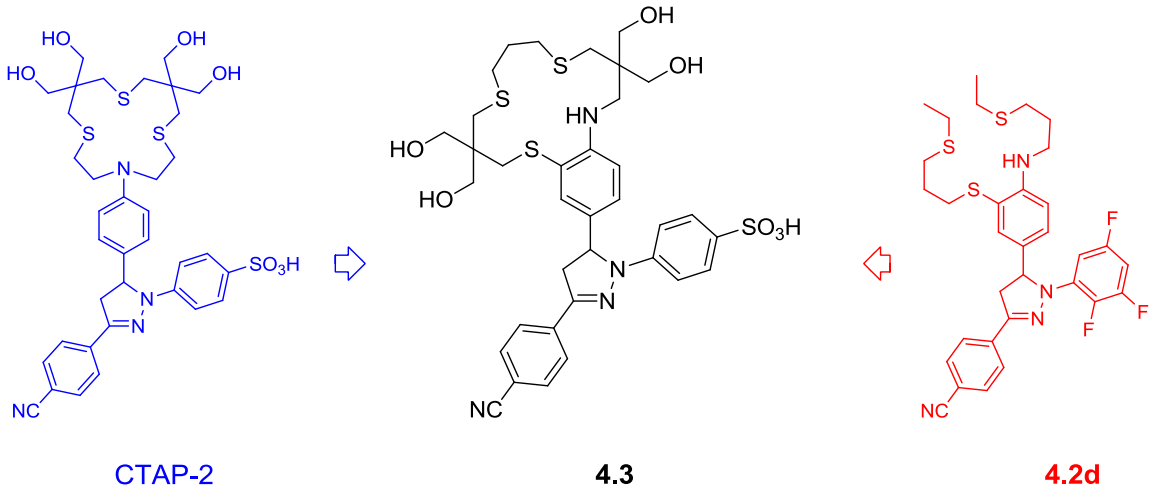

Figure 4.2: Conception of aqueous Cu(I)-probe **4.3**

As shown in the above figure, the macrocyclic ligand topology of CTAP-2 was retained for **4.3** even though **4.2d** has an acyclic ligand for easier synthetic accessibility. It was thought that the reduced conformational flexibility of a macrocyclic ligand would result in better resistance toward ternary complex formation, particularly against relatively strong monodentate ligands such as thiols, which are ubiquitous in biological environments.

4.4. Synthesis of probe 4.3

4.4.1. Construction of the ligand framework

The macrocyclic ligand framework of probe **4.3** was rendered synthetically accessible by combining the thietane ring-opening strategy developed for CTAP-2 with a recently introduced low-valent titanium-based method that, in contrast to standard dissolving-metal reduction, cleaves benzyl thioethers with high selectivity over thiophenol ethers.[9] As shown in Scheme 4.1, ring opening of thietane **3.15** with benzyl chloride in the presence of sodium iodide gave neopentyl iodide **4.4**, which proved sufficiently reactive to cleanly alkylate the acidic NH unit of benzothiazolin-2-one upon deprotonation in DMSO solution. The resulting intermediate was converted directly to the corresponding thiophenolate with sodium hydroxide, which was subsequently alkylated with a second equivalent of iodide **4.4**. This three-step, one pot synthesis furnished the bis(benzyl thioether) **4.5** in 75% yield. Thioether **4.5** was cleaved to the corresponding dithiol **4.6** by the titanium-catalyzed method of Akao et al,[9] and **4.6** was cyclized with 1,3-diiodopropane under Kellogg conditions[10] to give macrocycle **4.7** (Scheme 4.1).

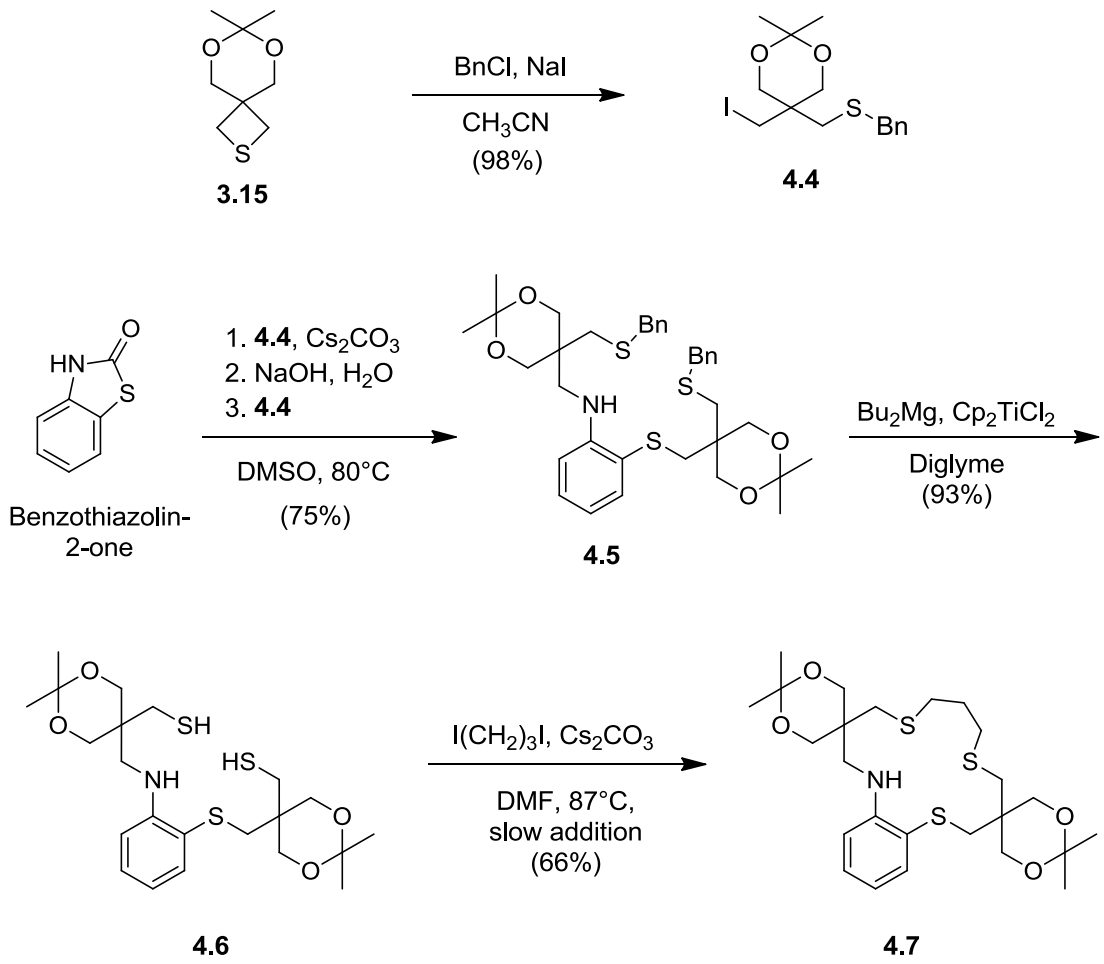

Scheme 4.2: Synthesis of the integrated arylamine-thiazacrown ligand framework

4.4.2. Assembly of the triarylpyrazoline fluorophore

To construct the triarylpyrazoline fluorophore, a carbon-based substituent such as an aldehyde must first be introduced para to the NH moiety of intermediate **4.7**. As shown in Scheme 4.2, this was accomplished by a two step Bouveault-type formylation: Amine **4.7** was selectively brominated at the para-position without oxidizing the sensitive aliphatic thioethers using 2,4,4,6-tetrabromocyclohexadienone under anhydrous conditions, and the resulting bromide **4.8** was subjected to metal-halogen exchange followed by addition of dimethylformamide and aqueous workup to decompose the resulting carbinolamine to the aldehyde. Although lithium-halogen exchange is normally

facile for aryl bromides even at low temperature, **4.8** was unreactive toward exchange with n-butyllithium at -78°C, presumably due to the strong electron-donating effect of the deprotonated secondary amine. Simply increasing the reaction temperature would likely result in N-alkylation of the deprotonated amine by the byproduct n-butyl bromide, so the metal-halogen exchange was instead carried out using the more reactive t-BuLi after initial deprotonation of the NH unit by n-BuLi. Addition of DMF followed by aqueous workup gave aldehyde **4.9** in 91% yield after recrystallization. To the knowledge of the author, this is the first published example of the Bouveault-type *para*-formylation of a secondary n-alkylarylamine.

Aldehyde **4.9** was condensed with 4-cyanoacetophenone to form chalcone **4.10**, the immediate precursor to the triarylpyrazoline fluorophore. In contrast to **3.26**, the chalcone precursor of CTAP-2 (Chapter 3), **4.10** did not spontaneously crystallize from the ethanolic reaction mixture, allowing extensive side-product formation and providing the desired product in only 48% yield after chromatographic purification. In a second run, a small aliquot of the reaction mixture was removed early in the reaction and the impure chalcone crystallized from hexane-dichloromethane. The remainder of the reaction mixture was seeded with this crystalline material, causing *in situ* crystallization of the product. After the reaction proceeded to completion, sufficiently pure chalcone **4.10** was obtained in 91% yield by simple filtration from the reaction mixture.

In contrast to the case of CTAP-2, fluorinated analogs of **4.3** were not desired for the initial stages of characterization. Therefore, the sulfonate protective group strategy developed for CTAP-2 was bypassed by condensing the chalcone with commercially available 4-hydrazinobenzenesulfonic acid in one pot following hydrolysis of the acetonide moieties to directly produce the triarylpyrazoline sulfonic acid **4.3**, which was isolated as its ammonium salt by HPLC in 82% yield (Scheme 4.2). Remarkably, the final product **4.3** was obtained in 21% overall yield from the simple thietane **3.15** over only eight separate synthetic steps.

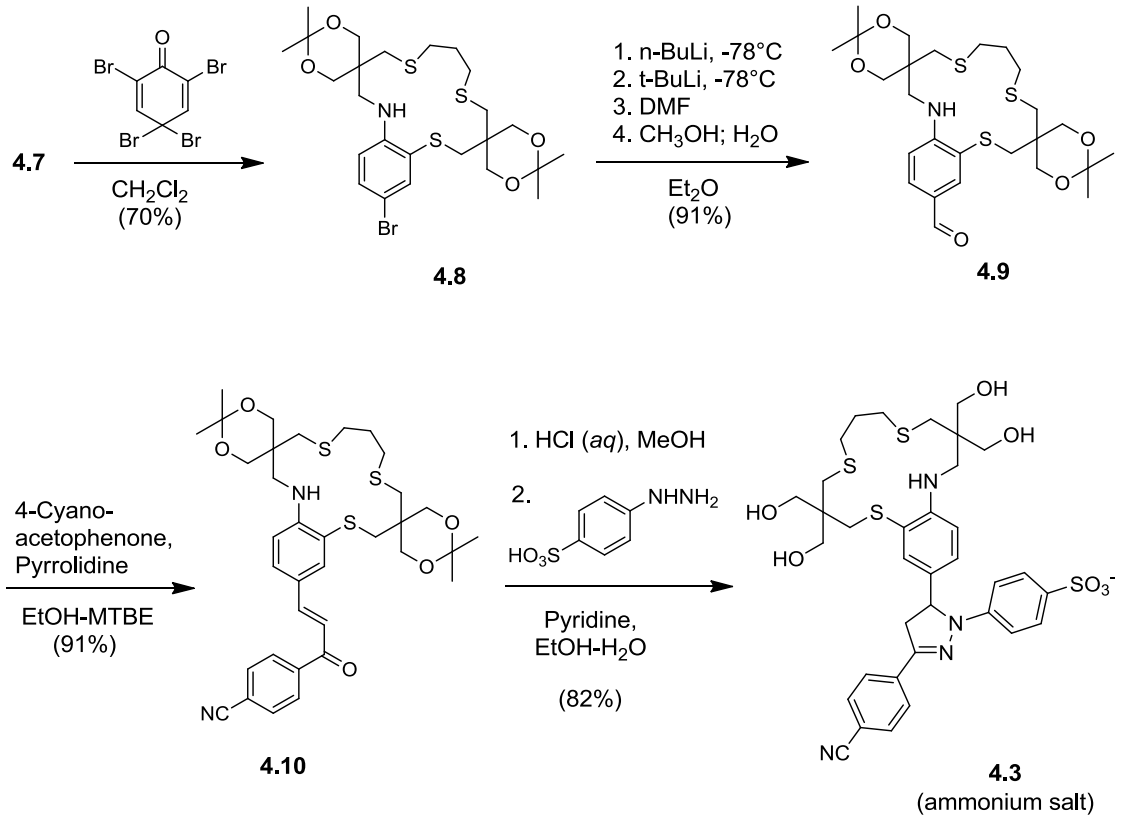

Scheme 4.3: Synthesis of Cu(I)-probe **4.3** from ligand precursor **4.7**

4.5. Cu(I) binding stoichiometry, analyte selectivity, and fluorescence response to Cu(I) and acidification

Similarly to CTAP-2, the ammonium salt of probe **4.3** was found to dissolve rapidly in pure water to millimolar concentrations. At micromolar concentrations in MOPS/K^+ buffer (10 mM, pH 7.2), **4.3** gave a strong fluorescence turn-on response to Cu(I), saturating sharply at 1 molar equivalent under deoxygenated conditions and giving a constant emission maximum of 506 nm throughout the titration (Figure 4.3).

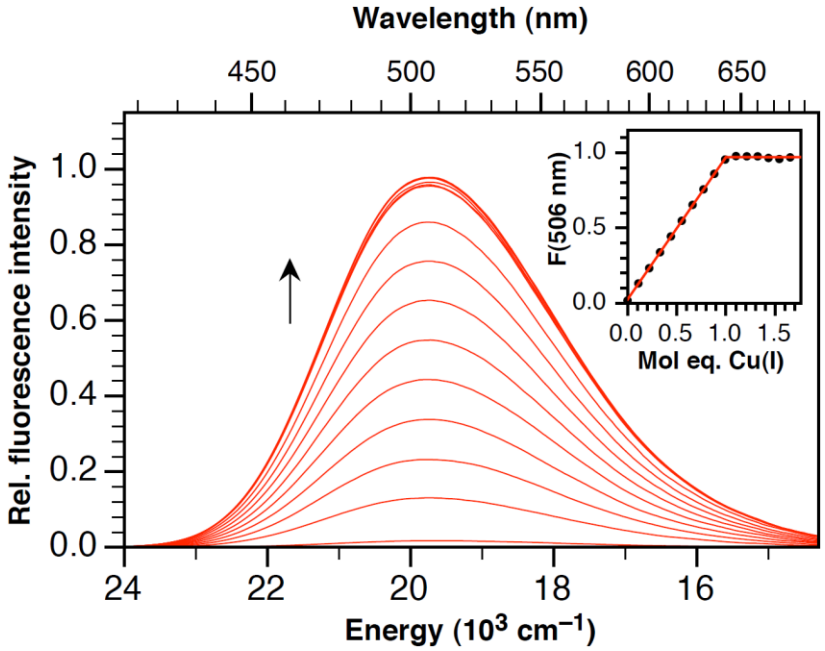

Figure 4.3: Titration of probe **4.3** with Cu(I) provided by *in situ* reduction of $CuSO_4$ with ascorbate. Inset: Fluorescence intensity at 506 nm versus amount of Cu(I) added. Probe concentration 4.6 µM.

The response of **4.3** proved highly selective for Cu(I) over all other cations tested, including Cu(II) and Hg(II), and identical fluorescence enhancements were obtained whether Cu(I) was provided directly as $Cu(MeCN)_4PF_6$ or by in situ reduction of Cu(II) with excess ascorbate (Figure 4.4).

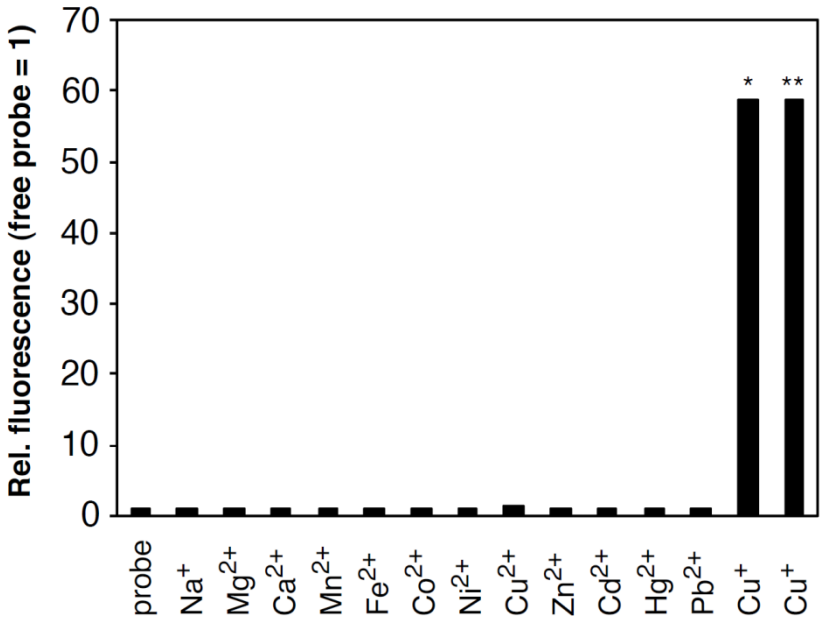

Figure 4.4: Analyte selectivity of probe **4.3** (4.6 µM in MOPS buffer)**.** *10 µM $Cu(MeCN)_4PF_6$. **10 µM $CuSO_4$ + 150 µM sodium ascorbate.

Contrary to our expectations, the fluorescence quantum yield (0.074) and contrast ratio (57) of **4.3** upon saturation with Cu(I) do not represent an improvement over CTAP-2, which gave a fluorescence quantum yield and contrast ratio of 0.083 and 65, respectively. The response of **4.3** to acidification is also surprisingly weak, reaching a maximum fluorescence quantum yield of only 0.070 at 100 mM HCl versus 0.25 at 5 mM HCl for CTAP-2. While such behavior is desirable in that it decreases the susceptibility of the probe to interference from pH changes, it challenges our previous assumptions about the intrinsic fluorophore quantum yield; calculating the fluorescence recovery upon Cu(I)-binding for probe **4.3** as for CTAP-2 --using the fluorescence quantum yield under acidic conditions as the reference point-- gives an impossible value of 106%. Clearly, a previously unrecognized fluorescence quenching mechanism is involved for probe **4.3** and possibly also CTAP-2 in acidic solution.

4.6. Investigating the intrinsic fluorophore quantum yield and effects of acidification

4.6.1. A pH-independent analog of the protonated Cu(I)-probes

To gauge the intrinsic fluorescence quantum yield of the common fluorophore moiety of CTAP-2 and **4.3** in neutral aqueous solution, we devised reference triarylpyrazoline **4.11**, in which the amine moiety of the 5-aryl ring is replaced with a cationic trimethylammonium group, permanently deactivating the 5-aryl ring toward oxidative electron transfer and exerting an electron-withdrawing effect comparable to a protonated amine at any pH. As shown in Scheme 4.3, pyrazoline **4.11** was prepared by quaternization of the dimethylamino-substituted chalcone **4.12** with methyl triflate to give chalcone **4.13**, which was subsequently condensed with 4-hydrazinobenzenesulfonic acid to give the desired triarylpyrazoline. Unexpectedly, this reaction initially halted at the chalcone hydrazone stage, and a change of solvent and temperature was required to achieve cyclization to the pyrazoline. Nevertheless, the zwitterionic product was readily isolated by crystallization.

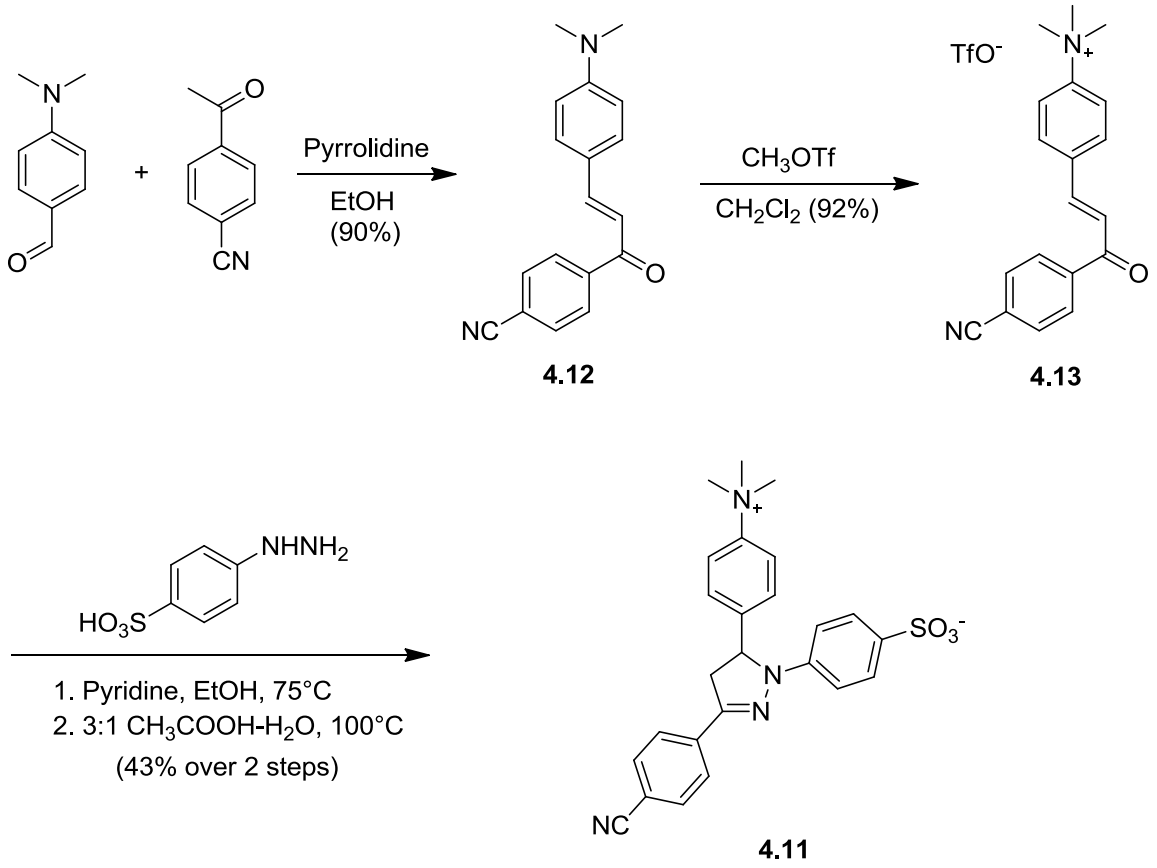

Scheme 4.4: Synthesis of the zwitterionic reference fluorophore **4.11**

In neutral aqueous solution (10 mM MOPS/K^+, pH 7.2), reference compound **4.11** showed very similar fluorescence properties to protonated CTAP-2 in 5 mM HCl: The absorption and emission maxima are nearly identical (see table 4.2) and the observed fluorescence quantum yield of 0.28 for compound **4.11** is only slightly higher than the value of 0.25 previously recorded for protonated CTAP-2. Consistent with this observation, the quantum yield of **4.11** was reduced by only 4% in 5 mM HCl versus neutral solution. In 100 mM HCl, however, the fluorescence quantum yield of **4.11** decreased by half to 0.14. No such decrease was observed in 100 mM KCl, confirming that the effect is mediated by the hydronium ion and is not due to the increase in ionic strength or chloride concentration. Although protonation of the pyrazoline imine nitrogen

in the ground state at pH 1 might be reasonably expected, the absorption spectra of **4.11** in 100 mM HCl and 100 mM KCl are superimposable, as are those in 1 M HCl and 1M KCl, suggesting that the observed fluorescence quenching by acid is due to an excited state proton transfer (ESPT) process and not to ground state protonation. Furthermore, the normalized emission spectra in neutral buffer and 100 mM HCl are superimposable, indicating that the species produced by ESPT is nonemissive.

Table 4.2: Steady state photophysical properties of **4.3**, **4.11**, and CTAP-2 in aqueous solution.

Compound	Conditions	Abs. λ_{max}/nm	Em. λ_{max}/nm	Φ_f
4.3	Buffer[a]	394	506	0.0014
	Buffer + Cu(I)	388	506	0.074[c]
	100 mM HCl	391	504	0.070
CTAP-2[d]	Buffer[a]	396	512	0.0015
	Buffer + Cu(I)	392	512	0.083[c]
	5 mM HCl	388	512	0.25
4.11	Buffer[a,b]	387	511	0.28
	5 mM HCl	387	511	0.27
	100 mM HCl	387	511	0.14

[a] 10 mM MOPS/K^+ pH 7.2. [b] Identical values were observed in unbuffered H_2O. [c] The ratio of Φ_f (free)/ Φ_f (Cu(I)) is slightly less than the observed contrast ratio at 380 nm excitation due to a small shift in the absorption spectra upon Cu(I) complexation. [d] The original value of 508 nm reported for the emission maximum of CTAP-2[1] is due to a slight error in emission monochromator calibration. The fluorescence quantum yields are not affected.

4.6.2. Analyzing the response of probe 4.3 to acidification

Armed with new knowledge regarding the direct effects of acidification on the fluorophore, we investegited the behavior of probe **4.3** under acidic conditions in more

detail. In contrast to reference compound **4.11**, probe **4.3** showed a significant shift in the absorption spectrum upon acidification, with the absorption maximum changing from 394 nm in 1 M KCl to 388 nm in 1M HCl. As a similar shift from 396 to 388 nm is observed upon protonation of CTAP-2 with 5 mM HCl, these shifts presumably correspond to protonation of the arylamine Cu(I)-ligand. In 100 mM HCl, probe **4.3** gave an absorption maximum of 391 nm, exactly halfway between the values observed in 1 M HCl and neutral solution, suggesting a pKa near 1 for protonation of the arylamine moiety. This remarkably low pKa was confirmed by Pritha Bagchi by nonlinear least-squares fitting of a series of absorption spectra acquired in aqueous HCl-KCl mixtures of varying $[H^+]$ but constant ionic strength using the SpecFit software package,[11] which yielded an extrapolated pKa value of 1.0 at 0.1 M ionic background.

Together with the observed fluorescence quenching of reference compound **4.11** under acidic conditions, the surprisingly low arylamine pKa of probe **4.3** fully explains the unexpectedly low fluorescence quantum yield observed in acidic solution: Relatively large acid concentrations are required to protonate the PET donor arylamine moiety to a significant extent, but high acid concentrations also directly quench the pyrazoline fluorophore by ESPT. At 100 mM HCl, only half of **4.3** is in the protonated form, and the fluorescence quantum yield is further reduced by half due to ESPT, thus bringing the quantum yield down from 0.28 (the value for reference compound **4.11** in neutral solution) to the observed value of 0.070. Taking the fluorescence quantum yield of **4.11** in neutral solution as the intrinsic fluorophore quantum yield, the fluorescence recovery of probe **4.3** upon Cu(I)-coordination is 26%, and that of CTAP-2 is 30%.

4.7. Reduced Cu(I)-binding affinity: a manifestation of poor Cu-N coordination?

The slightly lower fluorescence recovery upon Cu(I)-saturation of **4.3** compared to CTAP-2 suggests that the strength of the Cu(I)-N interaction is not improved for **4.3**

despite the integrated arylamine ligand design. This behavior is consistent, however, with the very low pKa of the arylamine nitrogen of probe **4.3**, which is nearly 1000-fold less basic than that of CTAP-2 (pKa 3.97).[1] Such a feebly basic amine nitrogen donor would be expected to coordinate only weakly, if at all, to the Cu(I) center. Inadequate donor strength of the arylamine nitrogen, however, would likely manifest not only in an attenuated fluorescence response but also in a reduced Cu(I)-binding affinity for probe **4.3** compared to related ligands.

Initially, we attempted to determine the Cu(I)-binding affinity of **4.3** as previously described for CTAP-2 using the Cu(II)-binding affinity and the ligand-bound Cu(II)/Cu(I) redox potential (Section 3.7.3). Attempts to determine the Cu(II) affinity of **4.3**, however, were complicated by a slow redox reaction between Cu(II) and the probe itself. In the presence of 10 μM (2 molar equivalents) of Cu(II), the fluorescence output of **4.3** slowly increased with time, reaching an emission enhancement of 6-fold after 30 minutes. Addition of only 0.4 molar equivalents of the relatively high affinity tripodal Cu(I)-chelator PEMEA[8] (log $K^{Cu(I)}$ = 15.4 at pH 7.2) reduced the fluorescence output by more than 60% within 1 minute. This indicates that the time-dependent fluorescence enhancement observed with Cu(II) is largely mediated by reduction to probe-bound Cu(I), presumably with the free probe serving as the electron source. A similar behavior was previously observed for **4.2d** in methanolic solution.[6]

In addition to the difficulty in determining the Cu(II) binding affinity, the electrochemical behavior of the **4.3**-Cu(I) complex was also unsuitable for affinity determination: Cyclic voltammetry experiments conducted by Pritha Bagchi revealed a one-electron process with a peak separation of 266 mV and a formal potential of 0.480 V vs. SHE for Cu(I)-saturated **4.3** at pH 5 (50 mV/s scan rate). Such a large peak separation indicates that substantial structural changes occur following oxidation of the Cu(I) complex or reduction of the Cu(II) complex, and the resulting formal potential is not suitable for affinity determination via the thermodynamic cycle method applied for

CTAP-2.[1] Instead, the Cu(I) affinity of **4.3** was determined by Pritha Bagchi via direct fluorescence-monitored titration using acetonitrile as a competing Cu(I) ligand.[2,12,13] This gave a uniform value of log $K^{Cu(I)}$ = 9.72 ± 0.03 at pH 7.2 for probe **4.3** whether the titration was conducted by varying the concentration of Cu(I) in the presence of a constant concentration of acetonitrile or *vice versa*. This binding affinity is nearly120 fold weaker than that of the corresponding tetrathioether macrocycle [15]aneS_4 (log $K^{Cu(I)}$ = 11.8)[14] and 50 fold weaker than that of CTAP-2 (log $K^{Cu(I)}$ = 11.4).[1] Although the reduced Cu(I)-binding affinity of **4.3** compared to these ligands may perhaps be attributable to other factors, it would certainly be consistent with an unusually low donor ability of the arylamine nitrogen in **4.3** toward Cu(I), which in turn is consistent with the unusually low pKa.

4.8. Fluorescence recovery limited by incomplete Cu(I)-N coordination: Evidence from fluorescence decay profiles

Previously, the Fahrni *et al.* demonstrated that the incomplete Cu(I)-N coordination and concomitant ternary complex formation responsible for the low fluorescence recovery of methanolic Cu(I) probes such as **2.4b** can be detected by picoseconds time-resolved fluorescence spectroscopy; each of the rapidly equilibrating coordination species has a distinct fluorescence lifetime, resulting in a multiexponential fluorescence decay profile which can be resolved into separate components. To gain further insight into the mechanism responsible for incomplete fluorescence recovery of **4.3** and CTAP-2, we applied the same technique to these aqueous Cu(I)-probes. As shown in Figure 4.5, both CTAP-2 and **4.3** gave multiexponential fluorescence decay profiles upon saturation with Cu(I), which appear as curved traces when plotted on a logarithmic y-axis. Reference compound **4.11**, by contrast, gave a cleanly monoexponential decay with a lifetime (τ_f) of 2.07 ns, which appears as a straight line.

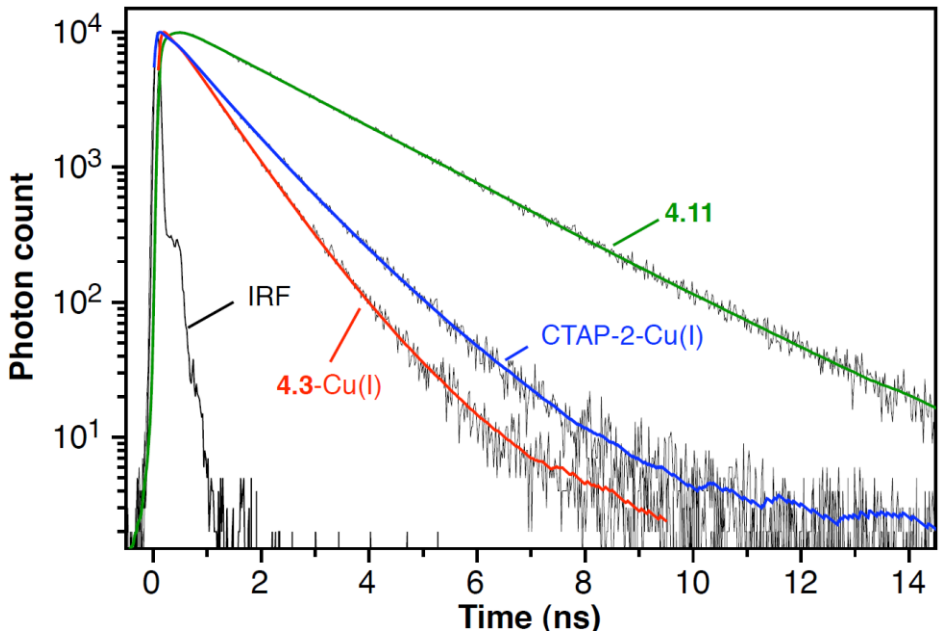

Figure 4.5: Fluorescence decay profiles of **4.3**-Cu(I), CTAP-2-Cu(I), and **4.11** in aqueous buffer.

The decay profiles of both CTAP-2-Cu(I) and **4.3**-Cu(I) fit well to a biexponential model with components of 0.82 ns (67%) and 1.36 ns (33%) for CTAP-2 and similar components of 0.72 ns (93%) and 1.44 ns (7%) for **4.3**. Interestingly, the minor, longer-lived species detected in the decay profile of **4.3**-Cu(I) recovers 70% of the fluorescence lifetime of reference compound **4.11**. This is comparable to the ultra-high contrast methanolic Cu(I)-probe **4.2d** (Section 4.2), which recovered 76% of the fluorescence lifetime of the corresponding triarylpyrazoline lacking a PET quencher (lifetimes 2.80 vs. 3.70 ns).[15] The substantially shorter lifetime of the predominant component, however, indicates that this species is substantially quenched by residual PET from the arylamine donor, suggesting little or no direct Cu(I)-N bonding interaction. As the Cu(I)-complexes of both CTAP-2 and **4.3** give biexponential fluorescence decay profiles with a predominant short lived component, it is evident that the fluorescence recoveries of both probes are limited by incomplete Cu(I)-N coordination.

4.9. Uncovering the cause of the low intrinsic fluorophore quantum yield

4.9.1. Suspected fluorescence quenching pathways

The 2.07 ns fluorescence lifetime observed for compound **4.11** in aqueous buffer is significantly shorter than those previously observed for triarylpyrazolines in methanol or acetonitrile, which are typically 3-4 ns for cyano-substituted derivatives. [REF] Consistent with a high nonradiative deactivation rate, the fluorescence quantum yield is correspondingly low at 0.28 compared to 0.4-0.7 for comparable triarylpyrazolines in polar organic solvents. Organic fluorophores quite commonly show a reduced fluorescence quantum yield in aqueous solution due to aggregation, but the fluorescence versus absorbance profile of **4.11** used in quantum yield determination (Figure 4.6) shows good linearity over a four-fold concentration range from 0.4 to 1.6 µM, indicating that the fluorescence quantum yield is independent of concentration and therefore that a significant aggregation effect is unlikely.

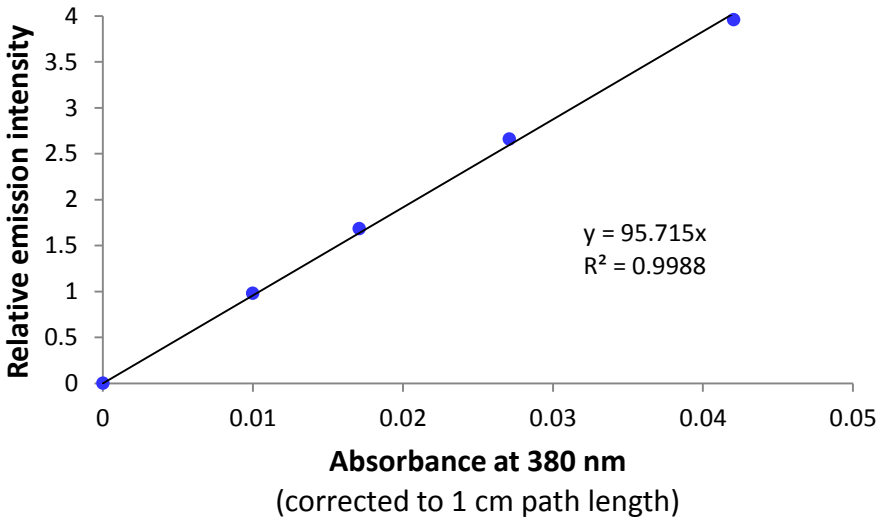

Figure 4.6: Fluorescence versus absorbance profile for triarylpyrazoline **4.11** in aqueous solution (10 mM MOPS, pH 7.2).

Another potential cause of the low fluorescence quantum yield and short lifetime could be an efficient internal conversion process involving the sulfonate moiety or its hydrogen-bonded solvation shell, and it is common for fluorophores to suffer a slight reduction in quantum yield upon sulfonation;[16] however, the 62% fluorescence quantum yield in acidic aqueous solution shown by triarylpyrazoline **3.3c**, a difluorinated analog of CTAP-2 (Chapter 3), speaks against the sulfonate moiety itself as the cause of the low fluorescence quantum yield of **4.11**.

A third possible explanation for the low fluorescence quantum yield of **4.11** is donor-excited PET, in which an electron is transferred from the excited fluorophore to an electron acceptor, in this case the 5-aryl ring. In simplified terms, the transferred electron can be considered to originate from the molecular orbital corresponding to the LUMO of the ground-state fluorophore. Striking evidence for such an effect is apparent in the fluorescence quantum yields of a series of triarylpyrazolines investigated by Rivett *et al.*[17,18] As shown in Figure 4.7, placement of strongly electron-withdrawing substituents such as cyano-, methanesulfonyl-, or carboxymethyl- on the 5-aryl ring results in dramatic fluorescence quenching when the 3-aryl ring is unsubstituted. The presence of a strong electron-withdrawing group on the 3-aryl ring, which should significantly lower the LUMO energy of the fluorophore, suppresses this quenching effect almost completely, while an electron-withdrawing group on the 1-aryl ring alone, which should primarily lower the HOMO energy, is ineffective. While the original reports offer no explanation for this behavior, it is certainly consistent with donor-excited PET with the 5-aryl ring acting as the electron acceptor.

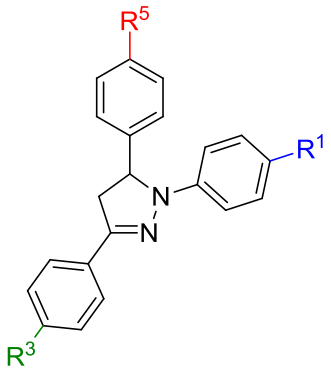

R^1	R^3	R^5	Φ_r[a]
H	H	H	0.46
CN	H	H	0.91
H	CN	H	0.66
H	H	CN	<0.1
H	H	SO_2Me	<0.05
H	H	CO_2Me	<0.05
CN	H	CN	<0.05
H	CN	CN	0.52
CN	CN	CN	0.98
H	SO_2Me	SO_2Me	0.66

[a] Relative fluorescence quantum yield in methanol (9,10-diphenylanthracene $\Phi_r = 1$).

Figure 4.7: Relative fluorescence quantum yields of triarylpyrazolines bearing electron-withdrawing substituents at the 1-, 3-, or 5-aryl rings. Data from Rivett *et al.*[17,18]

If donor-excited PET to the cationic 5-aryl ring were the primary factor responsible for the low fluorescence quantum yield of triarylpyrazolines such as **4.11** and protonated CTAP-2, then a similar quenching effect might also be expected for related compounds containing fluoro-substituents rather than the sulfonate moiety such as **2.4b**-H+, but this is not observed. It seems reasonable, however, that direct attachment of the anionic sulfonate group to the fluorophore might facilitate donor-excited PET via a field effect. Furthermore, Cody *et al.* previously observed evidence of donor-excited PET upon protonation of pyrazolines bearing a 5-aryl dimethylamino group and an unsubstituted 3-aryl ring,[5] indicating that a substituted arylammonium ion is a viable electron acceptor.

Due to the cationic 5-aryl ring and anionic fluorophore, donor-excited PET in triarylpyrazoline **4.11** would likely result in a net decrease in charge separation, and if this is the case then the fluorescence quantum yield should actually be higher in water than in a less polar solvent. Contrary to this notion, changing the solvent from water to methanol dramatically increased the quantum yield of **4.11** from 0.28 to 0.58. The fluorescence lifetime increased similarly from 2.07 to 3.58 ns, indicating that the

improvement in quantum yield is primarily due to a large decrease in k_{nr}, although a small increase in k_r also occurs (Table 4.3). Furthermore, the fluorescence lifetime and quantum yield of **4.11** in methanol are quite comparable to those of other cyano-substituted triarylpyrazolines previously reported, indicating that the low quantum yield observed in aqueous solution is due to a solvent effect rather than an inherent property of the compound.

4.9.2. ESPT in neutral solution revealed by solvent isotope effects

Given the fluorescence quenching by ESPT apparent for **4.11** under acidic conditions, a likely explanation for the substantially increased nonradiative deactivation rate of **4.11** in aqueous solution would be a second ESPT pathway with H_2O itself as the proton donor. Addition of 0.1 M NaOH had no effect on the fluorescence spectrum or quantum yield of **4.11**, indicating that any excited state protonation that occurs must be irreversible and kinetically controlled. Consistent with a fluorescence quenching mechanism involving a rate-limiting proton transfer from the solvent, the fluorescence quantum yield of **4.11** showed a substantial solvent deuterium isotope effect, increasing 1.7-fold from 0.28 to 0.48 when the solvent was changed from H_2O to D_2O with no effect on the absorption or normalized emission spectrum. The fluorescence lifetime increased proportionally from 2.07 to 3.56 ns, indicating that the improvement in quantum yield is due solely to a decrease in the nonradiative deactivation rate k_{nr} while k_r remains constant. Notably, the fluorescence lifetime and k_{nr} values obtained in D_2O are similar to those in methanol (Table 4.3), suggesting that ESPT is likely inhibited to a large extent in both solvents.

Table 4.3: Photophysical properties of **4.11** in H_2O, D_2O, and CH_3OH

Solvent	Abs. λ_{max}/nm	Em. λ_{max}/nm	Φ_f	τ_f /ns	k_r[c,e] /10^8 s^{-1}	k_{nr}[d,e] /10^8 s^{-1}
H_2O[a,b]	387	511	0.28	2.07	1.35	3.48
D_2O[a]	387	511	0.48	3.56	1.35	1.46
CH_3OH[a]	390	496	0.58	3.58	1.62	1.17

[a] Air-saturated conditions. [b] Deoxygenation had a negligible effect on the fluorescence lifetime. [c] $k_r = \Phi_f/\tau_f$. [d] $k_{nr} = (1-\Phi_f)/\tau_f$. [e] The third digit is not significant but is included to show the level of internal consistency.

While the above effects have been interpreted as evidence of ESPT, a substantial increase in fluorescence quantum yield in D_2O versus H_2O sometimes occurs for fluorophores which engage in hydrogen bonding with the solvent but have no obvious sites for excited-state protonation or deprotonation, such as 5-dimethylaminonaphthalene-1-sulfonate. In these cases, the increased nonradiative deactivation rate in H_2O is presumably due to an internal conversion mechanism involving transfer of energy to the high frequency O-H stretching vibrations of the solvent.[19] The similarly low k_{nr} values of **4.11** in D_2O versus CH_3OH, however, indicate that the mere presence of a solvent O-H stretch does not explain the fast nonradiative deactivation rate observed in H_2O. ESPT appears a more likely explanation, as remarkably similar decreases in k_{nr} in either D_2O or CH_3OH versus H_2O have been previously reported for several indole derivatives known to undergo fluorescence quenching by excited state protonation at C2 or C3 of the indole ring.[20] Furthermore, comparable solvent isotope effects on fluorescence quantum yield and lifetime have been previously observed in methanolic solution for 1,3,5-triarylpyrazolines lacking the strongly electron-withdrawing 3-aryl cyano-group and 1-aryl sulfonate moiety. These effects, which were completely absent in aprotic solvents such as benzene or acetonitrile, were attributed to excited-state protonation, and were enhanced by electron-donating substituents but diminished by electron-withdrawing substituents on the 1-aryl ring.[21] The latter observation mirrors a trend observed for the

CTAP-2 series probes **3.3a-d**, where the fluorescence quantum yields of the probes under acidic conditions rose dramatically as electron-withdrawing substituents were added to the 1-aryl ring (Chapter 3, Table 3.2).

4.10. The Relative importance of ESPT versus residual PET in the fluorescence quantum yield of Cu(I)-probes

Based on the data presented in this chapter, the fluorescence quantum yields upon Cu(I)-saturation of **4.3** and CTAP-2 are limited both by incomplete fluorescence recovery, which is apparently due to inadequate Cu(I)-N coordination resulting in residual PET, and a low intrinsic fluorophore quantum yield, which appears to be due to excited-state protonation of the fluorophore in aqueous solution. The relative importance of these two factors is determined by the contribution of each to the overall nonradiative deactivation rate constant k_{nr}. For **4.3** and CTAP-2, which exhibit a biexponential fluorescence decay rather than a single τ_f value, a combined k_{nr} can be calculated based on the natural decay lifetime, which is the average of the two lifetime components (τ_n) weighted by the fractional contribution (f_n) of each component (Table 4.4).

Table 4.4: Fluorescence decay data for Cu(I)-saturated probes CTAP-2 and **4.3**

Probe	Solvent	τ_1 (f_1)	τ_2 (f_2)	$\chi^{2\,c}$	Φ_f	$k_r^{\,d}$ /10^8 s^{-1}	$k_{nr}^{\,d}$ /10^8 s^{-1}
CTAP-2	H_2O[a]	0.82 (0.67)	1.36 (0.33)	1.031	0.083	0.83	9.2
4.3	H_2O[a]	0.72 (0.93)	1.44 (0.07)	1.094	0.074	0.95	12
4.3	D_2O[b]	0.94 (0.90)	2.04 (0.10)	1.141	0.089	0.84	8.6

[a] Deoxygenated 10 mM MOPS/K^+, pH 7.2. [b] Deoxygenated 10 mM MOPS/K^+, pH* 7.3 in D_2O, equivalent to pH 7.2 in H_2O.[22] [c] Goodness-of-fit parameter for biexponential fit. [d] Calculated as in Table 4.3 but using $\tau_f = \tau_1 f_1 + \tau_2 f_2$.

The contribution of ESPT to the overall value of k_{nr} can be estimated from the difference in k_{nr} for compound **4.11** in H_2O versus D_2O. Although quenching by an analogous mechanism may occur to a small extent even in D_2O, the k_{nr} value for **4.11** in this solvent is within the range observed for related triarylpyrazolines in acetonitrile solution,[5] where ESPT cannot occur, thus indicating that the contribution of such a pathway to k_{nr} should be relatively small. Subtracting $k_{nr}(D_2O)$ from $k_{nr}(H_2O)$ gives an estimated ESPT rate constant (k_{ESPT}) of approximately 2.0 x 10^8 s^{-1} for compound **4.11**, which is rather small compared to the overall effective k_{nr} values for the Cu(I)-probes (Table 4.4).

Assuming that the rate constants for ESPT and all other nonradiative deactivation pathways except for PET are similar for **4.11**, **4.3**-Cu(I), and CTAP-2-Cu(I), the effective rate constants of residual PET for the Cu(I)-probes can be estimated by subtracting the k_{nr} value of **4.11** in H_2O from the overall k_{nr} of each probe. For **4.3**-Cu(I), this yields an estimate of 8.5 x 10^8 s^{-1}, more than four-fold larger than the estimated k_{ESPT}, indicating that residual PET is the more important limiting factor for the fluorescence quantum yield of this probe. The same applies for CTAP-2-Cu(I), for which we estimate an effective residual PET rate constant of 5.7 x 10^8 s^{-1}. To check the validity of these conclusions, we predicted the fluorescence quantum yield of **4.3**-Cu(I) in the absence of ESPT, then measured the actual value in buffered D_2O. Subtracting the estimated k_{ESPT} of 2.0 x 10^8 s^{-1} from the overall k_{nr} of 1.2 x 10^9 s^{-1} for **4.3**-Cu(I) in H_2O yields a predicted k_{nr} of 1.0 x 10^9 s^{-1} in D_2O. Assuming the same k_r as in H_2O, the predicted quantum yield is $\Phi_f = k_r/(k_r + k_{nr}) = 0.088$, which is in excellent agreement with the experimentally determined value of 0.089. The striking accuracy of this quantum yield prediction is partially coincidental given the less exact agreement in k_r and k_{nr} (Table 4.3), but the results nevertheless substantiate the conclusion that residual PET is the major process limiting the quantum yield of low fluorescence recovery Cu(I)-probes such as **4.3** and CTAP-2, while ESPT plays a smaller but still significant role. The importance of the ESPT quenching pathway,

however, should become more important at higher degrees of PET inhibition. This is demonstrated by compound **4.11**, in which acceptor-excited PET is presumably abolished. In this case, elimination of the ESPT pathway results in a 70% improvement in fluorescence quantum yield from 0.28 to 0.48, and a comparable effect would be expected for a triarylpyrazoline-based probe that achieves nearly complete inhibition of PET upon Cu(I)-coordination. Furthermore, elimination of ESPT would improve the fluorescence contrast ratio almost in proportion to the quantum yield of the Cu(I)-bound probe, because the quantum yield of the free probe should be little affected by ESPT given the much larger rate of PET in the absence of analyte. Therefore, if the degree of PET inhibition upon Cu(I)-binding can be significantly improved in future aqueous Cu(I)-probes, simultaneous suppression of the ESPT pathway will give a synergistic improvement in contrast ratio and quantum yield.

4.11. Conclusions

In an effort to improve upon the fluorescence sensing performance offered by our recently developed aqueous Cu(I) probe CTAP-2 (Chapter 3), we combined the balanced aqueous solubilization strategy and macrocyclic ligand topology of this probe with a new design principle entailing integration of the PET donor aryl ring into the ligand backbone. Based on previous results obtained in methanolic solution, we expected the new ligand design to give a substantial improvement in fluorescence contrast ratio and quantum yield upon Cu(I)-saturation by enforcing complete coordination of the PET donor nitrogen to the Cu(I)-center. While the new probe **4.3** gave a strong fluorescence turn-on response with high selectivity for Cu(I), it did not exceed CTAP-2 in contrast ratio or quantum yield. To gain insight into the factors limiting the performance of these Cu(I) probes, we conducted more detailed studies with probe **4.3**, CTAP-2 and reference fluorophore **4.11**. These uncovered two separate effects that limit the fluorescence response of both **4.3** and

CTAP-2 to Cu(I): residual PET due to incomplete Cu-N coordination limits fluorescence recovery upon Cu(I) binding, and fluorescence quenching by excited-state protonation hinders the intrinsic fluorophore quantum yield even in neutral aqueous solution. The former effect, which was suspected for CTAP-2 based on previous studies in methanolic solution,[4] was confirmed for both probes by fluorescence decay analysis. The latter, which was discovered through solvent isotope effects on the fluorescence quantum yield and lifetime of reference fluorophore **4.11**, was initially unexpected but later found to have a literature precedent involving more electron-rich 1,3,5-triarylpyrazolines studied in methanolic solution.[21]

Although the reduction in fluorescence quantum yield due to ESPT is relatively minor compared to the effect of residual PET for the current Cu(I)-probes CTAP-2 and **4.3**, the ESPT pathway will become increasingly important at higher degrees of PET inhibition. As essentially complete PET inhibition upon Cu(I)-binding has already been demonstrated in methanol,[15] the ESPT pathway will likely be a critical consideration for the design of triarylpyrazoline-based aqueous Cu(I)-probes once a ligand design is found that more effectively enforces Cu(I)-N coordination in aqueous solution.

4.12. Experimental section

The experimental work carried out by the author is described below. Details regarding determination of the pKa, Cu(I)-binding affinity, and electrochemical behavior of **4.3** can be found in the original reference.[7]

4.12.1. Synthesis

General

Materials and reagents: 2,4,4,6-tetrabromocyclohexadienone was purchased from Alfa Aesar and the purity was determined via ^{1}H NMR ($CDCl_3$) shortly before use (impurity is 2,4,6-tribromophenol). Diglyme (diethylene glycol dimethyl ether) was distilled from sodium-benzophenone and stored under argon. Dry diethyl ether and dry DMF (EMD DriSolv® grade) were used as received. Other solvents and reagents were purchased from standard commercial sources and used as received. The synthesis of thietane **3.15** and CTAP-2 are described in Chapter 3. NMR: Spectra were recorded at 400 MHz (^{1}H, ppm vs. internal TMS), 376 MHz (^{19}F, ppm vs. internal CCl_3F), and 100 MHz (^{13}C, ppm vs. TMS, referenced to $CDCl_3$ (77 ppm) or CD_3OD (49 ppm) chemical shifts). Spectra were recorded at ambient temperature (20-23°C) unless stated otherwise. For ^{1}H spectra, the abbreviation "ad" denotes an apparent doublet with additional partially resolved coupling (AA'XX' spin system). In the ^{13}C spectra, isochronous chemical shifts for nonequivalent carbon nuclei were observed for **4.3**, **4.6**, and **4.7**. The coincident peaks were identified via integration, and the number of carbon nuclei represented by each peak is given in parentheses.

5-((benzylthio)methyl)-5-(iodomethyl)-2,2-dimethyl-1,3-dioxane (**4.4**)

A mixture of thietane **3.15** (8.19 g, 47 mmol), benzyl chloride (5.62 mL 48.9 mmol), NaI (10.6 g, 70.5 mmol), Na_2CO_3 (1g), and CH_3CN (20 mL) was stirred for 10 d in the dark. The resulting yellow mixture was stirred with aqueous Na_2SO_3 until colorless, diluted with water (200 mL), and extracted with MTBE (200 mL). The extract was washed with water (200 mL) followed by brine (20 mL), dried with $MgSO_4$, and concentrated. The yellow residue was taken up in dichloromethane (100 mL), stirred with silica gel (5g), filtered, and concentrated to give the product as a colorless oil which was used without further purification. Yield 18.1 g (98%). ^{1}H NMR ($CDCl_3$) δ 1.38 (s, 3H), 1.39 (s, 3H), 2.60 (s, 2H), 3.39 (s, 2H) 3.68 (d, *J* = 11.6 Hz, 2H), 3.72 (d, *J* = 11.6 Hz, 2H), 3.76 (s, 2H), 7.22-7.30 (m, 5H). ^{13}C NMR ($CDCl_3$) δ 12.9, 23.2, 23.9, 35.8, 36.7,

37.9, 66.3, 76.7, 98.6, 127.1, 128.5, 129.0, 138.0. EI-MS *m*/*z* 392 (27, $[M]^+$), 334 (68), 91 (100). EI-HRMS *m*/*z* calcd for $[M]^+$ $C_{15}H_{21}IO_2S$ 392.0307, found 392.0303.

Dibenzyl thioether intermediate **4.5**

A mixture of iodide **4.4** (8.13 g, 20.7 mmol), benzothiazolin-2-one (3.13 g, 20.7 mmol), Cs_2CO_3 (8.1 g, 25 mmol) and DMSO (9 mL) was stirred under argon overnight at 80°C. The mixture was diluted with 30 mL DMSO, and 20% w/v aq. NaOH (16.6 mL, 83 mmol) was slowly injected. A further 28 mL of DMSO was added simultaneously with NaOH as needed to prevent separation of the intermediate from the reaction mixture. After 35 min, acetic acid (1.42 mL, 25 mmol) was added to destroy excess NaOH, and a further 20.7 mmol of **4.4** was added as a solution in DMSO (11 mL). After 30 min, the mixture was allowed to cool, poured into water (300 mL) and extracted with MTBE (250 mL). The extract was washed with water + brine (2 x (250 mL + 10 mL)), dried with $MgSO_4$, and concentrated. The residue was purified by column chromatography (hexanes-MTBE) to give the product as a yellow oil. Yield 10.2 g (75%). ^{1}H NMR ($CDCl_3$) δ 1.36 (s, 3H), 1.40 (s, 3H), 1.44 (s, 3H), 2.57 (s, 2H), 2.72 (s, 2H), 2.85 (s, 2H), 3.35 (d, *J* = 6.6 Hz, 2H), 3.66 (s, 2H), 3.69-3.75 (m, 10H), 5.22 (t, *J* = 6.7 Hz, 1H), 6.61 (td, *J* = 7.5, 1.2 Hz, 1H), 6.77 (dd, J = 8.3, 1.0 Hz, 1H), 7.19 (ddd, J = 8.6, 7.5, 1.6 Hz, 1H), 7.21-7.27 (m, 10H), 7.39 (dd, J = 7.6, 1.6 Hz, 1H). ^{13}C NMR ($CDCl_3$) δ 22.5, 22.7, 24.7, 25.0, 34.7, 34.8, 37.8, 38.0, 38.3, 38.4, 38.8, 45.9, 65.4, 66.2, 98.3, 98.4, 110.4, 117.0, 117.7, 127.0, 127.1, 128.4, 128.5, 128.9, 129.0, 130.2, 135.8, 137.9, 138.2, 149.4. MALDI-HRMS (matrix: dithranol) *m*/*z* calcd for $[M+H]^+$ $C_{36}H_{48}NO_4S_3$ 654.2745 found 654.2767.

Dithiol **4.6**

An oven-dried 250 mL three-necked rb flask equipped with a gas inlet, thermometer, magnetic stir bar, and rubber septum was charged with a solution of **4.5**

(10.1 g, 15.4 mmol) in benzene (20 mL). The solution was concentrated under a stream of argon at 80°C, and diglyme (62 mL) was added. The mixture was stirred in an ice bath, and dibutylmagnesium solution (1 M in heptane, 62 mL) was added at a rate such that the temperature did not rise above 15°C. The Ar flow rate was then increased, the rubber septum was removed, solid Cp_2TiCl_2 (384 mg, 1.54 mmol) was added, and the septum was quickly replaced. The ice bath was removed after 5 min, and after 30 min the reaction was quenched with methanol (10 mL). The mixture was treated with citrate buffer (0.5 M trisodium citrate, 0.5 M citric acid, 120 mL), diluted with water (200 mL), and extracted with MTBE (250 mL). The organic layer was back-extracted with 5% aq. NaOH + methanol (3 x (60 mL + 10 mL)). The combined aqueous extracts were washed with hexanes (200 mL), acidified with citrate buffer (100 mL) + 1 M HCl (180 mL), and the resulting emulsion was extracted with 1:1 MTBE-toluene (300 mL). The extract was washed with water (3 x 500 mL), dried with $MgSO_4$, and concentrated to give the product as a pale pink oil. Yield 6.82 g (93%). ^{1}H NMR ($CDCl_3$) δ 1.16 (t, *J* = 9.2 Hz, 1H), 1.35 (t, *J* = 8.8 Hz, 1H), 1.38 (s, 3H), 1.39 (s, 3H), 1.43 (s, 3H), 1.47 (s, 3H), 2.74 (d, *J* = 8.8 Hz, 2H), 2.80 (d, *J* = 9.2 Hz, 2H), 3.35 (d, *J* = 6.4 Hz, 2H), 3.70 (d, *J* = 11.8 Hz, 2H), 3.75 (d, *J* = 11.8 Hz, 2H), 3.78 (s, 4H), 5.16 (t, *J* = 6.4 Hz, 1H), 6.65 (td, *J* = 7.5, 1.2 Hz, 1H), 6.79 (dd, J = 8.3, 1.1 Hz, 1H), 7.22 (ddd, *J* = 8.5, 7.5, 1.6 Hz, 1H), 7.43 (dd, *J* = 7.6, 1.6 Hz, 1H). ^{13}C NMR ($CDCl_3$) δ 22.5, 23.2, 24.2, 24.7, 27.2 (2C), 37.6, 37.90, 37.92, 45.2, 65.1, 66.0, 98.4, 98.6, 110.5, 117.4, 117.6, 130.5, 136.0, 149.3. EI-MS *m*/*z* 473 ($[M]^+$, 100), 458 (25), 312 (48), 254 (49), 137 (30), 136 (64), 87 (21).). EI-HRMS *m*/*z* calcd for $[M]^+$ $C_{22}H_{35}NO_4S_3$ 473.1728, found 473.1731.

Macrocycle **4.7**

Solutions of dithiol **4.6** (6.81 g, 14.4 mmol) and 1,3-diiodopropane (4.25 g, 14.4 mmol) in DMF (each 23 mL total volume) were added via a syringe pump over 18 h to a stirred suspension of Cs_2CO_3 (18.7 g, 57.5 mmol) in DMF (800 mL) under argon at 87°C

(internal temperature). After cooling, the liquid phase was decanted, and the solid was washed with warm xylenes (3 x 100 mL). The combined liquid phases were concentrated to dryness, and the residue was stirred in toluene (250 mL). After 10 min, the mixture was filtered through Celite and concentrated to dryness. The residue was purified by column chromatography (hexane-MTBE), and crystallized from boiling cyclohexane (20 mL) by addition of hexanes (25 mL) under stirring to give the product as a colorless crystalline powder. Yield 4.91 g (66%). Mp 123-123.5 °C ^{1}H NMR ($CDCl_3$) δ 1.41 (s, 3H), 1.45 (s, 3H), 1.48 (s, 3H), 1.95 (p, *J* = 6.6 Hz, 2H), 2.66 (s, 2H), 2.77 (t, *J* = 6.6 Hz, 2H), 2.82 (t, *J* = 6.7 Hz, 2H), 2.85 (s, 2H), 2.94 (s, 2H), 3.52 (d, *J* = 7.0 Hz, 2H), 3.67 (d, J = 11.9 Hz, 2H), 3.73 (d, J = 11.4 Hz, 2H), 3.75 (s, 4H), 5.58 (t, *J* = 7.0 Hz, 1H), 6.62 (td, *J* = 7.4, 1.2 Hz, 1H), 6.89 (dd, *J* = 8.3, 1.1 Hz, 1H), 7.20 (ddd, *J* = 8.5, 7.5, 1.6 Hz, 1H), 7.42 (dd, *J* = 7.6, 1.6 Hz, 1H). ^{13}C NMR ($CDCl_3$) δ 20.9, 22.7, 24.6, 26.6, 27.8, 31.4, 31.8, 34.9 (2C), 37.8, 38.5, 39.7, 44.8, 65.8, 66.7, 98.4, 98.5, 110.7, 117.0, 117.1, 130.4, 136.2, 150.2. EI-MS *m*/*z* 513 ($[M]^+$, 100), 498 (27), 220 (18), 150 (33), 137 (80), 136 (74), 83 (18). EI-HRMS *m*/*z* calcd for $[M]^+$ $C_{25}H_{39}NO_4S_3$ 513.2041, found 513.2042.

Bromide **4.8**

Macrocycle **4.7** (3.43 g, 6.68 mmol) was dissolved in CH_2Cl_2 (25 mL, dried over 4Å ms) in a 50 mL three-necked flask equipped with a gas inlet, thermometer, and stir bar. The mixture was cooled in an ice bath under Ar, and solid 2,4,4,6-tetrabromocyclohexadienone (4.10 g of 80% pure material, 8.0 mmol) was added in small portions against a gentle argon current at 0-10°C. After 10 minutes, the reaction was quenched with a solution of Na_2SO_3 (1.7 g, 13 mmol) and 20% aq. NH_3 (1.2 mL, 13 mmol) in H_2O (20 mL), then diluted with MTBE (100 mL). The aqueous layer was removed, and the organic layer was washed with water + 5% aq. NaOH (3 x (100 mL + 10 mL)), dried with Na_2SO_4, and concentrated. The residue was taken up in boiling hexanes (35 mL), filtered through cotton, and crystallized from hexanes-ethanol to give

the product as a colorless crystalline powder. Yield 2.78 g (72%). Mp 121-122.5°C. ^{1}H NMR ($CDCl_3$) δ 1.41 (s, 3H), 1.43 (s, 3H), 1.45 (s, 3H), 1.47 (s, 3H), 1.95 (p, *J* = 6.6 Hz, 2H), 2.60 (s, 2H), 2.77 (t, *J* = 6.5 Hz, 2H), 2.81 (t, *J* = 6.7 Hz, 2H), 2.83 (s, 2H), 2.94 (s, 2H), 3.52 (d, *J* = 7.0 Hz, 2H), 3.62 (d, *J* = 12.1 Hz, 2H), 3.71 (d, *J* = 12.1 Hz, 2H), 3.74 (s, 4H), 5.60 (t, *J* = 7.0 Hz, 1H), 6.81 (d, *J* = 8.8 Hz, 1H), 7.27 (dd, *J* = 8.8, 2.4 Hz, 1H), 2.53 (d, *J* = 2.4 Hz, 1H). ^{13}C NMR ($CDCl_3$) δ 20.4, 20.8, 24.4, 27.0, 27.6, 31.3, 31.9, 34.9, 35.0, 37.7, 38.5, 39.7, 44.7, 65.7, 66.7, 98.5, 98.6, 107.6, 112.2, 118.6, 133.0, 137.9, 149.3. EI-MS *m*/*z* 593 (100), 591 ($[M]^+$, 92), 578 (14), 576 (13), 217 (50), 215 (50), 214 (40), 83 (39). EI-HRMS *m*/*z* calcd for $[M]^+C_{25}H_{38}NO_4S_3Br$ 591.1146, found 591.1145.

Aldehyde **4.9**

Bromide **4.8** (2.59 g, 4.37 mmol) was added to an oven-dried two-necked flask equipped with a thermometer and magnetic stir bar, and the flask was sealed with a rubber septum and flushed with argon. Dry Et_2O (48 mL) was added, and the mixture was stirred until the bromide completely dissolved, then cooled in a dry ice-acetone bath. n-Butyllithium solution (2.5 M in hexanes, 3.5 mL, 8.7 mmol) was added dropwise at a rate such that the temperature did not exceed -60°C. *tert*-Butyllithium solution (1.6 M in pentane, 8.2 mL, 13 mmol; *Caution: highly pyrophoric*) was then added likewise. After 30 minutes, dry DMF (2.7 mL, 35 mmol) was added, the dry ice bath was removed, and the reaction was quenched with methanol (5 mL) once the internal temperature reached -30 °C. The mixture was then partitioned between toluene (70 mL) and water (70 mL). The aqueous layer was removed, and the organic layer was washed with water (3 x 70 mL) followed by brine (10 mL), dried with $MgSO_4$, stirred with silica gel (5 g) and filtered. The drying agent and silica were washed with MTBE, and the combined filtrates were concentrated under reduced pressure to give a brown oil. This material crystallized from boiling cyclohexane-ethyl acetate (30 mL + 5 mL), and the colorless crystalline powder was collected by filtration after cooling. Yield 2.15 g (91%). Mp 149-150°C. ^{1}H

NMR ($CDCl_3$) δ 1.42 (s, 3H), 1.43 (s, 3H), 1.46 (s, 3H), 1.50 (s, 3H), 1.97 (p, *J* = 6.4 Hz, 2H), 2.58 (s, 2H), 2.81-2.86 (m, 6H), 2.93 (s, 2H), 3.60 (d, *J* = 12.2 Hz, 2H), 3.70-3.74 (m, 4H), 3.76 (s, 4H), 6.44 (t, *J* = 7.0 Hz, 1H), 7.02 (d, *J* = 8.6 Hz, 1H), 7.71 (dd, *J* = 8.6, 2.0 Hz, 1H), 7.98 (d, *J* = 2.0 Hz, 1H), 9.69 (s, 1H). ^{13}C NMR ($CDCl_3$) δ 19.8, 22.6, 24.6, 27.1, 27.6, 31.1, 32.2, 34.8, 35.0, 37.6, 38.7, 39.7, 43.8, 65.6, 66.7, 98.5, 98.6, 109.6, 116.9, 126.3, 133.4, 138.8, 154.8, 189.5. EI-MS *m*/*z* 541 ($[M]^+$, 100), 526 (16), 178 (18), 165 (87), 164 (53), 83 (29). EI-HRMS *m*/*z* calcd for $[M]^+$ $C_{26}H_{39}NO_5S_3$ 541.1990, found 541.1996.

Chalcone **4.10**

Aldehyde **4.9** (523 mg, 965 µmol) and 4-cyanoacetophenone (147 mg, 1.01 mmol) were dissolved in ethanol (5 mL) + MTBE (2.5 mL) at 63°C (bath temperature). Pyrrolidine (160 µL, 1.9 mmol) was added, and the flask was sealed with a Teflon stopper. After 2 hours, a 150 µL aliquot of the reaction mixture was transferred to a glass vial, concentrated to dryness, and crystallized from CH_2Cl_2-hexanes (0.3 mL each). The crystal slurry was concentrated to dryness, taken up in MTBE, and added back to the reaction mixture, which rapidly transformed from a deep red solution to an orange crystalline slurry. The mixture was stirred for 1 h at 63°C, then for 36 h at 45-50°C. After cooling slowly to 4°C, the product was collected by filtration, washed with cold ethanol, and dried to give the product as an orange crystalline powder. Yield 588 mg (91%). Mp 148-151°C. ^1H NMR ($CDCl_3$) δ 1.43 (s, 6H), 1.46 (s, 3H), 1.51 (s, 3H), 1.97 (p, *J* = 6.4 Hz, 2H), 2.58 (s, 2H), 2.81-2.86 (m, 6H), 2.98 (s, 2H), 3.62 (d, *J* = 12.1 Hz, 2H), 3.69-3.74 (m, 4H), 3.77 (s, 4H), 6.27 (t, *J* = 7.1 Hz, 1H), 7.00 (d, *J* = 8.7 Hz, 1H), 7.26 (d, *J* = 15.4 Hz, 1H), 7.54 (dd, *J* = 8.7, 2.1 Hz, 1H), 7.74 (d, *J* = 15.4 Hz, 1H), 7.77-7.80 (m, 3H), 8.05-8.08 (m, 2H). ^{13}C NMR ($CDCl_3$) δ 19.8, 23.4, 23.9, 27.1, 27.7, 31.3, 32.2, 35.0, 35.2, 37.7, 38.8, 39.7, 44.0, 65.6, 66.8, 98.6, 98.7, 110.5, 115.4, 116.3, 117.1, 118.2, 123.2, 128.7, 132.1, 132.3, 137.9, 142.3, 146.6, 152.8, 188.8. EI-MS *m*/*z* 668

([M]$^+$, 100), 653 (10), 305 (18), 292 (75), 291 (52), 130 (17), 83 (20). EI-HRMS *m/z* calcd for [M]$^+$ $C_{35}H_{44}N_2O_5S_3$ 668.2412, found 668.2413.

Triarylpyrazoline **4.3** ammonium salt

A mixture of chalcone **4.10** (56.7 mg, 85 µmol), methanol (3 mL), and 1 M aq. HCl 68 µL) was boiled under stirring in a 90°C bath until the starting material dissolved completely (10 min). Water (0.8 mL) was then added, and the mixture was concentrated to ca. 1 mL. Ethanol (3 mL) was added, and the mixture was concentrated to dryness. Water (1 mL), ethanol (1.2 mL), 4-hydrazinobenzenesulfonic acid hemihydrate (25 mg, 130 µmol) and pyridine (16 µL, 200 µmol) were added. The reaction vessel was flushed with Ar, sealed, and stirred at 90°C for 16 h. The mixture was allowed to cool, then concentrated to dryness under a stream of Ar in a 35°C bath. The residue was completely dissolved in aq. NH_4HCO_3 (34 mg, 420 µmol, 3 mL), concentrated to dryness, redissolved in 4 mL water, and subjected to RP-HPLC to give the product as a yellow glassy solid after redissolution in methanol to decompose NH_4HCO_3 followed by drying under high vacuum. Yield 50.4 mg (82%). HPLC t_r = 16.8 min. (gradient 0-20 min., 28% to 35% MeCN / 0.5% aq. NH_4HCO_3 at 4 mL/min, 30 x 1 cm C18 column). ^{1}H NMR (CD_3OD, 25°C) δ 1.83 (p, *J* = 6.9 Hz, 2H), 2.54 (t, *J* = 6.8 Hz, 2H), 2.57 (overlapping t, *J* ≈ 7 Hz), 2.60 (s, 2H), 2.75 (s, 2H), 2.87 (d, *J* = 12.5 Hz, 1H), 2.92 (d, *J* = 12.5 Hz, 1H), 3.10 (dd, *J* = 17.4, 6.2 Hz, 1H), 3.18 (s, 2H) 3.47 (d, *J* = 11.1 Hz, 1H), 3.51 (d, *J* = 11.1 Hz, 1H), 3.53-3.56 (m, 6H), 3.80 (dd, *J* = 17.4, 12.3 Hz, 1H), 5.37 (dd, *J* = 12.3, 6.2 Hz, 1H), 6.66 (d, *J* = 8.6 Hz, 1H), 6.97 (dd, *J* = 8.5, 2.2 Hz, 1H), 7.10 (ad, *J* = 9.0 Hz, 2H), 7.27 (d, *J* = 2.2 Hz, 1H), 7.62 (ad, *J* = 9.0 Hz, 2H), 7.70 (ad, *J* = 8.7 Hz, 2H), 7.86 (ad, *J* = 8.7 Hz, 2H). ^{13}C NMR (CD_3OD) δ 30.0, 32.1, 32.4, 33.9, 34.9, 40.1, 43.6, 45.9, 46.0, 46.4, 65.0 (br, 2C), 65.06, 65.12, 65.16, 111.7, 112.3, 114.1, 119.8, 120.9, 127.4, 127.9, 128.0, 130.7, 133.5 (3C, 2 equivalent, 1 coincident) 136.7, 138.5, 146.6, 147.8, 150.1. ESI-HRMS *m/z* calcd for [M]$^-$ $C_{35}H_{41}O_7N_4S_4$ 757.1853, found 757.1845.

1-(4-cyanophenyl)-3-(4-dimethylaminophenyl)-prop-2-ene-1-one (**4.12**)[5]

p-Dimethylaminobenzaldehyde (744 mg, 4.99 mmol) and 4-acetylbenzonitrile (742 mg, 5.11 mmol) were stirred in ethanol (5 mL) until completely dissolved. Pyrrolidine (209 µL, 2.5 mmol) was added, and the mixture was stirred rapidly for ~ 20 min. until a red precipitate began to form then stirred slowly overnight. After 14 hours, the mixture was diluted with ethanol (7 mL) and cooled to 0°C, and the product was collected by filtration, washed with cold ethanol, and dried. Yield 1.24 g (90%). ^{1}H NMR spectrum is identical to that previously reported.[5]

Chalcone triflate **4.13**

Chalcone **4.12** (655 mg, 2.37 mmol) was completely dissolved in CH_2Cl_2, (10 mL) and methyl triflate (402 µL, 3.56 mmol) was added dropwise to the stirred solution. After 20 h, the precipitated product was collected by filtration, washed with CH_2Cl_2 followed by diethyl ether, and dried under vacuum to give the product as an off-white crystalline powder. Yield 964 mg (92%). Mp 224-225°C. ^{1}H NMR (DMSO-d_6) δ 3.66 (s, 9H), 7.85 (d, *J* = 15.7 Hz, 1H), 8.05-8.13 (m, 5H), 8.19 (ad, *J* = 9.1 Hz, 2H), 8.33 (ad, *J* = 8.6 Hz, 2H). ^{19}F NMR (DMSO-d_6) δ –77.3 (s, 3F). ESI-HRMS *m*/*z* calcd for $[M]^+$ $C_{19}H_{19}ON_2$ 291.1492, found 291.1484.

Triarylpyrazoline **4.11**

Chalcone **4.13** (490 mg, 1.11 mol), 4-hydrazinobenzenesulfonic acid hemi-hydrate (241 mg, 1.22 mmol), pyridine (136 µL, 1.67 mmol) and methanol (4 mL) were stirred overnight in a sealed vessel under Ar at 75°C. After cooling, the mixture was diluted with water + 20% aqueous ammonia (4 mL + 0.15 mL) and stirred for 1 h at 0°C. A yellow powder (390 mg) was collected by filtration and determined by ^{1}H NMR (DMSO-d_6) to be a mixture of isomeric hydrazones. This material was stirred in acetic

acid (3 mL) + water (1 mL) for 3 hours at 100°C under Ar. After cooling, the reaction mixture was diluted with CH_3CN under rapid stirring, and the resulting yellow crystalline powder was collected by filtration, washed with MeOH, and dried under vacuum to give **11** as a fine orange powder. Yield 220 mg (43% overall). To prepare an analytical sample, the product was dissolved in a minimum volume of 2,2,2-trifluoroethanol, filtered through a tight cotton plug, and diluted 10-fold with water to give yellow needles after standing overnight. The needles crumbled to a fine orange powder upon drying. Mp 262°C (dec). UV λ_{max} (H_2O) 387 nm ($\varepsilon = 2.6 \times 10^4\ M^{-1}\ cm^{-1}$). ^1H NMR (2 M LiCl in CD_3OD, 35°C) δ 3.17 (dd, *J* = 17.6, 5.8 Hz, 1H), 3.73 (s, 9H), 4.05 (dd, *J* = 17.6, 12.4 Hz, 1H), 5.78 (dd, *J* = 12.4, 5.8 Hz), 7.09 (ad, *J* = 8.9 Hz, 2H), 7.57 (ad, *J* = 9.1 Hz, 2H), 7.61 (ad, *J* = 8.9 Hz, 2H), 7.77 (ad, *J* = 8.5 Hz, 2H), 7.94 (ad, *J* = 8.5 Hz, 2H), 8.02 (ad, *J* = 9.1 Hz). ESI-HRMS *m*/*z* calcd for $[M+H]^+$ $C_{25}H_{25}O_3N_4S$ 461.1642, found 461.1636.

4.12.2. Steady-state absorption and fluorescence spectroscopy

Sample solutions were filtered through 0.45 μm nylon membrane filters to remove interfering dust particles or fibers. UV-vis absorption spectra were recorded at 22 °C using a Varian Cary Bio50 UV-vis spectrometer with constant-temperature accessory. Steady-state emission and excitation spectra were recorded with a PTI fluorimeter at ambient temperature (22 ± 2°C). Path lengths were 1 cm with a cell volume of 3.0 mL. The fluorescence spectra have been corrected for the spectral response of the detection system (emission correction file provided by instrument manufacturer) and for the spectral irradiance of the excitation channel (via a calibrated photodiode). The mole-ratio titration with Cu(I) was carried out by addition of aqueous copper (II) sulfate stock solution to a 4.6 μM working solution of probe **4.3** under argon in deoxygenated MOPS-K^+ buffer containing 100 μM sodium ascorbate as a reducing agent. The fluorescence quantum yields of triarylpyrazoline **4.11** in aqueous 10 mM pH 7.2 MOPS buffer and in

methanol were determined at 380 nm excitation using norharmane in 0.1 N H_2SO_4 as the fluorescence standard ($\Phi_f = 0.58$)[23] with a 10 cm path length for absorbance measurements to provide high accuracy. Other fluorescence quantum yields were subsequently determined using **4.11** in MOPS buffer as the fluorescence standard with 1 cm path lengths for both absorption (380 nm) and fluorescence measurements.

4.12.3. Analyte selectivity of probe 4.3

A 4.6 μM solution (100 mL) of **4.3** in 10 mM pH 7.2 MOPS buffer was prepared and the fluorescence spectrum was recorded over the emission range 400 to 700 nm with 380 nm excitation. Each cation tested was added to a 3 mL aliquot of the probe solution. The solution was mixed thoroughly, and the fluorescence spectrum was recorded after a 1 minute equilibration period. Emission spectra were integrated over the range of 486-526 nm, and the resulting intensities were divided by that of the free probe. Metal cations were supplied as aqueous stock solutions of the following salts: Mg(II), Ca(II), Co(II), and Ni(II) as nitrates, Na^+ as $NaClO_4$, Cd(II) as $CdCl_2$, Hg(II) as $Hg(OAc)_2$, and Mn(II), Fe(II), Cu(II) and Zn(II) as sulfates. $Cu^I(MeCN)_4PF_6$ was supplied as a 2.5 mM stock solution in MeCN. To avoid aerial oxidation, Fe(II) stock solution was prepared immediately before use.

4.12.4. Time-resolved fluorescence spectroscopy

Fluorescence decay data of **4.3**-Cu(I) (5 μM), CTAP-2-Cu(I) (5 μM), and **4.11** (2 μM) were acquired at the respective emission maxima using a single photon counting spectrometer (Edinburgh Instruments, LifeSpec Series) equipped with a pulsed laser diode as the excitation source (372 nm, FWHM = 80 ps, 10 MHz repetition rate, 1024 channel resolution). Sample solutions of the fluorophore saturated with Cu(I) were

prepared based on steady-state fluorescence titrations as described above, and the steady state spectrum was checked after each decay measurement to confirm stability of the solution. Probe **4.3**-Cu(I) solutions were found to be unstable in air saturated solution, so the fluorescence decay profiles of both probe-Cu(I) complexes were subsequently acquired under deoxygenated conditions. To ensure a relevant comparison, the fluorescence decay of **4.11** in H_2O was measured under both air-saturated and deoxygenated conditions, and the two fluorescence lifetimes were the same within experimental error (2.07 and 2.09 ns, respectively). The time decay data were analyzed by non-linear least squares fitting with deconvolution of the instrumental response function using the FluoFit software package.[24]

4.13. References

(1) Morgan, M. T.; Bagchi, P.; Fahrni, C. J. *J. Am. Chem. Soc.* **2011**, *133*, 15906.

(2) Yang, L.; McRae, R.; Henary, M. M.; Patel, R.; Lai, B.; Vogt, S.; Fahrni, C. J. *Proc Natl Acad Sci U S A* **2005**, *102*, 11179.

(3) Verma, M.; Chaudhry, A. F.; Morgan, M. T.; Fahrni, C. J. *Org. Biomol. Chem.* **2010**, *8*, 363.

(4) Chaudhry, A. F.; Verma, M.; Morgan, M. T.; Henary, M. M.; Siegel, N.; Hales, J. M.; Perry, J. W.; Fahrni, C. J. *J. Am. Chem. Soc.* **2010**, *132*, 737.

(5) Cody, J.; Mandal, S.; Yang, L.; Fahrni, C. J. *J. Am. Chem. Soc.* **2008**, *130*, 13023.

(6) Chaudhry, A. F.; Mandal, S.; Hardcastle, K. I.; Fahrni, C. J. *Chem. Sci.* **2011**, *2*, 1016.

(7) Morgan, M. T.; Bagchi, P.; Fahrni, C. J. *Dalton Trans.* **2013**, *42*, 3240.

(8) Ambundo, E. A.; Deydier, M. V.; Grall, A. J.; Aguera-Vega, N.; Dressel, L. T.; Cooper, T. H.; Heeg, M. J.; Ochrymowycz, L. A.; Rorabacher, D. B. *Inorg. Chem.* **1999**, *38*, 4233.

(9) Akao, A.; Nonoyama, N.; Yasuda, N. *Tetrahedron Lett.* **2006**, *47*, 5337.

(10) Buter, J.; Kellogg, R. M. *J. Org. Chem.* **1981**, *46*, 4481.

(11) Binstead, R. A.; Zuberbühler, A. D.; 3.0.27 ed.; Spectrum Software Associates, Marlborough MA 01752: 2001.

(12) Balakrishnan, K. P.; Kaden, T. A.; Siegfried, L.; Zuberbühler, A. D. *Helv. Chim. Acta* **1984**, *67*, 1060.

(13) Kamau, P.; Jordan, R. B. *Inorg. Chem.* **2001**, *40*, 3879.

(14) Bernardo, M. M.; Schroeder, R. R.; Rorabacher, D. B. *Inorg. Chem.* **1991**, *30*, 1241.

(15) Chaudhry, A. F.; Mandal, S.; Hardcastle, K. I.; Fahrni, C. J. *Chem. Sci.* **2011**, *2*, 1016.

(16) Valeur, B. *Molecular Fluorescence: Principles and Applications*; Wiley-VCH: Weinheim, 2001.

(17) Rivett, D. E.; Rosevear, J.; Wilshire, J. F. K. *Aust. J. Chem.* **1979**, *32*, 1601.

(18) Rivett, D. E.; Rosevear, J.; Wilshire, J. F. K. *Aust. J. Chem.* **1983**, *36*, 1649.

(19) Forster, T.; Rokos, K. *Chem. Phys. Lett.* **1967**, *1*, 279.

(20) Yu, H. T.; Colucci, W. J.; McLaughlin, M. L.; Barkley, M. D. *J. Am. Chem. Soc.* **1992**, *114*, 8449.

(21) Davidson, R. S.; Pratt, J. E. *Photochem Photobiol* **1984**, *40*, 23.

(22) Krezel, A.; Bal, W. *J. Inorg. Biochem.* **2004**, *98*, 161.

(23) Pardo, A.; Reyman, D.; Poyato, J. M. L.; Medina, F. *J. Lumin.* **1992**, *51*, 269.

(24) Enderlein, J.; Erdmann, R. *Optics Commun.* **1997**, *134*, 371.

CHAPTER 5

RAISING THE BAR: IMPROVING THE MAXIMUM FLUORESCENCE CONTRAST RATIO AND QUANTUM YIELD AVAILABLE FOR AQUEOUS COPPER(I) PROBES BY MODIFYING BOTH THE LIGAND AND FLUOROPHORE DESIGNS

5.1. Introduction:

In the previous chapter, we attempted to improve upon the fluorescence contrast ratio and quantum yield offered by our aqueous Cu(I)-probe CTAP-2[1] using a new ligand design strategy previously demonstrated to improve these parameters in methanolic Cu(I)-probes.[2] This entailed fusion of the PET donor aryl ring to the Cu(I)-ligand backbone while retaining all other design features of CTAP-2, including the sulfonated triarylpyrazoline fluorophore, the macrocyclic ligand topology, and two geminal pairs of hydroxymethyl groups attached to the three-carbon bridges of the ligand structure. While the new design (probe **4.3**) did not yield the expected improvements in contrast ratio and quantum yield, it did provide a strong and highly selective fluorescence turn-on response to Cu(I) with a reduced pH sensitivity compared to CTAP-2. More importantly, we uncovered the primary factors limiting the fluorescence response of CTAP-2 and **4.3** to Cu(I) in aqueous solution, which are incomplete Cu-N coordination resulting in residual PET in the probe-Cu(I) complex and fluorescence quenching by excited-state proton transfer (ESPT).[3] In this chapter, both of these issues are addressed by iterative modification of the ligand and fluorophore designs, ultimately resulting in a dramatic

improvement in both the fluorescence contrast ratio and quantum yield available from aqueous Cu(I)-probes.

5.2. Improving the intrinsic fluorophore quantum yield in aqueous solution

5.2.1. Suppression of ESPT by electron-withdrawing substituents

As discussed in Chapter 4, the intrinsic fluorescence quantum yield of the CTAP-2 fluorophore is significantly limited by ESPT in neutral aqueous solution. This was shown for the trimethylammonium analog **4.11** by substantial solvent deuterium isotope effects on the fluorescence quantum yield and lifetime, which both increased by over 70% in D_2O versus H_2O solution.[3] Although the ESPT pathway appears to be suppressed for **4.11** in methanol, triarylpyrazolines lacking strong electron-withdrawing groups do show strong solvent isotope effects in methanolic solution, and the magnitude of the effect is significantly influenced by the electron-donating or withdrawing character of substituents on the 1-aryl ring.[4] For example, the parent 1,3,5-triphenylpyrazoline shows an increase in fluorescence quantum yield of 1.31-fold in CH_3OD vs. CH_3OH, but the effect increases to 1.71-fold when an amino-group is placed at the para-position of the 1-aryl ring. By contrast, the effect is reduced to 1.13-fold by a cyano-group and 1.06-fold by a nitro-group at the same position. The substitution pattern of the 3-aryl ring appears to be less important, as a para-amino group on this ring increases the solvent isotope effect only slightly to 1.46-fold.[4]

Interestingly, the above data mirror trends in the fluorescence quantum yields of 1,3,5-triarylpyrazolines reported earlier by Rivett *et al*, who noted that the quantum yields in methanolic solution are increased by electron-withdrawing substituents and strongly diminished by electron-donating substituents on the 1-aryl ring, while no such effect is observed in cyclohexane solution.[5] As shown for a representative selection of

these *para*-substituted triarylpyrazolines in Table 5.1, the effects on fluorescence quantum yield correlate with the Hammett constants (σ_p) of the 1-aryl substituents, with stronger electron-withdrawing groups giving greater improvements in fluorescence quantum yield, while substituents on the 3-aryl ring exert a similar but substantially weaker effect.

Table 5.1: Relative Fluorescence quantum yield versus Hammett substituent constant for monosubstituted triarylpyrazolines characterized by Rivett *et al* in methanolic solution

Substituent	σ_p [a]	Φ_r [b] (1-Aryl substituted)	Φ_r [b] (3-Aryl substituted)
OMe	-0.27	<0.05	0.39
H	0	0.46	0.46
Cl	0.23	0.52	0.51
CN	0.66	0.91	0.66
SO_2Me	0.72	1.00	0.85

[a] Hammett para-substituent constant.[6] [b] Relative fluorescence quantum yield in methanolic solution (9,10-diphenylanthracene $\Phi_r = 1$).[5]

Based on the data presented above, the adverse effect of ESPT on the fluorescence quantum yields of 1,3,5-triarylpyrazolines in methanolic solution can be abolished by substitution of the 1-aryl ring with sufficiently powerful electron-withdrawing groups. It appears that this effect can also be harnessed in aqueous solution given the high fluorescence quantum yield (0.62) of the difluorinated CTAP-2 analog **3.3c** under acidic conditions (Chapter 3). Increasing the electron-withdrawing power of the 1-aryl ring, however, also results in a blue shift in absorption and emission wavelengths, which corresponds to a higher excited-state energy and thus a greater PET driving force. For Cu(I)-probes, the benefit of ESPT inhibition may be overpowered by a large increase in PET driving force if the 1-aryl ring is too electron-deficient, as demonstrated by the very low quantum yield of 0.01 observed for **3.3c**-Cu(I).

5.2.2. A sulfonamide-substituted triarylpyrazoline fluorophore with high fluorescence quantum yield in aqueous solution

5.2.2.1. Fluorophore design

Considering that the CTAP-2 fluorophore suffers from significant ESPT-mediated quenching while its difluorinated analog **3.3c** gives an excessive PET driving force, the monofluorinated derivative **3.3b** might be expected to provide an ideal compromise in electron-withdrawing character of the 1-aryl ring. This compound, however, gave only a slight improvement over CTAP-2 for the fluorescence quantum yield in acidic solution (0.31 vs. 0.25) but a 2.5-fold reduction in quantum yield of the Cu(I)-saturated form (0.033 vs. 0.083). Therefore, we investigated an alternative set of electron-withdrawing substituents.

We had previously considered the use of sulfonamide moieties as electron-withdrawing groups for water-soluble electronically tuned triarylpyrazoline fluorophores, particularly as an alternative to the 3-aryl cyano-substituent that would facilitate future design elaboration, such as conjugation to a protein or auxiliary fluorophore, via N-alkylation. As indicated by the Hammett substituent constant σ_p of 0.65 for the dimethylaminosulfonyl ($-SO_2NMe_2$) group, the electron-withdrawing power of an S-linked sulfonamide substituent is quite similar to that of a cyano-group ($\sigma_p = 0.66$) and significantly greater than that of a sulfonate moiety ($\sigma_p = 0.36$).[6] Therefore, replacing the 1-aryl sulfonate in addition to the 3-aryl cyano-group of the CTAP-2 fluorophore with sulfonamide moieties would be expected to reduce fluorescence quenching by ESPT. To maintain high aqueous solubility, the sulfonamide nitrogens can be functionalized with ionizable groups. For this purpose we chose ethanesulfonic acid units, thus permitting characterization over a large pH range while introducing minimal additional hydrophobic surface area. For initial evaluation of this fluorophore design, a 5-aryl dimethylamino-group was included as a PET switch that can be protonated by relatively low acid

concentrations, thus reducing the potential for interference from the acid-mediated ESPT quenching pathway (Chapter 4) during characterization. The chosen design (compound **5.1**) is shown in Figure 5.1.

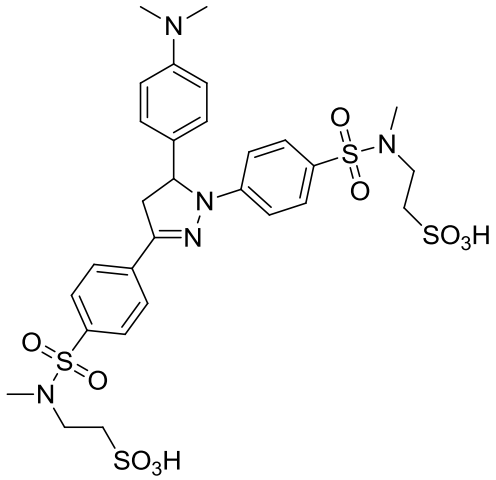

5.1

Figure 5.1: Sulfonamide-substituted triarylpyrazoline **5.1**

5.2.2.2. Synthesis

The triarylpyrazoline core of **5.1** was assembled via an analogous route to the compounds described in Chapters 3 and 4: The sulfonamide-substituted arylhydrazine **5.2** was prepared from 4-fluorobenzenesulfonyl chloride by reaction with aqueous methylamine followed by nucleophilic aromatic substitution with hydrazine. The sulfonamide-substituted acetophenone **5.3,** also obtained by reaction of a commercially available sulfonyl chloride with methylamine, was subjected to pyrrolidine-catalyzed condensation with *p*-dimethylaminobenzaldehyde to give chalcone **5.4** followed by acid-catalyzed condensation with arylhydrazine **5.2** to give triarylpyrazoline **5.5** (Scheme 5.1).

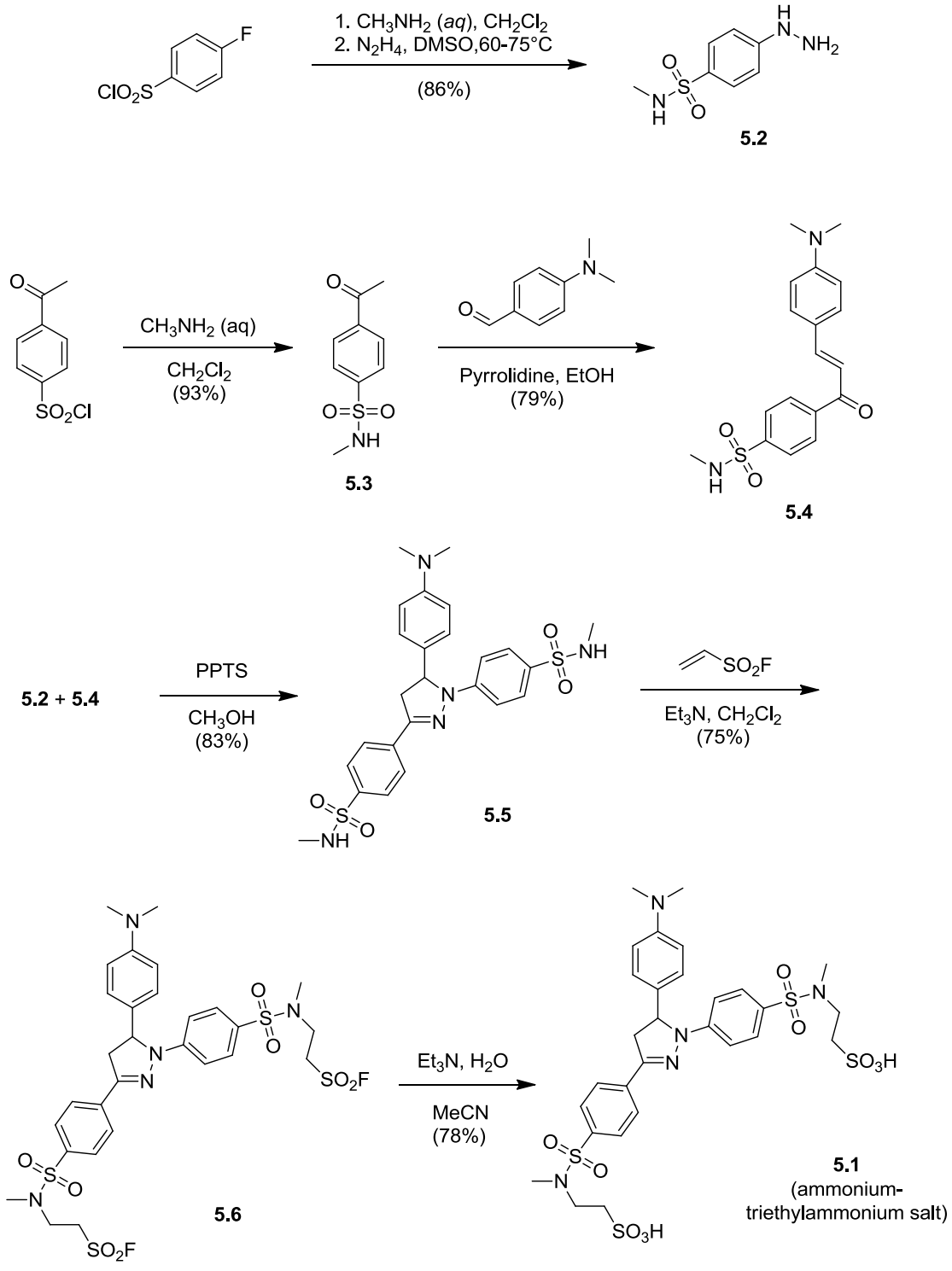

Scheme 5.1: Synthesis of sulfonamide reference fluorophore **5.1**

As shown above, the secondary sulfonamide moieties of **5.5** were functionalized to give the sulfonyl fluoride intermediate **5.6** by base-catalyzed conjugate addition to the potent Michael acceptor ethenesulfonyl fluoride (ESF). Interestingly, no literature precedent could be found for this reaction, and ESF in the absence of base has in fact been employed to selectively functionalize other nucleophilic moieties in the presence of primary or secondary sulfonamides.[7] The sulfonyl fluoride moieties were hydrolyzed to sulfonate anions using a triethylamine-water-acetonitrile mixture, which also gave moderate amounts of secondary sulfonamide side products, apparently by a competing base-catalyzed elimination reaction. Nevertheless, the desired triarylpyrazoline could be purified by HPLC using an ammonium bicarbonate-containing mobile phase, and was obtained in good yield as a mixed ammonium-triethylammonium salt.

5.2.2.3. Characterization and evaluation

Triarylpyrazoline **5.1** was found to be freely soluble in water, giving very weak fluorescence at neutral pH and bright fluorescence upon acidification. In 1 mM HCl, where the dimethylamino-group is expected to be completely protonated, **5.1** gave a fluorescence quantum yield of 0.59, which is more than double that of protonated CTAP-2 or its quaternary ammonium fluorophore analog **4.11,** at the expense of only a small blue-shift of the absorption and emission maxima (Table 5.2).

Table 5.2: Photophysical properties of **5.1** versus other water-soluble triarylpyrazolines

Compound	Medium	Abs. λ_{max}/nm	Em. λ_{max}/nm	ΔE_{00}/eV[b]	Φ_f
	Buffer[a]	387	491	2.87	0.006[c]
5.1	1 mM HCl	383	491	2.88	0.59
	5 mM HCl	383	491	2.88	0.55[d]
4.11	Buffer[a]	387	511	2.81	0.28
CTAP-2	5 mM HCl	388	512	2.82	0.25
3.3b	5 mM HCl	367	502	2.92	0.31
3.3c	5 mM HCl	348	478	3.08	0.62

[a] 10 mM MOPS pH 7.2. [b] Estimated as the mean of the excitation and emission energies. [c] This value decreased to 0.002 upon addition of 10 mM NaOH. [d] Calculated from Φ_f in 1 mM HCl and the respective fluorescence lifetimes assuming no change in k_r (see Table 5.3).

Notably, **5.1** has a longer wavelength absorption maximum and similar excited-state energy compared to the monofluorinated CTAP-2 analog **3.3b**, but the fluorescence quantum yield is substantially higher. Based on a computationally derived effective Hammett substituent constant of $\sigma^c = 0.28$ for an ortho-fluoro-substituent,[8] the combined electron-withdrawing power of the 1-aryl -F and $-SO_3^-$ substituents of **3.3b** ($\Sigma\sigma = 0.64$) is expected to be similar to that of the 1-aryl sulfonamide substituent of **5.1** ($\sigma_p = 0.65$). Based on the above data and given the similar electron-withdrawing ability of cyano- and dialkylaminosulfonyl-groups, it appears that the sulfonamide moieties of **5.1** provide a greater fluorescence quantum yield in aqueous solution than a combination cyano, fluoro- and sulfonate substituents with comparable overall electron-withdrawing power.

5.2.3. Confirming the origin of the improved fluorescence quantum yield of the bis-sulfonamide fluorophore

While the arenesulfonamide compound **5.1** clearly provides a superior fluorescence quantum yield in aqueous solution compared to the arenesulfonate-based triarylpyrazoline fluorophore of CTAP-2 and **4.11**, we questioned whether such a large effect could be fully explained by ESPT inhibition mediated by the greater electron-withdrawing power of a sulfonamide versus a sulfonate substituent on the 1-aryl ring, especially given the lower quantum yield of the electronically similar triarylpyrazoline **3.3c** (see above). The 3-aryl cyano-group of the previous sulfonated triarylpyrazolines might itself serve as a proton acceptor in the excited state, an effect previously noted for cyano-substituted donor-acceptor biphenyls.[9] If this were the case, then the fluorescence quantum yield in aqueous solution might be improved without increasing the PET driving force simply by replacing the 3-aryl cyano-group with a comparably electron-withdrawing sulfonamide substituent without modification of the 1-aryl ring. To test this possibility, we prepared reference compound **5.7**, a direct analog of **4.11** containing a dimethylaminosulfonyl-substituent in place of the cyano-group (Figure 5.2).

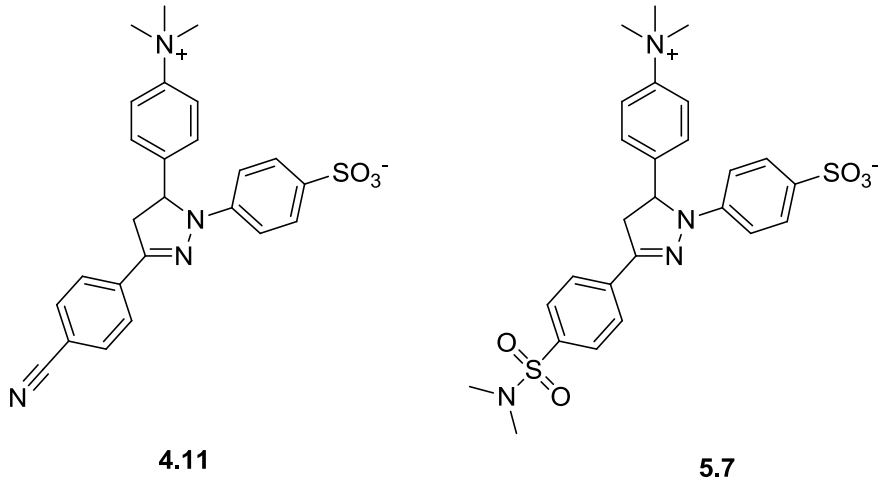

Figure 5.2: Structures of reference fluorophores **4.11** and **5.7**

Compared to **4.11**, triarylpyrazoline **5.7** gave very similar spectral properties, with a slight blue shift in absorption and emission maxima from 387 and 511 nm to 381 and 508 nm for **4.11** and **5.7**, respectively. The fluorescence quantum yield in neutral aqueous solution was also nearly identical for the two compounds, increasing only from 0.28 to 0.30. Therefore, it appears that the change from a cyano- to a sulfonamide substituent at the 3-aryl ring does not explain the greatly increased fluorescence quantum yield of **5.1**. Furthermore the fluorescence quantum yield of **5.7** increased from 0.30 in H_2O to 0.50 in D_2O, demonstrating a nearly identical solvent isotope effect to that of **4.11** (1.67 vs. 1.71), and implying that ESPT-mediated quenching is equally important for the two compounds.

To determine whether ESPT inhibition is indeed the primary factor responsible for the improved fluorescence quantum yield of sulfonamide-substituted triarylpyrazoline **5.1** relative to the sulfonate **4.11**, we measured the fluorescence decay profiles of **5.1** in acidified H_2O and D_2O by picosecond time-resolved fluorescence spectroscopy as previously described in Chapter 4 to determine the solvent isotope effect on the fluorescence lifetime. The results are shown below in Figure 5.3 and Table 5.3.

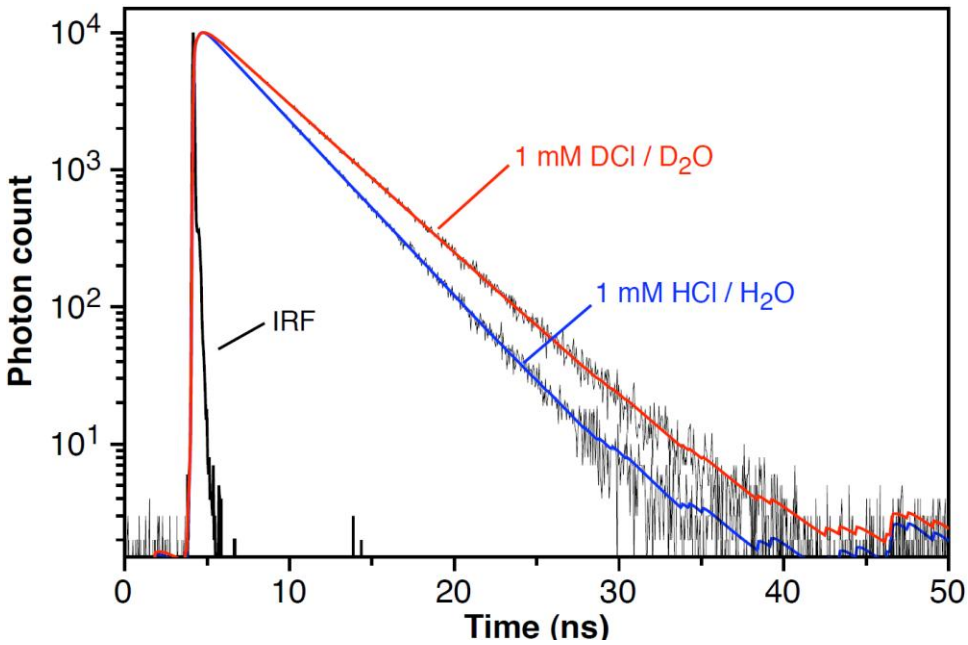

Figure 5.3: Fluorescence decay profiles of triarylpyrazoline **5.1** in acidic H_2O and D_2O solution

As shown above, the difference in the fluorescence decay profile of **5.1** in D_2O versus H_2O is rather small. In fact, the fluorescence lifetime of **5.1** increased by only 19% from 3.38 ns in H_2O to 3.99 ns in D_2O (Table 5.3), which stands in marked contrast to the 72% increase observed for **4.11**. The fluorescence quantum increased proportionally to the lifetime, indicating that the isotopic composition of the solvent affects only the nonradiative deactivation rate constant k_{nr} and not the radiative deactivation rate constant k_r. Estimating the rate constant of ESPT in H_2O as $k_{ESPT} = k_{nr}(H_2O) - k_{nr}(D_2O)$ yields a value of only 4.5×10^7 s^{-1} for **5.1**, which is more than four-fold lower than the value of 2.0×10^8 s^{-1} for **4.11**. Additionally, k_r is slightly higher for **5.1**, but this effect is less important than the large reduction in ESPT rate.

Table 5.3: Fluorescence decay data for compound **5.1** versus **4.11** in H_2O and D_2O

Compound	Medium	τ_f/ns	$\chi^{2\,a}$	$k_r^{b,d}$ /10^8 s^{-1}	$k_{nr}^{c,d}$ /10^8 s^{-1}
5.1	1 mM HCl in H_2O	3.38	0.973	1.75	1.21
	5 mM HCl in H_2O	3.13	1.08	1.75[e]	1.45
	1 mM DCl in D_2O	3.99	1.06	1.75	0.76
4.11	H_2O	2.07	1.17	1.35	3.48
	D_2O	3.36	1.03	1.35	1.46

[a] Goodness-of-fit parameter. All fits include a risetime of 0.25-0.4 ns. [b] $k_r = \Phi_f/\tau_f$. [c] $k_{nr} = (1-\Phi_f)/\tau_f$. [d] The third digit is not significant in absolute terms but is included for internal consistency. [e] Assumed.

Concluding from the above data, it appears that replacing the 1-aryl sulfonate of the CTAP-2 fluorophore by a more electron-withdrawing sulfonamide substituent produces a large increase in fluorescence quantum yield in aqueous solution due primarily to inhibition of ESPT in addition to a small contribution from an increased k_r.

5.3. Testing the new sulfonamide-based fluorophore with an existing Cu(I)-ligand design

5.3.1. Probe design

While the bis-sulfonamide fluorophore of **5.1** provides a substantially larger fluorescence quantum yield than the CTAP-2 fluorophore in the absence of PET quenching, its utility for Cu(I) probes will depend on the PET driving force it provides with the available Cu(I)-ligand-PET donor designs. As discussed in the previous section, the fluorophore of **5.1** is expected to be electronically similar to that of the monofluorinated CTAP-2 analog **3.3b**, and is therefore likely to provide a somewhat larger PET driving force than the unfluorinated CTAP-2 fluorophore when combined

with the same Cu(I)-ligand moiety. The difference in PET driving force between the two fluorophore designs cannot be estimated directly from the Rehm-Weller equation (Chapter 2), because the reduction potentials of 1,3,5-triarylpyrazolines are typically well outside of the accessible window in aqueous solution. Therefore, before optimizing the ligand design, we gauged the PET driving force of the new bis-sulfonamide fluorophore by combining it with the integrated arylamine thiazacrown ligand of the CTAP-2 analog **4.3** (Chapter 4), allowing a side-by-side comparison of the two fluorophore designs with the same Cu(I)-ligand. The resulting probe **5.8** and its predecessor **4.3** are shown below.

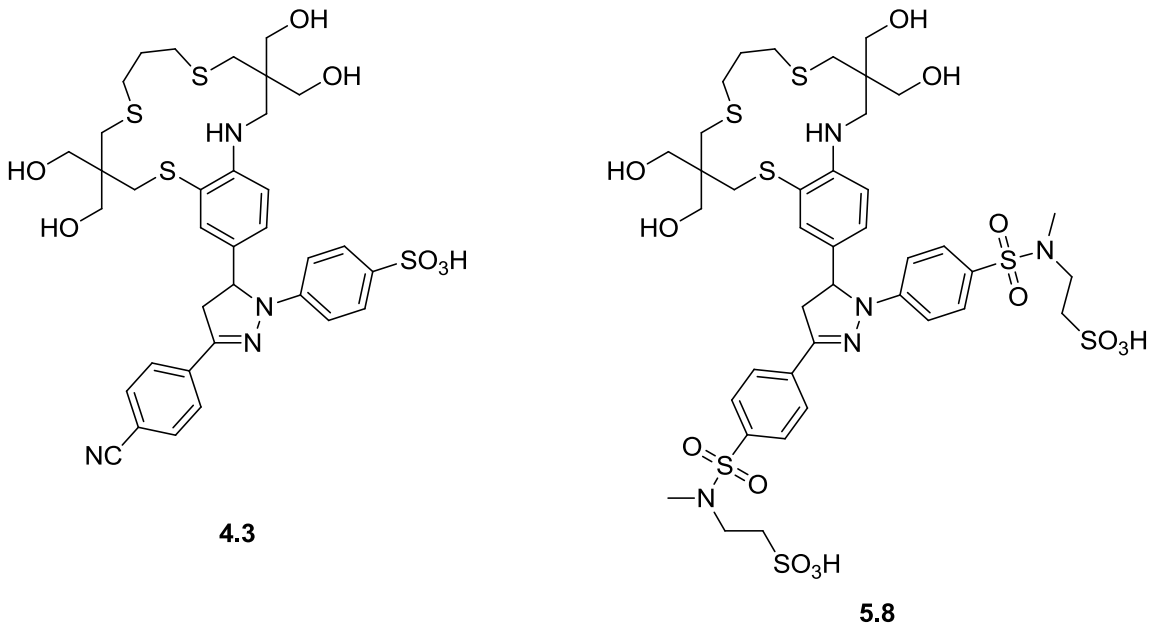

Figure 5.4: Structures of Cu(I)-probes **4.3** and **5.8**

5.3.2. Synthesis

Probe **5.8** was synthesized analogously to **5.1** using the previously prepared aldehyde **4.9** (Chapter 4). Condensation with acetophenone derivative **5.3** gave chalcone

5.9, which was converted to triarylpyrazoline **5.10** in good yield using a one-pot procedure involving cleavage of the acetonide moieties, acid-catalyzed condensation with arylhydrazine **5.2** in methanolic solution, and re-acetalization with 2,2-dimethoxypropane. In the initial acetonide cleavage step, the volatile byproducts are evaporated under a stream of inert gas before addition of the arylhydrazine, thus preventing its conversion to the corresponding acetone hydrazone and providing a shorter reaction time and higher yield than the two-step method previously employed for the CTAP-2 series.

The sulfonamide NH moieties of triarylpyrazoline **5.10** were readily functionalized with ESF under basic conditions without significant alkylation of the arylamine NH. Notably, this chemoselectivity is exactly opposite to that previously reported in the literature for an arylamine-sulfonamide substrate heated with ESF in DMF solution.[7] Furthermore, the sulfonyl fluoride moiety itself is unreactive toward sulfonamide formation with arylamines even at elevated temperatures,[7] and thus should be compatible with a wide variety of secondary amine Cu(I)-ligand designs. The sulfonyl fluoride **5.11** was hydrolyzed by a one-pot, two-step procedure involving addition of aqueous HCl to a solution of the substrate in acetonitrile to hydrolyze the acetonide moieties followed by addition of excess triethylamine to promote sulfonyl fluoride hydrolysis, which furnished the desired product **5.8** in moderate yield as the ammonium salt after HPLC purification (Scheme 5.2).

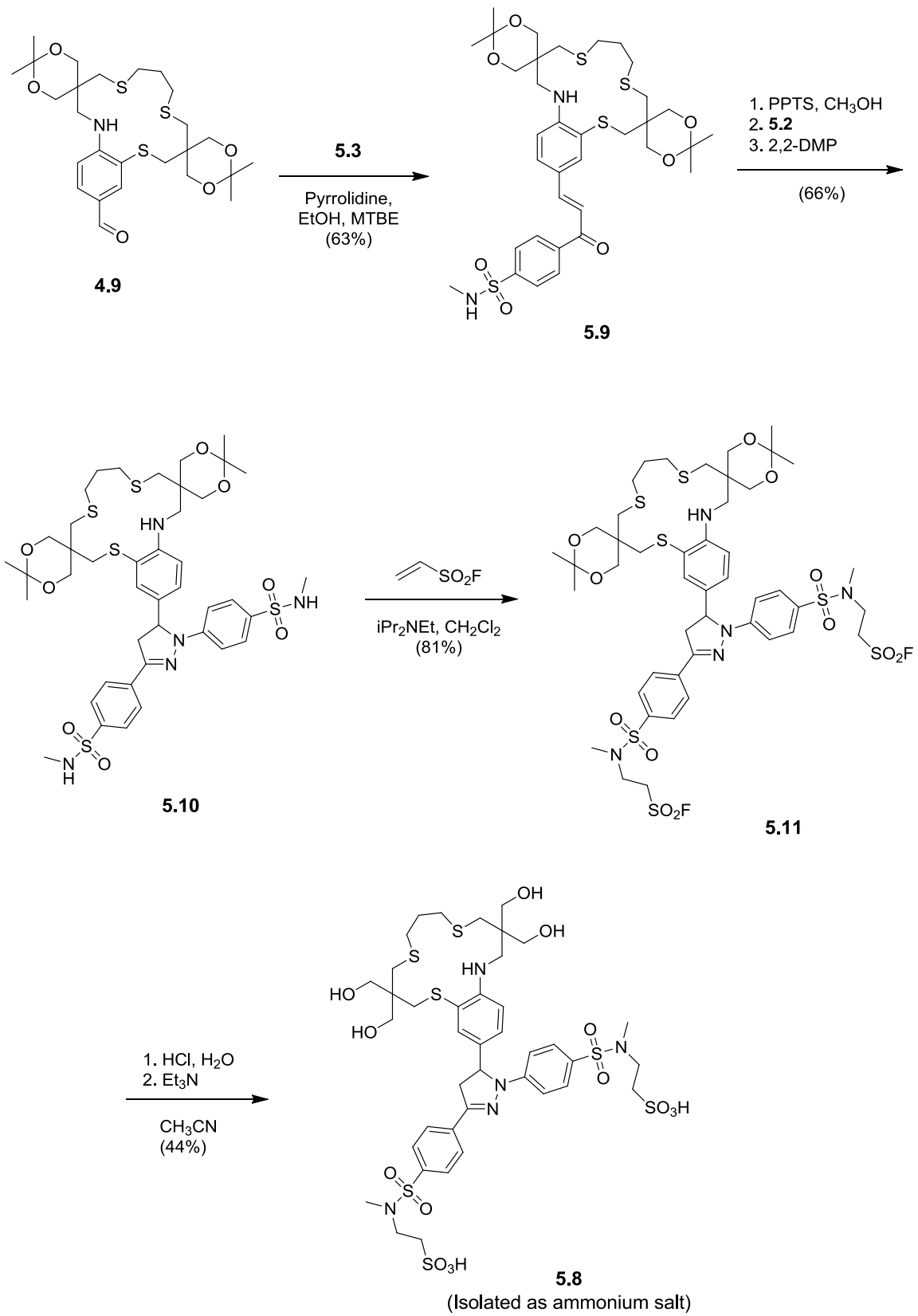

Scheme 5.2: Synthesis of probe **5.8**

5.3.3. Characterization and evaluation

Probe **5.8** was found to be freely soluble in water as expected and has very similar spectral properties to its fluorophore analog **5.1**. In neutral aqueous buffer (10 mM MOPS, pH 7.2), **5.8** gave an absorption maximum identical to that of **5.1** at 387 nm. Upon saturation with Cu(I), **5.8** gave a 30-fold fluorescence turn-on response with an emission maximum of 497 nm, but reached a peak fluorescence quantum yield of only 0.03. This is substantially lower than the value of 0.074 observed for probe **4.3**, which is indicative of a stronger PET driving force for the bis-sulfonamide fluorophore. Notably, the fluorescence quantum yield upon Cu(I)-saturation of **5.8** is similar to the value of monofluorinated CTAP-2 analog **3.3b** (0.033), suggesting that the PET driving force is similar for these two compounds as expected based on the electronic similarity of the fluorophores. In fact, the proportional decrease in quantum yield for **5.8** versus **4.3** is the same as for **3.3b** versus CTAP-2.

Based on the above data, the increase in PET driving force for the new sulfonamide-based fluorophore versus the previous sulfonate-based platform is significant but appears to be comparable to the addition of a single fluoro-substituent to the 1-aryl ring. An increase of this size should not be insurmountable through better ligand design; in fact, the value of initial PET driving force ($-\Delta G^0_{et}$) required for maximum contrast ratio actually increases for a ligand providing a greater increase in donor potential upon Cu(I)-binding, as exemplified by the additional fluoro-substituent required for optimum contrast ratio in probe **4.2d** versus its N-arylthiazacrown forerunner **2.4c** (See Chapter 4, Table 4.1). [2,10] Therefore, bis-sulfonamide fluorophore design should provide a suitable platform for optimization of the Cu(I)-ligand structure.

5.4. Cleaving the thiazacrown ring substantially improves contrast ratio and quantum yield

5.4.1. Probe design

There are several possible explanations for the apparent low degree of Cu-N coordination[3] and poor fluorescence recovery observed for the integrated arylamine-thiazacrown ligand of **4.3** and **5.8,** including reduced basicity of the arylamine nitrogen due to an inductive effect of the nearby hydroxymethyl groups, participation of one of the OH-groups as a donor toward Cu(I) in place of the arylamine nitrogen, or geometric constraints imposed by the sterics of the highly substituted and relatively rigid benzo-fused thiazacrown structure. To investigate the latter possibility, we designed probe **5.12**, in which the trimethylene bridge connecting the two aliphatic thioethers of **5.8** has been replaced by two methyl groups, giving a closer analog to the ultra high-contrast methanolic Cu(I)-probe[2] **4.2d**. The structures of **5.12** and also **4.2d** for comparison are shown in Figure 5.5.

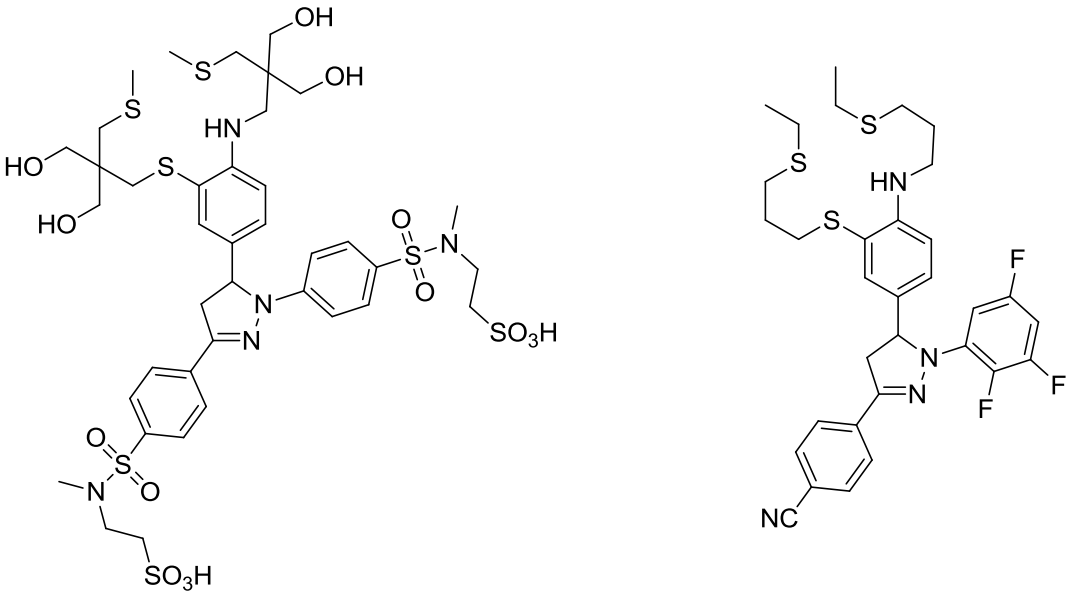

5.12 **4.2d**

Figure 5.5: Structure of aqueous Cu(I)-probe **5.12** and methanolic Cu(I) probe **4.2d**

5.4.2. Synthesis

As shown in Scheme 5.3, The Cu(I)-ligand moiety of **5.12** was prepared as its protected aldehyde derivative **5.13** by a similar route as for its macrocyclic analog **4.9** (Chapter 4), except that the aldehyde moiety was introduced at the beginning of the synthesis via the previously described[11] benzothiazolinone aldehyde **5.14**. This compound was N-alkylated with neopentyl iodide derivative **5.15**, which itself was prepared from the thietane intermediate **3.15** previously utilized in the synthesis of CTAP-2. The resulting product **5.16** was treated with aqueous sodium hydroxide in hot DMSO solution to cleave the thiocarbamate moiety, and the resulting thiolate was alkylated in situ with iodide **5.15** to give aldehyde **5.13**. This aldehyde was condensed with acetophenone derivative **5.3** to produce chalcone **5.17**, which was subsequently converted to triarylpyrazoline **5.18**, sulfonyl fluoride **5.19**, and finally to probe **5.12** using the methodology established for probe **5.8**. The final product was isolated by HPLC as its ammonium salt; the low isolated yield is due to difficulty in isolation and does not reflect the actual chemical conversion.

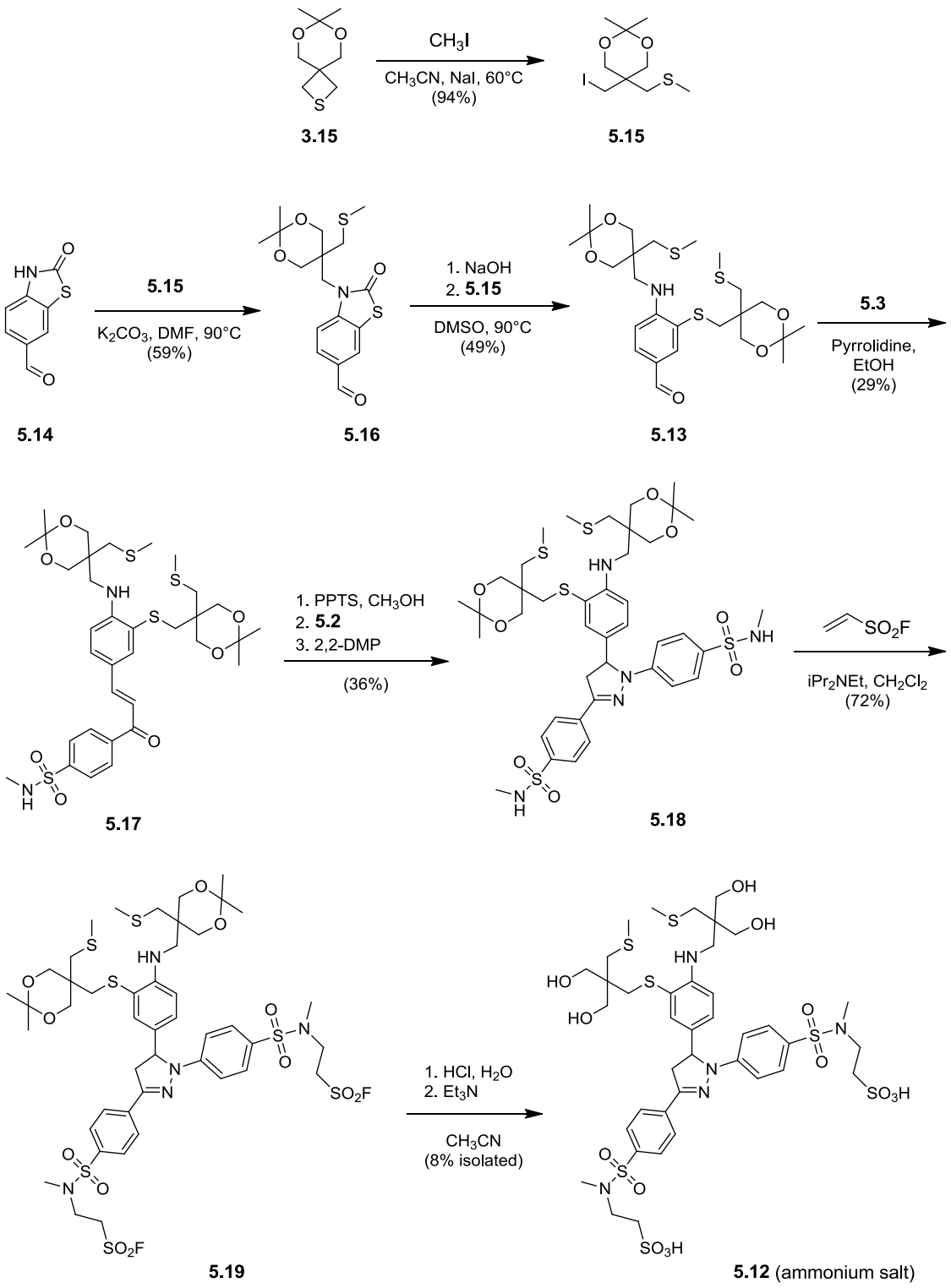

Scheme 5.3: Synthesis of probe **5.12**

5.4.3. Characterization and evaluation

Probe **5.12** dissolves rapidly in water and gives an absorption maximum identical to that of its macrocyclic congener **5.8** at 387 nm in neutral buffer. The fluorescence emission maximum upon addition of Cu(I) is also identical at 487 nm, but the intensity of the fluorescence response to Cu(I) is dramatically improved, reaching a contrast ratio of 100 and a fluorescence quantum yield of approximately 0.11. This represents the first actual performance improvement over CTAP-2 in aqueous solution. Given that the structures of **5.8** and **5.12** differ only by a single carbon atom at a site far removed from the fluorophore and PET donor, the more than three-fold improvement in fluorescence quantum yield and contrast ratio for **5.12** versus **5.8** provides a striking demonstration of the importance of cation binding mode for achieving a high-contrast response in PET-based fluorescence turn-on probes. Interestingly, **5.12** is also more responsive to acidification than its macrocyclic analog, reaching maximum fluorescence intensity at only 40 mM HCl versus 100 mM HCl for **5.8**. This difference is surprising given the identical fluorophore and PET donor structure of these compounds, and suggests that the pKa of the arylamine moiety in **5.8** is somehow influenced by the steric constraints of the macrocyclic ligand.

Although **5.12** gave a substantial improvement in performance relative to previous water-soluble Cu(I)-probes, the fluorescence decay profile upon saturation with Cu(I) is clearly multiexponential (Figure 5.6), suggesting that Cu-N coordination is incomplete even for this probe. The decay could could be fit to a biexponential model with components of 0.88 ns (62%) and 1.52 ns (38%) or to a triexponential model with components of 1.56 ns (32%), 0.93 ns (67%), and 0.25 ns (1%) (χ^2 = 1.09, blue trace).

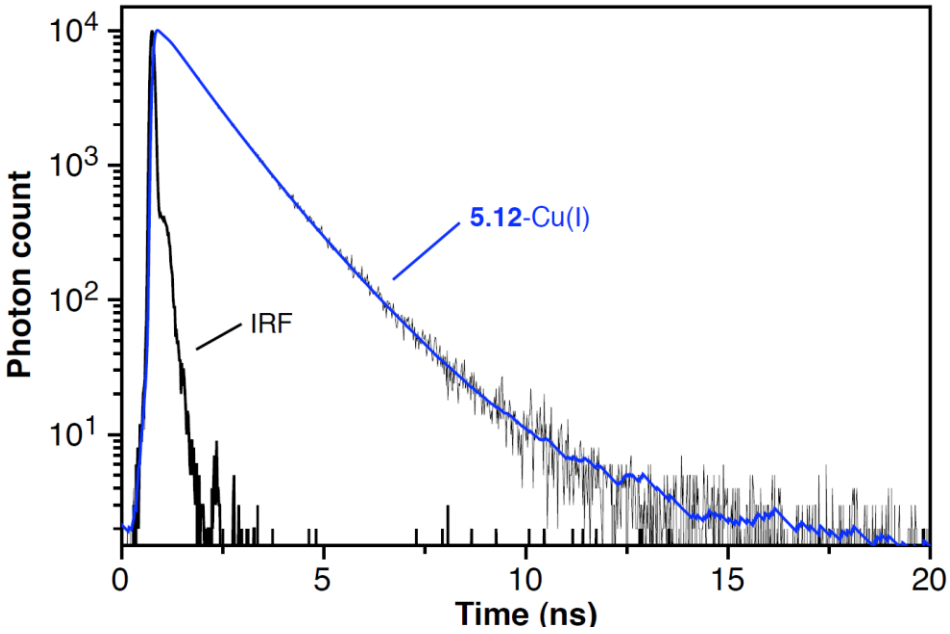

Figure 5.6: Fluorescence decay profile of Cu(I)-saturated **5.12**.

5.5. Removing a geminal pair of hydroxymethyl groups to reduce steric congestion in the Cu(I)-complex

5.5.1. Probe design

The large improvement in fluorescence contrast ratio and quantum yield obtained simply by opening the macrocyclic ring of probe **5.8** to give **5.12** suggests that the low Cu-N coordination apparent for the tetrahydroxylated thiazacrown ligand design of **4.3** and **5.8** is primarily due to steric effects. While the open-chain ligand design of **5.12** substantially improves the fluorescence response to Cu(I), this probe nevertheless gives a multiexponential fluorescence decay profile and does not achieve a fluorescence recovery comparable to that of the methanolic Cu(I)-probe **4.2d**, which gave a monoexponential decay profile.[2] Since the most substantial difference in ligand architecture between **4.2d** and **5.12** is the presence of geminal pairs of hydroxymethyl groups on the trimethylene

bridges of the ligand backbone, a likely contributing factor to the apparently lower degree of Cu-N coordination for **5.12** is that steric strain imposed by one or both pairs of hydroxymethyl groups disfavors direct Cu-N coordination. In fact, inspection of the crystal structure[2] of the related ligand **4.1**-Cu(I) complex, which contains a direct Cu-N bond, indicates that hydroxymethylation of the middle CH_2 of the S-S bridge will likely result in steric clashes with the aromatic ring reminiscent of those suspected for the earlier N-arylthiazacrown Cu(I)-ligand design. Removal of both pairs of hydroxymethyl groups would leave a strongly amphiphilic, detergent-like structure, so we elected to remove only the hydroxymethyl groups of the S-S bridge of probe **5.12** to give design **5.20** (Figure 5.7).

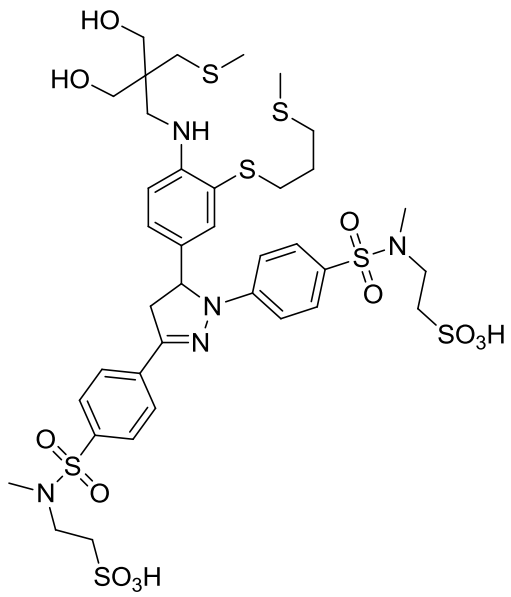

5.20

Figure 5.7: Structure of Cu(I)-probe **5.20**

5.5.2. Synthesis

Probe **5.20** was obtained by a similar route as for **5.12** except that the aldehyde functionality was introduced after assembly of the complete Cu(I)-ligand framework. This route was chosen due to the relatively low yield observed for the hydrolysis-alkylation step in the presence of an aldehyde group during the synthesis of **5.12**. As shown in Scheme 5.4, the synthesis instead began with the brominated benzothiazolinone **5.21**. N-alkylation with iodide **5.15** gave intermediate **5.22**, which was converted in high yield to the brominated ligand precursor **5.23** by the one pot hydrolysis-alkylation procedure. Bromide **5.23** was converted to aldehyde **5.24** in good yield using the metal-halogen exchange-based procedure originally developed for aldehyde **4.9** (Chapter 4), except that a solvent change from diethyl ether to THF was required to increase the solubility of the lithiated intermediates. Aldehyde **5.24** was converted sequentially to chalcone **5.25**, triarylpyrazoline **5.26**, and sulfonyl fluoride **5.27** using the same methodology as in the syntheses of probes **5.8** and **5.12**.

To avoid the elimination side reactions encountered in the synthesis **5.8** and **5.12** and difficult HPLC purification of the triethylamine-containing product mixture, we sought a different procedure for the final sulfonyl fluoride hydrolysis step. Interestingly, pyridine, which is often used to promote substitution reactions of sulfonyl chlorides and might be expected to serve as a nucleophilic catalyst, was found to be practically inert toward the sulfonyl fluoride moieties of intermediate **5.6**, which remained almost completely intact after stirring overnight in a solution of 10% water in pyridine! In marked contrast, sodium hydroxide in a methanol-THF-water mixture (63:32:5) was highly effective, cleaving the sulfonyl fluoride moieties completely in only 120 minutes, and only trace amounts of elimination side products were apparent by TLC. This method, combined with an initial acidic hydrolysis step, was applied to sulfonyl fluoride **5.27**, furnishing probe **5.20** in 75% yield as the ammonium salt after HPLC purification. The complete synthesis is shown in Scheme **5.4**.

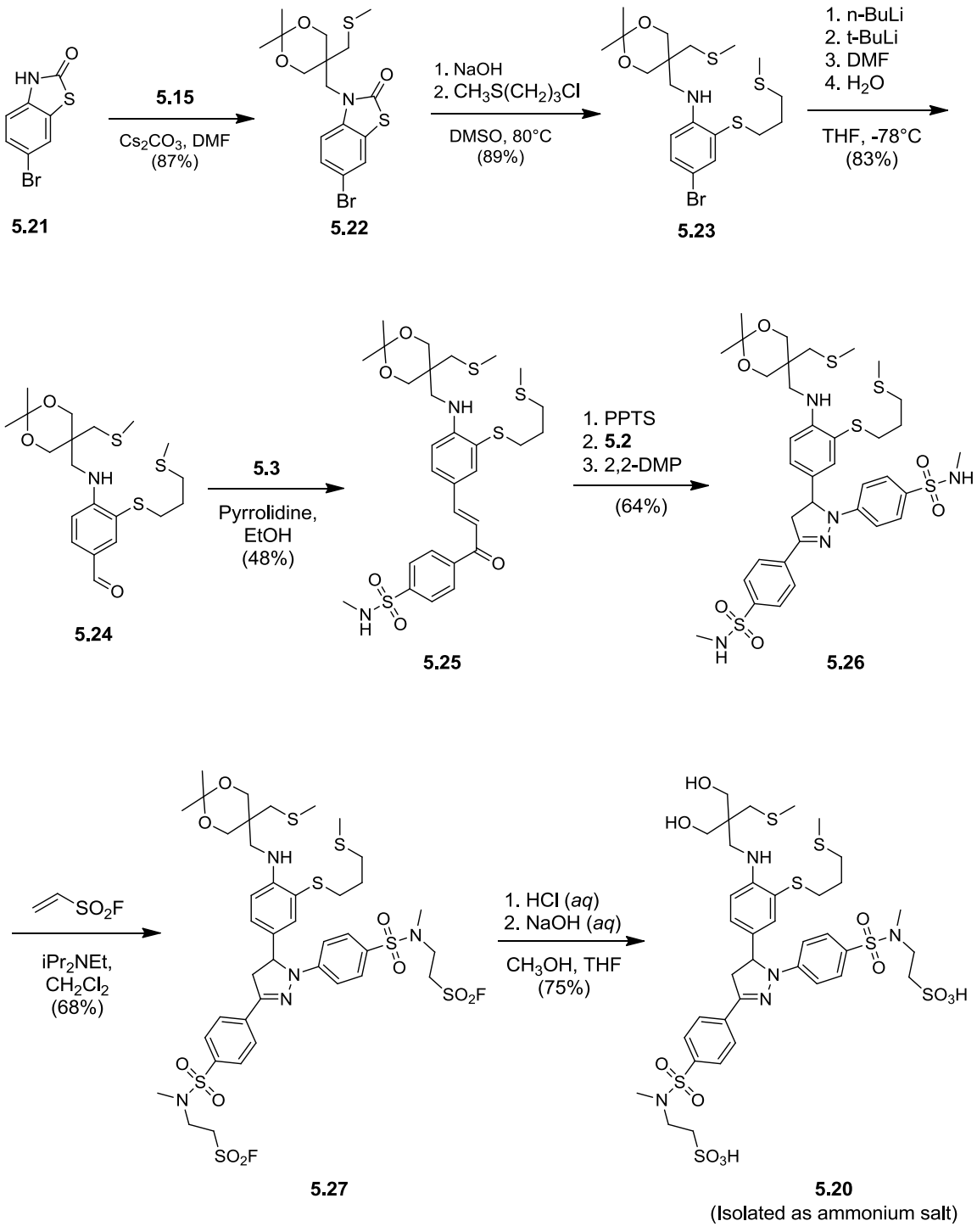

Scheme 5.4: Synthesis of probe **5.20**

5.5.3. Characterization and evaluation

Despite the removal of two hydroxyl groups, probe **5.20** dissolves directly in water to millimolar concentrations; however, the resulting solution foams readily, indicating a surfactant effect not apparent for the tetrahydroxylated probes **5.8** and **5.12**. Nevertheless, at the low micromolar concentrations used for characterization of its fluorescence properties, **5.20** gave no spectral evidence of increased aggregation, yielding a UV absorption spectrum indistinguishable from that of **5.12** with a maximum at 387 nm (Figure 5.8).

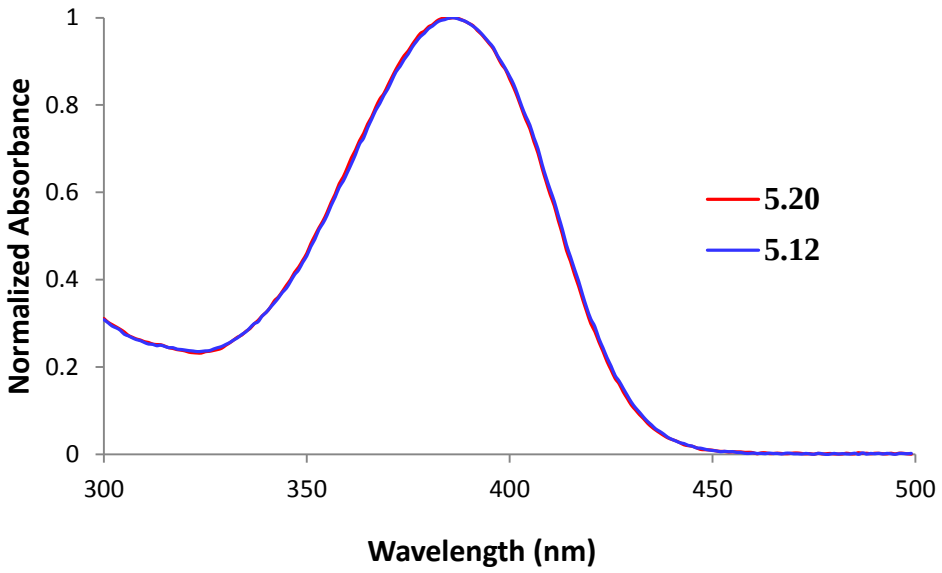

Figure 5.8: Normalized absorption spectra of probes **5.20** and **5.12** at a concentration of 1.25 µM (approximate)

Upon saturation with Cu(I), **5.20** gave a strong fluorescence turn-on response with an emission maximum identical to those of **5.8** and **5.12** at 487 nm and a contrast ratio near 160. A single-point fluorescence quantum yield measurement yielded an approximate value of 0.16 for **5.20** versus 0.11 for **5.12** under the same conditions, which

is consistent with the observed increase in contrast ratio. A more rigorous four-point measurement as described in Chapter 4 yielded a slightly lower quantum yield of 0.14 for **5.20**-Cu(I) after correction for a small shift in the absorption spectrum upon Cu(I) binding; the observed shift in absorption maximum from 387 to 381 nm is similar in magnitude to that observed for CTAP-2 and **4.3** (Chapter 4).

While the 160-fold fluorescence enhancement achieved by aqueous Cu(I) probe **5.20** approaches the maximum contrast ratio of 220 reached by related Cu(I)-probes in methanolic solution,[2] the fluorescence quantum yield of 0.14 is much lower than the value of 0.49 observed for the contrast-optimized methanolic Cu(I)-probe **4.2d** and corresponds to a fluorescence recovery of only 24% versus reference fluorophore **5.1**. Furthermore, the fluorescence decay profile (Figure 5.9) of Cu(I)-saturated **5.20** is obviously multiexponential, indicating that multiple coordination species providing significantly different degrees of PET inhibition are present even after removal of the hydroxymethyl moieties from the S-S bridge of the ligand moiety. The fluorescence decay of **5.20**-Cu(I) fit well to a biexponential model (Figure 5.9, blue trace), with decay components of 1.64 ns (21%) and 0.87 ns (79%) and a risetime of 0.26 ns ($\chi^2 = 1.08$).

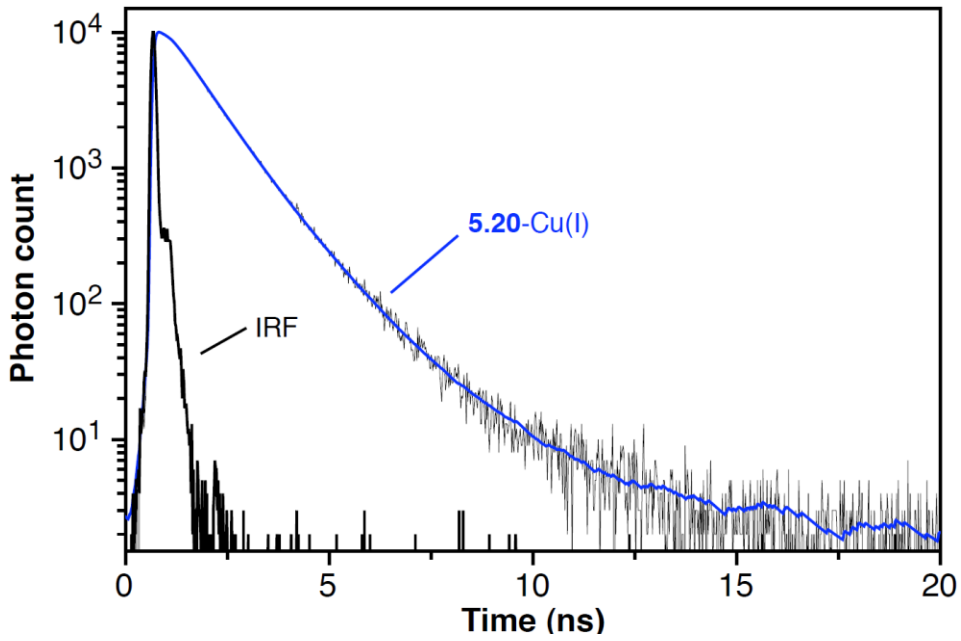

Figure 5.9: Fluorescence decay profile of Cu(I)-saturated **5.20**

The fluorescence decay profile of **5.20**-Cu(I) is surprisingly similar to that of **5.12**-Cu(I), which is seemingly at odds with the substantially higher quantum yield and contrast ratio upon Cu(I)-saturation observed for **5.20**. In fact, the respective fits actually show a decreased fractional contribution of the longer-lived decay component for **5.20** versus **5.12** (21% versus 32-38%), which would seem to imply a lower degree of Cu-N coordination. These fractional contributions, however, are not necessarily an accurate reflection of the actual species distribution in the sample, as significantly different fits providing similar χ^2 values can sometimes be found for a given multiexponential decay profile, especially when two decay components are relatively closely spaced as for **5.12**. Furthermore, the risetime observed for both **5.1**-H^+ and **5.20**-Cu(I) was not found for **5.12**-Cu(I), which instead yielded a low amplitude, short-lived decay component of 0.25 ns in the triexponential fit, suggesting that the true abundance of the fast-decaying species of **5.12**-Cu(I) may be masked by a risetime of equal length.

5.6. Improving the fluorescence quantum yield by decreasing the PET driving force

5.6.1. Rationale for decreasing the PET driving force

As discussed in the previous section, probe **5.20** achieves an excellent contrast ratio approaching that of the optimized methanolic Cu(I)-probe[2] **4.2d**, but the quantum yield upon Cu(I)-saturation remains relatively low at 0.14, corresponding to a fluorescence recovery of only 24%. Fluorescence decay analysis appears to implicate the ligand design as the cause of low fluorescence recovery, as the obviously multiexponential decay profile of **5.20**-Cu(I) presumably corresponds to the presence of multiple coordination species in contrast to the monoexponential fluorescence decay of **4.2d**-Cu(I).[2] A re-examination of unpublished data, however, revealed that the fluorescence decay profile upon Cu(I)-saturation of **4.2e**, an analog of **4.2d** with an additional *ortho*-fluoro-substituent on the pyrazoline 1-aryl ring and therefore a higher PET driving force, is actually multiexponential as well. Given that the 5-aryl ring comprising the ligand moiety is only weakly electronically coupled to the 1-aryl ring, it appears unlikely that a single additional 1-aryl fluoro-substituent would have a significant effect on Cu(I)-coordination. It is therefore probable that multiple coordination species actually exist for **4.2d**-Cu(I) as well, but the difference in fluorescence lifetime between these species is not large enough to be easily resolved from the decay profile. Such an outcome would be expected if the PET rate constant for each species is small compared to the intrinsic excited-state deactivation rate constant k_0 of the fluorophore, as in this case PET is not the major factor determining the fluorescence lifetime.

Based on the above reasoning, the obviously multiexponential decay profile of **5.20**-Cu(I) does not necessarily indicate that the ligand design is less effective than that of **4.2d** and may instead be an indication of a higher than optimal PET driving force. In fact, the contrast ratio of 160 provided by **5.20** is equal to that of the over-tuned probe **4.2e**, which has an estimated PET driving force ($-\Delta G^0_{et}$) 100 meV higher than that of

4.2d.[2] Therefore, an analog of **5.20** with a moderately decreased PET driving force might give an even higher contrast ratio as well as a higher fluorescence quantum yield upon Cu(I)-saturation.

5.6.2. Reducing electron-withdrawing power at the 3-aryl ring by transposing the sulfonamide substituent

While previous efforts to tune the PET driving force of triarylpyrazoline-based Cu(I)-probes have focused on modification of the 1-aryl ring, it now appears that a large degree of electron-withdrawing character at this ring is required to achieve a high fluorescence quantum yield in aqueous solution through inhibition of ESPT. As discussed in Section 5.2, however, the degree of ESPT-mediated fluorescence quenching appears to be significantly less sensitive to the nature of the 3-aryl ring. Since electron-withdrawing substituents at either ring yield a comparable increase in PET driving force,[8,12] it should be possible to create a Cu(I)-probe with significantly reduced PET driving force but similar intrinsic fluorophore quantum yield compared to **5.20** by decreasing the electron-withdrawing power at the 3-aryl ring while retaining the 1-aryl sulfonamide substituent. To significantly reduce the electron-withdrawing power without sacrificing the hydrophilic character and ease of functionalization provided by the sulfonamide moiety, we realized that the SO_2 and NR groups of the original N-methylarenesulfonamide design can simply be transposed to an N-arylmethanesulfonamide. The effect of this subtle modification should be quite substantial given the reported Hammett substituent constants of $\sigma_p = 0.65$ for $-SO_2NMe_2$ versus 0.24 for $N(Me)SO_2Me$.[6] To avoid possibly facilitating ESPT or donor-excited PET by introducing a π-donor in conjugation with the imine nitrogen of the pyrazoline core, the attachment point can also be moved from the *para*- to the *meta*-position of the 3-aryl ring with little expected change to the electron-withdrawing power ($\sigma_m = 0.21$ for $N(Me)SO_2Me$[6]). Applying these modifications to

probe **5.20** and its reference fluorophore **5.1** yields probe design **5.28** and reference fluorophore **5.29**, which are shown below in Figure 5.10.

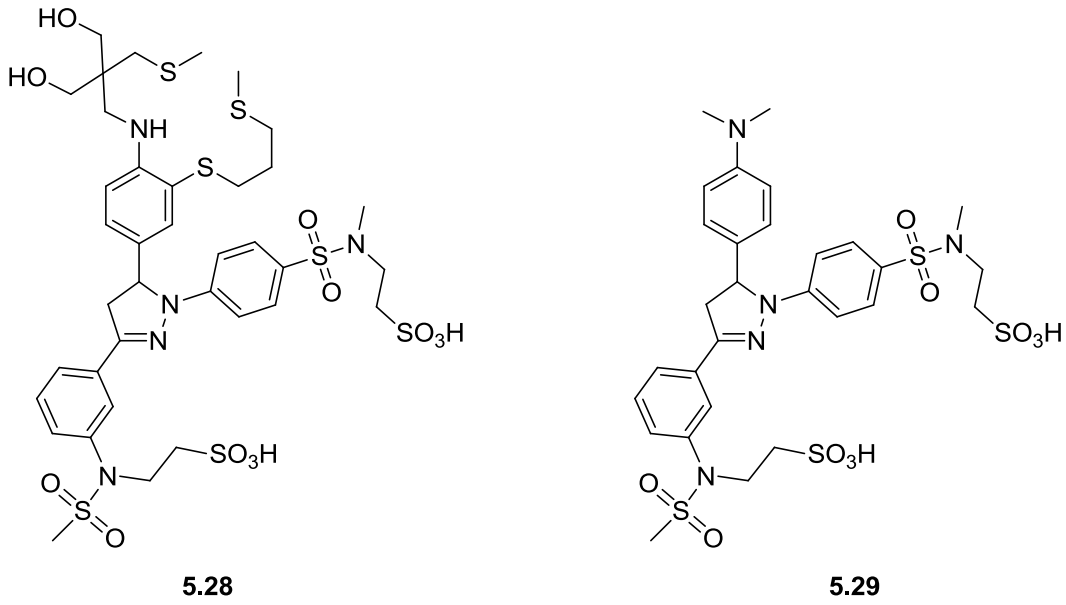

Figure 5.10: Structures of Cu(I)-probe **5.28** and reference triarylpyrazoline **5.29**

5.6.3. Synthesis and characterization of the N-arylmethanesulfonamide reference fluorophore

Before preparing Cu(I)-probe **5.28**, we first synthesized and characterized the reference compound **5.29** to ensure that the new fluorophore design achieves a sufficient fluorescence quantum yield in aqueous solution. As shown in Scheme 5.5, the synthesis proceeded similarly to that of the isomeric reference pyrazoline **5.1** up to the stage of the sulfonyl fluoride. The acetophenone derivative **5.30**, prepared from commercially available 3-aminoacetophenone and methanesulfonyl chloride, was condensed with 4-dimethylaminobenzaldehyde to give chalcone **5.31**, which was subsequently condensed

with arylhydrazine **5.2** to give triarylpyrazoline **5.32**. This mixed secondary sulfonamide readily underwent base-catalyzed conjugate addition to ESF to give the bis(sulfonyl fluoride) **5.33**. Interestingly, the first addition step proceeded more rapidly than expected and was complete within 30 minutes, while the second addition required several hours to approach completion as usual. This difference in reactivity is presumably due to greater acidity of the N-arylsulfonamide NH compared to that of an N-alkylsulfonamide. If this is the case, the N-arylsulfonamide should also be a better leaving group, and the reverse of the conjugate addition, E1cB-type elimination, may also proceed more rapidly, thus exacerbating the elimination side reactions previously encountered in the subsequent sulfonyl fluoride hydrolysis step. Given this possibility, we tested the ESF adduct of chalcone **5.31** as a simpler model substrate for sulfonyl fluoride hydrolysis before attempting the conversion with triarylpyrazoline sulfonyl fluoride **5.33**. Chalcone **5.31** reacted rapidly with ESF in the presence of triethylamine, giving clean conversion to a single product in minutes. When the resulting adduct was subjected to the conditions previously employed for efficient hydrolysis of the triarylpyrazoline sulfonyl fluoride **5.27** (Scheme 5.4), it underwent rapid elimination, returning the secondary sulfonamide **5.31** as the chief product by TLC. By contrast, treatment with an acetonitrile-water solution of DABCO (1,4-diazabicyclo[2,2,2]octane), a tertiary amine reported to be even more nucleophilic than 4-dimethylaminopyridine,[13] gave roughly equal amounts of **5.31** and a highly polar product consistent with a sulfonate salt. A solution containing equal parts of DABCO and its bicarbonate salt in 2:1 water-THF gave still better results, producing primarily the salt product with only a trace of **5.31**. Application of similar conditions to sulfonyl fluoride **5.33** gave the desired reference pyrazoline **5.29** as its ammonium salt after HPLC purification, although the yield of purified product is low due to an initial unsuccessful attempt to isolate the product as a crystalline potassium salt.

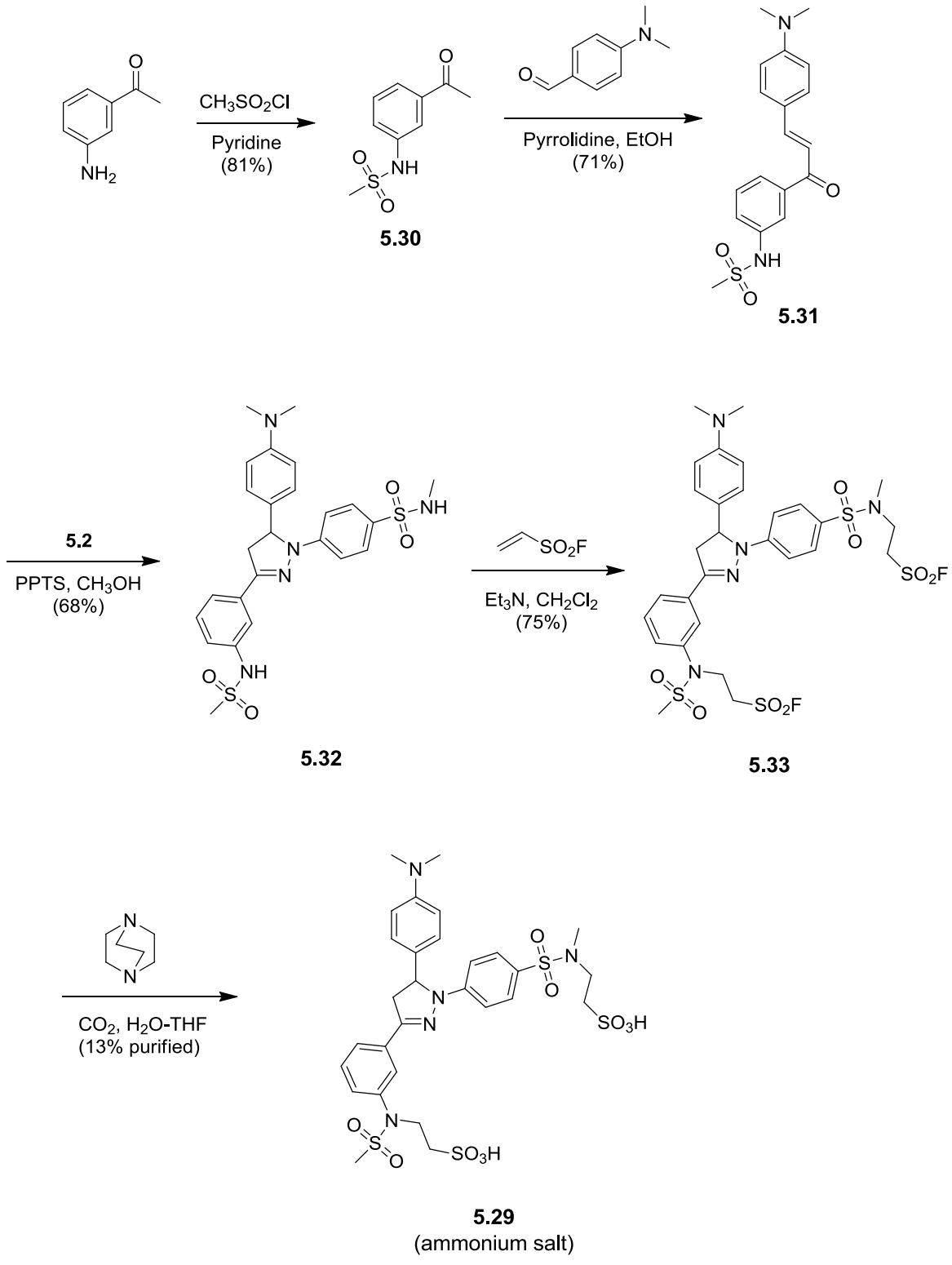

Scheme 5.5: Synthesis of N-arylmethanesulfonamide reference triarylpyrazoline **5.29**

Triarylpyrazoline **5.29** dissolves readily in water similar to its isomer **5.1**. In 1 mM aqueous HCl, the absorption and emission maxima (364 and 463 nm, respectively) of **5.29** are significantly blue-shifted relative to those of **5.1** under the same conditions, corresponding to a substantial increase in estimated excited-state energy from 2.88 to 3.04 eV. While such an increase in ΔE_{00} would appear to increase the PET driving force according to the Rehm-Weller equation (Chapter 2), previous data for 1,3,5-triarylpyrazolines in acetonitrile solution indicate that the increase in excited-state energy upon removal of electron-withdrawing groups from the 3-aryl ring is more than offset by a concomitant decrease in $E(A/A^-)$, yielding a net decrease in the PET driving force ($-\Delta G_{et}$) of similar magnitude to the observed increase in ΔE_{00}.[8,12,14]

Compound **5.29** gave an outstanding fluorescence quantum yield of 0.68 in 1 mM aqueous HCl, which is even higher than the value of 0.59 observed for **5.1** and compares favorably to previously reported fluorescence quantum yields for triarylpyrazolines in organic solvents,[8,10,12,14] including those in the aprotic solvent acetonitrile. The fluorescence lifetime of **5.29** in 1 mM HCl is also somewhat greater than that of **5.1** at 3.84 versus 3.38 ns, indicating that the improvement in fluorescence quantum yield is largely due to a lower k_{nr} of 8.3 x 10^7 s^{-1} for **5.29** versus 1.2 x 10^8 s^{-1} for **5.1**, while k_r is essentially unchanged (1.77 and 1.75 x 10^8 s^{-1}, respectively).

Based on its observed properties, it appears that the N-arylmethanesulfonamide triarylpyrazoline fluorophore of **5.29** is well suited for fluorescent probe design and will most likely yield a decreased PET driving force as well as a higher intrinsic fluorescence quantum yield in aqueous solution compared to its bis(arenesulfonamide) isomer **5.1**. Therefore, we proceeded to Cu(I) probe **5.28** as described in the next section.

5.6.4. Combining the best of the ligand and fluorophore designs

5.6.4.1. Synthesis

Cu(I)-probe **5.28** was prepared by a combination of the methodologies developed for related compounds throughout this chapter as shown in Scheme 5.6. Aldehyde **5.24**, the common precursor to probe **5.20**, was condensed with acetophenone derivative **5.30** to give chalcone **5.34**, which was subsequently converted to triarylpyrazoline **5.35** and sulfonyl fluoride **5.36**.

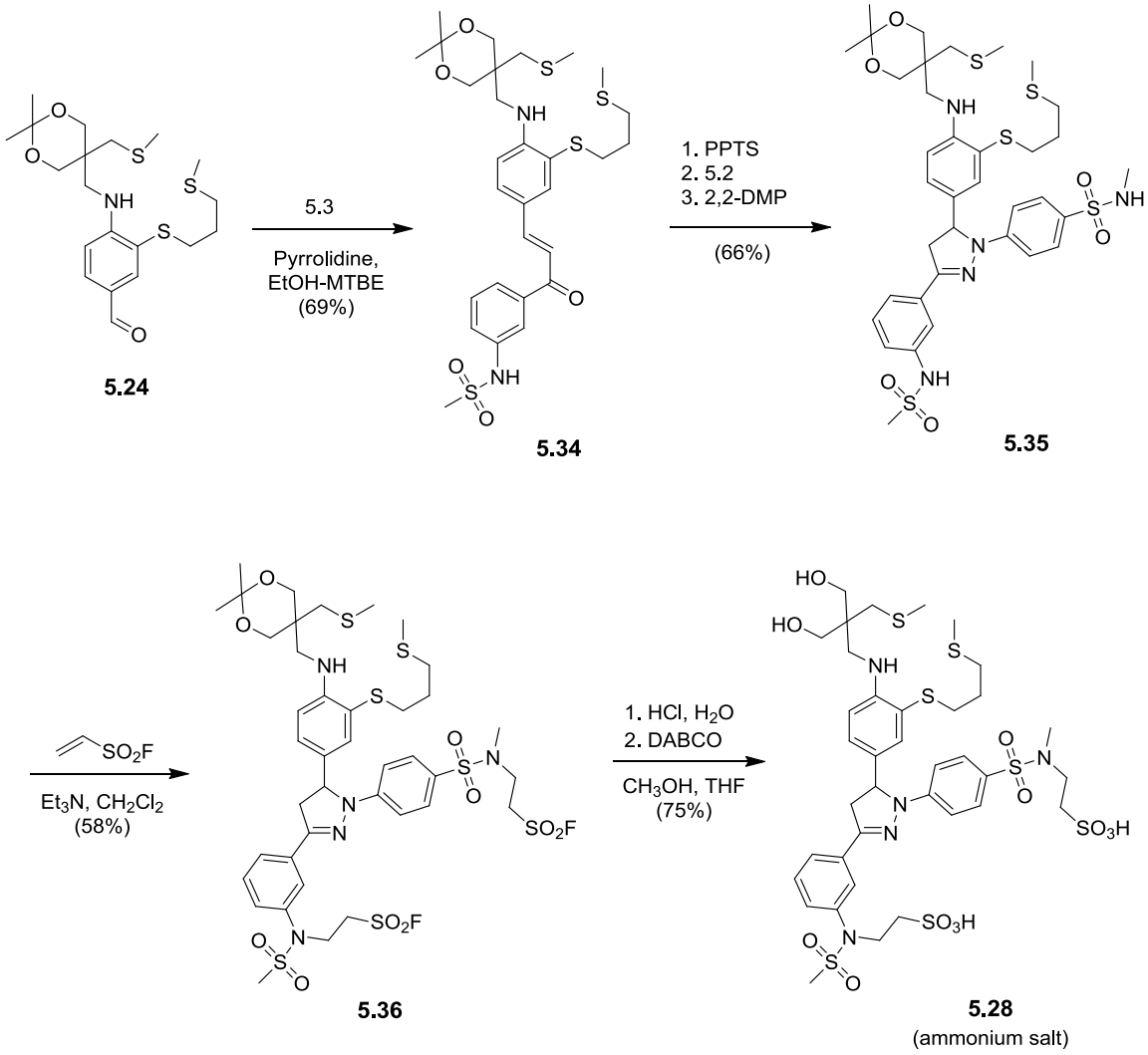

Scheme 5.6: Synthesis of Cu(I)-probe **5.28**

The final conversion to probe **5.28** was achieved by a brief acidic hydrolysis step in a methanol-THF-water mixture to free the hydroxyl groups followed by addition of excess DABCO to cleave the sulfonyl fluoride moieties to sulfonates, and the desired product was isolated as the ammonium salt by HPLC in good yield.

5.6.4.2. Characterization

Probe **5.28** dissolves readily in water and exhibits spectral properties similar to those of reference compound **5.29**, with an absorption maximum of 387 nm in neutral buffer. Upon saturation with Cu(I), **5.28** gave a powerful fluorescence turn-on response (Figure 5.11), reaching a contrast ratio of 180 with a fluorescence quantum yield of 0.41, which is approximately three-fold higher than that of the isomeric Cu(I)-probe **5.20** (0.14) and almost five-fold higher than that of CTAP-2 (0.083). Notably, such a result would not have been possible regardless of the ligand structure using the original sulfonated fluorophore design of CTAP-2, probe **4.3**, and reference compound **4.11**, as studies with the latter demonstrated that the quantum yield is limited to less than 30% in aqueous solution by ESPT (Chapter 4).[3]

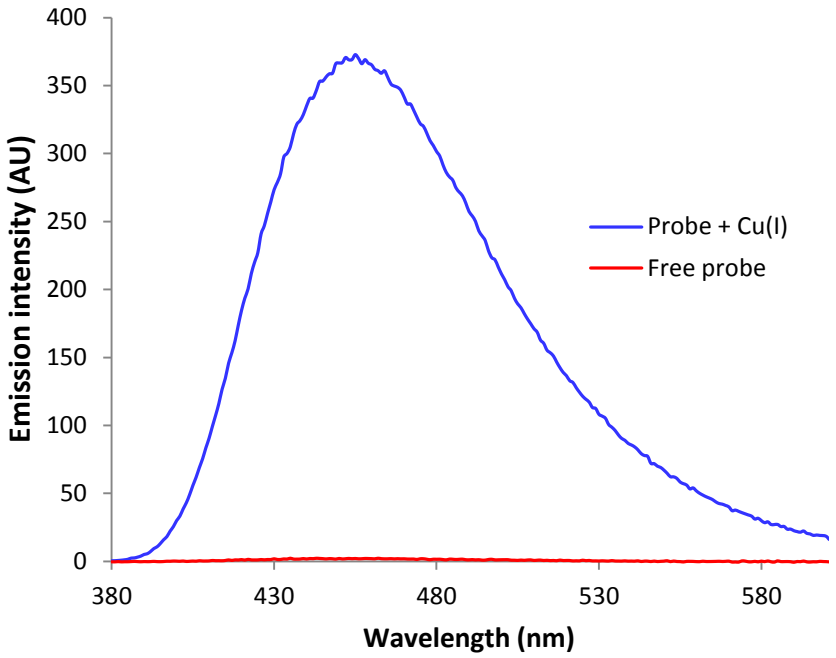

Figure 5.11: Emission spectra of probe 5.28 (1.2 µM) in pH 7.2 MOPS buffer before and after addition of Cu(I) (generaged by in-situ reduction of 2.5 µM Cu(II) with 100 µM ascorbate). Note: Buffer contains 1 µM of the tripodal chelator **6.1** (Chapter 6) to suppress background copper contamination. The fluorescence response was fully reversible by addition of a further 4 µM of **6.1**.

To reassess the PET switching performance provided by the ligand design shared by **5.20** and **5.28**, we measured the fluorescence decay profile of **5.28**-Cu(I). Based on the reasoning described in Section 5.6.1, if all major coordination modes of the ligand-Cu(I) complex provide a substantial increase in donor potential versus the free ligand, then at lower PET driving force the differences in fluorescence lifetime between the various coordination species should decrease, potentially resulting in a decay profile that appears monoexponential.

The observed decay profile (Figure 5.12) indeed shows this effect. In dramatic contrast to the decay profile of **5.20**-Cu(I), the deviation from linearity on a logarithmic scale is barely perceptible **5.28**-Cu(I), and the data can be fit with a single decay

component of 2.48 ns (blue trace) yielding a reasonable χ^2 value of 1.59. For comparison, the optimized methanolic Cu(I)-probe **4.2d** gave χ^2 = 1.32 for a monoexponential fit by the same procedure.[2] A biexponential fit (red trace) with components of 2.27 ns (85%) and 3.68 ns (15%) gave an improved χ^2 of 1.06, although the difference between the two fits is apparent only near the end of the acquisition window.

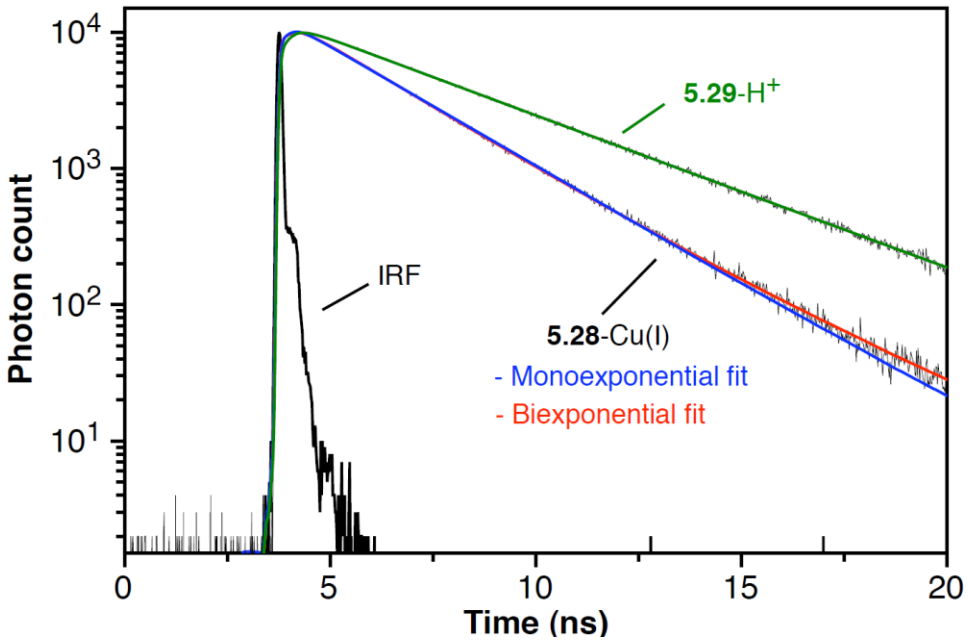

Figure 5.12: Fluorescence decay profiles of probe **5.28** and reference compound **5.29**

The decay profile of reference compound **5.29** in 1 mM HCl and its monoexponential fit (τ_f = 3.86 ns, green trace) are also shown for comparison. All three fits include a risetime component of 0.19-0.32 ns.

Given the very high contrast ratio achieved by probe **5.28** and the fact that even the shorter component in the biexponential decay fit recovers more than half of the fluorescence lifetime of the reference fluorophore **5.29**-H^+, it appears that the Cu(I)-ligand design shared by this probe and its isomer **5.20** is actually a rather effective PET

switch despite the presence of multiple coordination species. In fact, it is possible that the shorter-lived species is not a ternary complex with solvent as observed for N-arylthiazacrown-based probes[10] but simply a different coordination isomer of the binary complex presumably responsible for the longer decay component. Either way, both the contrast ratio and fluorescence quantum yield provided by **5.28** rival those of the best methanolic Cu(I)-probe **4.2d**, and further modifications to the ligand design are unnecessary with respect to these parameters.

5.7. Review and Conclusions

Taking into account the ESPT-mediated fluorescence quenching pathway previously determined to limit the fluorescence quantum yield achievable with the CTAP-2 fluorophore design in aqueous solution, we developed a new fluorophore design containing sulfonamide substituents as electron-withdrawing groups. Based on previous evidence that a similar excited-state protonation pathway operating in methanolic solution is highly sensitive to the electron-donating or electron-withdrawing power of substituents on the triarylpyrazoline 1-aryl ring, we expected that replacement of the 1-aryl sulfonate moiety of CTAP-2 with a more strongly electron-withdrawing sulfonamide substituent may suppress ESPT-mediated quenching in aqueous solution. Consistent with suppression of ESPT, the new fluorophore design exhibited more than double the fluorescence quantum yield of protonated CTAP-2 or its fluorophore analog **4.11**, as well as a substantially reduced solvent isotope effect on the fluorescence lifetime versus the latter. Combining the sulfonamide-based fluorophore with a previously investigated Cu(I)-ligand moiety, however, resulted in a decreased fluorescence quantum yield upon Cu(I)-saturation relative to the original fluorophore architecture, presumably due to an increased PET driving force. Subsequent modifications to the ligand design lead to probe 5.20, which gave more than twice the contrast ratio of CTAP-2, but the fluorescence

quantum yield upon Cu(I)-saturation remained relatively low at 14% and the fluorescence decay profile was obviously multiexponential. Based on previous observations with methanolic Cu(I)-probes, the behavior of 5.20 is consistent with an excessive PET driving force. To decrease the PET driving force while maintaining resistance to ESPT in aqueous solution, the 1-aryl sulfonamide substituent was left unmodified while the 3-aryl substituent was isomerized from a strongly electron-withdrawing N-methyl-arenesulfonamide at the para-position to a weakly electron-withdrawing N-aryl-methanesulfonamide at the meta-position (probe 5.28). This subtle modification resulted in a nearly three-fold increase in fluorescence quantum yield upon Cu(I)-saturation to 41% and a further improvement in contrast ratio to 180, rivaling the best performing methanolic Cu(I) probes, yet 5.28 dissolves directly in water as easily as CTAP-2. While the binding affinity and selectivity of 5.28 remain to be determined, it is unlikely that these parameters will differ dramatically from those observed for CTAP-2 and 4.3 given the surprisingly small differences in coordination behavior previously reported for acyclic versus macrocyclic polythioethers.[15,16] Disregarding the earlier reported Cu(I)-probe CS3,[17] which was demonstrated to form a colloidal precipitate at micromolar concentrations,[1] the challenge of obtaining bright, high-contrast fluorescence turn-on response to Cu(I) in aqueous solution has at last been met.

5.8. Experimental section

Absorption, steady-state fluorescence, and time-resolved fluorescence spectroscopy were conducted as described in the experimental section of Chapter 5. Compound synthesis and characterization for this chapter are described below.

General

Materials: Ethenesulfonyl fluoride[7](ESF) and benzothiazolin-2-one-6-carboxaldehyde[11] (**5.14**) were prepared as previously described. The synthesis of thietane **3.15** is described in Chapter 3, and that of aldehyde **4.9** is described in Chapter 4. NMR: Spectra were recorded at 400 MHz (^{1}H, ppm vs. internal TMS, referenced directly or indirectly via the known residual proton signal of the solvent[18]), 376 MHz (^{19}F, ppm vs. internal CCl_3F), and 100 MHz (^{13}C, ppm vs. TMS, referenced to $CDCl_3$ (77 ppm) or CD_3OD (49 ppm) chemical shifts). Spectra were recorded at ambient temperature (20-23°C) unless stated otherwise. For ^{1}H spectra, the abbreviation "ad" denotes an apparent doublet with additional partially resolved coupling (AA'XX' or AA'MM' spin system); only the largest (first order) coupling constant is given for these systems. In cases where the product as isolated contained a substantial amount of solvent, the solvent content was calculated from the initial ^{1}H NMR integrals and a second ^{1}H NMR spectrum was acquired after removal of solvent by repeated dissolution in $CDCl_3$ followed by concentration to dryness. MS: Spectra were acquired by the Georgia Tech Mass Spectrometry Facility. Column chromatography: Flash chromatography on Sorbent Technologies general purpose silica gel (60 Å pore size, 250 mesh).

Arylhydrazine **5.2**

A solution of 4-fluorobenzenesulfonyl chloride (8.49 g, 43.6 mmol) in DCM (60 mL) was cooled in an ice bath and methylamine solution (7 ml, 40% aqueous, d = 0.9 g/mL, 4 equiv.) was added slowly under stirring. Gentle boiling occurred, and the ice bath was removed once this had subsided. After 15 minutes, the mixture was diluted with crushed ice and carefully acidified with concentrated HCl (10 mL). The organic layer was separated, and the aqueous layer was extracted with DCM (2 x 20 mL). The combined organic layers were dried with Na_2SO_4 and concentrated. The residue was transferred to a 50 mL rb flask and dissolved in DMSO (12 mL). The flask was sealed under argon, and

hydrazine (4.1 mL, 3.0 equiv.) was added. The reaction vessel was vented to an oil bubbler, and the mixture was stirred at 50°C overnight. A further 2 mL (1.5 equiv.) of hydrazine were added, and the mixture was stirred at 60°C for 24 hours. After cooling, the mixture was slowly diluted with cold water (100 mL), and the resulting precipitate was collected by filtration, washed with cold water, and recrystallized from ethanol to give the product as colorless needles. Yield 7.54 g (37.5 mmol, 86%). Mp 140-141°C (lit.[19] mp 137°C) ^{1}H NMR (DMSO-d_6) δ 2.32 (d, *J* = 5.2 Hz, 3H), 4.19 (br. s, 2H), 6.82 (ad, *J* = 8.9 Hz, 2H), 6.94 (q, *J* = 5.2 Hz, 1H), 7.45 (ad, *J* = 8.9 Hz, 2H), 7.54 (br. s, 1H). ^{13}C NMR (DMSO-d_6) δ 28.7, 110.0, 124.5, 128.3, 155.2. EI-MS *m/z* 201 ($[M]^+$, 100), 171(50), 123 (55), 107 (60), 90 (40). EI-HRMS *m/z* calcd for $C_7H_{11}N_3O_2S$ 201.0572, found 201.0574.

Acetophenone **5.3**

A solution of 4-acetylbenzenesulfonyl chloride (4.52 g, 20.7 mmol) in DCM (45 mL) was cooled in an ice bath, and methylamine solution (7 ml, 40% aqueous, d = 0.9 g/mL, 4 equiv.) was added slowly under rapid stirring. After 20 minutes, the solution was acidified with aqueous HCl, and the organic layer was separated. The aqueous layer was extracted with DCM (2 x 15 mL), and the combined organic layers were dried with MgSO4 and concentrated. The residue was recrystallized from boiling ethyl acetate-cyclohexane under slow stirring to give the product as a colorless crystalline powder. Yield 4.09 g (19.2 mmol, 93%). ^{1}H NMR ($CDCl_3$) δ 2.67 (s, 3H), 2.69 (d, *J* = 5.3 Hz, 3H), 4.92 (br, q, *J* = 5.2 Hz, 1H), 7.95-7.98 (m, 2H), 8.08-8.11 (m, 2H). ^{13}C NMR ($CDCl_3$) δ 26.9, 29.3, 127.4, 128.9, 140.0, 142.7, 196.9. EI-MS *m/z* 213 ($[M]^+$, 55), 198 (100), 134 (25), 119 (24), 91(20), 76 (27). EI-HRMS *m/z* calcd for $C_9H_{11}NO_3S$ 213.0460, found 213.0461.

Chalcone **5.4**

Acetophenone **5.3** (480 mg, 2.25 mmol) and 4-dimethylaminobenzaldehyde (320 mg, 2.14 mmol) were stirred in ethanol (4 mL) at 50°C until completely dissolved, and pyrrolidine (180 µL, 2.14 mmol) was then added. After 1 hour, the deep red solution was cooled under rapid stirring to initiate crystallization of the product, and the resulting orange slurry was stirred overnight at 50°C. After cooling, the product was collected by filtration, washed with cold ethanol, and dried by suction and then under vacuum to give an orange crystalline powder. Yield 583 mg (1.69 mmol, 79%). Mp 153-154°C. ^{1}H NMR ($CDCl_3$) δ 2.70 (s, 3H), 3.05 (s, 6H), 4.88 (br, s, 1H), 6.68 (ad, *J* = 9.0 Hz, 2H), 7.26 (d, *J* = 15.4 Hz, 1H), 7.55 (ad, *J* = 8.9 Hz, 2H), 7.79 (d, *J* = 15.4 Hz, 1H), 7.97 (ad, *J* = 8.6 Hz, 2H), 8.08 (ad, *J* = 8.6 Hz, 2H). ^{13}C NMR ($CDCl_3$) δ 29.3, 40.0, 111.8, 116.0, 122.0, 127.3, 128.8, 130.8, 141.6, 142.6, 147.5, 152.4, 189.5. EI-MS *m/z* 344 ($[M]^+$, 100), 343 (25), 250 (24), 174 (33).

Triarylpyrazoline **5.5**

A mixture of chalcone **5.4** (393 mg, 1.14 mmol), arylhydrazine 5.2 (321 mg, 1.4 equiv.), PPTS (400 mg, 1.4 equiv.) and methanol (4 mL) was stirred under argon in a sealed vessel at 90°C for 3 hours. The mixture was poured into water (50 mL) and an attempt was made to extract the product with toluene (50 mL). A large amount of insoluble material remained so MTBE (25 mL) and dichloromethane (25 mL) were added, resulting two clear liquid phases after agitation and settling. The organic layer (top) was separated, dried with Na_2SO_4, and concentrated. The residue was subjected to column chromatography (DCM-MTBE) to give the product as a yellow glassy solid containing 0.6 molar equiv. of MTBE by ^{1}H NMR. Crystallization from DCM-hexane under stirring gave a yellow-green, strongly fluorescent crystalline powder. Yield 501 mg (0.949 mmol, 83%) Mp ~155°C (dec.). ^{1}H NMR ($CDCl_3$) δ 2.59 (d, *J* = 5.4 Hz, 3H), 2.66 (d, *J* = 5.4 Hz, 3H), 2.92 (s, 6H), 3.19 (dd, *J* = 17.3, 6.0 Hz, 1H), 3.84 (dd, *J* = 17.3, 12.3 Hz, 1H), 4.48 (q, *J* = 5.4 Hz, 1H), 4.78 (q, *J* = 5.4 Hz, 1H), 5.34 (dd, *J* = 12.3, 6.0 Hz,

1H), 6.66 (ad, *J* = 8.8 Hz, 2H), 7.09 (ad, *J* = 8.8 Hz, 2H), 7.16 (ad, *J* = 9.0 Hz, 2H), 7.63 (ad, *J* = 9.0 Hz, 2H), 7.83-7.88 (m, 4H). ^{13}C NMR ($CDCl_3$) δ 29.27, 29.29, 40.4, 43.3, 63.7, 112.9, 113.0, 126.3, 126.5, 127.5, 127.6, 128.0, 128.7, 136.4, 138.5, 146.9, 147.4, 150.2.

Sulfonyl fluoride **5.6**

Triarylpyrazoline 5.5 (102 mg, 193 µmol) and triethylamine (54 µL, 2 equiv.) were stirred in dry DCM (4 mL) under argon. Ethenesulfonyl fluoride (48 µL, d = 1.32 g/mL, 3.0 equiv.) was added. TLC (10:1 DCM-MTBE) indicated almost complete consumption of the starting material (R_f 0.2) after 8 minutes and formation of two products (R_f 0.5 and 0.8). The latter is the desired product and the former is presumably the mono-N-alkylated intermediate. After 4 hours, the starting material was completely consumed but the intermediate remained. After 18 hours the reaction had progressed very little since the 4 hour point, so a further 3 equiv. of ESF were added. After 10 minutes, the intermediate at R_f 0.5 had been completely consumed. The mixture was diluted with toluene (3 mL) and evaporated to dryness under a stream of argon in a 40°C bath. The residue was subjected to column chromatography (2:1 DCM-hexanes with a gradient from 0 to 3.3% MTBE) to give the product as a yellow glassy solid containing 0.74 molar equiv. (8 mass%) of MTBE calculated from the ^{1}H NMR integrals. Yield 117 mg raw (108 mg corrected for solvent content, 145 µmol, 75%). ^{1}H NMR ($CDCl_3$) δ 2.80 (s, 3H), 2.89 (s, 3H), 2.94 (s, 6H), 3.21 (dd, *J* = 17.4, 6.0 Hz, 1H), 3.47-3.51 (m, 2H), 3.55-3.59 (m, 2H), 3.69-3.79 (m, 4H), 3.87 (dd, *J* = 17.4, 12.3 Hz, 1H), 5.37 (dd, *J* = 12.3, 6.0 Hz, 1H), 6.68 (ad, *J* = 8.9 Hz, 2H), 7.10 (ad, *J* = 8.8 Hz, 2H), 7.19 (ad, *J* = 9.0 Hz, 2H), 7.59 (ad, *J* = 9.1 Hz, 2H), 7.83 (ad, *J* = 8.7 Hz, 2H), 7.90 (ad, *J* = 8.7 Hz, 2H). ^{19}F NMR ($CDCl_3$) δ 56.3 (t, *J* = 4.8 Hz, 1F), 56.6 (t, *J* = 4.7 Hz, 1F). ESI$^+$-HRMS calcd for $[M+H]^+$ $C_{29}H_{36}O_8N_5F_2S_4$ 748.1409, found 748.1405.

Reference triarylpyrazoline **5.1**

Sulfonyl fluoride 5.6 (74 mg of material containing 8% MTBE, 91 μmol) was stirred in 1 mL of a mixture containing acetonitrile (45%), triethylamine (45%) and water (10 %). After 10 min, TLC (10:1 DCM-MTBE) indicated a mixture of the starting material (R_f 0.8), a small amount of single-elimination product (R_f 0.5) and a trace of double elimination product (R_f 0.2, identical to triarylpyrazoline **5.5**), as well as hydrolysis products ($R_f \approx 0$). After stirring overnight, only the hydrolysis products and double-elimination product remained. The mixture was concentrated to dryness under a stream of argon, and the residue was taken up in methanol (2 mL) + concentrated ammonia (~100 μL) and concentrated again. The residue was dissolved in water (2 mL), and the product was isolated by RP-HPLC using a gradient of 25-33% CH3CN in 0.1% aqueous NH_4HCO_3 to give a yellow glassy solid after repeated evaporation with methanol and vacuum drying. The ^{1}H NMR spectrum of this material is consistent with a mixed ammonium-triethylammonium salt containing 44 mol% Et_3NH^+, corresponding to a formula weight of 815 g/mol. Yield 74 mg (71 μmol, 78%). ^{1}H NMR (CD_3OD) δ 1.30 (t, J = 7.3 Hz, 4H (0.44 Et_3NH^+)) 2.72 (s, 3H), 2.83 (s, 3H), 2.90 (s, 6H), 2.98-3.04 (m, 4H), 3.19 (dd, $J \approx$ 17.7, 5.8 Hz, 1H, partly obscured by subsequent signal), 3.20 (q, J = 7.3 Hz, 2.6H (0.44 Et_3NH^+)), 3.34-3.43 (m, 2H), 3.47-3.51 (m, 2H), 3.95 (dd, J = 17.6, 12.2 Hz, 1H), 5.48 (dd, J = 12.2, 5.8 Hz, 1H), 6.76 (ad, J = 8.8 Hz, 2H), 7.13 (ad J = 8.8 Hz, 2H), 7.23 (ad, J = 9.0 Hz, 2H), 7.58 (ad, J = 9.0 Hz, 2H), 7.86 (ad, J = 8.7 Hz, 2H), 7.99 (ad, J = 8.7 Hz, 2H). ESI-HRMS *m/z* calcd for $[M]^{2-}$ $C_{29}H_{35}N_5O_{10}S_4$ 370.5639, found 370.5630.

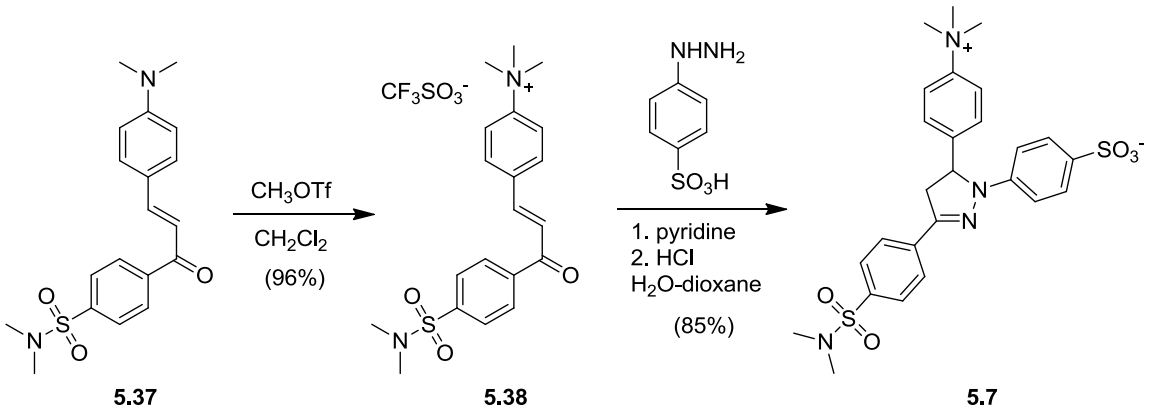

Scheme 5.7: Synthesis of reference fluorophore **5.7**

Chalcone **5.37**

This compound was synthesized as described for chalcone **5.4** using N-(4-acetyl-benzenesulfonyl) dimethylamine (304 mg, 1.34 mmol), p-dimethylaminobenzaldehyde (220 mg, 1.1 equiv.), and pyrrolidine (56 µL, 0.5 equiv.). Yield 360 mg (1.00 mmol, 75%), orange crystalline powder. ^{1}H NMR ($CDCl_3$) δ 2.75 (s, 6H), 3.06 (s, 6H), 6.70 (ad, *J* = 9.0 Hz, 2H), 7.28 (d, *J* = 15.4 Hz, 1H), 7.76 (ad, *J* = 8.8 Hz, 2H), 7.81 (d, *J* = 15.4 Hz, 1H), 7.88 (ad, *J* = 8.6 Hz, 2H), 8.11 (ad, *J* = 8.6 Hz, 2H). ^{13}C NMR ($CDCl_3$) δ 37.9, 40.1, 111.7, 116.0, 122.0, 127.8, 128.7, 130.8, 138.2, 142.7, 147.4, 152.3, 189.5. EI-MS *m/z* 358 ($[M]^+$, 100), 250 (40), 174 (32). EI-HRMS *m/z* calcd for $[M]^+$ $C_{19}H_{22}N_2O_3S$ 358.1351, found 358.1345.

Chalcone **5.38**

Chalcone 5.37 (303 mg, 845 µmol) was dissolved in dry dichloromethane (5 mL) and methyl trifluoromethanesulfonate (140 µL, 1.5 equiv.) was added. The solution was stirred rapidly until crystallization initiated and then stirred slowly overnight. The product was collected by filtration, washed with 1:1 dichloromethane-diethyl ether, and dried under nitrogen flow to give a pale peach colored crystalline powder. Yield 422 mg (808

μmol, 96%). Mp 245-246°C. ^{1}H NMR (DMSO-d_6) δ 2.68 (s, 6H), 3.66 (s, 9H), 7.87 (d, *J* = 15.7 Hz, 1H), 7.95 (ad, *J* = 8.6 Hz, 2H), 8.08 (ad, *J* = 9.2 Hz, 2H), 8.12 (d, *J* = 15.7 Hz, 1H), 8.20 (ad, *J* = 9.2 Hz, 2H), 8.40 (ad, *J* = 8.7 Hz, 2H). ^{13}C NMR (DMSO-d_6) δ 37.5, 56.4, 121.1, 124.3, 127.9, 129.5, 130.3, 136.1, 138.6, 140.5, 142.5, 148.2, 186.6. Note: the ^{13}C signal corresponding to the triflate anion, which should show low l intensity and strong ^{19}F-^{13}C coupling, was not distinguished over baseline noise. ESI-HRMS *m/z* calcd for $[M]^+$ $C_{20}H_{25}N_2O_3S$ 373.1580, found 373.1572.

Triarylpyrazoline **5.7**

A mixture of chalcone **5.38** (232 mg, 444 μmol), 4-hydrazinobenzenesulfonic acid hemihydrate (114 mg, 1.3 equiv.), pyridine 47 μL, water (1.8 mL) and dioxane (0.6 mL) was stirred under argon at 90°C. The solids dissolved within minutes give a clear red-orange solution which transformed to a canary-yellow slurry within two hours. A small sample of the solid material was removed and found to be poorly soluble in water and non-fluorescent in aqueous solution. Aqueous HCl (6 M, 96 μL, 1.3 equiv.) and dioxane (0.6 mL) were added, and the mixture was sealed under argon and stirred at100°C. After 26 minutes, the yellow solid had dissolved completely. The mixture was allowed to cool, diluted slowly with ethanol under rapid stirring to the point of permanent turbidity, and then diluted dropwise with water until clear. After 30 min., the product separated as a light yellow, strongly fluorescent crystalline powder. Yield 204 mg (376 μmol, 85%) ^{1}H NMR (3:1 D_2O : CD_3CN) δ 2.64 (s, 6H), 3.09 (dd, *J* = 17.7, 6.1 Hz, 1H), 3.56 (s, 9H), 3.86 (dd, *J* = 17.7, 12.5 Hz, 1H), 5.51 (dd, *J* = 12.5, 6.1 Hz, 1H), 7.03 (ad, *J* = 8.9 Hz, 2H), 7.44 (ad, *J* = 9.1 Hz, 2H), 7.57 (ad, *J* = 8.9 Hz, 2H), 7.76-7.79 (m, 4H), 7.90 (ad, *J* = 8.6 Hz, 2H).

Chalcone **5.9**

Aldehyde **4.9** (488 mg, 901 µmol) and acetophenone **5.3** (202 mg, 1.05 equiv.) were stirred in a mixture of ethanol (4.5 mL) and MTBE (2 mL) at 50°C until completely dissolved. Pyrrolidine (150 µL, 2 equiv.) was added, and the mixture was stirred for 2 hours at 50°C then allowed to cool to rt, producing a red, gummy precipitate. After two days of stirring at rt, the mixture was stirred at 50°C for 3 hours and then poured into water (50 mL) + 1 M NaH_2PO_4 (10 mL). The resulting emulsion was extracted with MTBE, and the organic layer was dried with MgSO4, concentrated to dryness, and separated by column chromatography (2:1 DCM-hexanes + increasing MTBE) to give the product as an orange glassy solid. Yield 415 mg (63%). ^{1}H NMR ($CDCl_3$) δ 1.425 (s, 3H), 1.428 (s, 3H), 1.46 (s, 3H), 1.51(s, 3H), 1.97 (p, *J* = 6.4 Hz, 2H), 2.59 (s, 2H), 2.71 (d, *J* = 5.3 Hz, 3H), 2.81-2.86 (m, 6H), 2.97 (s, 2H), 3.60-3.80 (m, 10H), 4.60 (q, *J* = 5.3 Hz, 1H), 6.26 (t, *J* = 7.1 Hz, 1H), 7.00 (d, *J* = 8.7 Hz, 1H), 7.28 (d, *J* = 15.5 Hz, 1H), 7.55 (dd, *J* = 8.7, 2.1 Hz, 1H), 7.73 (d, *J* = 15.5 Hz, 1H), 7.80 (d, *J* = 2.1 Hz, 1H), 7.97 (ad, *J* = 8.5 Hz, 2H), 8.10 (ad, *J* = 8.5 Hz, 2H). EI-MS *m/z* 736 ($[M]^+$, 100), 360 (55), 265 (20), 198 (15), 83 (19). EI-HRMS *m/z* calcd for $C_{35}H_{48}N_2O_7S_4$ 736.2344, found 736.2375.

Triarylpyrazoline **5.10**

Chalcone **5.9** (209 mg, 284 µmol) and PPTS (143 mg, 2 equiv.) were stirred in boiling methanol for 15 min. The mixture was concentrated to dryness under a stream of argon and the residue was dissolved in methanol (1.5 mL). Arylhydrazine **5.2** (86 mg, 1.5 equiv.) was added, and the deep red solution was stirred in a sealed vessel under argon at 90°C for 4 hours. The resulting brownish-yellow solution was allowed to cool and concentrated to dryness. The residue was dissolved in acetone (2 mL) and 2,2-dimethoxypropane (2 mL) and p-TsOH • H_2O (108 mg, 2 equiv.) were added. After stirring for 15 minutes, the reaction was quenched with triethylamine (240 µL, 6 equiv.), and the mixture was diluted with DCM (50 mL) and washed with H_2O (50 mL) + 1 M

aqueous NaH_2PO_4 (10 mL). The aqueous layer was extracted with DCM (20 mL), and the combined organic layers were dried with Na_2SO_4 and concentrated to dryness. The residue was separated by column chromatography (DCM-MTBE) to give the product as a yellow glassy solid containing 0.65 molar equiv. (6 mass%) MTBE by ^{1}H NMR. Yield 182 mg (171 mg corrected for solvent content, 186 μmol, 66%). ^{1}H NMR ($CDCl_3$) δ 1.38 (s, 3H), 1.40 (s, 3H), 1.43 (s, 3H), 1.44 (s, 3H), 1.94 (p, *J* = 6.4 Hz, 2H), 2.58 (s, 2H), 2.61 (d, *J* = 5.4 Hz, 3H), 2.68 (d, *J* = 5.4 Hz, 3H), 2.73-2.81 (m, 6H), 2.92 (d, *J* = 11.8 Hz, 1H), 2.97 (d, *J* = 11.8 Hz, 1H), 3.18 (dd, *J* = 17.3, 6.1 Hz, 1H), 3.50-3.72 (m, 10H), 3.84 (dd, *J* = 17.3, 12.3 Hz, 1H), 4.44 (q, *J* = 5.4 Hz, 1H), 4.69 (q, *J* = 5.4 Hz, 1H), 5.29 (dd, J = 12.3, 6.1 Hz, 1H), 5.66 (t, *J* = 7.1 Hz, 1H), 6.90 (d, *J* = 8.6 Hz, 1H), 7.04 (dd, *J* = 8.6, 2.2 Hz, 1H), 7.16 (ad, *J* = 9.0 Hz, 2H), 7.35 (d, *J* = 2.2 Hz, 1H), 7.65 (ad, *J* = 9.0 Hz, 2H), 7.84-7.89 (m, 4H).). ^{13}C NMR ($CDCl_3$) δ 20.0, 23.5, 23.8, 27.4, 27.5, 29.3, 29.4, 31.3, 31.9, 35.0, 35.1, 37.8, 38.5, 39.4, 43.2, 44.5, 63.5, 65.6, 65.7, 66.5, 66.7, 98.4, 98.6, 111.2, 113.0, 117.4, 126.3, 127.5, 127.7, 127.8, 128.7, 128.8, 133.4, 136.3, 138.5, 146.8, 147.3, 150.1.

Sulfonyl fluoride **5.11**

Triarylpyrazoline **5.10** (150 mg of material containing 6% MTBE, 153 μmol) and N,N-diisopropylethylamine (200 μL, 7.5 equiv.) were dissolved in anhydrous DCM (1.5 mL) under argon, and ethenesulfonyl fluoride (38 μL, 3 equiv.) was added to the stirred mixture. After 3 hours, the mixture was diluted with toluene (3 mL) and concentrated to dryness. The residue was separated by column chromatography (2:1 DCM-hexanes plus 0 →17% MTBE) to give the product as a yellow glassy solid after solvent evaporation under high vacuum. Yield 142 mg (81%). ^{1}H NMR ($CDCl_3$) δ 1.38 (s, 3H), 1.41 (s, 3H), 1.436 (s, 3H), 1.443 (s, 3H), 1.94 (p, *J* = 6.4 Hz, 2H), 2.57 (s, 2H), 2.75-2.80 (m, 6H), 2.82 (s, 3H), 2.90 (s, 3H), 2.96 (d, *J* = 11.7 Hz, 1H), 3.00 (d, *J* = 11.7 Hz, 1H), 3.20 (dd, *J* = 17.4, 6.1 Hz, 1H), 3.49-3.52 (m, 2H), 3.56-3.62 (m, 6H), 3.67-3.79 (m, 10H), 3.87 (dd,

J = 17.4, 12.3 Hz, 1H), 5.30 (dd, *J* = 12.3, 6.1 Hz, 1H), 5.69 (t, *J* = 7.1 Hz, 1H), 6.90 (d, *J* = 8.6 Hz, 1H), 7.03 (dd, *J* = 8.6, 2.2 Hz, 1H), 7.19 (ad, *J* = 8.9 Hz, 2H), 7.38 (d, *J* = 2.2 Hz, 1H), 7.61 (ad, *J* = 9.1 Hz, 2H), 7.84 (ad, *J* = 8.7 Hz, 2H), 7.90 (ad, *J* = 8.7 Hz, 2H). ^{19}F NMR ($CDCl_3$) δ 56.3 (t, J = 4.8 Hz 1F), 56.6 (t, J = 4.7 Hz, 1F). ESI-HRMS *m/z* calcd for $[M+H]^+$ $C_{46}H_{64}N_5O_{12}S_7F_2$ 1140.2559, found 1140.2561.

Probe **5.8**

Sulfonyl fluoride **5.11** (117 mg, 103 µmol) was dissolved in acetonitrile (1.7 mL) and 3 M aqueous HCl (340 µL, 10 equiv. HCl, ~190 equiv. H_2O) was added to the stirred mixture. After 15 minutes, triethylamine (570 µL, 40 equiv.) was added. The mixture was stirred overnight and then concentrated to dryness. The residue was taken up in methanol (3 mL) and heated in a 40°C bath. $NaHCO_3$ 129 mg, 15 equiv. was added, followed by sufficient water for complete dissolution. The mixture was concentrated to dryness, taken up in methanol-water mixture, and concentrated again. After repetition of this procedure to remove triethylamine, the residue was taken up in methanol (4 mL), diluted with ethanol (2 mL), filtered to remove NaCl, and concentrated to dryness. The product was obtained as the ammonium salt by RP-HPLC as described for reference compound **5.1** as a yellow glassy solid. Yield 49 mg (45 µmol, 44%). ^{1}H NMR (CD_3OD) δ 1.82 (p, *J* ≈ 7 Hz, 2H), 2.50 (t, *J* = 6.8 Hz, 2H), 2.56 (t, *J* = 6.9 Hz, 2H), 2.59 (s, 2H), 2.72 (s, 3H), 2.76 (s, 2H), 2.82 (s, 3H), 2.88 (d, *J* = 12.4 Hz, 1H), 2.96 (d, *J* = 12.4 Hz 1H), 3.00-3.06 (m, 4H), 3.16-3.22 (m, 3H), 3.38-3.42 (m, 2H), 3.47-3.58 (m, 10H), 3.90 (dd, *J* = 17.6, 12.2 Hz, 1H), 5.41 (dd, *J* = 12.2, 5.8 Hz, 1H), 6.69 (d, *J* = 8.6 Hz, 1H), 7.01 (dd, *J* = 8.5, 2.1 Hz, 1H), 7.22 (ad, *J* = 9.0 Hz, 2H), 7.33 (d, *J* = 2.1 Hz, 1H), 7.58 (ad, *J* = 9.1 Hz, 2H), 7.85 (ad, *J* = 8.6 Hz, 2H), 7.96 (ad, *J* = 8.6 Hz, 2H). ESI-HRMS *m/z* calcd for $[M]^{2-}$ $C_{40}H_{55}O_{14}N_5S_7$ 526.5901, found 526.5891.

Iodide **5.15**

A mixture of thietane **3.15** (10.08 g, 57.8 mmol), methyl iodide (4.3 mL, 1.2 equiv.), powdered K_2CO_3 (200 mg), and acetonitrile (15 mL) was stirred under argon at 60°C for 20 hours. The mixture was concentrated under reduced pressure, and the oily residue was taken up in DCM (50 mL), stirred with silica gel (3 g), and filtered through a 2 x 2 cm pad of silica gel. The silica gel was washed with a further 50 mL of DCM, and the combined filtrate and washing were concentrated under reduced pressure to give the product as a colorless oil. Yield 17.23 g (54.5 mmol, 94%). ^{1}H NMR ($CDCl_3$) δ 1.41 (s, 3H), 1.42 (s, 3H), 2.19 (s, 3H), 2.69 (s, 2H), 3.42 (s, 2H), 3.73 (d, *J* = 11.8 Hz, 2H), 3.80 (d, *J* = 11.8 Hz, 2H). Note: in some samples, a partly resolved long-range coupling (< 0.5 Hz) is observed in the methyl signals at 1.41 and 1.42 ppm. ^{13}C NMR ($CDCl_3$) δ 12.9, 17.9, 23.1, 24.0, 37.1, 39.2, 66.3, 98.6. EI-MS *m/z* 316 ($[M]^+$, 65), 301 (67), 131 (82), 101 (55), 83 (82), 61 (100), 55 (62). EI-HRMS *m/z* calcd for $C_9H_{17}IO_2S$ 315.9994, found 315.9999.

Benzothiazolinone **5.16**

A mixture of benzothiazolin-2-one-6-carboxaldehyde[11] (**5.14**, 255 mg, 1.42 mmol), iodide **5.15** (562 mg, 1.25 equiv.), and K_2CO_3 (600 mg, 3 equiv.) in DMF (5 mL) was stirred at 90°C for 12 hours. The mixture was diluted into a solution of 1 M NaOH in 20% aqueous methanol (100 mL), and the resulting emulsion was extracted with MTBE (100 mL). The extract was washed with a further 100 mL of the aqueous-methanolic NaOH solution, dried with Na2SO4, and concentrated under reduced pressure to a yellow oily residue. Crystallization from diethyl ether-pentane under stirring gave the product as a slightly tan crystalline powder. Yield 306 mg (833 µmol, 59%). Mp 134-134.5°C ^{1}H NMR ($CDCl_3$) δ 1.49 (br. s, 6H), 2.13 (s, 3H) 2.66 (s, 2H), 3.64 (d, *J* = 12.5 Hz, 2H), 4.03 (d, *J* = 12.5 Hz, 2H), 4.24 (s, 2H), 7.74 (d, *J* = 8.5 Hz, 1H), 7.87 (dd, *J* = 8.5, 1.6 Hz, 1H), 7.97 (d, *J* = 1.6 Hz, 1H), 9.95 (s, 1H). ^{13}C NMR ($CDCl_3$) δ 18.4, 21.0, 26.7, 38.1,

40.1, 46.6, 64.7, 98.6, 111.7, 123.3, 123.4, 129.4, 132.0, 143.1, 171.4, 190.2. EI-HRMS *m/z* calcd for C_{17} $H_{21}NO_4S_2$ 367.0912, found 367.0921

Aldehyde **5.13**

A solution of intermediate **5.16** (253 mg, 688 µmol) in DMSO (10 mL) was heated to 80°C under argon, and 15% aqueous NaOH (830 µL, 4.5 equiv.) was added under rapid stirring. After 50 minutes, iodide **5.15** (272 mg, 1.25 equiv. was added as a solution in DMSO (2 mL). After 30 minutes, the mixture was partitioned between water (80 mL) and MTBE (80 mL). The organic layer was separated, washed with twice with water (80 mL) plus brine (10 mL), dried with $MgSO_4$, and concentrated. The residue was separated by column chromatography (hexanes-MTBE) to give the product as a pale yellow oil. Yield 181 mg (342 µmol, 50%). ^{1}H NMR ($CDCl_3$) δ 1.39 (s, 3H), 1.41 (s, 3H), 1.46 (s, 3H), 1.48 (s, 3H), 2.12 (s, 3H), 2.17 (s, 3H), 2.59 (s, 2H), 2.75 (s, 2H), 2.98 (s, 2H), 3.58 (d, *J* = 6.6 Hz, 2H), 3.71 (d, *J* = 12.2 Hz, 2H), 3.77 (s, 4H), 3.83 (d, *J* = 12.2 Hz, 2H), 6.11 (t, *J* = 6.6 Hz, 1H), 6.93 (d, *J* = 8.6 Hz, 1H), 7.71 (dd, *J* = 8.6, 2.0 Hz, 1H), 7.98 (d, *J* = 2.0 Hz, 1H), 9.69 (s, 1H). ^{13}C NMR ($CDCl_3$) δ 17.7, 21.1, 23.6, 23.7, 26.3, 38.0, 38.1, 38.5, 38.8, 38.9, 45.4, 65.3, 66.2, 98.5, 98.6, 109.4, 118.0, 126.3, 133.0, 138.1, 154.0, 189.6. EI-MS m/z 529 ($[M]^+$, 100), 354 (25), 180 (27), 164 (40), 117 (55), 61 (50). EI-HRMS *m/z* calcd for $[M]^+$ $C_{25}H_{39}NO_5S_3$ 529.1990, found 529.1993.

Chalcone **5.17**

A solution of aldehyde **5.13** (764 mg, 1.44 mmol), acetophenone **5.3** (308 mg, 1.44 mmol), and pyrrolidine (241 µL, 2.88 mmol) in ethanol (6 mL) was stirred for 2 days at 50°C. The resulting oily biphasic mixture was poured into water (50 mL) + 1 M NaH_2PO_4 (10 mL) and extracted with MTBE (60 mL). The extract was dried with $MgSO_4$ and concentrated, and the residue was separated by column chromatography (2:1 DCM-hexanes + 0→17% MTBE) to give the product as an orange-red glassy solid. Yield

305 mg (420 µmol, 29%). ^{1}H NMR ($CDCl_3$) δ 1.39 (s, 3H), 1.42 (s, 3H), 1.47 (s, 3H), 1.49 (s, 3H), 2.13 (s, 3H), 2.17 (s, 3H), 2.61 (s, 2H), 2.71 (d, *J* = 5.3 Hz, 3H), 2.76 (s, 2H), 3.00 (s, 2H), 3.55 (d, *J* = 6.6 Hz, 2H), 3.72 (d, *J* = 12.1 Hz, 2H), 3.78 (s, 4H), 3.83 (d, *J* = 12.1 Hz, 2H), 4.67 (q, *J* = 5.3 Hz, 1H), 5.89 (t, *J* = 6.6 Hz, 1H), 6.91 (d, *J* = 8.7 Hz, 1H), 7.29 (d, *J* = 15.5 Hz, 1H), 7.53 (dd, *J* = 8.7, 2.1 Hz, 1H), 7.73 (d, *J* = 15.5 Hz, 1H), 7.80 (d, *J* = 2.1 Hz 1H), 7.98 (ad, *J* = 8.6 Hz, 2H), 8.11 (ad, *J* = 8.6 Hz, 2H). ^{13}C NMR ($CDCl_3$) δ 17.8 (2C), 21.3, 23.5, 23.9, 26.2, 29.3, 38.1, 38.2, 38.6, 38.9, 39.1, 45.5, 65.4, 66.3, 98.5, 98.6, 110.2, 116.8, 118.3, 123.4, 127.3, 128.9, 131.7, 137.0, 141.8, 142.4, 146.5, 151.8, 189.3. EI-MS *m/z* 724 ($[M]^+$, 100), 375 (40), 373 (25), 198 (25), 131 (30), 117 (83), 61 (92). EI-HRMS *m/z* calcd for $[M]^+$ $C_{34}H_{48}N_2O_7S_4$ 724.2344, found 724.2350.

Triarylpyrazoline **5.18**

This compound was synthesized according to the procedure described for triarylpyrazoline **5.10** using chalcone **5.17** (162 mg, 223 µmol), PPTS (112 mg, 2 equiv.), and arylhydrazine **5.2** (90 mg, 2 equiv.) Yield 74 mg (81 µmol, 36%), yellow glassy solid.^{1}H NMR ($CDCl_3$) δ 1.35 (s, 3H), 1.39 (s, 3H), 1.44 (s, 6H), 2.06 (s, 3H), 2.14 (s, 3H), 2.60-2.63 (m, 5H), 2.66-2.69 (m, 5H), 2.88 (d, *J* = 12.9 Hz, 1H), 2.94 (d, *J* = 12.9 Hz, 1H), 3.19 (dd, *J* = 17.3, 6.0 Hz 1H), 3.41 (dd, *J* = 6.6, 2.1 Hz, 2H), 3.68-3.81 (m, 8H), 3.84 (dd, *J* = 17.3, 12.3 Hz, 1H), 4.37 (q, *J* = 5.5 Hz, 1H), 4.59 (q, *J* = 5.4 Hz, 1H), 5.30 (dd, *J* = 12.3, 6.0 Hz, 1H), 5.33 (t, *J* = 6.6 Hz, 1H), 6.81 (d, *J* = 8.6 Hz, 1H), 7.05 (dd, *J* = 8.6, 2.2 Hz, 1H), 7.16 (ad, *J* = 9.0 Hz 2H), 7.32 (d, *J* = 2.2 Hz 1H), 7.65 (ad, *J* = 9.0 Hz, 2H), 7.84-7.89 (m, 4H). ^{13}C NMR ($CDCl_3$) δ 17.77, 17.83, 21.6, 23.7, 23.7, 25.9, 29.3, 29.4, 38.0, 38.3, 38.6, 38.72, 38.73, 43.2, 45.9, 63.4, 65.3, 65.4, 65.4, 66.2, 98.4, 98.5, 111.1, 113.1, 118.6, 126.4, 127.5, 127.6, 127.9, 128.75, 128.83, 132.9, 136.4, 138.6, 146.8, 147.4, 149.3.

Sulfonyl fluoride **5.19**

This compound was synthesized as described for sulfonyl fluoride **5.11** using triarylpyrazoline **5.18** (60 mg, 66 µmol), ethenesulfonyl fluoride (39 µL, 7 equiv.), and diisopropylethylamine (202 µL, 18 equiv.) with a reaction time of 2 hours. Yield 54 mg (48 µmol, 72%), yellow glassy solid. ^{1}H NMR ($CDCl_3$) δ 1.36 (s, 3H), 1.40 (s, 3H), 1.44 (s, 6H), 2.07 (s, 3H), 2.15 (s, 3H), 2.60 (s, 2H), 2.65 (d, *J* = 13.3 Hz 1H), 2.69 (d, *J* = 13.3 Hz, 1H), 2.82 (s, 3H), 2.90 (s, 3H), 2.91 (d, *J* = 12.8 Hz, 1H), 2.96 (d, *J* = 12.8 Hz, 1H), 3.21 (dd, *J* = 17.4, 6.0 Hz, 1H), 3.38-3.46 (m, 2H), 3.49-3.52 (m, 2H), 3.56-3.59 (m, 2H), 3.68-3.82 (m, 12H), 3.86 (dd, *J* = 17.4, 12.2 Hz, 1H), 5.31 (dd, *J* = 12.2, 6.0 Hz, 1H), 5.36 (t, *J* = 6.7 Hz, 1H), 6.82 (d, *J* = 8.6 Hz, 1H), 7.05 (dd, *J* = 8.5, 2.2 Hz, 1H), 7.19 (ad, *J* = 8.9 Hz, 2H), 7.34 (d, *J* = 2.2 Hz, 1H), 7.61 (ad, *J* = 9.1 Hz, 2H), 7.84 (ad, *J* = 8.7 Hz, 2H), 8.00 (ad, *J* = 8.7 Hz, 2H). ^{19}F NMR δ 56.3 (t, *J* = 4.8 Hz, 1F), 56.6 (t, *J* = 4.7 Hz,1F). ESI-HRMS calcd for $[M+H]^+$ $C_{45}H_{64}N_5O_{12}S_7F_2$ 1128.2559, found 1128.2560.

Probe **5.12**

This compound was synthesized as described for probe **5.8** except that K_2CO_3 (10 equiv.) was used in place of $NaHCO_3$ during workup for more efficient removal of triethylamine. Starting material: sulfonyl fluoride **5.19** (50.6 mg, 44 µmol). Isolated yield of pure product ammonium salt 3.5 mg (3.6 µmol, 8%), yellow glassy solid containing ~ 1 molar equiv. (3%) methanol by ^{1}H NMR. The low yield is due to difficult HPLC separation requiring low column loading, and only a small fraction of the total yield has been purified. ^{1}H NMR (CD_3OD) δ 1.98 (s, 3H), 2.10 (s, 3H), 2.54 (d, *J* = 13.0 Hz, 1H), 2.57 (d, *J* = 13.0 Hz, 1H), 2.69 (s, 2H), 2.73 (s, 3H), 2.79 (d, *J* = 12.7 Hz, 1H), 2.83 (s, 3H), 2.84 (d, *J* ≈ 13 Hz, 1H, obscured by previous signal), 2.97-3.05 (m, 4H), 3.21-3.55 (m, 11H, partly obscured by CHD_2OH and CH_3OH signals), 3.71 (m, 4H), 3.95 (dd, *J* = 17.5, 12.2 Hz, 1H), 5.46 (dd, *J* = 12.2, 5.6 Hz, 1H), 6.72 (d, *J* = 8.6 Hz, 1H), 7.08 (dd, *J* = 8.6, 2.2 Hz, 1H), 7.27 (ad, *J* = 9.0 Hz, 2H), 7.35 (d, *J* = 2.2 Hz, 1H), 7.62 (ad, *J* = 9.1 Hz,

2H), 7.88 (ad, *J* = 8.6 Hz, 2H), 8.01 (ad, *J* = 8.6 Hz, 2H). ESI-HRMS *m/z* calcd for $[M]^{2-}$ $C_{39}H_{55}N_5O_{14}S_7$ 520.5901, found 520.5891.

Benzothiazolinone **5.22**

A mixture of 6-bromobenzothiazolin-2-one (**5.21**, 4.37 g, 19.0 mmol), iodide **5.15** (6.61 g, 1.1 equiv.), Cs_2CO_3 (9.3g, 1.5 equiv.), and DMF (10 mL) was stirred at 90°C under argon overnight. The mixture was diluted with water (100 mL) and extracted with MTBE (100 mL). The extract was washed with 5% aqueous NaOH (100 mL) followed by water (100 mL) + brine (10 mL), dried with MgSO4, filtered, and concentrated to give a yellow oil that solidified on contact with methanol. The resulting material was recrystallized from methanol under stirring to give a colorless crystalline powder. Yield 6.90 g (87%). ^{1}H NMR ($CDCl_3$) δ 1.47 (s, 6H), 2.13 (s, 3H), 2.66 (s, 2H), 3.62 (d, *J* = 12.5 Hz, 2H), 4.00 (d, *J* = 12.5 Hz, 2H), 4.14 (s, 2H), 7.44 (dd, *J* = 8.7, 1.7 Hz, 1H), 7.47 (dd, *J* = 8.7, 0.6 Hz, 1H), 7.54 (dd, *J* = 1.7, 0.6 Hz, 1H). ^{13}C NMR ($CDCl_3$) δ 18.4, 21.4, 26.3, 38.1, 40.2, 46.4, 64.6, 98.5, 112.9, 115.8, 124.1, 124.8, 129.6, 137.4, 170.7. EI-MS *m/z* 419 (27) 417 ($[M]^+$, 25), 404 (35), 402 (32), 361 (35), 359 (32), 328 (50), 326 (45), 135 (52), 97 (100), 82 (80), 61 (70). EI-HRMS *m/z* calcd for $[M]^+$ $C_{16}H_{20}NO_3S_2{}^{79}Br$ 417.0068, found 417.0050.

Bromide **5.23**

Benzothiazolinone 5.22 (4.80 g, 11.5 mmol) was dissolved in DMSO (40 mL) under argon at 80°C. Aqueous NaOH (5 M, 8.3 mL, 3.6 equiv.) was injected as a slow stream into the rapidly stirred solution. After 30 minutes, the reaction was complete by TLC (5:1 hexane-EtOAc). The mixture was cooled to 60°C and acetic acid (0.85 mL, 1 equiv) was added, followed by 1-chloro-3-methylthiopropane (1.43 g, 1 equiv.) in DMSO (2 mL). After 30 minutes, a trace of the intermediate thiophenol remained distinguishable by TLC, so a further 0.1 equiv. (143 mg) of 1-chloro-3-methylthiopropane was added.

After 15 minutes, TLC indicated complete consumption of the thiophenol. The mixture was partitioned between water (300 mL) and MTBE (140 mL), and the organic layer was washed twice with water (200 mL) + brine (10 mL), dried with $MgSO_4$, and concentrated. The residue was separated by column chromatography (hexanes-MTBE) to give the product as a colorless oil. Yield 4.93 g (10.3 mmol, 89%). ^{1}H NMR ($CDCl_3$) δ 1.45 (s, 3H), 1.46 (s, 3H), 1.83 (p, *J* = 7.1 Hz, 2H), 2.06 (s, 3H), 2.16 (s, 3H), 2.58 (t, *J* = 7.0 Hz, 2H), 2.60 (s, 2H), 2.81 (t, *J* = 7.1 Hz, 2H), 3.38 (d, *J* = 6.6 Hz, 2H), 3.71 (d, *J* = 12.0 Hz, 2H), 3.78 (d, *J* = 12.0 Hz, 2H), 5.32 (t, *J* = 6.5 Hz, 1H), 6.71 (d, *J* = 8.8 Hz, 1H), 7.28 (dd, *J* = 8.8, 2.4 Hz, 1H), 7.48 (d, *J* = 2.4 Hz, 1H). ^{13}C NMR ($CDCl_3$) δ 15.4, 17.8, 21.8, 25.6, 28.5, 32.8, 33.6, 38.3, 38.7, 45.9, 65.4, 98.5, 107.6, 111.7, 119.1, 132.8, 137.6, 148.7. EI-MS *m/z* 481 (70), 479 ($[M]^+$, 65), 306 (43), 304 (39), 216 (40), 214 (35), 89 (100), 61 (63). EI-HRMS *m/z* calcd for $[M]^+$ $C_{19}H_{30}NO_2S_3{}^{79}Br$ 479.0622, found 479.0610.

Aldehyde **5.24**

An oven-dried 50 mL rb flask was charged with bromide 5.23 (642 mg, 1.34 mmol), sealed with a rubber septum, and flushed with argon. Anhydrous THF (14 mL) was added, and the solution was cooled in a dry ice-acetone bath. After 15 min, *n*-butyllithium (2.5 M in hexanes, 1.1 mL, 2 equiv.) was added dropwise to the stirred solution. After 5 min, *t*-butyllithium (1.6 M in pentane, 2.5 mL, 3 equiv.) was added dropwise. After 30 min, anhydrous DMF (1.0 mL, 10 equiv.) was added, the cooling bath was removed, and the mixture was quenched with water once the temperature rose to ~0°C. The mixture was partitioned between water (100 mL) and MTBE (100 mL), and the organic layer was washed with water + brine (100 mL + 10 mL), dried with MgSO4, and concentrated. The residue was separated by column chromatography (hexanes-MTBE) to give the product as a pale yellow oil. Yield 458 mg (83%). ^{1}H NMR ($CDCl_3$) δ 1.46 (s, 3H), 1.49 (s, 3H), 1.84 (p, *J* = 7.1 Hz, 2H), 2.05 (s, 3H), 2.17 (s, 3H), 2.57 (s,

2H), 2.59 (t, *J* = 7.0 Hz, 2H), 2.83 (t, *J* = 7.1 Hz, 2H), 3.56 (d, *J* = 6.5 Hz, 2H), 3.70 (d, *J* = 12.2 Hz, 2H), 3.82 (d, *J* = 12.2 Hz, 2H), 6.16 (t, *J* = 6.4 Hz, 1H), 6.91 (d, *J* = 8.6 Hz, 1H), 7.72 (dd, *J* = 8.6, 2.0 Hz, 1H), 7.92 (d, *J* = 2.0 Hz, 1H), 9.70 (s, 1H). ^{13}C NMR ($CDCl_3$) δ 15.3, 17.8, 21.1, 26.3, 28.5, 32.7, 33.7, 38.2, 38.7, 45.5, 65.4, 98.7, 109.2, 117.5, 126.1, 133.1, 138.2, 154.2, 189.6. EI-MS *m/z* 429 ($[M]^+$, 85), 254 (38), 164 (34), 89 (100), 61 (40). EI-HRMS calcd for $C_{20}H_{31}NO_3S_3$ 429.1466, found 429.1475.

Chalcone **5.25**

A solution of aldehyde **5.24** (420 mg, 978 µmol), acetophenone **5.3** (208 mg, 1 equiv.), and pyrrolidine (163 µL, 2 equiv.) in ethanol (5 mL) was stirred at 45°C for two days. The resulting biphasic mixture was partitioned between water (100 mL) + 1 M NaH_2PO_4 (10 mL) and MTBE (100 mL). The organic layer was dried with $MgSO_4$ and concentrated, and the residue was separated by column chromatography (DCM-MTBE) to give the product as a red-orange glassy solid. Yield 296 mg (474 µmol, 48%). ^{1}H NMR ($CDCl_3$) δ 1.47 (s, 3H), 1.49 (s, 3H), 1.85 (p, *J* = 7.1 Hz, 2H), 2.05 (s, 3H), 2.18 (s, 3H), 2.59 (s, 2H), 2.60 (t, *J* = 7.0 Hz, 2H), 2.70 (d, *J* = 5.3 Hz, 3H), 2.84 (t, *J* = 7.1 Hz, 2H), 3.53 (d, *J* = 6.5 Hz, 2H), 3.72 (d, *J* = 12.1 Hz, 2H), 3.83 (d, *J* = 12.1 Hz, 2H), 4.97 (q, *J* = 5.3 Hz, 1H), 5.96 (t, *J* = 6.5 Hz, 1H), 6.89 (d, *J* = 8.7 Hz, 1H), 7.29 (d, *J* = 15.5 Hz, 1H), 7.55 (dd, *J* = 8.7, 2.1 Hz, 1H), 7.74 (d, *J* = 15.4 Hz, 1H), 7.75 (d, *J* = 2.1 Hz, 1H), 7.98 (ad, *J* = 8.5 Hz, 2H), 8.10 (ad, *J* = 8.5 Hz, 2H). ^{13}C NMR ($CDCl_3$) δ 15.3, 17.7, 21.2, 26.2, 28.4, 29.3, 32.7, 33.7, 38.2, 38.7, 45.5, 65.4, 98.6, 110.0, 116.6, 117.6, 123.0, 127.3, 128.8, 131.8, 137.4, 141.7, 142.2, 146.5, 152.0, 189.2. EI-MS *m/z* 624 ($[M]^+$, 70), 449 (25), 89 (100), 61 (25). EI-HRMS *m/z* calcd for $[M]^+$ $C_{29}H_{40}N_2O_5S_4$ 624.1820, found 624.1804.

Triarylpyrazoline **5.26**

This compound was synthesized according to the procedure described for triarylpyrazoline **5.10** using chalcone **5.25** (126 mg, 202 µmol), arylhydrazine **5.2** (61 mg, 1.5 equiv.), and PPTS (101 mg, 2 equiv.). Yield 105 mg (129 µmol, 64%). ^{1}H NMR ($CDCl_3$) δ 1.44 (s, 6H), 1.69 (p, *J* = 7.1 Hz, 2H), 2.00 (s, 3H), 2.15 (s, 3H), 2.44-2.55 (m, 2H), 2.59 (s, 2H), 2.61 (d, *J* = 5.5 Hz, 3H), 2.68 (d, *J* = 5.4 Hz, 3H), 2.74 (t, *J* = 7.1 Hz, 2H), 3.19 (dd, *J* = 17.4, 5.9 Hz, 1H), 3.35-3.43 (m, 2H), 3.70 (d, *J* = 12.0 Hz, 2H), 3.79 (d, *J* ≈ 12 Hz, 2 H), 3.85 (dd, *J* = 17.4, 12.3 Hz, 1H), 4.42 (q, *J* = 5.5 Hz, 1H), 4.66 (q, *J* = 5.4 Hz, 1H), 5.31 (dd, *J* = 12.3, 5.9 Hz, 1H), 5.39 (t, *J* = 6.6 Hz, 1H), 6.80 (d, *J* = 8.6 Hz, 1H), 7.08 (dd, *J* = 8.5, 2.2 Hz, 1H), 7.15 (ad, *J* = 9.0 Hz, 2H), 7.25 (d, *J* = 2.2 Hz, 1H), 7.65 (ad, *J* = 9.1 Hz, 2H), 7.84-7.90 (m, 4H). ^{13}C NMR ($CDCl_3$) δ 15.4, 17.8, 21.6, 25.9, 28.4, 29.30, 29.34, 32.6, 33.4, 38.3, 38.6, 43.2, 45.9, 63.4, 65.4, 65.5, 98.6, 110.9, 113.0, 117.8, 126.4, 127.6, 127.6, 127.9, 128.5, 128.7, 133.3, 136.3, 138.6, 146.7, 147.4, 149.5. MALDI-HRMS m/z calcd for $[M+H]^+$ $C_{36}H_{50}N_5O_6S_5$ 808.2365, found 808.2395.

Sulfonyl fluoride **5.27**

This compound was synthesized according to the procedure described for sulfonyl fluoride **5.11** using triarylpyrazoline **5.26** (78 mg, 97 µmol), ethenesulfonyl fluoride (40 µL, 5 equiv.), and diisopropylethylamine (211 µL, 12.6 equiv.). Yield 67 mg (65 µmol, 68%). ^{1}H NMR ($CDCl_3$) δ 1.44 (s, 6H), 1.71 (p, *J* = 7.1 Hz, 2H), 2.01 (s, 3H), 2.15 (s, 3H), 2.49-2.56 (m, 2H), 2.58 (s, 2H), 2.75 (t, *J* = 7.1 Hz, 2H), 2.82 (s, 3H), 2.90 (s, 3H), 3.21 (dd, *J* = 17.4, 5.9 Hz, 1H), 3.40 (d, *J* = 6.7 Hz, 2H) 3.49-3.53 (m, 2H), 3.56-3.59 (m, 2H), 3.68-3.81 (m, 8H), 3.87 (dd, *J* = 17.4, 12.3 Hz, 1H), 5.32 (dd, *J* = 12.3, 5.9 Hz, 1H), 5.42 (t, *J* = 6.6 Hz, 1H), 6.81 (d, *J* = 8.6 Hz, 1H), 7.08 (dd, *J* = 8.5, 2.2 Hz, 1H), 7.19 (ad, *J* = 9.0 Hz, 2H), 7.26 (d, *J* = 2.2 Hz, 1H), 7.61 (ad, *J* = 9.1 Hz, 2H), 7.84 (ad, *J* = 8.7 Hz, 2H), 7.90 (ad, *J* = 8.7 Hz, 2H). ^{19}F NMR δ 56.3 (t, *J* = 4.8 Hz, 1F), 56.6 (t, *J* = 4.7 Hz,

1F). MALDI-HRMS m/z calcd for $[M+H]^+$ $C_{40}H_{56}N_5O_{10}S_7F_2$ 1028.2040, found 1028.2002.

Probe **5.20**

Sulfonyl fluoride 5.27 (48 mg, 47 µmol) was stirred in a mixture of methanol (1.5 mL), THF (0.5 mL), and 3 M aqueous HCl (47 µL, 3 equiv.). After 40 min, the mixture was concentrated to dryness under a stream of argon, and the residue was stirred in a mixture of methanol (2 mL), THF (1 mL), and 5 M NaOH (112 µL, 12 equiv.). After 4 hours, the reaction was quenched by adding a small piece of dry ice and concentrated to dryness. The residue was taken up in methanol (5 mL), filtered through cotton to remove $NaHCO_3$, and concentrated to dryness. The resulting material was taken up in 75% H_2O/25% CH_3CN and separated by RP-HPLC using a gradient of 30-34% CH3CN in 0.1% aqueous NH4HCO4 to give the product ammonium salt as a yellow glassy solid after drying under high vacuum. Purification of 37.5% of the total crude material gave 13.3 mg (13 µmol, 75% yield). ^{1}H NMR (CD_3OD) δ 1.62 (p, *J* = 7.0 Hz, 2H), 1.93 (s, 3H), 2.09 (s, 3H), 2.39-2.52 (m, 2H), 2.66 (s, 2H), 2.71-2.74 (m, 5H), 2.83 (s, 3H), 2.97-3.04 (m, 4H), 3.21 (s, 2H), 3.22 (dd, *J* = 17.5, 5.7 Hz, 1H), 3.36-3.44 (m, 2H), 3.47-3.51(m, 2H), 3.59 (s, 4H), 3.94 (dd, *J* = 17.5, 12.2 Hz, 1H), 5.47 (dd, *J* = 12.2, 5.6 Hz, 1H), 6.73 (d, *J* = 8.6 Hz, 1H), 7.12 (dd, *J* = 8.5, 2.2 Hz, 1H), 7.23-7.25 (m, 3H), 7.61 (ad, *J* = 9.0 Hz, 2H), 7.87 (ad, *J* = 8.5 Hz, 2H), 8.00 (ad, *J* = 8.5 Hz, 2H). ^{13}C NMR ($CDCl_3$) δ 15.3, 17.7, 29.5, 33.4, 33.8, 35.9, 36.0, 37.8, 44.1, 46.2, 47.2, 47.7, 47.8, 50.7, 50.8, 64.7, 64.8, 111.7, 114.3, 118.9, 127.3, 127.8, 128.9, 128.9, 129.9, 130.0, 134.7, 138.1, 138.6, 148.6, 149.8, 151.1. ESI-HRMS *m/z* calcd for $[M]^{2-}$ $C_{37}H_{51}N_5O_{12}S_7$ 490.5795, found 490.5787.

Acetophenone **5.30**

m-Aminoacetophenone (9.09 g, 67.3 mmol) was dissolved in pyridine (27 mL, 5 equiv.), and the solution was cooled in an ice bath under a slow stream of argon. Methanesulfonyl chloride (6.8 mL, 1.3 equiv.) was added dropwise to the stirred solution. After 5 min, the reaction was quenched by adding crushed ice and poured over a slurry of crushed ice (~100 g) and concentrated HCl (25 mL). The resulting red emulsion was extracted with dichloromethane (100 mL) + MTBE (200 mL). The yellow organic layer (top), dried with MgSO4, filtered, and concentrated. The residue was recrystallized from cyclohexane-ethyl acetate to give the product as a slightly yellowish crystalline powder. Yield 10.41 g (48.8 mmol, 73%) A further 1.26 g of pure product was recovered from the emulsion layer remaining after extraction, bringing the total yield to 11.67 g (81%). ^{1}H NMR ($CDCl_3$) δ 2.63 (s, 3H), 3.06 (s, 3H), 7.38 (br. s, 1H), 7.48 (t, *J* = 7.9 Hz 1H), 7.56 (ddd, *J* = 8.1, 2.3, 1.1 Hz, 1H), 7.77 (dt, *J* = 7.7, 1.2 Hz, 1H), 7.84 (t, *J* = 1.8 Hz, 1H). ^{13}C NMR ($CDCl_3$) δ 26.7, 39.6, 120.0, 125.1, 125.2, 130.0, 137.5, 138.4, 197.7.

Chalcone **5.31**

A solution of acetophenone **5.30** (2.10 g, 9.85 mmol), 4-dimethylaminobenzaldehyde (1.50 g, 1.02 equiv.), and pyrrolidine (250 µL, 0.3 equiv.) in ethanol (30 mL) was stirred for 2 days at 40-50°C. The resulting dark red slurry was allowed to cool, and the product was collected by filtration, washed with cold ethanol until the washings were yellow-orange rather than red, and dried under high vacuum at 50°C to give a yellow-orange crystalline powder. Yield 2.42 g (7.03 mmol, 71%). Mp 215-217°C ^{1}H NMR (DMSO-d_6) δ 3.01 (s, 6H), 3.05 (s, 3H), 6.75 (ad, *J* = 9.0 Hz, 2H), 7.46-7.49 (m, 1H), 7.51-7.56 (m, 2H), 7.68-7.72 (m, 3H), 7.85 (br. t, *J* ≈ 1.8 Hz, 1H), 7.90 (dt, *J* = 7.5, 1.2 Hz, 1H), 9.97 (br. s,1H). ^{13}C NMR ($CDCl_3$) δ 39.4, 39.6, 111.7, 116.0, 118.9, 121.8, 123.4, 123.7, 129.6, 130.7, 138.8, 139.4, 145.4, 152.0,188.3. EI-MS

m/z 344 ([M]$^+$, 100), 265 (45), 174 (38). EI-HRMS *m/z* calcd for [M]$^+$ $C_{18}H_{20}N_2O_3S$ 344.1195, found 344.1187.

Triarylpyrazoline **5.32**

A mixture of chalcone **5.31** (488 mg, 1.42 mmol), arylhydrazine 5.2 (399 mg, 1.4 equiv.), and PPTS (496 mg, 1.4 equiv.) in methanol (4 mL) was stirred under argon in a sealed vessel at 90°C for 3 hours. The mixture was partitioned between water (100 mL) and DCM (40 mL). The organic layer was collected, and the aqueous layer was extracted with DCM (2 x 20 mL). The combined organic layers were dried with MgSO4 and concentrated to a foamy glassy solid. This material was dissolved in a small volume of DCM and scratched with a Pasteur pipette until crystals appeared. A seed crystal was collected, and the remaining material was concentrated to dryness, dissolved in acetone, filtered through a tight cotton plug to remove a small amount of insoluble material, and diluted with MTBE to the point of permanent turbidity (required 30 mL). The mixture was diluted dropwise with acetone until clear and then seeded with the initial crystalline material. After 4 hours of slow stirring, the product was collected by filtration, washed with MTBE, and dried under high vacuum to give a colorless crystalline powder. Yield 510 mg (967 µmol, 68%). Mp 183-184°C. ^{1}H NMR (Acetone-d_6) δ 2.49 (d, *J* = 5.3 Hz, 3H), 2.89 (s, 6H), 3.04 (s, 3H), 3.17 (dd, *J* = 17.5, 5.7 Hz, 1H), 3.97 (dd, *J* = 17.5, 12.1 Hz, 1H), 5.49 (dd, *J* = 12.1, 6.7 Hz, 1H), 5.99 (q, *J* = 5.3 Hz, 1H), 6.71 (ad, *J* = 8.8 Hz, 2H), 7.15 (ad, *J* = 8.8 Hz, 2H), 7.19 (ad, *J* = 8.9 Hz, 2H), 7.38-7.41 (m, 1H), 7.42-7.46 (m, 1H), 7.56-7.61 (m, 3H), 7.84 (br. t, *J* ≈ 1.7 Hz, 1H), 8.69 (br. s, 1H). EI-MS *m/z* 527 ([M]$^+$, 95), 223 (25), 147 (100), 146 (40). EI-HRMS *m/z* calcd for [M]$^+$ $C_{25}H_{29}N_5O_4S_2$ 527.1661, found 527.1664.

Sulfonyl fluoride **5.33**

A mixture of triarylpyrazoline **5.32** (254 mg, 481 µmol), triethylamine (201 µL, 3 equiv.), and ethenesulfonyl fluoride (241 µL, 6 equiv.) in dry DCM (5 mL) was stirred under argon for 5 hours. The mixture was diluted with toluene (2 mL), concentrated to dryness under a stream of nitrogen, and partitioned between DCM (50 mL) and water + 1 M NaH_2PO_4 (50 mL + 10 mL). The organic layer was collected, and the aqueous layer was extracted with DCM (25 mL). The combined organic layers were dried with MgSO4, filtered, and concentrated to dryness. The residue was dissolved in DCM and filtered through a 3 cm plug of silica gel in a Pasteur pipette. The silica plug was washed with 10:1 DCM-MTBE (5 mL), and the combined filtrate and washings were concentrated to dryness. The residue was crystallized from boiling acetone-MTBE under slow stirring to give the product as an ivory-colored crystalline powder. Yield 269 mg (360 µmol, 75%). Mp 182-183°C ^{1}H NMR ($CDCl_3$) δ 2.80 (s, 3H), 2.94 (s, 6H), 3.00 (s, 3H), 3.20 (dd, *J* = 17.4, 6.0 Hz, 1H) 3.47-3.50 (m, 2H), 3.68-3.74 (m, 4H), 3.86 (dd, *J* = 17.4, 12.2 Hz, 1H), 4.27 (br. t, *J* ≈ 7 Hz, 2H), 5.32 (dd, *J* = 12.2, 6.0 Hz, 1H), 6.68 (ad, *J* = 8.8 Hz, 2H), 7.11 (ad, *J* = 8.8 Hz, 2H), 7.17 (ad, *J* = 9.0 Hz, 2H), 7.36 (ddd, *J* = 8.0, 2.1, 0.9 Hz, 1H), 7.50 (t, *J* = 7.9 Hz, 1H), 7.58 (ad, *J* = 9.1 Hz, 2H), 7.70-7.72 (m, 1H), 7.76 (br. t, *J* ≈ 1.8 Hz, 1H). ^{19}F NMR ($CDCl_3$) δ 56.3 (t, *J* = 4.8 Hz, 1F) 57.3 (t, *J* = 4.3 Hz, 1F).

Reference triarylpyrazoline **5.29**

A mixture of sulfonyl fluoride **5.33** (101 mg, 135 µmol), 1M aqueous DABCO (1.08 mL, 8 equiv), 1 M aqueous DABCO saturated with CO_2 (540 µL), water (540 µL), and THF (1.44 mL) was stirred overnight and then concentrated to dryness. Excess DABCO was removed by sublimation under high vacuum, and the residue was taken up in methanol (2 mL). A solution of K_2CO_3 (47 mg, 2.5 equiv) in 4:1 methanol-water (3 mL) was added, and the resulting precipitate was collected by filtration and dried. This material (51 mg), which was expected to be the potassium salt of the desired product, was

not pure by 1H NMR, so the filtrate was concentrated to dryness, taken up in water, and separated by RP-HPLC with a gradient of acetonitrile in 0.5% aqueous NH_4HCO_3 to obtain the product ammonium salt as a pale yellow glassy solid. Yield 14 mg (13%). ^{1}H NMR (CD_3OD) δ 2.72 (s, 3H), 2.90 (s, 6H), 2.98-3.04 (m, 4H), 3.04 (s, 3H), 3.18 (dd, *J* = 17.6, 5.8 Hz, 1H), 3.33-3.45 (m, 2H), 3.94 (dd, *J* = 17.6, 12.1 Hz, 1H), 4.12-4.16 (m, 2H), 5.43 (dd, *J* = 12.1, 5.8 Hz, 1H), 6.79 (ad, *J* = 8.7 Hz, 2H), 7.14 (ad, *J* = 8.8 Hz, 2H), 7.20 (ad, *J* = 9.0 Hz, 2H), 7.45-7.47 (m, 1H), 7.49-7.53 (m, 1H), 7.57 (ad, *J* = 9.0 Hz, 2H), 7.79-7.80 (m, 1H), 7.84 (br. dt, *J* = 7.6, 1.3 Hz, 1H). ESI-HRMS *m/z* calcd for $[M]^{2-}$ $C_{29}H_{35}N_5O_{10}S_4$ 370.5639, found 370.5632.

Chalcone **5.34**

A solution of aldehyde **5.24** (975 mg, 2.27 mmol), acetophenone **5.30** (484 mg, 1 equiv.) and pyrrolidine (95 µL, 0.5 equiv.) in ethanol (6 mL) was stirred for 25 hours at 45°C, producing a red, oily biphasic mixture. A small aliquot (~50 µL) of the lower phase was removed, concentrated, and separated by column chromatography in a Pasteur pipette (2:2:1 hexanes-DCM-MTBE). The presumed chalcone product (bright orange band) was crystallized from MTBE-hexane. The bulk reaction mixture was diluted with 6 mL MTBE, stirred until homogeneous, and seeded with the crystalline material. The resulting crystalline slurry was stirred for 4 days at 30°C, diluted into toluene (100 mL) and washed with a mixture of sat. aqueous Na_2CO_3 (15 mL), sat. aqueous $NaHCO_3$ (15 mL) and water (70 mL) followed by 1 M NaH_2PO_4 (25 mL). The organic layer was dried with Na2SO4 and concentrated, and the residue was separated by column chromatography (2:2:1 hexanes-DCM-MTBE). The resulting orange, glassy, slightly impure product was crystallized from MTBE to give chocolate-colored leaflets that turned yellow-orange after drying under vacuum. Yield 981 mg (1.57 mmol, 69%). ^{1}H NMR ($CDCl_3$) δ 1.47 (s, 3H), 1.49 (s, 3H), 1.86 (p, *J* = 7.1 Hz, 2H), 2.06 (s, 3H), 2.18 (s, 3H), 2.60 (s, 2H), 2.61 (t, *J* = 7.0 Hz, 2H), 2.85 (t, *J* = 7.2 Hz, 2H), 3.06 (s, 3H), 3.53 (d,

J = 6.5 Hz, 2H), 3.72 (d, *J* = 12.1 Hz, 2H), 3.82 (d, *J* = 12.1 Hz, 2H), 5.92 (t, *J* = 6.5 Hz, 1H), 6.88 (d, *J* = 8.7 Hz, 1H), 7.37 (d, *J* = 15.4 Hz, 1H), 7.51 (t, *J* = 7.9 Hz, 1H), 7.61 (dd, *J* = 8.7, 2.0 Hz, 1H), 7.72 (ddd, *J* = 8.1, 2.3, 0.9 Hz, 1H), 7.81 (d, *J* = 2.0 Hz, 1H), 7.83-7.85 (m, 1H), 7.97 (d, *J* = 15.4 Hz, 1H), 8.10 (br. s, 1H), 8.14 (br. t, *J* = 1.9 Hz, 1H). ^{13}C NMR ($CDCl_3$) δ 15.4, 17.8, 21.4, 26.1, 28.6, 32.8, 33.8, 38.3, 38.8, 39.5, 45.5, 65.5, 98.7, 110.0, 116.0, 117.7, 120.6, 123.5, 124.1, 124.8, 129.8, 132.1, 137.3, 138.2, 139.9, 146.8, 151.9. EI-MS *m/z* 624 ($[M]^+$, 45), 198 (10), 121 (12), 89 (100), 73 (45), 61 (37). EI-HRMS m/z calcd for $[M]^+$ $C_{29}H_{40}N_2O_5S_4$ 624.1820, found 624.1833.

Triarylpyrazoline **5.35**

A mixture of chalcone **5.34** (343 mg, 549 µmol) and PPTS (276 mg, 2 equiv.) in methanol (5 mL) was boiled for 15 min, then concentrated to an oily residue under a stream of argon. Arylhydrazine **5.2** (144 mg, 1.3 equiv.) and methanol (3 mL) were added, and the mixture was stirred under argon in a sealed vessel at 90°C for 2 hours. The mixture was concentrated to dryness, and the residue was taken up in acetone (5 mL) + 2,2-dimethoxypropane (3 mL). The mixture was boiled for 15 min, allowed to cool, and partitioned between water (100 mL) and DCM (50 mL). The organic layer was collected, and the aqueous layer was extracted with DCM (20 mL). The combined organic layers were dried with Na_2SO_4 and concentrated, and the residue was separated by column chromatography (DCM-MTBE) to give the product as a pale yellow glassy solid. Yield 282 mg (349 µmol, 64%). ^{1}H NMR ($CDCl_3$) δ 1.440 (s, 3H), 1.444 (s, 3H), 1.69 (p, *J* = 7.1 Hz, 2H), 2.00 (s, 3H), 2.14 (s, 3H), 2.44-2.55 (m, 2H), 2.59 (s, 2H), 2.60 (d, *J* = 5.4 Hz, 3H), 2.73 (t, *J* = 7.1 Hz, 2H), 3.05 (s, 3H), 3.15 (dd, *J* = 17.3, 5.9 Hz, 1H), 3.34-3.43 (m, 2H), 3.70 (d, *J* = 12.0 Hz, 2H), 3.79 (d, *J* ≈ 12 Hz, overlaps with subsequent signal, 2H), 3.81 (dd, *J* = 17.3, 12.2 Hz, 1H), 4.45 (q, *J* = 5.5 Hz, 1H), 5.23 (dd, *J* = 12.2, 6.0 Hz, 1H), 5.37 (t, *J* = 6.6 Hz, 1H), 6.79 (d, *J* = 8.6 Hz, 1H), 7.06 (br. s, 1H), 7.07 (dd, *J* = 8.5, 2.2 Hz, 1H), 7.11 (ad, *J* = 9.0 Hz, 2H), 7.24 (d, *J* = 2.2 Hz, 1H), 7.29 (ddd, *J* = 8.0, 2.2,

1.0 Hz, 1H), 7.38 (t, *J* = 7.9 Hz, 1H), dt (*J* = 7.9, 1.2 Hz, 1H), 7.61-7.74 (m, 3H). ^{13}C NMR ($CDCl_3$) δ 15.3, 17.8, 21.7, 25.8, 28.4, 29.4, 32.6, 33.4, 38.3, 38.7, 39.5, 43.5, 45.9, 63.1, 65.4, 65.5, 98.6, 110.8, 112.8, 117.8, 118.0, 121.2, 122.9, 127.0, 127.7, 128.7, 128.9, 130.0, 133.3, 133.7, 137.3, 147.1, 148.5, 149.4.

Sulfonyl fluoride **5.36**

A solution of triarylpyrazoline 5.35 (169 mg, 209 µmol), triethylamine (87 µL, 3 equiv.), and ethenesulfonyl fluoride (105 µL, 6 equiv.) in dry DCM (2 mL) was stirred under argon for 3 hours, then diluted with toluene (2 mL) and concentrated to dryness. The residue was separated by column chromatography (1:1 DCM-hexanes plus increasing MTBE) and the resulting glassy product was crystallized from DCM-MTBE to give an ivory-colored crystalline powder. Yield 125 mg (122 µmol, 58%). ^{1}H NMR ($CDCl_3$) δ 1.44 (br. s, 6H), 1.72 (p, *J* = 7.1 Hz, 2H), 2.01 (s, 3H), 2.15 (s, 3H), 2.46-2.57 (m, 2H), 2.59 (s, 2H), 2.75 (t, *J* = 7.1 Hz, 2H), 2.81 (s, 3H), 3.01 (s, 3H), 3.19 (dd, *J* = 17.4, 6.0 Hz 1H), 3.40 (d, *J* = 6.6 Hz, 2H), 3.48-3.52 (m, 2H), 3.70 (d, *J* = 11.8 Hz, 2H), 3.71-3.76 (m, 4H), 3.80 (d, *J* = 11.8 Hz, 2H), 3.86 (dd, *J* = 17.4, 12.2 Hz, 1H), 4.28 (br. t, *J* ≈ 7 Hz, 2H), 5.27 (dd, *J* = 12.2, 6.0 Hz, 1H), 5.41(t, *J* = 6.6 Hz, 1H), 6.81 (d, *J* = 8.6 Hz, 1H) 7.09 (dd, *J* = 8.5, 2.2 Hz, 1H), 7.16 (ad, *J* = 9.0 Hz, 2H), 7.27 (d, *J* = 2.2 Hz, 1H), 7.37 (ddd, *J* = 8.0, 2.1, 1.0 Hz, 1H), 7.51 (t, *J* = 7.9 Hz, 1H), 7.60 (ad, *J* = 9.1 Hz, 2H), 7.72 (dt, *J* ≈ 8.0, 1.2 Hz, 1H), 7.76 (t, *J* = 1.8 Hz, 1H). ^{19}F NMR ($CDCl_3$) δ 56.3 (t, *J* = 4.9 Hz, 1F), 57.3 (t, *J* = 4.3 Hz, 1F.

Probe **5.28**

Sulfonyl fluoride **5.36** (60 mg, 58 µmol) was stirred in a mixture of methanol (1 mL), THF (0.5 mL), and 1 M aqueous HCl (116 µL, 2 equiv.). The resulting suspension was heated briefly to boiling until the starting material completely dissolved and then concentrated to ~0.3 mL under a stream of argon. Methanol (0.5 mL), 1 M aqueous

DABCO (0.7 mL) and THF (0.3 mL) were added, and the mixture was stirred overnight and then concentrated to dryness. The product was isolated as the ammonium salt by RP-HPLC with a gradient of acetonitrile in 0.5% aqueous NH4HCO3 to give a pale yellow glassy solid after drying under high vacuum. Isolated yield 38 mg (37 μmol) separated from 83% of the total crude material, 77%. ^{1}H NMR ($CDCl_3$) δ 1.62 (p, *J* = 7.0 Hz, 2H), 1.93 (s, 3H), 2.09 (s, 3H), 2.39-2.52 (m, 2H), 2.66 (s, 2H), 2.72 (s, 3H), 2.73 (t, *J* = 7.0 Hz, 2H), 2.98-3.02 (m, 4H), 3.03 (s, 3H), 3.20 (dd, *J* = 17.6, 5.6 Hz, 1H), 3.21 (s, 2H), 3.37-3.41 (m, 2H), 3.59 (m, 4H), 3.93 (dd, *J* = 17.6, 12.1 Hz, 1H), 4.12-4.16 (m, 2H), 5.41 (dd, *J* = 12.1, 5.6 Hz, 1H), 6.72 (d, *J* = 8.6 Hz, 1H), 7.11 (dd, *J* = 8.5, 2.2 Hz, 1H), 7.21 (ad, *J* = 9.0 Hz, 2H), 7.24 (d, *J* = 2.2 Hz, 1H), 7.44-7.47 (m, 1H), 7.50 (t, *J* ≈ 7.7 Hz, 1H), 7.59 (ad, *J* = 9.1 Hz, 2H), 7.80 (br. t, *J* = 1.7 Hz, 1H), 7.85 (dt, *J* = 7.6, 1.4 Hz, 1H). ^{13}C NMR ($CDCl_3$) δ 13.8, 16.3, 28.0, 32.0, 32.3, 24.5, 36.3, 36.6, 42.9, 44.7, 45.7, 46.3, 49.4, 50.0, 63.0, 63.3, 110.3, 112.6, 117.4, 125.2, 125.4, 126.1, 127.4, 128.6, 128.7, 129.0, 129.5, 133.3, 133.9, 139.8, 147.4, 149.2, 149.5. ESI-HRMS m/z calcd for $[M]^{2-}$ $C_{37}H_{51}N_5O_{12}S_7$ 490.5795, found 490.5787.

5.9. References

(1) Morgan, M. T.; Bagchi, P.; Fahrni, C. J. *J. Am. Chem. Soc.* **2011**, *133*, 15906.

(2) Chaudhry, A. F.; Mandal, S.; Hardcastle, K. I.; Fahrni, C. J. *Chem. Sci.* **2011**, *2*, 1016.

(3) Morgan, M. T.; Bagchi, P.; Fahrni, C. J. *Dalton Trans.* **2013**, *42*, 3240.

(4) Davidson, R. S.; Pratt, J. E. *Photochem. Photobiol.* **1984**, *40*, 23.

(5) Rivett, D. E.; Rosevear, J.; Wilshire, J. F. K. *Aust. J. Chem.* **1979**, *32*, 1601.

(6) Hansch, C.; Leo, A.; Taft, R. W. *Chem. Rev.* **1991**, *91*, 165.

(7) Krutak, J. J.; Burpitt, R. D.; Moore, W. H.; Hyatt, J. A. *J. Org. Chem.* **1979**, *44*, 3847.

(8) Verma, M.; Chaudhry, A. F.; Fahrni, C. J. *Org. Biomol. Chem.* **2009**, *7*, 1536.

(9) Maus, M.; Rurack, K. *New J. Chem.* **2000**, *24*, 677.

(10) Chaudhry, A. F.; Verma, M.; Morgan, M. T.; Henary, M. M.; Siegel, N.; Hales, J. M.; Perry, J. W.; Fahrni, C. J. *J. Am. Chem. Soc.* **2010**, *132*, 737.

(11) DeOrazio, R. J.; Maeng, J.-H.; Manning, D. D.; Sherer, B. A.; Scott, I. L.; Nikam, S. S. *Synth. Commun.* **2011**, *41*, 3551.

(12) Fahrni, C. J.; Yang, L. C.; VanDerveer, D. G. *J. Am. Chem. Soc.* **2003**, *125*, 3799.

(13) Baidya, M.; Kobayashi, S.; Brotzel, F.; Schmidhammer, U.; Riedle, E.; Mayr, H. *Angew. Chem., Int. Ed. Engl.* **2007**, *46*, 6176.

(14) Cody, J.; Mandal, S.; Yang, L.; Fahrni, C. J. *J. Am. Chem. Soc.* **2008**, *130*, 13023.

(15) Ambundo, E. A.; Deydier, M. V.; Grall, A. J.; Aguera-Vega, N.; Dressel, L. T.; Cooper, T. H.; Heeg, M. J.; Ochrymowycz, L. A.; Rorabacher, D. B. *Inorg. Chem.* **1999**, *38*, 4233.

(16) Bernardo, M. M.; Schroeder, R. R.; Rorabacher, D. B. *Inorg. Chem.* **1991**, *30*, 1241.

(17) Dodani, S. C.; Domaille, D. W.; Nam, C. I.; Miller, E. W.; Finney, L. A.; Vogt, S.; Chang, C. J. *Proc. Natl. Acad. Sci. U. S. A.* **2011**, *108*, 5980.

(18) Gottlieb, H. E.; Kotlyar, V.; Nudelman, A. *J. Org. Chem.* **1997**, *62*, 7512.

(19) Lespagnol, A.; Bar, D.; Erb-Debruyne, M.; Delhomenie-Sauvage, M. *Bull. Soc. Chim. Fr.* **1960**, 490.

CHAPTER 6

SULFONATED THIOETHER-BASED LIGANDS AND THEIR CRYSTALLINE COPPER(I)-COMPLEXES AS COLORLESS, WATER-SOLUBLE, AND AIR-STABLE AFFINITY STANDARDS

6.1. Introduction

6.1.1. The need for copper(I)-affinity standards

For an accurate understanding of the molecular mechanisms of copper trafficking in living organisms, knowledge of the copper binding affinities of the ligands involved is essential. Accurate binding affinity determination for Cu(I)-transport proteins, however, is not straightforward, and gross inconsistencies abound in the literature. For example, the values reported for Cu(I)-binding affinity of the metallochaperone Atox1 span a range of more than two trillion-fold from 2.5×10^5 to 5.6×10^{17} M^{-1}.[1,2]

Difficulties in binding affinity determination for biologically relevant Cu(I)-ligands stem from several different sources. As mentioned in Chapter 1, aqueous Cu^+ is highly reactive toward molecular oxygen. It is also prone to disproportionation at concentrations above about 1 μM and to precipitation as Cu_2O at neutral pH,[3] all of which may lead to losses during titrations with copper(I). Furthermore, while the most reliable reported binding affinities of Cu(I)-proteins are generally above 10^{12} M^{-1}, metal-protein binding affinities much above 10^6 M^{-1} are difficult to determine by direct titration because the protein and cation will be almost completely associated even at the lowest concentrations suitable for monitoring by non-disruptive techniques.[4]

Metal-binding affinities which are too high to measure by direct titration can instead be determined by competition experiments, where the metal ion is allowed to equilibrate between the ligand under study and another ligand of known binding affinity. In the case of Cu(I), use of a competing ligand can also protect against aerial oxidation or disproportionation, provided that the ligand selected preferentially stabilizes Cu(I) over Cu(II). There are two additional requirements, however, for determining metal binding affinities through ligand competition methods: The affinity standard ligand and test ligand must not form heteroleptic ternary complexes with the metal cation to a significant extent under the conditions of measurement, and the binding affinity of the standard must be accurately known.

6.1.2. Ligands previously employed as copper(I)-affinity standards

For Cu(I), the above conditions have been surprisingly difficult to meet with previously available ligands. Strong monodentate ligands such as cyanide[5] or thiourea[6] are sometimes employed as Cu(I) affinity standards, but this is likely to result in heteroleptic complex formation during competition experiments, as Cu(I) typically exhibits a coordination number of up to four.[7] Dithiothreitol (DTT), a 1,4-dithiol typically employed as a reducing agent for protein disulfides, has also been utilized as a competitive ligand against Cu(I) –binding proteins, but is far from ideal due to its high reactivity with oxygen and variable coordination stoichiometry.[8]

The water-soluble, ortho-substituted bipyridine-type ligands bicinchoninic acid (BCA) and bathocuproine disulfonic acid (BCS) (Figure 6.1) yield colored, air-stable 2:1 complexes with Cu(I) and are frequently used as affinity standards,[4] but their binding affinities have been controversial in the literature, with values of the 2:1 ligand metal complex stability constant β_2 ranging from log β_2 = 11.4 to 17.3 for BCA[8,9] and 19.5 to 22.5 for BCS.[9,10] Furthermore, these bidentate chelators, though more sterically

demanding than small monodentate ligands such as cyanide and thiourea, are presumably still prone to heteroleptic complex formation, particularly with other ligands of low denticity. As previously noted,[8] this is a likely source of error in an earlier attempt to determine the Cu(I)-complex stability constant of BCS by competition with cyanide.[9]

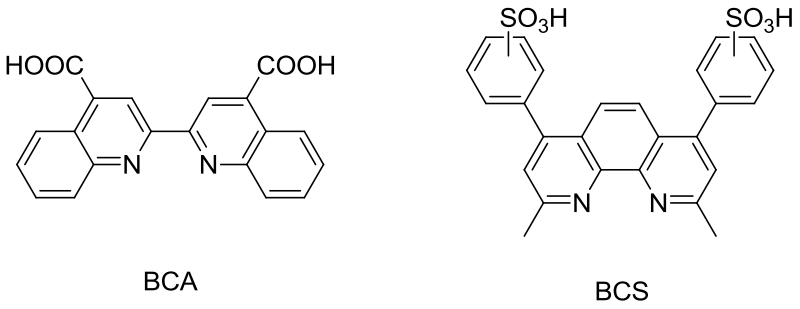

Figure 6.1: Structures of the Cu(I)-selective ligands BCA and BCS

6.1.3. The promising properties of tetradentate thioether-based ligands

Tetradentate sulfur-rich ligands including thiocrown macrocycles and tripodal thioether-amines have been extensively investigated as Cu(I)-ligands by Rorabacher and coworkers, and often form air-stable 1:1 complexes with Cu(I). By saturating the Cu(I) coordination sphere, these chelators should provide greater resistance to heteroleptic complex formation during Cu(I)-competition experiments than ligands of lower denticity. Additionally, these chelators often exhibit a low to moderate Cu(II)-binding affinity and electrochemically reversible interconversion of the Cu(II) and Cu(I) complexes, allowing the relatively high Cu(I)-binding affinity to be calculated from the directly measurable Cu(II) affinity and the ligand-bound Cu(II)/Cu(I) redox potential using a thermodynamic cycle method[11] as previously described for CTAP-2 (Chapter 3, Section 3.7.3). Furthermore, the Cu(I)-complexes of aliphatic polythioethers are typically colorless with the lowest-energy UV transitions occurring at wavelengths below 300 nm,[12] thus

providing the potential for spectrophotometric or fluorimetric monitoring of the Cu(I)-occupancy of the ligand under study rather than the affinity standard ligand in competition titrations. This is potentially a valuable asset for competition experiments with copper proteins: If the affinity standard ligand can be used in large excess over the protein, then it would yield a buffer-like effect rendering the concentration and initial copper occupancy of the protein, which may be imprecisely known, inconsequential to the results of the titration. The one major impediment to the use of previously reported thioether-rich tetradentate Cu(I)-ligands in direct competition experiments with copper proteins is their inherent lipophilicity, which not only results in limited aqueous solubility but might also lead to interfering hydrophobic interactions with the protein.

6.2. Sulfonated NS_3 Tripods

6.2.1. Ligand design

Previous studies by Rorabacher *et al* indicated that tripodal amine ligands have somewhat higher Cu(I)-association constants than linear or macrocyclic ligands with similar donor atom sets and also provide a greater stabilization of the Cu(I) oxidation state over Cu(II).[13,14] These trends are exemplified by the respective Cu(I)-association constants of log $K^{Cu(I)}$ = 13.6, 13.1, and 15.8 and the respective ligand-bound Cu(II)/Cu(I) reduction potentials of 0.38, 0.41, and 0.69 V vs. SHE for the chelators [14]aneNS_3-a, [14]aneNS_3-b, and TMMEA shown in Figure 6.2.[13,14] Replacing the NS_3-donor set of the macrocycles with S_4 improves the ligand-bound Cu(II)/Cu(I) reduction potential but not the Cu(I) affinity, which is instead somewhat decreased to log $K^{Cu(I)}$ = 12.1 and 12.2, respectively for [14]aneS_4-*a* and [14]aneS_4-*b*, the respective all-sulfur analogs of [14]aneNS_3-*a* and [14]aneNS_3-*b*.[14]

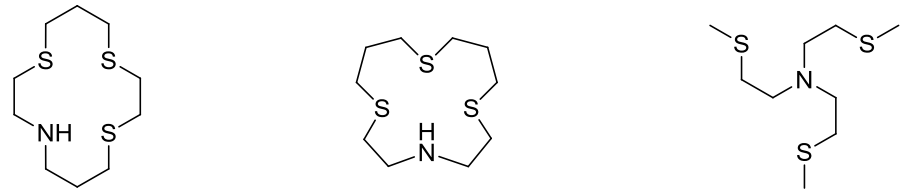

Figure 6.2: Structures of Cu(I)-ligands [14]aneNS$_3$-*a*, [14]aneNS$_3$-*b*, and TMMEA

Based on the higher affinity provided by the tripodal topology and a relatively recent report of subfemtomolar Cu(I)-binding affinity for Atox1 and related Cu(I)-transport proteins,[4] we chose TMMEA as a starting point for the design of water-soluble thioether-based Cu(I)-ligands. Replacing the methyl groups of TMMEA with ionic 3-sulfopropyl moieties yields design **6.1**, shown in Figure 6.3 as its sodium salt. Given the substantial distortion from the preferred tetrahedral coordination geometry of Cu(I) apparent in the x-ray crystal structure of the TMMEA-$CuClO_4$ complex,[13] we also devised ligand **6.2**, in which the N-S bridges are lengthened from two carbons to three, to determine whether this modification could increase the binding affinity by better accommodating the preferred tetrahedral ligand geometry of Cu(I).

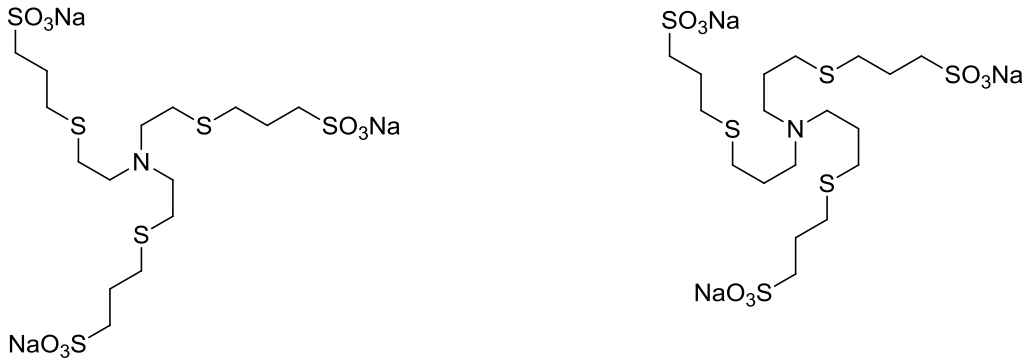

6.1 **6.2**

Figure 6.3: Structures of the sulfonated NS_3 tripodal ligands **6.1** and **6.2**

6.2.2. Synthesis and properties of the ligands and their Cu(I)-complexes

Both **6.1** and **6.2** were prepared from the corresponding tris(ω-chloroalkyl)amines by reaction with commercially available sodium 3-mercaptopropanesulfonate in the presence of sodium hydroxide. The desired products were separated from the byproduct sodium chloride by recrystallization from methanol-rich mixtures, as the solubility of sodium chloride exhibits a negative temperature dependence in methanol.[15] After drying under vacuum, both ligands were obtained as fine white powders that gave NMR spectra and elemental analyses consistent with the intended structures in anhydrous form. Ligands **6.1** and **6.2** were each reacted with a stoichiometric quantity of tetrakis(acetonitrile)copper(I) hexafluorophosphate to produce the respective copper complexes **6.3** and **6.4**, which were obtained as colorless crystalline powders from alcohol-water mixtures. These were dried under high vacuum to yield fine white powders, which were determined to be the 1:1 adducts with sodium hexafluorophosphate as shown in Scheme 6.1. The hexafluorophosphate stoichiometry was initially determined by a combination of ^{1}H and ^{19}F NMR using 2,2,2-trifluoroethanol as an internal standard to link the proton and fluorine NMR integrals, then confirmed by elemental analysis, which yielded results consistent with the proposed structures in anhydrous form. Recrystallization of complex **6.4** from ethanol-water had no effect on the hexafluorophosphate ^{19}F integral value.

Ligands **6.1** and **6.2** as well as their respective copper(I)-complexes **6.3** and **6.4** dissolve readily in water to concentrations greater than 100 mM. Remarkably, the Cu(I) complexes are air-stable in aqueous solution, showing no sign of oxidation to blue Cu(II) after several days. The formation of water-soluble, air-stable Cu(I)-complexes should be a valuable asset for the use of **6.1** and **6.2** as affinity standards in ligand competition experiments, because the fractional Cu(I)-occupancy of the ligand, and hence the

effective buffered concentration of Cu^{+}, can be varied using an aqueous stock solution of the pre-formed copper complex, thus eliminating the need for Cu(I)-stabilizing solvents such as acetonitrile which may participate in undesired additional coordination equilibria or promote denaturation of proteins. Additionally, the air-stability of the Cu(I)-complexes should eliminate the need for rigorous deoxygenation or the presence of reducing agents provided that the ligand under study is also air-stable.

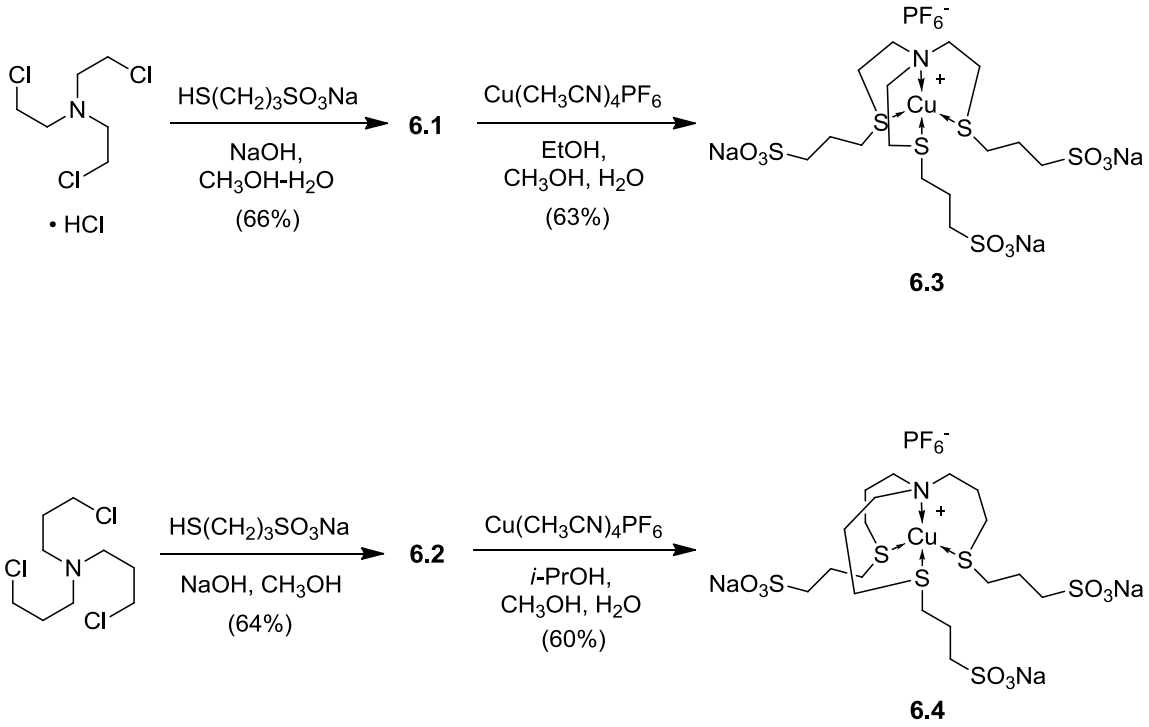

Scheme 6.1: Synthesis of ligands **6.1**-**6.2** and Cu(I) complexes **6.3**-**6.4**.

6.2.3. X-ray crystal structures of the Cu(I)-complexes

Initial attempts to obtain crystals of **6.3** or **6.4** suitable for x-ray diffraction analysis were unsuccessful, yielding only fibrous acicular crystals by thermal recrystallization from dilute solutions and fine powders by vapor diffusion or solvent evaporation. Surprisingly, preparation of a second batch of complex **6.4** yielded a small

amount of clear tablet-shaped granules in addition to the previously obtained fibrous crystals when recrystallization was conducted in the presence of a larger fraction of water than before (approximately 4:1 ethanol-water by volume). The granules yielded ^{1}H and ^{19}F NMR spectra identical to those of the fibrous form, and slow stirring overnight converted all of the fibrous material to the granular form. The granules slowly decomposed to a powder under dry argon or vacuum but were found to be completely stable in ambient air, remaining clear and colorless after drying under air flow overnight. Careful thermal recrystallization of the granular form from ethanol-water yielded a sample suitable for x-ray diffraction. Attempts to crystallize complex **6.3** under the conditions that yielded the granular form of **6.4** were unsuccessful, but crystallization in the presence of a large excess of sodium perchlorate in 2:1 ethanol-water yielded clear prisms suitable for x-ray diffraction.

Data collection and structural refinement for the crystals obtained from both **6.3** and **6.4** were carried out by Dr. John Bacsa of Emory University. The crystal structure of **6.4** contains the expected 1:1 Cu(I)-ligand complex with one equivalent of hexafluorophosphate per copper center. The asymmetric unit (Figure 6.4) contains two enantiomeric forms of the copper complex stacked in opposing directions with both sets of sulfonate groups bridged by sodium cations and water molecules, giving an overall composition of $Na_6(CuL)_2(PF_6)_2 \bullet 15\ H_2O$ where CuL represents the dianionic trisulfonated ligand-copper complex.

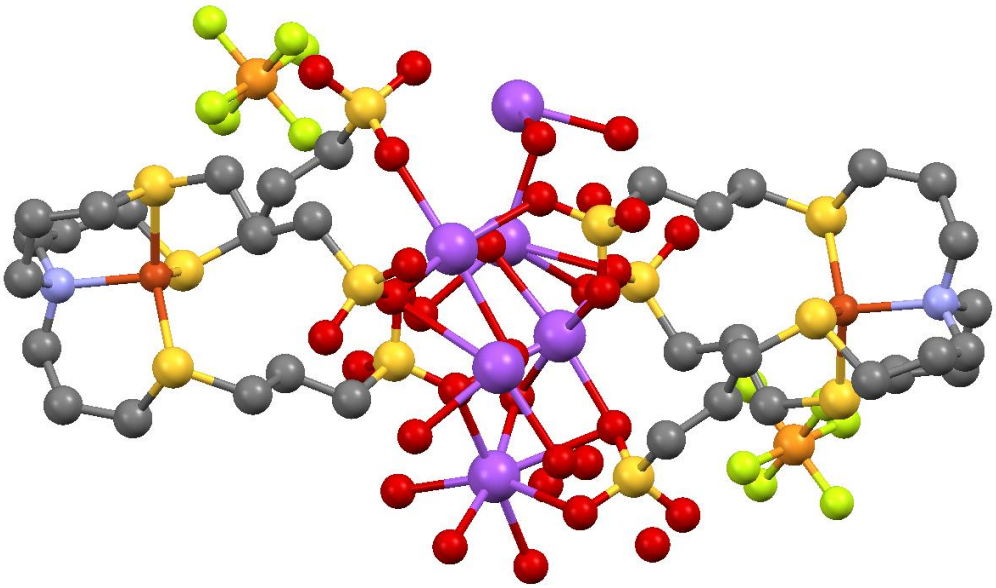

Figure 6.4: Ball-and-stick representation of the asymmetric unit of complex **6.4** (hydrogen atoms omitted for clarity)
Colored spheres represent atoms as follows: Gray, carbon; red, oxygen; blue, nitrogen; yellow, sulfur; purple, sodium; brown, copper; orange, phosphorus; yellow-green, fluorine. Image generated using the software Mercury 3.1[16]

The crystals obtained from complex **6.3** in the presence of perchlorate contain the expected 1:1 ligand-Cu(I) complex structure and form a sodium-bridged dimer similar to that observed for **6.4** but with the incorporation of three partly disordered perchlorate ions per two copper centers and no hexafluorophosphate, corresponding to a formula of $Na_7(CuL)_2(ClO_4)_3 \bullet 4\ H_2O$. This compound is hereafter referred to as **6.3**-ClO_4. For structural comparison, the dianionic copper-ligand complex structures for both **6.3**-ClO_4 and **6.4** are shown in ORTEP representation in Figure 6.5, and bond lengths and angles about the respective Cu(I) centers are given in Table 6.1. Atom numbers in the table correspond to those in the ORTEP figures.

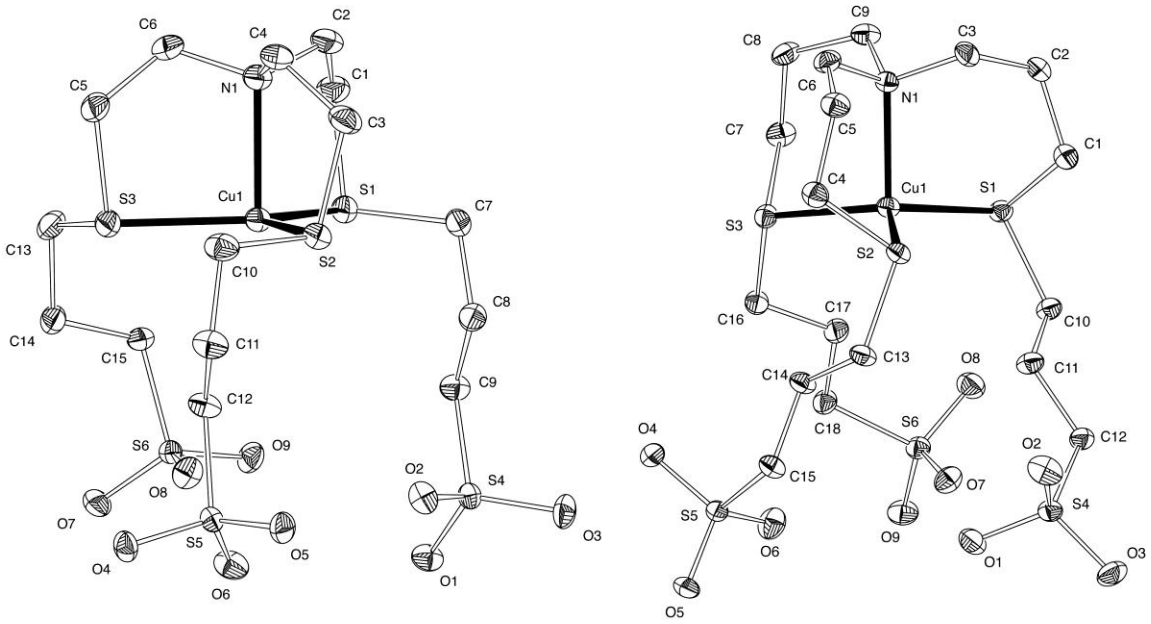

Figure 6.5: ORTEP representations of the dianionic Cu(I)-complex unit from the crystal structures of complexes **6.3**-ClO_4 (left) and **6.4** (right). Images generated by Dr. Christoph Fahrni using the software PLATON[17]

Table 6.1: Selected bond lengths and angles for Cu(I) complexes **6.3**-ClO_4 and **6.4**

	6.3-ClO_4	**6.4**
Bond lengths (angstroms)		
Cu(1)-S(1)	2.2486(7)	2.2868(6)
Cu(1)-S(2)	2.2886(7)	2.2870(6)
Cu(1)-S(3)	2.2680(7)	2.2889(6)
Cu(1)-N(1)	2.1610(17)	2.1261(17)
Bond angles (degrees)		
S(1)-Cu(1)-N(1)	91.91(6)	98.78(5)
S(2)-Cu(1)-N(1)	89.88(5)	97.86(5)
S(3)-Cu(1)-N(1)	91.32(5)	98.51(5)
S(1)-Cu(1)-S(2)	121.41(2)	117.60(2)
S(1)-Cu(1)-S(3)	125.49(2)	118.36(2)
S(2)-Cu(1)-S(3)	112.99(3)	117.77(2)
Sum of S-Cu-S	359.89	353.73

As is clearly visible in the ORTEP, the Cu(I)-center in **6.3**-ClO_4 is highly distorted from the preferred tetrahedral ligand arrangement of Cu(I), assuming instead a trigonal pyramidal structure with a near-planar CuS_3 unit. The S-Cu-N bond angles of this complex are all close to 90°, and the sum of the three S-Cu-S angles is 359.9°, nearly equal to the 360° sum expected for a perfectly planar arrangement. The Cu(I)-center in **6.4** is somewhat closer to tetrahedral, with S-Cu-N angles of 97.9-98.8° and an S-Cu-S bond angle sum of 353.7° versus 328.4° for a perfect tetrahedral arrangement. Neither the sulfonate groups nor the associated water molecules participate in Cu(I)-coordination in either complex; even though the Cu(I)-center of **6.3**-ClO_4 appears to present an open site for trigonal bipyramidal coondination, the nearest oxygen atom (O8) is over 4.2 Å away. Overall, the Cu(I)-coordination mode displayed by ligand **6.1** in **6.3**-ClO_4 is similar to that of TMMEA, which gave N-Cu-S angles of 91.2 ±0.6° and S-Cu-S angles 120 ± 2°.[13] As expected, ligand **6.2** provides a coordination geometry closer to tetrahedral in its Cu(I)-complex **6.4**, although the structure is still clearly distorted toward trigonal pyramidal coordination.

6.2.4. Coordination properties of ligands 6.1 and 6.2 in aqueous solution

All experiments described in Section 6.2.4 were conducted by Pritha Bagchi

The acid dissociation constants (pKa values) for the N-protonated forms of **6.1** and **6.2** were determined by direct potentiometric titration as 7.00 and 8.98, respectively at 0.1 M ionic strength. These concentration-based pKa values can be converted to mixed mode pKa values, in which H^+ is expressed in terms of activity, by adding a correction factor of 0.11.[18] Interestingly, the resulting value of 7.11 for ligand **6.1** is substantially lower than the mixed-mode pKa of 8.36 reported for the analogous ligand TMMEA.[13]

Like TMMEA,[13] ligand **6.1** forms a colored Cu(II) complex with a strong S-Cu(II) charge-transfer absorption at 374 nm. Direct spectrophotometric titration of **6.1**

with Cu^{2+} at pH 5 gave a complex stability constant of log $K_{Cu(II)}$ = 6.42 ± 0.02. Cyclic voltammetry revealed a quasi-reversible one-electron process for **6.1**-Cu(II) with a formal potential of 0.716 V vs. SHE, yielding a calculated Cu(I)-complex stability constant of log $K_{Cu(I)}$ = 16.33 by the thermodynamic cycle method.[11] Interestingly, this is actually slightly larger than reported for TMMEA (log $K_{Cu(I)}$ = 15.80)[13] despite the lower pKa of **6.1**.

Attempts to determine the Cu(I) affinity of **6.2** by similar methods were not successful, as this ligand gave no spectrophotometrically detectable interaction with Cu^{2+} at pH 5. While raising the pH would be expected to increase the apparent Cu(II) affinity by increasing the fraction of **6.2** present in its unprotonated form, a pH below about 5.3 is necessary for titrations with Cu(II) to prevent formation of hydroxo-Cu(II) species.[19] Consistent with a very low Cu(II) affinity, cyclic voltammetry of the pre-formed **6.2**-Cu(I)-complex **6.4** revealed only an irreversible process, suggesting dissociation of Cu(II) from the ligand upon oxidation of the Cu(I)-complex. The Cu(I)-affinity of ligand **6.2** was instead determined by competition titrations with BCA at pH 7, which in turn was calibrated against **6.1** at pH 5. Compared to **6.1**, the Cu(I)-complex stability constant of **6.2** was found to be over 1000-fold lower at log $K_{Cu(I)}$ = 13.08. This effect is probably due to a greater entropic penalty for conformational restriction of the longer N-S bridges of ligand **6.2** compared to **6.1**, which apparently overwhelms any enthalpic stabilization associated with the more favorable bond angles about the Cu(I)-center in the **6.2**-Cu(I) complex. At present, however, we have not attempted to dissect the Cu(I)-complex stability constants of these ligands into enthalpic and entropic terms.

In addition to the substantial difference in the actual Cu(I)-complex stability constant $K_{Cu(I)}$, the apparent Cu(I)-binding affinities of **6.1** and **6.2** at pH 7 diverge even further due to the higher pKa of **6.2**. This is explained as follows: For 1:1-binding ligands, the effective Cu(I)-binding affinity at a given pH is equal to the conditional complex stability constant $K'_{Cu(I)}$, which is defined similarly to the complex stability

constant $K_{Cu(I)}$ except that the free ligand concentration [L] is replaced with the total concentration of free and protonated ligand [L']. This is given by Equation 6.1, where [Cu(I)L] is the concentration of the ligand-Cu(I) complex and [Cu^+] is the effective concentration of free Cu^+.

$$K'_{Cu(I)L} = \frac{[Cu(I)L]}{[Cu^+][L']} \qquad (6.1)$$

Assuming any protonated forms of the ligand have negligible Cu(I)-affinity, the ratio $K'_{Cu(I)}/K_{Cu(I)}$ is equal to the fraction of the non(metal-bound) ligand present in un-protonated form, or [L]/[L'], which in turn is set by the pKa of the protonation site(s) and the pH of the medium. For a ligand with a single protonation site, the pH dependence of $K'_{Cu(I)}$ is given by Equation 6.2, where the pKa term is the mixed-mode value.

$$\frac{K'_{Cu(I)}}{K_{Cu(I)}} = \frac{[L]}{[L']} = \frac{1}{1 + 10^{pKa - pH}} \qquad (6.2)$$

Alternatively, the dependence of apparent binding affinity on pH can be expressed in logarithmic form as Equation 6.3.

$$\log K'_{Cu(I)} = \log K_{Cu(I)} - \log(1 + 10^{pKa-pH}) \qquad (6.3)$$

Note that when the ligand pKa exceeds the pH of the medium by more than about 1, the term $\log(1+ 10^{pKa - pH})$ can be approximated as pKa − pH, and the apparent Cu(I)-affinity can therefore be estimated as $\log K'_{Cu(I)} \approx \log K_{Cu(I)} + pH - pKa$. Therefore, the apparent Cu(I)-affinity at pH 7 of ligand **6.2**, which has a mixed-mode pKa of 9.09, will be lower than the Cu(I)-complex stability constant by approximately two orders of

magnitude. Based on Equation 6.3, the apparent Cu(I)-binding affinities at pH 7 of **6.1** and **6.2** are separated by nearly five orders of magnitude at log $K'_{Cu(I)}$ = 15.97 and 10.99 for **6.1** and **6.2**, respectively. Due to this very large difference in the apparent Cu(I) affinities at neutral pH, **6.1** and **6.2** alone cannot be used to provide a continuous range of buffered Cu(I) concentrations: Assuming that a metal occupancy of at least 5% and no more than 95% can be regarded as providing a useful buffering capacity, the buffering range of each ligand would be log[Cu^+] = log $K'_{Cu(I)}$ ± 1.3, requiring a difference in Cu(I)-affinity of no more than 2.6 log units for two 1:1-binding ligands to provide a continuous buffering range. Therefore, a third ligand of intermediate Cu(I)-affinity is required to bridge the gap between the Cu(I)-buffering ranges provided by **6.1** and **6.2** at neutral pH.

Although the relatively low apparent Cu(I)-affinity of **6.2** does not provide an overlapping buffering range with the higher affinity ligand **6.1**, it does offer an important potential benefit: the corresponding water-soluble and air-stable Cu(I)-complex **6.4** should be useful as a Cu(I)-supplying agent for quantitative metalation of higher affinity ligands such as copper proteins. This role is currently served mostly by tetrakis-(acetonitrile)copper(I) complexes such as $Cu(CH_3CN)_4PF_6$, which decomposes on prolonged exposure to ambient air, is oxidized almost instantly in aerated aqueous solution, and requires organic solvents such as acetonitrile for preparation of stable stock solutions. The hydrated granular crystalline form of **6.4** (Section 6.2.3) will likely be especially useful as a copper supplying agent, as it appears to be minimally hygroscopic and completely stable in air under ambient humidity.

6.3. A water-soluble tetrathioether macrocycle designed for enhanced Cu(I)-affinity

6.3.1. Ligand design

The area between the Cu(I)-buffering ranges offered by ligands **6.1** and **6.2** might in principle be covered using a third tripodal amine containing a mixture of 2- and 3-carbon N-S bridges; however, such a structure would be less symmetrical than **6.1** and **6.2** and may therefore be more difficult to purify by crystallization. Bridging the affinity gap with a water-soluble tetrathioether macrocycle would provide the additional benefit of a pH-independent Cu(I)-affinity standard, but the Cu(I)-complex stability constants of known tetradentate thiocrown ligands such as [16]aneS_4, [14]aneS_4-*a* and [14]aneS_4-*b* are too low (log $K_{Cu(I)}$ = 12.0-12.2) to provide a Cu(I)-buffering range contiguous with that of the high affinity tripodal ligand **6.1** at neutral pH. Furthermore, direct hydroxylation of the thiocrown ligand backbone, introduced by Rorabacher *et al.* as a means to increase aqueous solubility,[19-21] usually results in a decreased Cu(I)-affinity.[20,21] We suspected, however, that the ligand solubilization strategy previously developed for CTAP-2, which entails functionalization of the ligand backbone with geminal pairs of hydroxymethyl groups at the middle carbons of trimethylene bridges, might actually increase the Cu(I)-affinity of a flexible thiocrown such as [16]aneS_4 by favoring endo-conformations of the thioether moieties. A similar effect has been previously noted by Desper *et al.*[22] regarding the Ni(II)-affinities of methylated [14]aneS_4 derivatives, where the tetramethyl derivative **6.5** (Figure 6.6) yielded a 49-fold higher affinity than the parent structure [14]aneS_4-*a* in nitromethane solution.

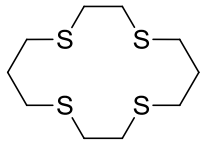

[14]aneS_4-*a*

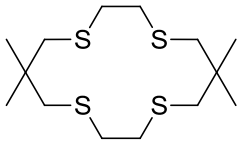

6.5

Figure 6.6: Structures of thiocrown ligands [14]aneS_4-*a* and **6.5**

While an effect observed for square planar Ni(II)-complexes in nitromethane is not necessarily expected to apply to tetrahedral Cu(I)-complexes in aqueous solution, the increased Ni(II) affinity of **6.5** appears to be due to destabilization of exodentate conformations of the thiocrown ring rather than a specific preorganization toward the preferred coordination geometry of the Ni(II) cation,[22] and is therefore likely to be general. An effect of equal magnitude applied to the Cu(I)-affinity of [16]aneS_4 (log $K_{Cu(I)}$ = 12.0) would provide a value of log $K_{Cu(I)}$ = 13.7, which is almost centered between the apparent Cu(I)-affinities of **6.1** and **6.2** at pH 7. To investigate this possibility, we devised ligand **6.6**, a derivative of [16]aneS_4 containing hydroxymethyl groups in analogous positions to the methyl groups of the [14]aneS_4 derivative **6.5**. Although it was unclear whether **6.6** itself would be adequately water-soluble for use as a Cu(I)-buffering agent, it could also serve as a precursor to the presumably more soluble tetrasulfonated derivative **6.7** (Figure 6.7).

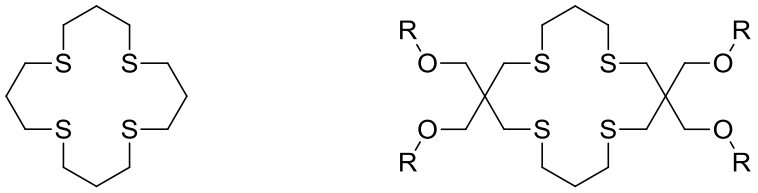

[16]aneS_4

6.6: R = H
6.7: R = $(CH_2)_3SO_3Na$

Figure 6.7: Structures of [16]aneS_4 and proposed water-soluble ligands **6.6** and **6.7**

6.3.2. Synthesis and properties of ligands 6.6 and 6.7 and their Cu(I)-complexes

Like the other hydroxylated thioether ligands reported in this work, **6.6** was derived from the versatile thietane precursor **3.15**. As shown in Scheme 6.2, double ring-opening with 1,3-diiodopropane gave diiodide **6.8**, which was cyclized with 1,3-

propanedithiol under Kellogg conditions to give thiocrown **6.9**. Interestingly, this macrocyclization proceeded in high yield despite its reliance on two consecutive nucleophilic substitutions at neopentyl centers. These apparently facile substitutions presumably proceed via the non-chain single electron transfer-radical coupling mechanism described by Ashby *et al.*, which is particularly favorable for alkyl iodides and is less sensitive to steric hindrance than the classic S_N2 pathway.[23]

Hydrolysis of the acetonide moieties of **6.9** under acidic conditions yielded ligand **6.6**, which was found to be highly crystalline and poorly soluble in most common solvents including water, alcohols, and even acetone. Reaction with tetrakis(acetonitrile)-copper(I) hexafluorophosphate gave the crystalline, air-stable copper(I) complex **6.10**, which dissolves readily in methanol or hot water.

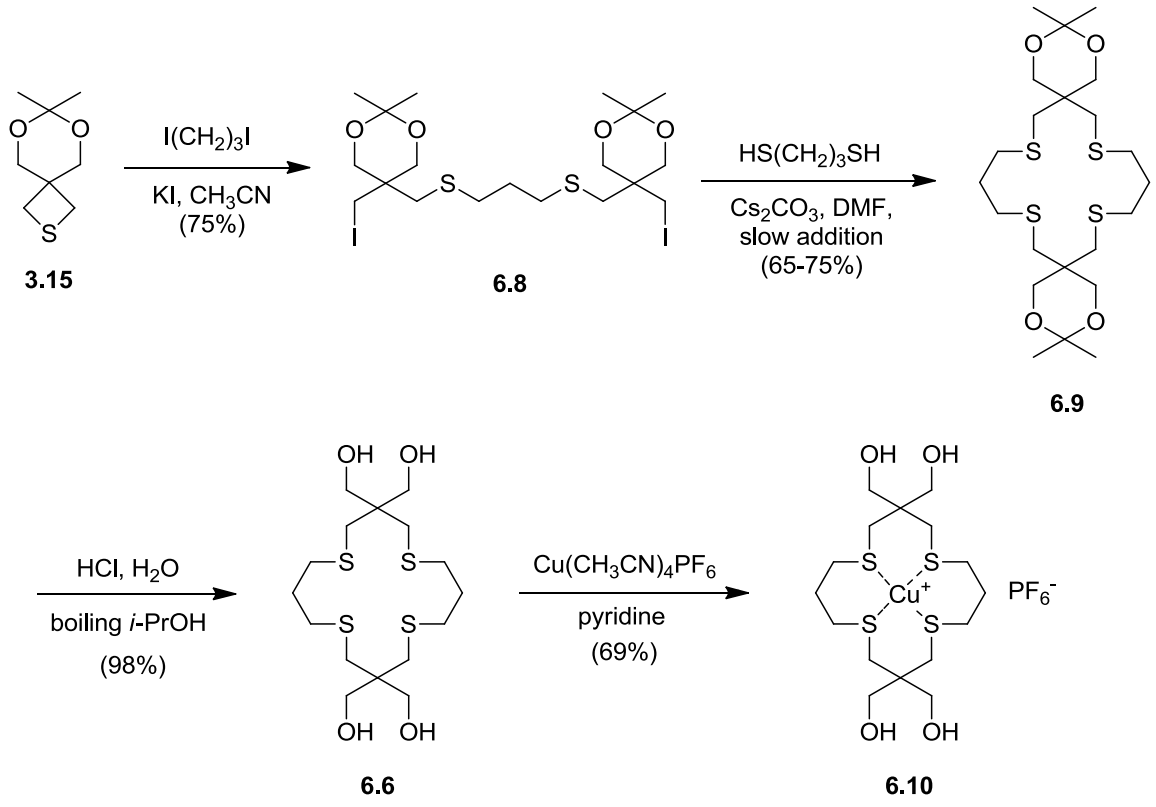

Scheme 6.2: Synthesis of ligand **6.6** and Cu(I)-complex **6.10**

Although the Cu(I)-complex is reasonably water soluble, efforts to accurately determine the Cu(I)-complex stability constant of ligand **6.6** were hampered by the exceedingly low solubility of the free ligand. Dilution of a DMSO stock solution of **6.6** to 10 μM in aqueous buffer yielded an initially homogeneous solution, but the ligand began to crystallize out within minutes even at this low concentration, indicating inadequate solubility for use as a Cu(I)-buffering agent. Therefore, we proceeded with the synthesis of the sulfonated derivative **6.7**.

An obvious route for the conversion of **6.6** to **6.7** is deprotonation of the hydroxyl moieties with a strong base such as sodium hydride followed by alkylation with 1,3-propanesultone, but this approach was unsuccessful. Treatment of **6.6** with 8 molar equivalents of NaH in DMF followed by addition of 8 molar equivalents of 1,3-propanesultone resulted in only about 60% alkylation of the hydroxyl groups as determined from the proton NMR spectrum of the product mixture in D_2O. This mixture, which was obtained as a colorless, water-soluble amorphous powder after washing with ethanol and vacuum drying, did not dissolve to any visible extent in DMF or DMSO even with heating, and further treatment with NaH and 1,3-propanesultone in DMF did not significantly alter the proton NMR integrals. Attempts to carry out the alkylation using potassium tert-butoxide and 1,3-propanesultone in DMSO yielded similar results. Apparently, the sodium or potassium sulfonate salts resulting from partial O-alkylation of **6.6** have insufficient solubility in aprotic solvents such as DMF and DMSO for further alkylation to proceed. We reasoned that this difficulty might be overcome using lithium as the counter-ion, as lithium salts of strong acids are generally much more soluble in polar organic solvents than the corresponding sodium and potassium salts. This was first attempted using n-butyllithium as the base in ether solvents, but **6.6** was surprisingly unreactive under these conditions, apparently due to exceedingly low solubility of both the starting material and its lithium alkoxides. Remarkably, a mixture containing the tetra-alcohol **6.6** and only 1 molar equivalent of n-butyllithium in dry diglyme

(diethylene glycol dimethyl ether) gave a positive test for unreacted alkyllithium (intense purple color with 1,10-phenanthroline) even after stirring for 1 hour at 80°C!

Since **6.6** is soluble in DMSO, the reaction was next attempted in this solvent. Although DMSO is itself deprotonated by n-BuLi, the resulting "dimsyllithium" is able to deprotonate alcohols, and has been previously employed for dialkylation of α-hydroxy-carboxylic acids to form α-alkoxy-esters.[24] Dropwise addition of n-butyllithium to a solution of **6.6** in anhydrous DMSO resulted in a transient white precipitate, presumably a sparingly soluble lithium alkoxide, which became permanent once the amount n-BuLi exceeded one molar equivalent. This precipitate began to redissolve upon addition of 1,3-propanesultone, consistent with conversion of the lithium alkoxide to a more soluble lithium sulfonate. Addition of alternating portions of n-butyllithium and 1,3-propanesultone eventually yielded a solution that remained clear upon further addition of n-BuLi. The solution remained homogeneous upon dilution with ethanol, but yielded a voluminous white precipitate upon addition of ethanolic sodium iodide, demonstrating the much lower solubility of the sodium sulfonate versus the lithium sulfonate. Recrystallization from ethanol-water gave the desired product **6.7** in 69% yield after vacuum drying as a colorless, water-soluble powder. Reaction of **6.7** with a stoichiometric quantity of with tetrakis(acetonitrile)copper(I) hexafluorophosphate followed by crystallization and vacuum drying gave the colorless, water-soluble, and oxygen-stable Cu(I)-complex **6.11**, which was determined by ^{1}H and ^{19}F NMR to be a 1:1 adduct with sodium hexafluorophosphate as previously noted for the sulfonated tripodal Cu(I)-complexes **6.3** and **6.4**. The synthesis of **6.7** and **6.11** is shown below in Scheme 6.3.

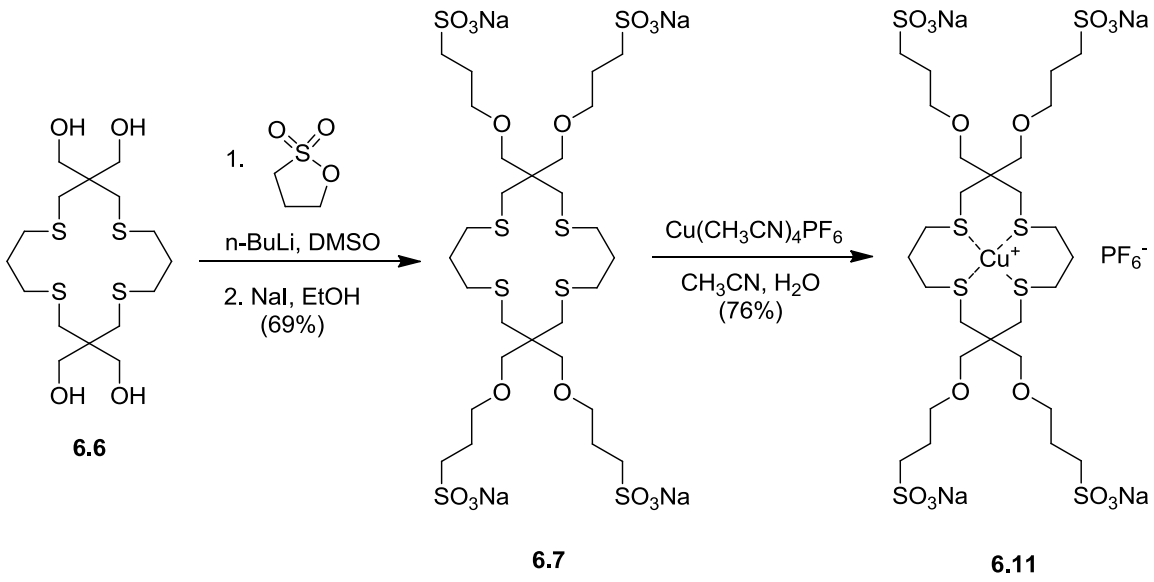

Scheme 6.3: Synthesis of ligand **6.7** and Cu(I)-complex **6.11**

6.3.3. Coordination properties of ligand 6.7

All experiments described in Section 6.3.3 were conducted by Pritha Bagchi

Similarly to the high-affinity tripodal ligand **6.1**, thiocrown ligand **6.7** was found to form a colored complex with Cu^{2+} at pH 5, allowing the Cu(II)-complex stability constant to be determined spectrophotometrically by direct titration with $CuSO_4$. The resulting value of log $K_{Cu(II)}$ = 3.47 is 18-fold higher than reported for the parent thiocrown ligand [16]aneS_4 (log $K_{Cu(II)}$ = 2.20),[12] but significantly lower than that of ligand **6.1** (log $K_{Cu(II)}$ = 6.42). Cyclic voltammetry of **6.7** in the presence of excess Cu^{2+} revealed a quasi-reversible single electron process with a formal potential of 0.729 V vs. SHE, which would correspond to log $K_{Cu(I)}$ = 13.6, but the observed peak separation (90 mV at 20 mV/s scan rate) is too large for this result to be considered reliable. Competition titrations with BCA and BCS, both of which had been cross-calibrated against ligand **6.1**, yielded a uniform complex stability constant of log $K_{Cu(I)}$ = 13.80 ± 0.03. This value is remarkably close to the figure of log $K_{Cu(I)}$ = 13.7 predicted on the

basis of the steric effect reported by Desper *et al*. for the Ni(II) affinities of [14]aneS_4 derivatives (See section 6.3.1) and is indeed nearly centered between the apparent Cu(I)-affinities at pH 7 of log $K'_{Cu(I)}$ = 10.99 and 15.97 for the tripodal ligands **6.2** and **6.1**, respectively. Together, ligands **6.2**, **6.7**, and **6.1** provide a nearly continuous buffering range extending from approximately 10^{-10} to 10^{-17} M Cu^{+}.

6.3.4. X-ray crystal structures of ligand 6.6 and Cu(I)-complex 6.10

To examine the Cu(I)-coordination mode of ligand **6.7** and also its degree of preorganization relative to the parent structure [16]aneS_4, we attempted to obtain crystal structures of both the free ligand and its Cu(I)-complex **6.11**. Although both compounds readily formed fibrous acicular crystals suitable for purification purposes, we were unable to obtain crystals suitable for x-ray diffraction after many attempts under a variety of conditions. Therefore, we turned to the neutral ligand **6.6** and its Cu(I)-complex **6.10** as model compounds. Ligand **6.6** could only be obtained as twinned needles, but these could be grown to a large size and otherwise good quality by recrystallization from DMSO-water. Copper complex **6.10** initially gave only very thin fibers from ethanol, methanol, or water. When the fibrous crystals were removed by filtration from a rapidly cooled ethanolic solution before crystallization was complete, a slower-growing form, consisting of clear, colorless prisms suitable for x-ray diffraction, nucleated after several hours. Data collection and structural refinement for both **6.6** and **6.10** were carried out by Dr. John Bacsa of Emory University.

The crystals obtained from **6.10** were found to be an ethanol solvate of the expected 1:1 Cu(I)-complex containing two diastereomeric conformers (A and B) of [**6.6**-Cu(I)]$^{+}$, two ethanol molecules, and two disordered hexafluorophosphate counter-ions per asymmetric unit. As shown in Figure 6.8 and Table 6.2, the Cu(I)-coordination geometry is distorted tetrahedral with S-Cu-S bond angles ranging from 97.0° to 118.9° for conformer A and 96.6° to 123.7° for conformer B.

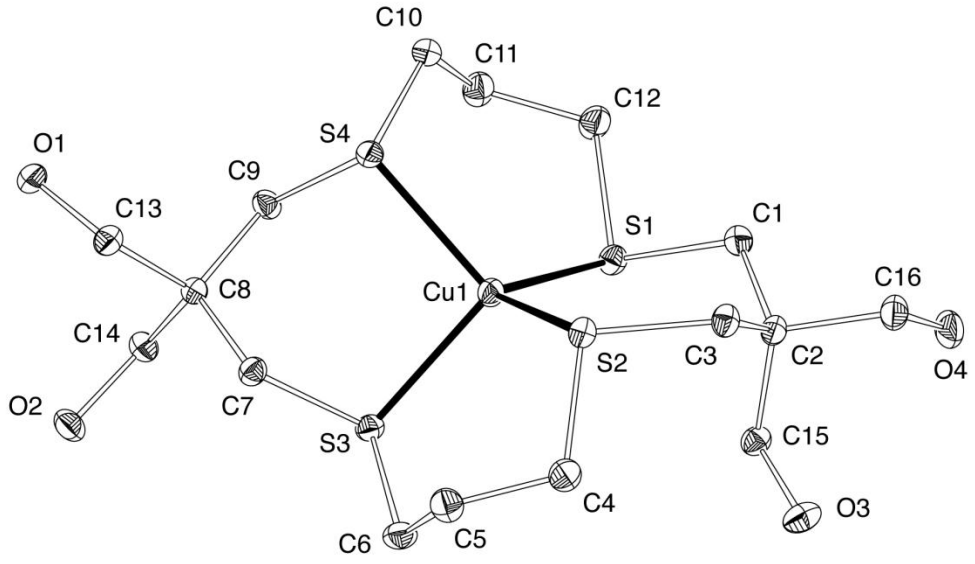

Figure 6.8: ORTEP representation of the cationic unit of Cu(I)-complex **6.10** (Conformer A). Image generated by Dr. Christoph Fahrni using PLATON[17]

Table 6.2: Selected bond lengths and angles in Cu(I)-complex **6.10**

	Conformer A	**Conformer B**
Bond lengths (angstroms)		
Cu(1)-S(1)	2.2558(2)	2.2729(3)
S(2)-Cu(1)	2.2577(2)	2.2576(2)
S(3)-Cu(1)	2.3024(2)	2.3339(2)
S(4)-Cu(1)	2.3108(2)	2.3088(3)
Average Cu-S	2.282	2.293
Bond angles (degrees)		
S(1)-Cu(1)-S(3)	118.896(9)	116.703(10)
S(1)-Cu(1)-S(4)	110.019(9)	104.482(9)
S(1)-Cu(1)-S(2)	106.648(9)	106.517(9)
S(2)-Cu(1)-S(3)	106.772(9)	109.358(9)
S(2)-Cu(1)-S(4)	117.871(9)	123.669(10)
S(3)-Cu(1)-S(4)	97.026(8)	96.580(9)

As observed for the tripodal ligand-Cu(I) complexes **6.3**-ClO_4 and **6.4**, the structure of **6.10** contains S-Cu-S bond angles that differ considerably from the tetrahedral ideal of 109.5°, but the Cu-S bond lengths average less than the typical value of 2.33 Å previously noted for Cu(I)-thioether complexes.[13]

The twinned crystals of **6.6** yielded a partly disordered structure, which was modeled using two components for one of the -$S(CH_2)_3S$- units to give a final R-factor of 10.1% for the structural refinement. The differences in atomic locations for the two components are not large, with maximum values of 0.42 Å for carbon and 0.41 Å for sulfur, so a single component was selected for structural comparison purposes. As shown in Figure 6.9, the respective crystal structures indicate that ligand **6.6** is indeed substantially preorganized toward Cu(I) coordination compared to the parent structure [16]aneS_4.[25] Two of the thioether moieties of [16]aneS_4 point directly away from the macrocyclic cavity, with a transannular S-S distance of 8.5 Å. By contrast, the maximum S-S distance in **6.6** is only 6.1 Å, which is significantly closer to the value of 4.0 Å observed in Cu(I)-complex **6.10**.

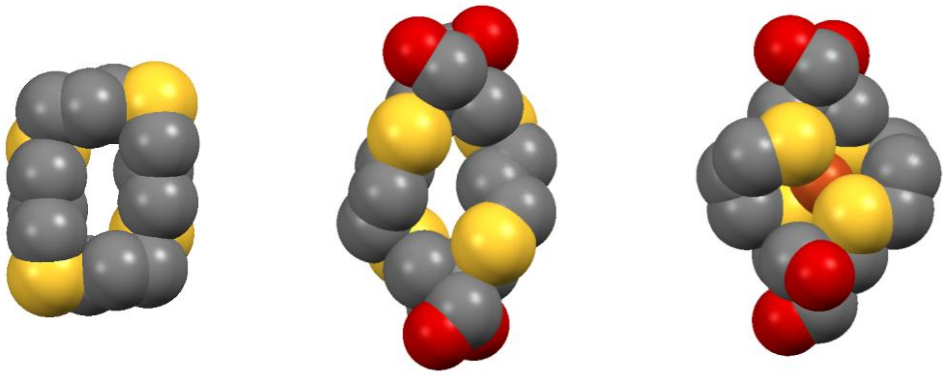

Figure 6.9: Comparison of the crystal structures of [16]aneS_4,[25] **6.6**, and **6.10** Hydrogen atoms omitted for clarity. Images generated using Mercury 3.1[16]

While the molecular geometries found in crystal structures do not necessarily represent the most abundant species in solution, particularly for a flexible structure such as 16aneS_4, the differences in ring conformation observed for **6.6** versus [16]aneS_4 are similar to those noted by Desper *et al*. for **6.5** versus [14]aneS_4-*a*. Assuming that functionalization of the hydroxyl groups of **6.6** does not significantly alter the conformational preferences of the macrocyclic ring, the increase in Cu(I)-complex stability constant for the sulfopropylated analog **6.7** versus [16]aneS_4 is most likely due to the intended preorganizational effect.

6.4. Applications of the water-soluble thioether ligands and Cu(I)-complexes

All experiments described in Section 6.4 were conducted by Pritha Bagchi

6.4.1. Verification of Cu(I)-complex stability constants

As discussed in Section 6.1.2, the water-soluble bidentate ligands BCA and BCS are frequently employed as Cu(I)-affinity standards, but there is no consensus in the literature as to the Cu(I)-complex stability constants of either of these ligands. Recently, Xiao *et al*.[8] determined the 2:1 ligand-Cu(I) complex stability constant β_2 of BCS based on the thermodynamic cycle method[11] using the corresponding Cu(II)-complex stability constant and ligand-bound Cu(II)/Cu(I) reduction potential, yielding a value of log β_2 = 19.9. The complex stability constant for BCA-Cu(I) was then determined as log β_2 = 17.3 based on indirect competition with BCS using a protein intermediary ligand.[8] These values, however, differ significantly from our results of log β_2 = 17.67 and 20.81 for BCA and BCS, respectively, which were obtained by direct competition with ligand **6.1**. Correct Cu(I)-complex stability constants for BCA and BCS are critical not only for the use of these ligands as Cu(I)-affinity standards but also for our determination of the

Cu(I)-complex stability constants of ligands **6.2** and **6.7**. Therefore we carefully investigated the source of the discrepancy.

In our hands, determination of log β_2 for BCS-Cu(I) using the thermodynamic cycle method did not agree with the results of Xiao *et al*. but instead yielded a value identical to that obtained by direct competition with **6.1**. There are two factors likely responsible for this disagreement. The first is the choice of reference potential for the aqueous Cu^{2+}/Cu^{+} couple. Xiao *et al*. used an older value of 0.164 V,[10] whereas we used a "concentration potential" of 0.130 V derived by correcting the standard reduction potential of 0.154 V for the activity coefficients of Cu^{2+} and Cu^{+} at 0.1 M ionic strength.[11] The significance of this difference is explained as follows: Cu(I) affinities are calculated by the thermodynamic cycle method according to Equation 3.1 as previously described in Chapter 3, where $E_{\mathrm{Cu(II/I)solv}}$ represents the reduction potential of the aqueous Cu^{2+}/Cu^{+} couple and $E_{\mathrm{Cu(II/I)L}}$ is the reduction potential of the ligand-bound Cu(II)/Cu(I) couple. Note that Equation 3.1 also holds for 2:1-binding ligands such as BCS provided that the Cu(I) and Cu(II)-ligand complexes have identical stoichiometries, and K is simply replaced by β_2.

$$E_{\mathrm{Cu(II/I)L}} = E_{\mathrm{Cu(II/I)solv}} - \frac{\ln(10)RT}{F}\log\frac{K_{\mathrm{Cu(II)}}}{K_{\mathrm{Cu(I)}}} \qquad (3.1)$$

At 25°C (298 K), the term ln(10)RT/F is equal to 0.0592 V, so the dependence of log $K_{\mathrm{Cu(I)}}$ on $E_{\mathrm{Cu(II/I)L}}$, $E_{\mathrm{Cu(II/I)solv}}$, and log $K_{\mathrm{Cu(II)}}$ can be expressed by Equation 6.4.

$$\log K_{\mathrm{Cu(I)}} = \log K_{\mathrm{Cu(II)}} + \frac{E_{\mathrm{Cu(II/I)L}} - E_{\mathrm{Cu(II/I)solv}}}{0.0592\ \mathrm{V}} \qquad (6.4)$$

According to Equation 6.4, log $K_{Cu(I)}$ (or log β_2) increases by 1 for every 59 mV increase in $E_{Cu(II/I)L} - E_{Cu(II/I)solv}$. Therefore, the 34 mV higher value used by Xiao *et al.* for $E_{Cu(II/I)solv}$ should reduce the apparent log β_2 for BCS-Cu(I) by 0.57.

The 0.3 log unit discrepancy remaining after the above correction is probably due to the methodology used to measure log β_2 for BCS-Cu(II). Xiao *et al*. determined this value by the Bjerrum method,[26] which relies on the shift in apparent acid dissociation constant of the protonated ligand in the presence of Cu(II). A BCS concentration of 4 mM was employed for direct potentiometric determination of the acid dissociation constant,[8] but BCS has been reported to aggregate significantly in aqueous solution at concentrations above about 1 mM.[27] To avoid aggregation, we determined log β_2 for BCS-Cu(II) at a BCS concentration of 0.3 mM by competition titrations against the ligand N,N-bis(2-hydroxyethyl)-N-(2-pyridylmethyl)amine (DHEAMP, Figure 6.10), and the Cu(II)-affinity of this ligand was in turn verified by direct titration with Cu^{2+}.

Based on the above considerations, our value for log β_2 of BCS-Cu(I) determined by the thermodynamic cycle method is most likely more accurate than that of Xiao *et al.,* and the internal consistency between the Cu(I)-affinities determined for **6.1** and BCS by this method is encouraging. Any inaccuracy in the value we employed for $E_{Cu(II/I)solv}$, however, would affect the apparent affinities of **6.1** and BCS equally, giving an undetected error in the Cu(I)-affinities not only for these ligands but also for BCA, **6.2**, and **6.7**. Therefore, we sought to independently verify the Cu(I)-complex stability constants of these ligands using an independent method. The Cu(I)-complex stability constants β_1, β_2, and β_3 of acetonitrile have been previously determined using a method based on the kinetics of Cu(I)-oxidation by Co(III) complexes,[7] which does not depend on the exact value of the Cu^{2+}/Cu^{+} reduction potential, but the Cu(I) affinity of acetonitrile is insufficient for competition with **6.1**. Furthermore, the Cu(I)-complexes of **6.1**, **6.2**, and **6.7** are colorless with no significant UV absorption above 300 nm, so

competition titrations between any of these ligands and acetonitrile, which also forms colorless Cu(I)-complexes, would be difficult to monitor spectrophotometrically. We realized, however, that the Cu(I)-complex stability constants of higher affinity ligands could be linked to those of acetonitrile using the tripodal pyridine-thioether ligand PEMEA[13] (Figure 6.10).

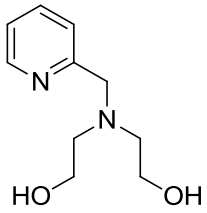

DHEAMP

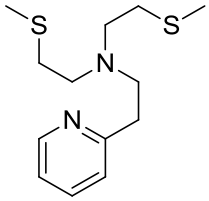

PEMEA

Figure 6.10: Structures of pyridine ligands DHEAMP and PEMEA

PEMEA is a 1:1-binding ligand with a Cu(I)-complex stability constant of log $K_{Cu(I)}$ = 15.76, but has two sites that can be protonated in dilute aqueous solution with mixed-mode pKa values of 7.33 and 3.26. As its upper pKa and its value of log $K_{Cu(I)}$ are similar to those of **6.1**, it should be suitable for competition titrations with **6.1** at pH 5 or above, and the pyridine ring should provide a spectroscopic handle for monitoring Cu(I)-occupancy. At pH values significantly below the lower pKa, however, Cu(I)-coordination will compete with two consecutive protonation equilibria, reducing log $K'_{Cu(I)}$ by approximately 2 for every unit reduction pH. At pH 2, log $K'_{Cu(I)}$ should fall to about 9.2, a value well suited for competition with acetonitrile. Furthermore, the PEMEA-bound Cu(II)/Cu(I) couple has a relatively high reduction potential of 0.595 V vs. SHE, so the PEMEA-Cu(I) complex should not be highly reactive toward oxygen.

For verification purposes, we re-determined the acid dissociation constants of PEMEA as well as the value of log $K_{Cu(I)}$ by the thermodynamic cycle method, then determined the Cu(I)-affinity independently by competiton with acetonitrile. Remarkably, the two different methods yielded exactly the same value of log $K_{Cu(I)}$ = 15.71 with an estimated uncertainty of ± 0.08 for the thermodynamic cycle and ± 0.02 for the competition titration. The Cu(I)-complex stability constants of **6.1** and BCA were then verified directly against PEMEA by competition titrations. The resulting value of log $K_{Cu(I)}$ = 16.33 for **6.1** exactly matches the result obtained by the thermodynamic cycle method, thus also verifying our value log β_2 for BCS, which was obtained by competition with **6.1** and verified independently by the thermodynamic cycle method. The value of log β_2 = 17.63 ± 0.05 obtained for BCA matches the result of log β_2 = 17.67 ± 0.03 obtained by competition with **6.1** within experimental error. The latter value was obtained using an aqueous stock solution of the air-stable Cu(I)-complex **6.3** as the copper source, so it is most likely more accurate than the former, which relied on an acetonitrile stock solution of $Cu(CH_3CN)_4PF_6$. Therefore, our values of log $K_{Cu(I)}$ for **6.2** and **6.7**, which were obtained by competition with BCA assuming log β_2 = 17.67, are also confirmed. Taken together, these results constitute a web of accurately cross-verified Cu(I)-affinity standards anchored in two independent primary methods for determining Cu(I)-complex stability constants. The Cu(I)-complex stability constants, concentration-mode pKa values, and apparent Cu(I)-complex stability constants at neutral pH for the three sulfonated thioether ligands **6.1**, **6.2**, and **6.7**, as well as the previous Cu(I)-affinity standards BCA and BCS, are compiled in Table 6.3. To facilitate comparison between 1:1 and 2:1 binding ligands, we have also included the values of pCu, which we define as the thermodynamic free Cu^+ concentration in a solution containing 10 μM ligand and 1μM Cu(I) by analogy to a similar metric used on iron coordination chemistry.[28] Notably, **6.1** actually binds Cu^+ more tightly than BCS at this relatively low concentration, even

though the 2:1 Cu(I)-complex stability constant of BCS is numerically much larger than the 1:1 Cu(I)-complex stability constant of ligand **6.1**. Increasing the ligand concentration to 500 μM while maintaining the same fractional occupancy, however, would result in -1og[Cu^+] = 18.3 for BCS, while the value for ligand **6.1** would remain constant at 16.9.

Table 6.3. Cu(I)-complex stability constants of water-soluble affinity standard ligands

Ligand	pKa	log $K_{Cu(I)}$ [a]	log $K'_{Cu(I)}$ (pH 7)	pCu [c]
6.1	7.00	16.33	15.97	16.9
6.2	8.98	13.08	10.99	11.9
6.7	-	13.80	13.80	14.8
BCA	3.80	17.66 [b]	17.66	13.5
BCS	5.70	20.81 [b]	20.76	16.6

[a] Mean value weighted inversely by the internal standard deviations of the individual determination methods. [b] log β_2. [c] [Cu^+] calculated for a solution containing 10 μM ligand and 1 μM Cu(I) at pH 7

6.4.2. Determination of the Cu(I)-affinity of the metallochaperone CusF

To demonstrate the utility of the new water-soluble thioether-based Cu(I)-ligands as affinity standards, we sought to determine the Cu(I)-binding affinity of a copper protein by ligand competition titrations. We selected the bacterial copper chaperone CusF in part because it contains a single tryptophan residue reported to engage directly in a cation-π interaction with Cu(I), which allows fluorimetric monitoring of Cu(I) occupancy due to nearly complete quenching of tryptophan fluorescence in the Cu(I)-bound protein.[29] The Cu(I) affinity of CusF has been determined previously as log $K'_{Cu(I)}$ = 6.43 by isothermal titration calorimetry and later as a relative value versus BCA as K_d x β_2 =

7300, where $K_d = 1/K'_{Cu(I)}$,[27] corresponding to log $K'_{Cu(I)} = 13.80$ based on our value of β_2 for BCA-Cu(I). As is common for the Cu(I)-binding affinities of proteins, these literature values disagree by over 7 orders of magnitude. If the latter value is correct, however, the Cu(I)-affinity of CusF is exactly the same as that of **6.7** (Table 6.3), making this ligand ideal for competition titrations.

Titration of the apo-form of CusF with Cu(I), which was produced in situ from $CuSO_4$ and 100 µM sodium ascorbate under deoxygenated conditions, gave a linear decrease in fluorescence intensity with sharp saturation at 1 molar equivalent. Back-titration with **6.7** gave a gradual increase in fluorescence intensity toward the original value, indicating effective competition (Figure 6.11).

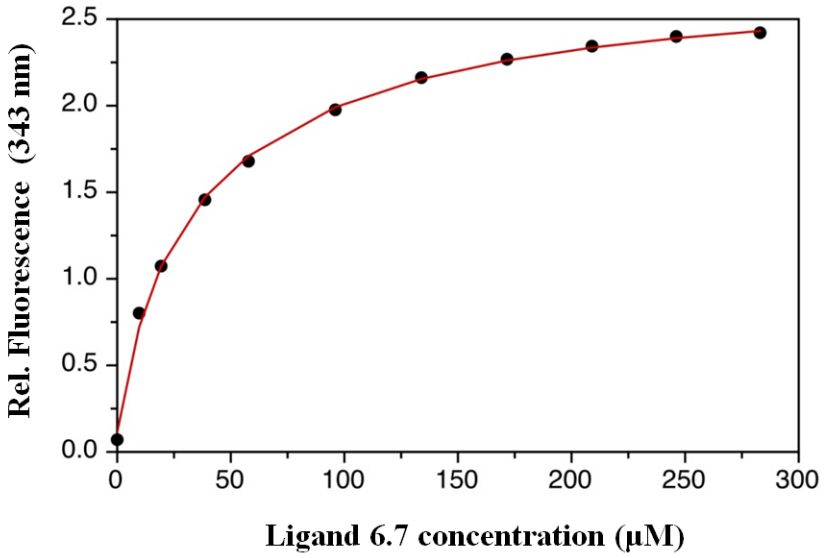

Figure 6.11: Fluorescence-monitored titration of Cu(I)-saturated CusF with ligand **6.7** Conditions: 20 µM CusF, 21µM Cu(I), 0-283 µM **6.7**, pH 7. Black points: experimental data. Red trace: fit. Experiment performed by Pritha Bagchi

The above competition titration yielded a value of log $K'_{Cu(I)} = 14.29 \pm 0.11$, which is 0.5 log units higher than the value determined Xue *et al*. by competition with

BCA (see above). Due to this discrepancy, we re-determined the Cu(I)-affinity of CusF by direct competition with BCA using spectrophotometric monitoring of the $BCA_2Cu(I)$ absorption at 562 nm. This was performed both by titrating a mixture of BCA and Cu(I) with the protein and by titrating a mixture of BCA and the protein with Cu(I), yielding identical results of $\log K'_{Cu(I)} = 14.21 \pm 0.03$ and confirming the value obtained by fluorimetric titration with **6.7** within experimental error. The discrepancy between our data and that obtained by Xue *et al.*[29] may be due to the choice of wavelength for spectrophotometric monitoring; the latter authors appears to have calculated the Cu(I)-occupancy of BCA using an absorption peak of the Cu(I)-complex at 358 nm,[29] which is overlapped slightly by the absorption spectrum of free BCA, whereas we used the completely isolated absorption peak at 562 nm. Based on these data, it appears that we have not only demonstrated the utility of sulfonated thioether-based Cu(I)-ligands as affinity standards for Cu(I)-proteins but also provided a more accurate value of $\log K'_{Cu(I)}$ for the bacterial metallochaperone CusF than was previously available.

6.5. Conclusions

To aid in the challenging problem of accurately determining the Cu(I)-binding affinities of biomolecules, we have created a series of water-soluble, 1:1-binding Cu(I)-ligands for use as affinity standards. These sulfonated thioether-based ligands form colorless, air-stable, and water-soluble Cu(I)-complexes that are optically transparent down to 300 nm, allowing spectrophotometric or fluorimetric monitoring of the Cu(I)-occupancy of other ligands under study, including proteins, without interference from the affinity standard ligand or its Cu(I) complex during competition experiments. In this respect, our sulfonated thioether ligands are complementary to the previously known Cu(I)-affinity standards BCA and BCS, which absorb strongly in the near UV but form colored Cu(I)-complexes suitable for spectrophotometric monitoring in the visible range.

All three sulfonated thioether ligands **6.1**, **6.2**, and **6.7** as well as their respective Cu(I)-complexes **6.3**, **6.4**, and **6.10** are readily isolated by recrystallization and stable in solid form, allowing preparation of solutions with precisely defined, buffered concentrations of available Cu^+ by mixing the free ligands and Cu(I)-complexes in the appropriate ratio without the need for auxiliary Cu(I)-ligands such as acetonitrile. Aqueous solutions of the Cu(I)-complexes are air-stable for many hours, consistent with the presence of little or no free Cu^+ in solution, yet rapid equilibration was observed in all ligand competition titrations, indicating that Cu(I)-exchange likely proceeds via an associative mechanism and is not limited by the slow kinetics of complete Cu(I)-dissociation from the ligand. This behavior is essential for high affinity ligands to be useful as Cu(I)-buffers or affinity standards: Ligand **6.1**, for example, has an apparent Cu(I) complex stability constant of nearly 10^{16} M^{-1} implying that even if the ligand-Cu^+ association reaction were to occur with a diffusion-limited rate constant of 10^8 M^{-2} s^{-1}, the reverse reaction would occur with a rate constant of only 10^{-8} M^{-1} s^{-1}, corresponding to a half-life of over two years for dissociation of the complex to free Cu^+.

In addition to use as an affinity standard, the isolated Cu(I)-complex **6.4**, which contains the lowest affinity ligand **6.2**, may also serve as an alternative to the previously available tetrakis(acetonitrile)-copper(I)-salts for quantitative metalation of higher affinity ligands such as copper proteins. Unlike Cu(I)-acetonitrile complexes, **6.4** forms a well-defined crystalline hydrate that is stable in ambient air and can be dissolved directly in water to provide air-stable aqueous stock solutions at concentrations up to 100 mM.

The Cu(I)-complex stability constants of **6.1**, **6.2**, and **6.7** have been accurately determined, along with those of BCA and BCS, by a network of competition titrations anchored in two independent primary methods, providing a unified series of five total affinity standard ligands able to provide buffered Cu(I)-concentrations ranging from approximately 10^{-10} to 10^{-19} M. We anticipate that this series will aid substantially in

accurate binding affinity determination for Cu(I)-proteins and possibly other biologically relevant Cu(I)-ligands.

6.6. Experimental section

Compound synthesis and crystallization procedures are described below. Potentiometric and ligand competition titrations, which were conducted by Pritha Bagchi, and full details of X-ray diffraction analysis and structural refinement, which were conducted by Dr. John Bacsa of Emory University, will be presented in an upcoming publication. Preliminary crystallographic data are given in Appendix 1.

6.6.1. Synthesis

General

NMR: ^{19}F spectra are reported in ppm relative to internal 2,2,2-trifluoroethanol (TFE), which was employed both as a chemical shift standard and an integration standard to link the ^{19}F and ^{1}H integrals. The resulting fluorine integration values were between 5.2 and 6 for the PF_6^- signal of all hexafluorophosphates. ^{1}H and ^{13}C spectra acquired in D_2O are referenced to internal sodium 3-trimethylsilylpropionate-2,2,3,3-d_6. ^{1}H spectra acquired in other solvents are reported in ppm relative to internal TMS, while ^{13}C spectra acquired in other solvents are referenced to the known chemical shift of the solvent peak ($CDCl_3$: 77 ppm, $(CD_3)_2SO$: 39.5 ppm).

Ligand **6.1**

A solution of tris(2-chloroethyl) amine hydrochloride (2.16 g, 8.97 mmol), sodium 3-mercaptopropanesulfonate 5.28 g, 3.3 equiv. and NaOH (1.58 g, 4.3 equiv.) in methanol (45 mL) plus water (5 mL) was stirred under argon overnight at 60°C. The resulting pasty mixture was diluted to 250 mL in 10:1 methanol-water and heated to

boiling. Water was then added slowly until almost all solids had dissolved (required 15 mL). The mixture was filtered while hot, boiled down to 200 mL, diluted back to 300 mL with methanol, and allowed to cool to room temperature under slow stirring. The resulting crystalline slurry was stirred for 2 hours at 0°C, and the colorless product was collected by filtration, washed with cold methanol followed by acetone, and dried under high vacuum to give a fine powder. Yield 3.75 g (5.95 mmol, 66%). ^{1}H NMR (D_2O, 400 MHz) δ 2.00-2.07 (m, 6H), 2.69-2.75 (m, 12H), 2.77-2.83 (m, 6H), 3.01-3.05 (m, 6H). ^{13}C NMR (D_2O, 100 MHz) δ 27.1, 30.4, 32.8, 52.6, 55.5. Elemental analysis calcd (%) for $C_{15}H_{30}NNa_3O_9S_6$ (629.76): C 28.61, H 4.80, N 2.22; found C 28.27, H 4.70, N 2.17.

Complex **6.3**

Solid $Cu(CH_3CN)_4PF_6$ (511 mg, 1.37 mmol) was added to a solution of **6.1** (864 mg, 1.37 mmol) in H_2O (10 mL). Ethanol (10 mL) was added, and the mixture was stirred in a 60°C bath until all solids dissolved. The resulting green solution was decolorized by adding the minimum amount (<100 mg) of sodium ascorbate, diluted with 40 mL ethanol, boiled down to half its original volume, and diluted slowly with ethanol until slightly turbid. The solution was then removed from the heat source and diluted dropwise with water to the point of clarity. Methanol (15 mL) was added, and the mixture was allowed to cool to room temperature under slow stirring. The resulting crystalline suspension was stirred in an ice bath for 2 hours, and the colorless product was collected by filtration, washed with ethanol, and dried under high vacuum to give a fine powder. Yield 719 mg (858 mmol, 63%). ^{1}H NMR (D_2O, 400 MHz) δ 2.11 (p, J = 7.4 Hz, 6H), 2.79-2.86 (m, 12H), 3.02-3.06 (m, 12H). ^{19}F NMR (D_2O, 376 MHz) δ (TFE) 4.62 (d, *J* = 708 Hz, 6F). Elemental analysis calcd (%) for $C_{15}H_{30}CuF_6NNa_3O_9PS_6$ (838.27): C 21.49, H 3.61, N 1.67; found C 21.38, H 3.52, N 1.64.

Ligand **6.2**

Tris(3-chloropropyl)amine (2.00 g, 8.11 mmol), sodium 3-mercaptopropane-sulfonate (4.48 g, 3.1 equiv.), and sodium hydroxide (1.01 g, 3.1 equiv.) were stirred in methanol (35 mL) under argon at 60 °C overnight. The resulting pasty mixture was diluted into 150 mL methanol + 10 mL water and heated to boiling. The resulting slightly turbid solution was suction-filtered through a pre-heated glass frit, re-heated to boiling, and allowed to cool to room temperature under slow stirring. The product separated as a colorless crystalline powder, which was collected by filtration, washed with methanol followed by diethyl ether, and dried under vacuum to give a fine powder. Yield 3.53 g (5.18 mmol, 64%) ^{1}H NMR (D_2O, 400 MHz) δ 1.75-1.83 (m, 6H), 1.99-2.07 (m, 6H), 2.58-2.64 (m, 12H), 2.72 (t, *J* = 7.2 Hz, 6H), 3/00-3.05 (m, 6H). ^{13}C NMR (D_2O, 100 MHz) δ 27.0, 28.0, 31.8, 32.6, 52.6, 54.9. Elemental analysis calcd (%) for $C_{18}H_{36}NNa_3O_9S_6$ (671.84): C 32.18, H 5.40, N 2.08; found C 31.79, H 5.41, N 2.06.

Complex **6.4** anhydrous

Ligand **6.2** (679 mg, 1.01 mmol) and $Cu(CH_3CN)_4PF_6$ (377 mg, 1.01 mmol) were stirred in methanol (20 mL). The mixture was heated to reflux under argon, and water was added slowly until all colorless solids had dissolved. A small amount of blue solid remained at this point, but dissolved upon addition of 60 µL (1 mmol) of acetic acid. The mixture was concentrated nearly to dryness, and the residue was stirred in boiling isopropanol (50 mL), decolorized with the minimum amount of sodium ascorbate, and diluted dropwise with water until all solids had dissolved. The resulting biphasic liquid was diluted with methanol until monophasic (required 15 mL), and allowed to cool to room temperature under slow stirring. The resulting colorless crystalline powder was collected by filtration, washed with cold isopropanol, and dried under vacuum. Yield 520 mg (0.607 mmol, 60%). ^{1}H NMR (D_2O, 400 MHz) δ 2.07-2.15 (m, 12H), 2.71-2.74 (m,

6H), 2.93-2.98 (m, 12H), 3.02-3.06 (m, 6H). ^{19}F NMR (D_2O, 376 MHz) δ (TFE) 4.64 (d, *J* = 708 Hz, 6F). Elemental analysis calcd (%) for $C_{18}H_{36}CuF_6NNa_3O_9PS_6$ (880.35): C 24.56, H 4.12, N 1.59; found C 24.47, H 4.22, N 1.59.

Complex **6.4** hemi(pentadecahydrate)

Ligand **6.2** (1.12 g, 1.67 mmol) and $Cu(CH_3CN)_4PF_6$ (621 mg, 1.67 mmol) were added to a 50 mL rb flask containing a magnetic stir bar. The flask was sealed and flushed with argon, and water (10 mL) and ethanol (10 mL) were injected. The mixture was stirred until all solids had dissolved and then shaken with air, which resulted in a blue coloration. Triethylamine (100 µL) was added, resulting in a small amount of blue precipitate which was removed by centrifugation. The mixture was heated to boiling, diluted slowly with ethanol (required 35 mL) to the point of permanent turbidity, and allowed to settle while hot. The clear solution was decanted, filtered through a glass frit, and allowed to cool. A mixture of fibrous acicular crystals and irregular hexagonal tablet-shaped granules was deposited. The fibrous crystalline form was separated from the granular crystalline form by swirling and decantation, and a sample of each crystalline form was collected by filtration and dried under argon flow. Both forms yielded ^{1}H and ^{19}F NMR spectra identical to those of anhydrous **6.4**. The two crystalline slurries were recombined, and the mixture was stirred slowly overnight, resulting in complete conversion to the granular form. This was collected by filtration, washed with cold 4:1 ethanol-water, and dried by suction in ambient air to give a free-flowing, colorless granular powder consisting of irregular hexagonal tablets. A sample of this material was recrystallized from 3:1 ethanol-water to give larger tablets of identical crystal habit. X-ray diffraction analysis yielded an empirical formula of $C_{36}H_{102}Cu_2F_{12}N_2Na_6O_{33}P_2S_{12}$ (2030.93 g/mol), corresponding to $C_{18}H_{36}CuNNa_3O_9S_6PF_6 \bullet 7.5\ H_2O$ (1015.46 g/mol) per copper equivalent. Yield 719 mg (0.708 mmol, 42%).

Diiodide **6.8**

A mixture of thietane **3.15** (10.70 g, 61.4 mmol), 1,3-diiodopropane (9.11 g, 30.8 mmol), potassium iodide (5.10 g, 30.7 mmol), and powdered potassium carbonate (200 mg, 1.5 mmol) was stirred under argon in a sealed, foil-wrapped flask for 3 days at 65°C followed by 8 days at 45 °C.[a] The mixture was diluted into methanol (120 mL), treated with concentrated aqueous ammonia (20 mL), heated briefly to boiling, and concentrated to a viscous oil. This material was stirred for 2 hours with 1 M aqueous citric acid (100 mL) and cyclohexane (200 mL). The organic layer was separated, dried with $MgSO_4$, concentrated under reduced pressure, and rotated under high vacuum overnight to completely remove cyclohexane, giving the product as a viscous, slightly yellow yellow oil which was used in the next step without further purification. Yield 14.83 g (20.0 mmol, 75%). ^{1}H NMR ($CDCl_3$, 400 MHz) δ 1.41 (s, 6H), 1.42 (s, 6H), 1.92 (p, *J* = 7.1 Hz, 2H), 2.69 (t, J = 7.1 Hz, 4H), 2.70 (s, 4H), 3.40 (s, 4H), 3.72 (d, *J* = 11.8 Hz, 8H), 3.78 (d, *J* = 11.8 Hz, 8H). ^{13}C NMR ($CDCl_3$, 100 MHz) δ 12.8, 23.4, 23.7, 29.6, 32.5, 36.7, 36.8, 66.3, 98.6. EI-MS *m/z* 644 (56, $[M]^+$), 375 (100), 343 (50), 45 (181), 83 (67). EI-HRMS *m/z* calcd for $[M]^+$ $C_{19}H_{34}NI_2O_4S_2$ 643.9988, found 643.9985. [a] Alternatively, the product can be obtained in 73% yield by column chromatography on silica gel (hexanes-MTBE) after reaction for only 4 days at 65 °C.

Macrocycle **6.9**

Solutions of diiodide **6.8** (14.81 g, 24.2 mmol) and 1,3-propanedithiol (2.62 g, 24.2 mmol) in DMF (20 mL total solution volume each) were loaded into all-plastic syringes and added by syringe pump over 48 hours to a stirred suspension of cesium carbonate (23.6 g, 72.5 mmol) in DMF (750 mL) at 80°C (internal temperature) under argon. The hot liquid phase was then decanted from the solid residue and concentrated to

dryness. The solids remaining after decantation were stirred in boiling toluene (200 mL), and the liquid phase was decanted and added to the residue remaining after evaporation of the initial liquid phase. The resulting mixture was concentrated to dryness, and the process was repeated. The residue was taken up in DCM (250 mL) and filtered through a 4 cm diameter column containing sequential beds of sand (3 cm), celite (3 cm) and silica gel (4 cm). The column was flushed with an additional 250 mL of DCM, and the combined fitlrates were concentrated under reduced pressure. The residue was taken up in boiling acetone (100 mL), diluted slowly with hot hexanes until crystallization initiated, and allowed to cool under slow stirring. The product was collected by filtration, washed with 5% acetone in hexanes, and dried by suction. Yield 7.82 g (65%).[b] Mp 131-132°C. ^{1}H NMR ($CDCl_3$, 400 MHz) δ 1.41 (s, 12H), 1.93 (p, *J* = 6.9 Hz, 4H), 2.74 (t, *J* = 6.9 Hz, 8H), 2.79 (s, 8H), 3.71 (s, 8H). ^{13}C NMR ($CDCl_3$, 100 MHz) δ 23.7, 28.7, 32.4, 35.2, 37.9, 66.7, 98.4. EI-MS *m/z* 496 (100, $[M]^+$), 355 (50), 106 (45). EI-HRMS *m/z* calcd for $[M]^+$ $C_{22}H_{40}O_4S_4$ 496.1809, found 496.1813. [b] With chromatographic purification of the starting diiodide **6.8**, macrocycle **6.9** was obtained in 75% yield following the above procedure at half scale.

Ligand **6.6**

Macrocycle **6.9** (7.58 g, 15.3 mmol) was dissolved in boiling isopropanol (200 mL) and 1 M aqueous HCl (15 mL) was added. The resulting crystalline slurry was boiled down to 150 mL total volume and then allowed to cool to room temperature under slow stirring. The colorless product was collected by filtration, washed with cold isopropanol followed by hexanes, and dried under high vacuum at 120 °C. Yield 6.25 g (98%). Mp 220.5-222°C. ^{1}H NMR (DMSO-D_6, 400 MHz) δ 1.80 (p, *J* = 7.0 Hz, 4H), 2.58 (s, 8H), 2.61 (t, *J* = 7.0 Hz, 8H), 3.30 (d, *J* = 5.1 Hz, 8H), 4.50 (t, *J* = 5.1 Hz, 4H). ^{13}C NMR (DMSO-D_6, 100 MHz) δ 28.9, 31.8, 34.1, 44.6, 62.5. EI-MS *m/z* 416 (100,

$[M]^+$), 241 (70), 106 (62). EI-HRMS *m/z* calcd for $[M]^+$ $C_{16}H_{32}O_4S_4$ 416.1183, found 416.1184.

Complex **6.10**

Ligand **6.6** (395 mg, 0.948 mmol) and $Cu(CH_3CN)_4PF_6$ (353 mg, 0.948 mmol) were stirred in pyridine (10 mL) under argon until all solids had dissolved. The mixture was concentrated to a thick paste, diluted with water (10 mL), and concentrated again to a thick paste under a stream of argon in a 50°C bath. The residue was taken up in methanol (15 mL), centrifuged to remove a small amount of pale blue precipitate, concentrated to dryness, and recrystallized from water to give the product as colorless fibrous crystals. Yield 408 mg (69%). ^{1}H NMR (DMSO-D_6, 400 MHz) δ 1.93-2.01 (br. m, 4H), 2.74 (s, 8H), 2.93 (br. t, $J \approx 5$ Hz, 8H), 3.39 (d, $J = 5.2$ Hz, 8H), 4.88 (t, $J = 5.2$ Hz, 4 H). ^{13}C NMR (DMSO-D_6, 100 MHz) δ 22.8 (br.), 34.6, 37.4, 43.3, 62.3.

Ligand **6.7**

Ligand **6.6** (1.52 g, 3.66 mmol) was added to an oven-dried 100 mL rb flask containing a 25 mm egg-shaped magnetic stir bar. The flask was sealed with a rubber septum and flushed with argon, and anhydrous DMSO (25 mL) was added. The mixture was stirred until the starting material had completely dissolved, and a solution of n-butyllithium in hexane (2.5 M, 3.07 mL, 2.1 equiv.) was added dropwise under rapid stirring. A white precipitate appeared and subsequently redissolved after addition of each drop, then became persistent once the amount of added n-BuLi exceeded 1.0 molar equiv. The resulting suspension was stirred for 30 minutes under a stream of argon to allow cooling by evaporation of hexane, and 1,3-propanesultone (893 mg, 2.0 equiv.) in anhydrous DMSO (2 mL) was added. The mixture was stirred for 4 hours, after which most of the precipitate had redissolved. A further 2 equiv. of n-BuLi followed by 2 equiv. of 1,3-propanesultone were added as described above, and the mixture was stirred

overnight. The reaction vessel was manually agitated to dislodge material deposited on the flask walls, and a further 1.4 equiv. of n-BuLi and 2 equiv. of 1,3-propanesultone were added as described above. After 4 hours, the mixture was almost clear. A final 1.0 equiv. of n-BuLi and 1.0 equiv. 1,3-propanesultone were added, and the mixture became completely clear after stirring overnight. The resulting solution was diluted with ethanol (75 mL), treated with activated carbon to remove colored material leached from the rubber septum, and filtered through Celite. The carbon-Celite pad was washed with 30 mL of ethanol, and the combined filtrate and washings were treated with a solution of sodium iodide in 15 mL ethanol, producing a voluminous white precipitate. The mixture was heated to boiling, diluted slowly with water under rapid stirring until the precipitate completely dissolved (required 20 mL) and allowed to cool to room temperature under slow stirring. The resulting crystalline slurry was cooled to 4 °C, and the slightly colored product was collected by filtration, dissolved in 25 mL water, filtered through cotton to remove a small amount of insoluble material, heated to boiling, and diluted gradually with ethanol (required 75 mL) to the point of permanent turbidity. The mixture was diluted dropwise with water until clear and then allowed to cool under slow stirring. The resulting colorless crystalline powder was collected by filtration and dried overnight at 100°C/0.05 torr to give a fine powder. Yield 2.52 g (2.54 mmol, 69%) ^{1}H NMR (D_2O, 400 MHz) δ 1.93-2.05 (m, 12H), 2.75 (s, 8H), 2.76 (t, *J* = 6.9 Hz, 8H), 2.97-3.01 (m, 8H), 3.44 (s, 8H), 3.62 (t, *J* = 6.2 Hz, 8H). ^{13}C NMR (D_2O, 100 MHz) δ 27.1, 31.2, 34.7, 37.2, 46.5, 50.9, 72.5, 74.6. Elemental analysis calcd (%) for $C_{28}H_{52}Na_4O_{16}S_8$ (993.18): C 33.86, H 5.28, S 25.83; found C 32.69, H 5.28, S 25.44.

Complex **6.11**

A solution of $Cu(CH_3CN)_4PF_6$ (221 mg, 0.593 mmol) in acetonitrile (10 mL) was added to a solution of ligand **6.7** (589 mg, 0.593 mmol) in water (10 mL). The mixture was concentrated to a viscous residue, which was taken up in boiling ethanol (50 mL) and concentrated to dryness. The resulting material was stirred in boiling ethanol (30 mL) and diluted gradually with water until almost all solids had dissolved to give a yellow, slightly turbid solution. This was decolorized with the minimum sufficient amount (< 50 mg) of ascorbic acid, allowed to settle while hot, decanted from the small amount of solid sediment, and allowed to cool under slow stirring to give a colorless crystalline slurry. The product was collected by filtration and dried overnight at 50°C/0.05 torr followed by 1 hour at 100°C/0.05 torr to give a fine powder. Yield 539 mg (0.449 mmol, 76%). ^{1}H NMR ($CDCl_3$, 400 MHz) δ 1.99-2.06 (m, 8H), 2.07-2.11 (m, 4H), 2.89 (s, 8H), 2.97-3.01 (m, 16H), 3.55 (s, 8H), 3.65 (t, *J* = 6.2 Hz, 8H). ^{13}C NMR ($CDCl_3$, 100 MHz) δ 25.6, 27.1, 38.0, 40.7, 45.4, 50.9, 72.5, 74.7. ^{19}F NMR (D_2O, 376 MHz) δ (TFE) 4.66 (d, *J* = 708 Hz, 6F). Elemental analysis calcd (%) for $C_{28}H_{52}CuF_6Na_4O_{16}PS_8 \cdot 2H_2O$ (993.18): C 27.17, H 4.56, S 20.73; found C 27.20, H 4.51, S 20.76.

6.6.2. Crystallization procedures for X-ray diffraction

Complex **6.3**-ClO_4

Complex 6.3 (20 mg) was dissolved in water (100 µL) and diluted with ethanol (200 µL.). To this solution was added 500 µL of a solution prepared by dissolving $NaClO_4 \cdot H_2O$ (3.0 g), in ethanol (8 mL) plus water (4 mL). The mixture was filtered through a 0.2 µM nylon membrane and allowed to stand overnight in a sealed vial, yielding clear, colorless triclinic prisms.

Complex **6.4**

The granular form of complex **6.4** (30 mg) was recrystallized from 3:1 ethanol-water (1 mL) using hot tap water as the heat source.[c] The resulting irregular hexagonal tablets contained areas of turbidity at the center, so they were broken, heated under hot tap water until a single clear fragment remained, and allowed to cool, giving a cluster of clear irregular hexagonal tablets up to about 3 mm in width. Due to the large size, the crystals were cut into smaller pieces for X-ray diffraction (carried out by Dr. John Bacsa).

[c] Heating the solution above about 45°C results in conversion to the fibrous crystalline form.

Ligand **6.6**

Ligand 6.10 (30 mg) was dissolved in DMSO (1 mL) and the mixture was diluted with water until crystallization occurred, resulting in fine needles. The mixture was repeatedly agitated under hot tap water (~40°C), and diluted further with DMSO until complete dissolution occurred. The resulting solution was filtered through a tightly packed cotton plug and allowed to stand overnight, resulting in clear, twinned needles up to about 6 mm in length.

Complex **6.10**

Complex 6.10 (35 mg) was dissolved in boiling ethanol (~ 1 mL) and filtered through a 0.2 mm nylon membrane. Long, twinned fibers, nearly identical to the anhydrous form obtained by crystallization from water, were deposited. The mother liquor was removed, and fresh ethanol (3 mL) was added. The solution was heated to boiling and loaded into an all-plastic syringe, which was fitted with a 0.2 μM nylon membrane filter. The assembly was quickly cooled to room temperature, initiating formation of fibrous crystals, which were removed by filtration as soon as clearly visible.

After several hours, the clear solution deposited tiny, shining prisms, which grew up to about 4 mm long after standing overnight.

6.7. References

(1) Wernimont, A. K.; Yatsunyk, L. A.; Rosenzweig, A. C. *J. Biol. Chem.* **2004**, *279*, 12269.

(2) Badarau, A.; Dennison, C. *J. Am. Chem. Soc.* **2011**, *133*, 2983.

(3) Beverskog, B.; Puigdomenech, I. *J. Electrochem. Soc.* **1997**, *144*, 3476.

(4) Xiao, Z. G.; Wedd, A. G. *Nat. Prod. Rep.* **2010**, *27*, 768.

(5) Changela, A.; Chen, K.; Xue, Y.; Holschen, J.; Outten, C. E.; O'Halloran, T. V.; Mondragon, A. *Science* **2003**, *301*, 1383.

(6) Zeng, L.; Miller, E. W.; Pralle, A.; Isacoff, E. Y.; Chang, C. J. *J. Am. Chem. Soc.* **2006**, *128*, 10.

(7) Kamau, P.; Jordan, R. B. *Inorg. Chem.* **2001**, *40*, 3879.

(8) Xiao, Z. G.; Brose, J.; Schimo, S.; Ackland, S. M.; La Fontaine, S.; Wedd, A. G. *J. Biol. Chem.* **2011**, *286*, 11047.

(9) Miras, R.; Morin, I.; Jacquin, O.; Cuillel, M.; Guillain, F.; Mintz, E. *J. Biol. Inorg. Chem.* **2008**, *13*, 195.

(10) Hawkins, C. J.; Perrin, D. D. *J. Chem. Soc.* **1963**, 2996.

(11) Bernardo, M. M.; Heeg, M. J.; Schroeder, R. R.; Ochrymowycz, L. A.; Rorabacher, D. B. *Inorg. Chem.* **1992**, *31*, 191.

(12) Bernardo, M. M.; Schroeder, R. R.; Rorabacher, D. B. *Inorg. Chem.* **1991**, *30*, 1241.

(13) Ambundo, E. A.; Deydier, M. V.; Grall, A. J.; Aguera-Vega, N.; Dressel, L. T.; Cooper, T. H.; Heeg, M. J.; Ochrymowycz, L. A.; Rorabacher, D. B. *Inorg. Chem.* **1999**, *38*, 4233.

(14) Galijasevic, S.; Krylova, K.; Koenigbauer, M. J.; Jaeger, G. S.; Bushendorf, J. D.; Heeg, M. J.; Ochrymowycz, L. A.; Taschner, M. J.; Rorabacher, D. B. *Dalton Trans.* **2003**, 1577.

(15) Pinho, S. P.; Macedo, E. A. *J. Chem. Eng. Data* **2005**, *50*, 29.

(16) Macrae, C. F.; Bruno, I. J.; Chisholm, J. A.; Edgington, P. R.; McCabe, P.; Pidcock, E.; Rodriguez-Monge, L.; Taylor, R.; Streek, J. v. d.; Wood, P. A. *J. Appl. Cryst.* **2008**, *41*, 466.

(17) Spek, A. L. *J. Appl. Cryst.* **2003**, 7.

(18) Martell, A. E. *Critical Stability Constants*; New York: Plenum Press, 1974.

(19) Pett, V. B.; Leggett, G. H.; Cooper, T. H.; Reed, P. R.; Situmeang, D.; Ochrymowycz, L. A.; Rorabacher, D. B. *Inorg. Chem.* **1988**, *27*, 2164.

(20) Krylova, K.; Jackson, K. D.; Vroman, J. A.; Grall, A. J.; Snow, M. R.; Ochrymowycz, L. A.; Rorabacher, D. B. *Inorg. Chem.* **1997**, *36*, 6216.

(21) Meagher, N. E.; Juntunen, K. L.; Heeg, M. J.; Salhi, C. A.; Dunn, B. C.; Ochrymowycz, L. A.; Rorabacher, D. B. *Inorg. Chem.* **1994**, *33*, 670.

(22) Desper, J. M.; Gellman, S. H.; Wolf, R. E.; Cooper, S. R. *J. Am. Chem. Soc.* **1991**, *113*, 8663.

(23) Ashby, E. C.; Park, W. S.; Goel, A. B.; Su, W. Y. *J. Org. Chem.* **1985**, *50*, 5184.

(24) Page, P. C. B.; Chan, Y. H.; Heaney, H.; McGrath, M. J.; Moreno, E. *Synlett* **2004**, 2606.

(25) Blake, A. J.; Gould, R. O.; Halcrow, M. A.; Schroder, M. *Acta Crystallogr., Sect. B: Struct. Sci.* **1993**, *49*, 773.

(26) Bjerrum, J. *Metal Amine Formation in Aqueous Solution. Theory of the Reversible Step Reactions*; P. Haase & Son: Copenhagen, 1957.

(27) Yao, S. G.; Cherny, R. A.; Bush, A. I.; Masters, C. L.; Barnham, K. J. *J. Pept. Sci.* **2004**, *10*, 210.

(28) Avdeef, A.; Sofen, S. R.; Bregante, T. L.; Raymond, K. N. *J. Am. Chem. Soc.* **1978**, *100*, 5362.

(29) Xue, Y.; Davis, A. V.; Balakrishnan, G.; Stasser, J. P.; Staehlin, B. M.; Focia, P.; Spiro, T. G.; Penner-Hahn, J. E.; O'Halloran, T. V. *Nat. Chem. Biol.* **2008**, *4*, 107.

CHAPTER 7

CONCLUSION AND OUTLOOK

7.1. Copper(I)-selective fluorescent probes

At the outset of the work described in this dissertation, the available copper(I)-selective fluorescence turn-on probes were best regarded as proofs of concept, providing fluorescence contrast ratios only up to 10 and fluorescence quantum yields up to 15% in response to aqueous Cu(I).[1,2] While preliminary cellular imaging experiments yielded promising results, especially for CTAP-1,[1] these experiments relied on high-dose copper supplementation involving direct exposure of cells to 100-150 μM $CuCl_2$ to produce an observable response. For comparison, 150 μM Cu^{2+} is approximately three times the human toxicity threshold[3] of 3 ppm for copper in drinking water.

Efforts to improve the utility of Cu(I)-probes for biological imaging applications have thus far concentrated primarily on improving the fluorescence contrast ratio and quantum yield, which has been a major focus of this work. The inherent fluorescence quenching abilities of Cu(I), formerly considered the greatest obstacle to effective fluorescent probe design, have now been definitively overcome using a PET-based fluorescence switching mechanism, resulting in fluorescence contrast ratios exceeding 150 and fluorescence quantum yields of up to 49% in methanolic solution or 41% in aqueous solution, the latter from probe **5.28** developed in Chapter 5.

During the course of this work, it became apparent that aqueous solubility and probe aggregation in aqueous solution are equally important factors, and much of the effort of this author was devoted to overcoming the inherent lipophilicity of the fluorophore and ligand structures previously applied for Cu(I)-sensing. This effort was not in vain, however, as it is now clear that the probe CTAP-2 developed in Chapter 3 is

in fact the first truly water-soluble Cu(I)-selective fluorescent indicator with a reversible turn-on response.

Subsequent refinements in probe design since CTAP-2 have now brought the fluorescence quantum yield and contrast ratio available from water-soluble Cu(I)-probes to a point which should be quite adequate for biological imaging applications, and the quest to optimize these parameters can now be considered complete. Based on the current best estimates[4] for the Cu(I)-binding affinity of copper chaperones such as Atox1, however, the Cu(I)-affinities of all previously reported Cu(I)-probes including CTAP-2 and its descendents are probably several orders of magnitude lower than required for imaging of endogenous intracellular Cu(I)-pools, despite reports to the contrary by Chang *et al.*[5,6] The latter are based on experiments with highly lipophilic probes characterized in aqueous buffer, draw sweeping conclusions from threshold-level data, and provide interpretations which are highly questionable in the opinion of this author. Furthermore, Price *et al.*[7] recently presented detailed studies demonstrating a lack of intracellular copper-sensing efficacy for Coppersensor-1, the first Cu(I)-selective fluorescent probe introduced by Chang *et al.*,[2] which has also been demonstrated to form colloidal aggregates in aqueous solution.[8]

While the achievements detailed here represent important steps toward development of Cu(I)-selective fluorescent probes truly worthy to serve as mainstream tools in the elucidation of copper(I)-biochemistry, this ultimate goal has not yet been achieved. In the opinion of this author, further development of water-soluble Cu(I)-selective fluorescent probes should first focus on improving Cu(I)-affinity.

7.2. Copper(I)-affinity standards

Small-molecule ligands that are freely water-soluble, easily purified, and form colorless, air-stable 1:1 Cu(I)-complexes could serve as ideal affinity standards for Cu(I),

but to the knowledge of this author, no ligands meeting all of the above characteristics existed prior to the work described in Chapter 6. Rorabacher *et al*.[9-11] came close, producing several moderately lipophilic, slightly water-soluble thiocrown Cu(I)-ligands that may otherwise meet the above characteristics, but these were not tested as affinity standards.

Due in part to a lack of suitable affinity standards, binding affinity determination for Cu(I)-proteins has been challenging, and to refer the aggregate literature on protein-Cu(I) affinities as inexact would be a gross understatement. Thanks in part to the synthetic contributions of the author, but more so to a total of roughly 170 painstakingly careful potentiometric and competition titrations conducted by Pritha Bagchi, we have now constructed a small but robust series of Cu(I) affinity standards, including three freely water-soluble sulfonated thioether-based ligands suitable for competition experiments with lower affinity Cu(I)-proteins. The sulfonated thioether ligands form colorless Cu(I) complexes which are air-stable even in aqueous solution, readily purified by crystallization, and have sufficiently low near-UV absorptivity to allow fluorimetric monitoring of the Cu(I) occupancy of the bacterial copper chaperone CusF during competition titrations without significant inner-filter effects from the Cu(I)-complex of the affinity standard. While we have currently demonstrated only one instance of protein Cu(I)-affinity determination using the new affinity standard series, our values for the Cu(I)-complex stability constants of the previously employed standards BCA and BCS, which have been cross-verified against our new ligands, could allow the re-assessment of published protein-Cu(I) affinities based on less accurate values. While the Cu(I)-affinities of the current sulfonated thioether ligands are not quite high enough for effective competition against eukaryotic copper chaperones such as Atox1, it is probable that the affinity range of the current series can be extended with new designs providing better ligand preorganization or more strongly coordinating donors, which would provide a substantial asset to the field of copper biochemistry.

7.3. References

(1) Yang, L.; McRae, R.; Henary, M. M.; Patel, R.; Lai, B.; Vogt, S.; Fahrni, C. J. *Proc. Natl. Acad. Sci. U. S. A.* **2005**, *102*, 11179.

(2) Zeng, L.; Miller, E. W.; Pralle, A.; Isacoff, E. Y.; Chang, C. J. *J Am Chem Soc* **2006**, *128*, 10.

(3) Pizarro, F.; Olivares, M.; Uauy, R.; Contreras, P.; Rebelo, A.; Gidi, V. *Environ. Health Perspect.* **1999**, *107*, 117.

(4) Xiao, Z. G.; Brose, J.; Schimo, S.; Ackland, S. M.; La Fontaine, S.; Wedd, A. G. *J. Biol. Chem.* **2011**, *286*, 11047.

(5) Domaille, D. W.; Zeng, L.; Chang, C. J. *J. Am. Chem. Soc.* **2010**, *132*, 1194.

(6) Dodani, S. C.; Domaille, D. W.; Nam, C. I.; Miller, E. W.; Finney, L. A.; Vogt, S.; Chang, C. J. *Proc. Natl. Acad. Sci. U. S. A.* **2011**, *108*, 5980.

(7) Price, K. A.; Hickey, J. L.; Xiao, Z. G.; Wedd, A. G.; James, S. A.; Liddell, J. R.; Crouch, P. J.; White, A. R.; Donnelly, P. S. *Chem. Sci.* **2012**, *3*, 2748.

(8) Morgan, M. T.; Bagchi, P.; Fahrni, C. J. *J. Am. Chem. Soc.* **2011**, *133*, 15906.

(9) Pett, V. B.; Leggett, G. H.; Cooper, T. H.; Reed, P. R.; Situmeang, D.; Ochrymowycz, L. A.; Rorabacher, D. B. *Inorg. Chem.* **1988**, *27*, 2164.

(10) Krylova, K.; Jackson, K. D.; Vroman, J. A.; Grall, A. J.; Snow, M. R.; Ochrymowycz, L. A.; Rorabacher, D. B. *Inorg. Chem.* **1997**, *36*, 6216.

(11) Meagher, N. E.; Juntunen, K. L.; Heeg, M. J.; Salhi, C. A.; Dunn, B. C.; Ochrymowycz, L. A.; Rorabacher, D. B. *Inorg. Chem.* **1994**, *33*, 670.

APPENDIX A

X-RAY CRYSTALLOGRAPHIC DATA

Table A1: Crystal data and structure refinement of complex **6.3**-ClO_4 **(**$[Cu(I)\text{-}(\mathbf{6.1})]_2Na_7(ClO_4)_3(H_2O)_4$)

Empirical formula	$C_{30}H_{68}Cl_3Cu_2N_2Na_7O_{34}S_{12}$	
Formula weight	1780.08	
Temperature	173(2)	
Wavelength	0.71073	
Crystal system	Triclinic	
Space group	P -1	
Unit cell dimensions	a = 9.8246(15) Å	α = 82.967(2)°
	b = 9.8488(15) Å	β = 84.686(2)°
	c = 18.657(3) Å	γ = 64.474(2)°
Volume	1615.2(4) $Å^3$	
Z	1	
Density (calculated)	1.830 g/cm^3	
Absorption coefficient	1.308 mm^{-1}	
F(000)	912	
Crystal size	0.721 x 0.249 x 0.092 mm	
Theta range for data collection	2.202 to 31.126°	
Index ranges	-14<=h<=14, -14<=k<=14, -27<=l<=27	
Reflections collected	25301	
Independent reflections	10289 [R(int) = 0.0316]	
Completeness to theta = 25.242°	100.0 %	
Absorption correction	numerical	
Max. and min. transmission	1.000 and 0.5883	
Refinement method	Full-matrix least-squares on F^2	
Data / restraints / parameters	10289 / 572 / 574	
Goodness-of-fit on F^2	1.029	
Final R indices [I>2sigma(I)]	R1 = 0.0390, wR2 = 0.1038	
R indices (all data)	R1 = 0.0474, wR2 = 0.1098	
Extinction coefficient	n/a	
Largest diff. peak and hole	1.026 and –0.603 $e.Å^{-3}$	

Table A2: Atomic coordinates (x 10^4) and equivalent isotropic displacement parameters ($Å^2$x 10^3) for complex **6.3**-ClO_4 **(**[Cu(I)-(**6.1**)]$_2$$Na_7(ClO_4)_3(H_2O)_4$). U(eq) is defined as one third of the trace of the orthogonalized U^{ij} tensor.

Atom Label	x	y	z	U(eq)
Cu(1)	6651(1)	1120(1)	1824(1)	17(1)
Cl(1A)	3097(2)	-2233(2)	1814(1)	24(1)
S(1)	8747(1)	1442(1)	1941(1)	18(1)
S(2)	6560(1)	-1133(1)	1789(1)	18(1)
S(3)	7086(1)	3356(1)	4243(1)	14(1)
S(4)	2455(1)	1625(1)	3965(1)	14(1)
S(5)	4317(1)	3117(1)	1799(1)	19(1)
S(6)	8896(1)	-1962(1)	3902(1)	13(1)
Na(1)	6015(1)	946(1)	4739(1)	17(1)
Na(2)	2527(1)	-1884(1)	3827(1)	18(1)
Na(3)	10000	0	5000	14(1)
Na(4)	1664(1)	4761(1)	4732(1)	25(1)
O(1)	7867(2)	2157(2)	4801(1)	19(1)
O(2A)	2856(6)	-1970(6)	2563(2)	68(1)
O(3A)	3020(5)	-871(4)	1415(2)	42(1)
O(4A)	4590(5)	-3410(7)	1680(4)	53(1)
O(5A)	1955(4)	-2615(4)	1597(2)	51(1)
O(6)	1716(2)	601(2)	4096(1)	19(1)
O(7)	3694(2)	1189(2)	4451(1)	22(1)
O(8)	1388(2)	3203(2)	3976(1)	22(1)
O(9)	9820(2)	-1208(2)	4053(1)	20(1)
O(10)	7280(2)	-971(2)	3953(1)	21(1)
O(11)	9282(2)	-3414(2)	4328(1)	21(1)
O(12)	6961(2)	4820(2)	4399(1)	22(1)
O(13)	3002(2)	5586(2)	3739(1)	29(1)
O(14)	4999(2)	-2176(2)	4142(1)	21(1)
O(15)	5636(2)	3353(2)	4123(1)	20(1)

Table A2 continued

N(1)	6864(2)	1408(2)	658(1)	20(1)
C(1)	9324(2)	1319(3)	986(1)	24(1)
C(2)	8023(3)	2001(3)	477(1)	24(1)
C(3)	5383(3)	2485(2)	377(1)	23(1)
C(4)	7361(3)	-118(2)	413(1)	23(1)
C(5)	6479(3)	-960(2)	810(1)	23(1)
C(6)	8134(2)	3438(2)	2049(1)	19(1)
C(7)	7255(2)	3822(2)	2769(1)	18(1)
C(8)	8175(2)	2904(2)	3422(1)	18(1)
C(9)	3330(2)	1414(2)	3084(1)	19(1)
C(10)	2213(2)	2217(3)	2489(1)	22(1)
C(11)	2994(2)	2282(3)	1747(1)	23(1)
C(12)	4535(3)	3763(2)	858(1)	25(1)
C(13)	9323(2)	-2310(2)	2984(1)	17(1)
C(14)	8571(3)	-3220(2)	2728(1)	21(1)
C(15)	8298(3)	-2850(2)	1920(1)	23(1)
Cl(1B)	3334(6)	-2371(6)	1917(3)	24(1)
O(2B)	3390(15)	-1807(16)	2580(5)	68(1)
O(3B)	2821(14)	-1145(12)	1347(6)	42(1)
O(4B)	4836(13)	-3409(18)	1699(10)	53(1)
O(5B)	2322(9)	-3087(10)	2001(5)	51(1)
Cl(2)	10040(20)	5030(20)	4(16)	26(1)
O(16)	8986(5)	6543(5)	-183(3)	55(2)
O(17)	10036(6)	4493(5)	736(2)	58(2)
O(18)	9597(6)	4035(6)	-425(3)	64(2)
O(19)	11544(5)	4749(5)	-306(3)	55(2)

Table A3: Crystal data and structure refinement of complex **6.4** ([Cu(I)-(**6.2**)]$_2$Na$_6$(PF$_6$)$_2$(H$_2$O)$_{15}$)

Empirical formula	$C_{36}H_{102}Cu_2F_{12}N_2Na_6O_{33}P_2S_{12}$	
Formula weight	2030.87	
Temperature	173(2)	
Wavelength	0.71073 Å	
Crystal system	Triclinic	
Space group	P -1	
Unit cell dimensions	a = 11.8551(17) Å	α = 91.273(2)°
	b = 11.9311(17) Å	β = 98.023(2)°
	c = 32.214(5) Å	γ = 119.384(2)°
Volume	3909.7(10) Å^3	
Z	2	
Density (calculated)	1.725 g/cm^3	
Absorption coefficient	1.047 mm^{-1}	
F(000)	2100	
Crystal size	0.783 x 0.451 x 0.316 mm	
Theta range for data collection	1.284 to 32.106°	
Index ranges	-17<=h<=17, -17<=k<=17, -45<=l<=46	
Reflections collected	50063	
Independent reflections	25380 [R(int) = 0.0266]	
Completeness to theta = 32.106°	99.7 %	
Absorption correction	none	
Max. and min. transmission	0.8602 and 0.6223	
Refinement method	Full-matrix least-squares on F^2	
Data / restraints / parameters	25380 / 54 / 1278	
Goodness-of-fit on F^2	1.022	
Final R indices [I>2sigma(I)]	R1 = 0.0484, wR2 = 0.1242	
R indices (all data)	R1 = 0.0631, wR2 = 0.1339	
Extinction coefficient	n/a	
Largest diff. peak and hole	1.926 and –1.299 e.Å^{-3}	

Table A4: Atomic coordinates (x 10^4) and equivalent isotropic displacement parameters ($Å^2$x 10^3) for complex **6.4** ([Cu(I)-(**6.2**)]$_2$$Na_6$($PF_6$)$_2$($H_2O$)$_{15}$). U(eq) is defined as one third of the trace of the orthogonalized U^{ij} tensor.

Atom Label	x	y	z	U(eq)
Cu(1)	-3220(1)	-1624(1)	233(1)	15(1)
Cu(2)	3196(1)	1603(1)	4774(1)	14(1)
S(1)	-4998(1)	-1427(1)	323(1)	15(1)
S(2)	-4964(1)	-3905(1)	1761(1)	15(1)
S(8)	397(1)	-698(1)	1740(1)	15(1)
S(3)	-425(1)	682(1)	3259(1)	17(1)
S(6)	3233(1)	3515(1)	4673(1)	15(1)
S(5)	4991(1)	1462(1)	4659(1)	15(1)
S(4)	4730(1)	4063(1)	3289(1)	16(1)
S(7)	1209(1)	-268(1)	4666(1)	15(1)
S(9)	-3317(1)	-3554(1)	346(1)	15(1)
S(10)	-1206(1)	215(1)	346(1)	15(1)
S(11)	-2878(1)	1435(1)	1726(1)	16(1)
S(12)	2952(1)	-1343(1)	3288(1)	17(1)
Na(3)	-2185(1)	-948(1)	2272(1)	23(1)
Na(5)	3065(1)	-867(1)	2307(1)	21(1)
Na(4)	2246(1)	997(1)	2828(1)	21(1)
Na(1)	3134(1)	3803(1)	2421(1)	25(1)
Na(6)	-2888(1)	-4041(1)	2606(1)	27(1)
Na(2)	3598(1)	6847(1)	2524(1)	34(1)
O(8)	3339(2)	3098(2)	3175(1)	22(1)
O(1)	-5688(2)	-4284(2)	2116(1)	22(1)
O(5)	-3575(2)	-2986(2)	1903(1)	24(1)
O(15)	-468(2)	-189(2)	1819(1)	20(1)
O(14)	1086(2)	-827(2)	2137(1)	21(1)
O(13)	2518(2)	-2299(2)	2925(1)	37(1)
O(11)	4078(2)	-1225(2)	3578(1)	24(1)
O(12)	3200(2)	-100(2)	3151(1)	33(1)

Table A4 continued

O(7)	438(2)	146(2)	3212(1)	21(1)
O(6)	-1008(2)	852(2)	2851(1)	23(1)
O(25)	-1421(2)	-84(2)	3513(1)	23(1)
O(9)	5300(2)	4522(2)	2912(1)	27(1)
O(26)	-897(2)	-2078(2)	2614(1)	39(1)
O(27)	-3051(2)	-2220(2)	2900(1)	44(1)
O(28)	-3204(3)	-5458(2)	2020(1)	50(1)
O(29)	-1637(2)	-4938(2)	2964(1)	29(1)
O(2)	2076(2)	4796(2)	2726(1)	41(1)
O(24)	1118(2)	1965(2)	2393(1)	26(1)
O(4)	3225(2)	2674(2)	1818(1)	29(1)
O(10)	4948(2)	5113(2)	3591(1)	26(1)
O(20)	4006(2)	1476(2)	2445(1)	24(1)
O(21)	5073(2)	-948(2)	2463(1)	23(1)
O(22)	1948(2)	-3135(2)	2031(1)	30(1)
O(3)	4588(2)	6912(2)	3200(1)	42(1)
O(23)	3474(2)	-537(2)	1615(1)	29(1)
O(16)	1304(2)	60(2)	1460(1)	23(1)
O(17)	-3122(2)	240(2)	1911(1)	22(1)
O(18)	-2393(2)	2525(2)	2052(1)	27(1)
O(19)	-4011(2)	1268(2)	1432(1)	26(1)
O(30)	-5170(2)	-5024(1)	1496(1)	20(1)
N(1)	3566(2)	1825(2)	5443(1)	15(1)
N(2)	-3562(2)	-1847(2)	-437(1)	14(1)
C(3)	-5639(2)	-3111(2)	1447(1)	17(1)
C(2)	-5079(2)	-2746(2)	1042(1)	17(1)
C(1)	-5494(2)	-1839(2)	832(1)	17(1)
C(9)	578(2)	2237(2)	3538(1)	19(1)
C(8)	1263(2)	2172(2)	3969(1)	19(1)
C(7)	2354(2)	3508(2)	4162(1)	17(1)
C(6)	5450(2)	1919(2)	4147(1)	17(1)
C(5)	5011(2)	2837(2)	3965(1)	18(1)
C(4)	5507(2)	3267(2)	3553(1)	19(1)

Table A4 continued

C(15)	6219(2)	2890(2)	5008(1)	19(1)
C(14)	6047(2)	2696(2)	5466(1)	20(1)
C(13)	4950(2)	2855(2)	5608(1)	19(1)
C(12)	2678(2)	2201(2)	5619(1)	19(1)
C(11)	2690(2)	3423(2)	5480(1)	20(1)
C(10)	2088(2)	3348(2)	5022(1)	19(1)
C(16)	3362(2)	603(2)	5615(1)	19(1)
C(17)	2019(2)	-609(2)	5476(1)	20(1)
C(18)	1712(2)	-1181(2)	5019(1)	19(1)
C(19)	813(2)	-1201(2)	4160(1)	17(1)
C(20)	2011(2)	-938(2)	3968(1)	18(1)
C(21)	1644(2)	-1871(2)	3576(1)	18(1)
C(22)	-645(2)	-2273(2)	1477(1)	17(1)
C(23)	-1349(2)	-2218(2)	1049(1)	19(1)
C(24)	-2465(2)	-3551(2)	863(1)	16(1)
C(25)	-2161(2)	-3422(2)	7(1)	20(1)
C(26)	-2728(2)	-3482(2)	-455(1)	21(1)
C(27)	-2665(2)	-2240(2)	-597(1)	20(1)
C(28)	-4943(2)	-2854(2)	-615(1)	19(1)
C(29)	-6038(2)	-2677(2)	-483(1)	20(1)
C(30)	-6225(2)	-2862(2)	-24(1)	19(1)
C(31)	-3317(2)	-613(2)	-608(1)	19(1)
C(32)	-1967(2)	579(2)	-466(1)	20(1)
C(33)	-1658(2)	1153(2)	-8(1)	20(1)
C(34)	-801(2)	1142(2)	853(1)	17(1)
C(35)	-1991(2)	903(2)	1049(1)	18(1)
C(36)	-1581(2)	1851(2)	1440(1)	17(1)
P(2)	475(1)	5284(1)	5853(1)	20(1)
F(1)	925(2)	4408(1)	6131(1)	28(1)
F(2)	-569(2)	4025(2)	5546(1)	39(1)
F(3)	1516(2)	6528(1)	6171(1)	36(1)
F(4)	1567(2)	5537(2)	5572(1)	37(1)
F(5)	-611(2)	5014(2)	6143(1)	35(1)

Table A4 continued

F(6)	36(2)	6154(2)	5584(1)	39(1)
P(3)	419(1)	5245(1)	833(1)	19(1)
F(7)	-575(2)	3908(2)	557(1)	44(1)
F(8)	-136(2)	5981(2)	539(1)	40(1)
F(9)	-650(2)	4983(2)	1128(1)	36(1)
F(10)	991(2)	4529(2)	1137(1)	36(1)
F(11)	1506(2)	5522(2)	548(1)	39(1)
F(12)	1417(2)	6596(1)	1118(1)	31(1)
O(31)	6419(2)	10356(2)	3264(1)	26(1)
O(32)	6701(2)	2403(2)	2803(1)	26(1)
O(33)	9883(2)	4908(2)	2385(1)	45(1)

Table A5: Crystal data and structure refinement of ligand **6.6**.

Empirical formula	$C_{16}H_{32}O_4S_4$	
Formula weight	416.65	
Temperature	173.15 K	
Wavelength	0.71073 Å	
Crystal system	Triclinic	
Space group	P -1	
Unit cell dimensions	a = 9.5948(9) Å	α = 100.741(2)°
	b = 9.6412(9) Å	β = 107.2010(10)°
	c = 12.1268(12) Å	γ = 97.413(2)°
Volume	1032.38(17) $Å^3$	
Z	2	
Density (calculated)	1.340 g/cm^3	
Absorption coefficient	0.477 mm^{-1}	
F(000)	448	
Crystal size	0.774 x 0.212 x 0.196 mm	
Theta range for data collection	1.809 to 31.051°	
Index ranges	-13<=h<=13, -13<=k<=13, 0<=l<=17	
Reflections collected	10217	
Independent reflections	10217	
Completeness to theta = 35.0°	98.3 %	
Absorption correction	semi-empirical from equivalents	
Refinement method	Full-matrix least-squares on F^2	
Data / restraints / parameters	10217 / 73 / 248	
Goodness-of-fit on F^2	1.054	
Final R indices [I>2sigma(I)]	R1 = 0.1009, wR2 = 0.2508	
R indices (all data)	R1 = 0.1150, wR2 = 0.2612	
Extinction coefficient	n/a	
Largest diff. peak and hole	2.342 and –0.789 $e.Å^{-3}$	

Table A6: Atomic coordinates (x 10^4) and equivalent isotropic displacement parameters ($Å^2$x 10^3) for ligand **6.6**. U(eq) is defined as one third of the trace of the orthogonalized U^{ij} tensor.

Atom Label	x	y	z	U(eq)
C(1)	6909(4)	1686(4)	1563(3)	23(1)
C(2)	7008(5)	2954(5)	2576(3)	24(1)
C(3)	8301(5)	3011(5)	3706(3)	29(1)
S(2A)	10104(6)	3426(13)	3483(10)	34(1)
C(4A)	11398(15)	3172(13)	4804(12)	43(2)
C(5A)	11487(16)	1619(13)	4817(14)	44(2)
C(6A)	12487(14)	1040(15)	4139(13)	39(2)
S(3A)	12432(4)	-815(5)	4186(3)	32(1)
S(2B)	10131(6)	3246(13)	3512(10)	34(1)
C(4B)	11121(15)	2923(13)	4917(11)	43(2)
C(5B)	11161(16)	1354(13)	4850(14)	44(2)
C(6B)	12060(14)	788(15)	4050(13)	39(2)
S(3B)	12046(4)	-1064(5)	3953(3)	32(1)
C(7)	13290(6)	-1365(5)	3064(4)	34(1)
C(8)	12806(5)	-2920(5)	2344(4)	28(1)
C(9)	11200(5)	-3246(6)	1490(4)	34(1)
C(10)	8990(5)	-2102(5)	62(4)	30(1)
C(11)	8645(5)	-1125(5)	1045(4)	26(1)
C(12)	6984(4)	-1148(5)	724(4)	26(1)
C(13)	13898(5)	-3156(5)	1659(4)	27(1)
C(14)	12861(6)	-3973(5)	3151(4)	34(1)
C(15)	5553(5)	2780(5)	2874(4)	30(1)
C(16)	7261(6)	4356(5)	2174(4)	31(1)
O(1)	13559(4)	-4590(4)	936(3)	32(1)
O(2)	14288(5)	-3748(4)	4033(3)	48(1)
O(3)	5544(4)	3990(4)	3759(3)	41(1)
O(4)	6069(4)	4390(4)	1146(3)	43(1)
S(1)	6456(1)	-55(1)	1862(1)	32(1)
S(4)	10941(2)	-2169(2)	392(1)	46(1)

Table A7: Crystal data and structure refinement of complex **6.10** ([(Cu(I)-**6.6**]PF_6•EtOH)

Empirical formula	$C_{18}H_{38}CuF_6O_5PS_4$	
Formula weight	671.26	
Temperature	110(2)	
Wavelength	0.71073 Å	
Crystal system	Triclinic	
Space group	P -1	
Unit cell dimensions	a = 13.4862(5) Å	α = 71.5710(10)°
	b = 13.6947(4) Å	β = 77.6760(10)°
	c = 15.8096(5) Å	γ = 78.8850(10)°
Volume	2681.45(15) $Å^3$	
Z	4	
Density (calculated)	1.663 g/cm^3	
Absorption coefficient	1.256 mm^{-1}	
F(000)	1392	
Crystal size	0.712 x 0.356 x 0.184 mm	
Theta range for data collection	1.376 to 40.718°	
Index ranges	-24<=h<=24, -24<=k<=25, -28<=l<=28	
Reflections collected	110771	
Independent reflections	33773 [R(int) = 0.1632]	
Completeness to theta = 35.0°	99.5 %	
Absorption correction	semi-empirical from equivalents	
Max. and min. transmission	0.9848 and 0.6912	
Refinement method	Full-matrix least-squares on F^2	
Data / restraints / parameters	33773 / 253 / 683	
Goodness-of-fit on F^2	1.022	
Final R indices [I>2sigma(I)]	R1 = 0.0374, wR2 = 0.0959	
R indices (all data)	R1 = 0.0454, wR2 = 0.1019	
Extinction coefficient	n/a	
Largest diff. peak and hole	1.974 and –0.883 $e.Å^{-3}$	

Table A8: Atomic coordinates (x 10^4) and equivalent isotropic displacement parameters ($Å^2$x 10^3) for complex **6.10** ([(Cu(I)-**6.6**]PF_6•EtOH). U(eq) is defined as one third of the trace of the orthogonalized U^{ij} tensor.

Atom Label	x	y	z	U(eq)
P(2A)	2414(1)	-2417(1)	9998(1)	19(1)
F(7A)	1461(1)	-3065(1)	10313(1)	28(1)
F(8A)	3389(2)	-1804(2)	9710(2)	41(1)
F(9A)	1681(1)	-1380(1)	9590(2)	50(1)
F(10A)	2652(1)	-2649(1)	9041(1)	34(1)
F(11A)	2195(2)	-2187(2)	10956(1)	57(1)
F(12A)	3153(1)	-3494(1)	10387(1)	46(1)
P(2B)	2475(4)	-2429(4)	10060(3)	19(1)
F(7B)	1647(5)	-3214(6)	10391(6)	28(1)
F(8B)	3225(8)	-1566(8)	9657(10)	41(1)
F(9B)	1563(5)	-1505(4)	10081(6)	50(1)
F(10B)	2371(5)	-2342(5)	9059(3)	34(1)
F(11B)	2499(7)	-2597(8)	11094(4)	57(1)
F(12B)	3304(5)	-3428(5)	10044(5)	46(1)
C(17)	5834(1)	240(1)	7347(1)	15(1)
C(18)	5434(1)	892(1)	8017(1)	13(1)
C(19)	5129(1)	2052(1)	7541(1)	15(1)
C(23)	2308(1)	2558(1)	4877(1)	15(1)
C(24)	2017(1)	1577(1)	4771(1)	13(1)
C(25)	2423(1)	556(1)	5436(1)	15(1)
C(26)	2529(1)	-733(1)	7188(1)	20(1)
C(27)	3601(1)	-1302(1)	6975(1)	19(1)
C(28)	4431(1)	-1070(1)	7381(1)	21(1)
C(29)	2482(1)	1444(1)	3831(1)	15(1)
C(30)	841(1)	1734(1)	4902(1)	17(1)
C(31)	4578(1)	423(1)	8755(1)	14(1)
C(32)	6360(1)	895(1)	8453(1)	16(1)
O(5)	2074(1)	2265(1)	3122(1)	18(1)
O(6)	515(1)	852(1)	4807(1)	26(1)
O(7)	4291(1)	1027(1)	9375(1)	18(1)

Table A8 continued

O(8)	6796(1)	-118(1)	8910(1)	18(1)
S(5)	4998(1)	78(1)	6650(1)	15(1)
S(6)	3826(1)	2410(1)	7298(1)	16(1)
S(7)	3659(1)	2458(1)	4949(1)	16(1)
S(8)	2274(1)	642(1)	6583(1)	14(1)
Cu(2)	3702(1)	1419(1)	6433(1)	15(1)
C(4)	235(1)	6259(1)	7688(1)	18(1)
O(2)	4700(1)	4256(1)	9722(1)	18(1)
O(4)	-1039(1)	3587(1)	5885(1)	22(1)
O(1)	3477(1)	2942(1)	11629(1)	17(1)
C(14)	4196(1)	3436(1)	9706(1)	14(1)
C(10)	1051(1)	1566(1)	10190(1)	17(1)
C(11)	1571(1)	1154(1)	9389(1)	18(1)
S(3)	2503(1)	4658(1)	8372(1)	13(1)
S(4)	1217(1)	2881(1)	10129(1)	13(1)
C(13)	2892(1)	3754(1)	11039(1)	15(1)
C(8)	3051(1)	3641(1)	10076(1)	12(1)
S(2)	-264(1)	5059(1)	8388(1)	13(1)
O(3)	-107(1)	5647(1)	5809(1)	20(1)
C(9)	2603(1)	2686(1)	10081(1)	14(1)
Cu(1)	1094(1)	3816(1)	8647(1)	13(1)
S(1)	1085(1)	2729(1)	7834(1)	14(1)
C(3)	-1029(1)	4822(1)	7669(1)	15(1)
C(2)	-538(1)	4154(1)	7023(1)	13(1)
C(6)	2142(1)	6035(1)	7844(1)	18(1)
C(15)	315(1)	4649(1)	6300(1)	15(1)
C(7)	2553(1)	4682(1)	9506(1)	14(1)
C(5)	1041(1)	6506(1)	8114(1)	18(1)
C(1)	-185(1)	3017(1)	7519(1)	15(1)
C(12)	958(1)	1433(1)	8619(1)	19(1)
C(16)	-1425(1)	4112(1)	6564(1)	18(1)
C(33)	9315(1)	-596(1)	7383(1)	24(1)
C(34)	9255(1)	515(1)	7377(1)	29(1)
O(10)	5054(1)	3866(1)	1720(1)	21(1)

Table A8 continued

C(35)	4924(1)	4234(1)	2494(1)	23(1)
O(9)	8324(1)	-927(1)	7745(1)	21(1)
C(36)	4039(1)	5090(1)	2513(1)	33(1)
C(20)	4040(1)	3696(1)	6495(1)	16(1)
C(21)	3292(1)	4053(1)	5803(1)	17(1)
C(22)	3611(1)	3800(1)	4983(1)	19(1)
C(20')	3789(2)	3748(2)	6618(2)	16(1)
C(21')	4266(2)	3912(2)	5647(2)	22(1)
C(22')	3807(2)	3745(2)	4908(2)	19(1)
P(1A)	7092(1)	2798(1)	4873(1)	22(1)
F(1A)	7916(4)	3586(4)	4427(4)	44(1)
F(2A)	6240(3)	2046(3)	5349(3)	45(1)
F(3A)	7588(5)	2136(4)	4186(3)	38(1)
F(4A)	6607(3)	3462(4)	5578(2)	49(1)
F(5A)	6350(4)	3519(5)	4187(4)	44(1)
F(6A)	7819(3)	2104(4)	5572(3)	64(1)
P(1B)	7332(1)	2511(1)	4869(1)	22(1)
F(1B)	8126(2)	3337(2)	4415(2)	44(1)
F(2B)	6530(2)	1708(1)	5316(1)	45(1)
F(3B)	7685(2)	2063(2)	4015(1)	38(1)
F(4B)	7010(1)	2978(2)	5724(1)	49(1)
F(5B)	6482(2)	3331(2)	4353(2)	44(1)
F(6B)	8187(2)	1714(2)	5377(1)	64(1)